Routes to novel nano-structured organoclay composites

Whilton, Nicola Tracey

Award date:
1997

Awarding institution:
University of Bath

ROUTES TO NOVEL NANO-STRUCTURED ORGANOCLAY COMPOSITES

Submitted by **NICOLA TRACEY WHILTON**

for the degree of Ph.D.

of the University of Bath

1997

ProQuest LLC
789 East Eisenhower Parkway
P.O. Box 1346
Ann Arbor, MI 48106-1346

SUMMARY

Investigations on two ordered lamellar nanocomposite systems were carried out; namely, the synthesis of organic anion-intercalated layered double hydroxides (LDHs) and organically-functionalized magnesium phyllosilicates. Solid-state characterization techniques, including XRD, CP MAS NMR, electron microscopy and thermal analysis were utilized for analysis of these organic-inorganic hybrid materials.

Negatively charged amino acids (aspartic acid, glutamic acid) and a related polymer, polyaspartate, were intercalated within the gallery spaces of magnesium-aluminium-LDHs. Synthesis of the bioinorganic composites was achieved *via* coprecipitation involving simultaneous formation of the inorganic sheets and intercalation of the anionic species. The organic species were electrostatically held within the interlayer regions by the positively charged inorganic sheets. Oligomeric/polymeric polyaspartate was also generated within the interlayer regions of the pre-formed nanocomposite *via in situ* thermal polycondensation of intercalated aspartate precursors and *via* a chemical carbodiimide-activated coupling approach.

A further study into the intercalation of amphiphilic 5-alkoxyisophthalate dianions *via* coprecipitation showed how variation in the alkoxy chain length had little effect on the expansion of the interlayer spacing of the layered organic-inorganic hybrid.

Layered inorganic-organic composites containing covalently linked organic functionalities and based on a 2:1 trioctahedral phyllosilicate (talc) framework were prepared. Successful one-pot nonhydrothermal syntheses, involving generation of a inorganic layered framework through co-condensation of magnesium and

organosilicon components, afforded a range of organically-derivatized layered phyllosilicate-type composites. Variations in the hydrolysis/condensation behaviour of the organofunctional alkoxysilanes necessitated a modification of the reaction conditions in some instances. Analogies were made between the formation and structural arrangement of these materials and the organophosphonates of the tetravalent metals, and in particular the zirconium phosphonates.

Finally, possible applications of magnesium (organo)phyllosilicates through exploitation of the structure of these materials and, in particular, the properties of the organic functionalities were explored. The reactivity of the organic substituents towards bimolecular inter- and intramolecular reactions and the ion/metal-binding affinities were investigated. Preliminary attempts were made to generate porosity in the layered system through the use of organically-bridged bis(methoxysilyl) precursors.

ACKNOWLEDGEMENTS

Many people have served to provide encouragement, entertainment and occasional enlightenment to my three years (and a bit) in Bath. I have been fortunate during my time here to have had friends and colleagues whom I could rely on for support and advice.

Firstly I would like to express my gratitude to my supervisor Professor Stephen Mann for giving me the opportunity to work in his research group and for his encouragement, help and interest during my Ph.D..

I am also indebted to Dr. Kim Wong and Dr. Dominic Walsh for continual support and postdoctoral words of wisdom. In particular I would like to thank them for their involvement in my 'pilots' training on the electron microscopes and help with the production of this thesis.

I would also like to thank Dr. Sandra Burkett for her collaboration on the magnesium (organo)phyllosilicate project and for introducing me to the wonderful world of silica and solid state NMR. Dr. Benedicte Lebeau is also thanked for enlightening me further on the intricacies of solid state NMR and for her hospitality during my stay with her. I am equally grateful to the residents of N° 5 Clarence Terrace (Chris, Vicky, Claire, David and Menna) and Eric for their company and floor-space during my visits to Bath and to Ron for the use of his computer during my writing-up period.

I would like to acknowledge the support staff at the University; Rev. Barry Chapman (PXRD), Alan Carver (elemental analysis and XRD), Robert and Ahmed (miscellaneous), Ursula Potter and Hugh Perrot (electron optics) and externally, Dr.

David Apperley, University of Durham (solid state NMR) and Chris Paynter, English China Clays International (TGA/DSC).

I am grateful to the NERC for financial support and for memorable conferences in Paris, San Francisco and Exeter.

I would finally like to thank my colleagues in the lab, including those that have come and gone (and maybe come back again) for spicing up my time there.

Special thanks to Steve Sims for invaluable advice on the construction of this thesis and to Katy and Kerry-Ann for their friendship and encouragement.

Finally, to my Mum, Dad and Paul for their love, support and patience, a big Thankyou.

CONTENTS

CHAPTER 1

GENERAL INTRODUCTION:

FABRICATION OF ORGANIZED

INORGANIC-ORGANIC COMPOSITES

GENERAL INTRODUCTION: FABRICATION OF ORGANIZED INORGANIC-ORGANIC COMPOSITES

The following review aims to present some of the most recent developments in ordered composite materials. Conceptual approaches linking biology and materials chemistry will introduce the idea of biomimetic construction of organized architectures, through the application of design strategies based on inorganic-organic interfacial recognition, supramolecular pre-organization and external processing. Later sections will concentrate on recent developments involving the synthesis of nanoscale objects of dimensionality two. Inorganic lamellar solids as host structures for organic molecules and the fabrication of layered mineral-polymer nanocomposites will be detailed. Also highlighted will be rational design strategies based on the supramolecular assembly of molecular components and nanostructural materials (e.g. mineral sheets) to generate ordered organic-inorganic compounds. In the closing section, more recent molecularly-tailored solids, which are amenable to systematic structural design by modulation of the ionic inorganic framework and covalently-attached organic constituents, will be reviewed.

GENERAL INTRODUCTION: FABRICATION OF ORDGANIZED INORGANIC-ORGANIC COMPOSITES

The following review aims to present some of the most recent developments in ordered composite materials. Conceptual approaches linking biology and materials chemistry will introduce the idea of biomimetic construction of organized architectures, through the application of design strategies based on inorganic-organic interfacial recognition, supramolecular pre-organization and external processing. Later sections will concentrate on recent developments involving the synthesis of nanoscale objects of dimensionality two. Inorganic lamellar solids as host structures for organic molecules and the fabrication of layered mineral-polymer nanocomposites will be detailed. Also highlighted will be rational design strategies based on the supramolecular assembly of molecular components and nanostructural materials (e.g. mineral sheets) to generate ordered organic-inorganic compounds. In the closing section, more recent molecularly-tailored solids, which are amenable to systematic structural design by modulation of the ionic inorganic framework and covalently-attached organic constituents, will be reviewed.

1.1 *Biomineralization and the Biomimetic Approach to Inorganic Materials Design*

Nature has a unique and elegant approach for the construction of inorganic materials which is based on ordering molecular interactions between supramolecular organic aggregates and inorganic components. Many of Nature's remarkable materials contain mixtures of molecules or microstructures in which inorganic crystals or glasses are formed and coexist with organic molecules. Organic components, such as proteolipids, polysaccharides and proteins, are self-assembled into enclosed protein cages, lipid vesicles, membranes, and extended organic networks to form the reaction environments which constitute the initial stage in biomineral fabrication. These organized organic surfaces more often than not dictate the nucleation and crystal growth of the inorganic phase and the resultant biominerals often display size uniformity, unusual crystal habits, organized textures, and defined structures and compositions. The preferential crystallographic alignment of bioinorganic materials relative to an associated organic matrix is a remarkable feature of biomineralization. Subsequent ordering of these organized inorganic-organic composites can result in hierarchical microstructures.

Biomimetic materials chemists attempt to mimic the approaches Nature employs to fabricate materials exhibiting novel properties and complex form across a range of length scales (Mann, 1993). Recent investigations of biomineralization have indicated specific molecular interactions at the inorganic-organic matrix interface to be the key to understanding the physicochemical processes that result in the controlled nucleation and growth of inorganic crystals (Mann *et al.* 1992). Synthetic systems have highlighted the importance of electrostatic binding or association, geometric

matching (epitaxy) and stereochemical correspondence in these recognition processes. The development of new strategies for the controlled synthesis of inorganic nanophases, the crystal engineering of bulk solids and the assembly of organized composite and ceramic materials, is currently underway based on these design principles. To this end, attempts to mimic Nature have reaped fruitful rewards, albeit on a less complex scale!

As in Nature, recent work has concentrated on the use of appropriate organic templating agents (molecules, polymers, micelles, vesicles, and foams), to orchestrate the positioning, interconnection, and stabilization of inorganic building blocks at the micro-, meso- and macroscale. The materials are frequently formed as composite materials involving specific molecular interactions between the inorganic and organic components. However, upon completion of mineralization the organic components may be removed leaving spatially controlled and organized inorganic structures.

In a strategy of transcriptive synthesis (Mann and Ozin, 1996), the pattern and form of an inorganic material corresponds closely with that of the self-assembled organic architecture. The organic template is pre-organized and relatively stable, with chemical and morphological information 'written' into the surface structure. Interfacial nucleation and crystal growth can result in direct materials replication of the preformed organic shape. Compressed Langmuir monolayers of surfactant molecules on aqueous subphases have been used to conduct 'crystal design' and demonstrate simply, but eloquently, that oriented inorganic nucleation can be controlled by molecular recognition between the two-dimensional organic template and embryonic inorganic aggregates. Influence over the resultant crystal morphology and habit was also evident [Heywood and Mann, 1994 (Figure 1.1a)]. Self-assembled

lipid tubules can be used as discreet three-dimensional templates for the controlled crystallization of inorganic oxides [Archibald and Mann, 1993 (Figure 1.1b)]. Tubular microstructures formed from a sugar-based galactocerebroside lipids and small amounts of anionic sulphated derivative (which provide nucleation sites) were used to induce the nucleation of magnetic and non-magnetic iron oxides, leading to 'decoration' of the external surface of the cylindrical organic template. The assembly of the mineral nuclei is generally considered to be governed by electrostatic, structural and stereochemical complementarity at the inorganic-organic interface.

Synthetic control over the size of inorganic crystals has also been illustrated by utilizing pre-organized model polymer matrices (Bianconi *et al.*, 1991), protein cages [Meldrum *et al.*, 1991; Meldrum *et al.*, 1992 (Figure 1.1c)], phospholipid vesicles (Mann *et al.*, 1986) and reverse micelles (Meyer *et al.*, 1984; Petit *et al.*, 1993,). The formation of inorganic phases within spatially-controlled microenvironments mimics an approach similar to that used in the construction of some biominerals.

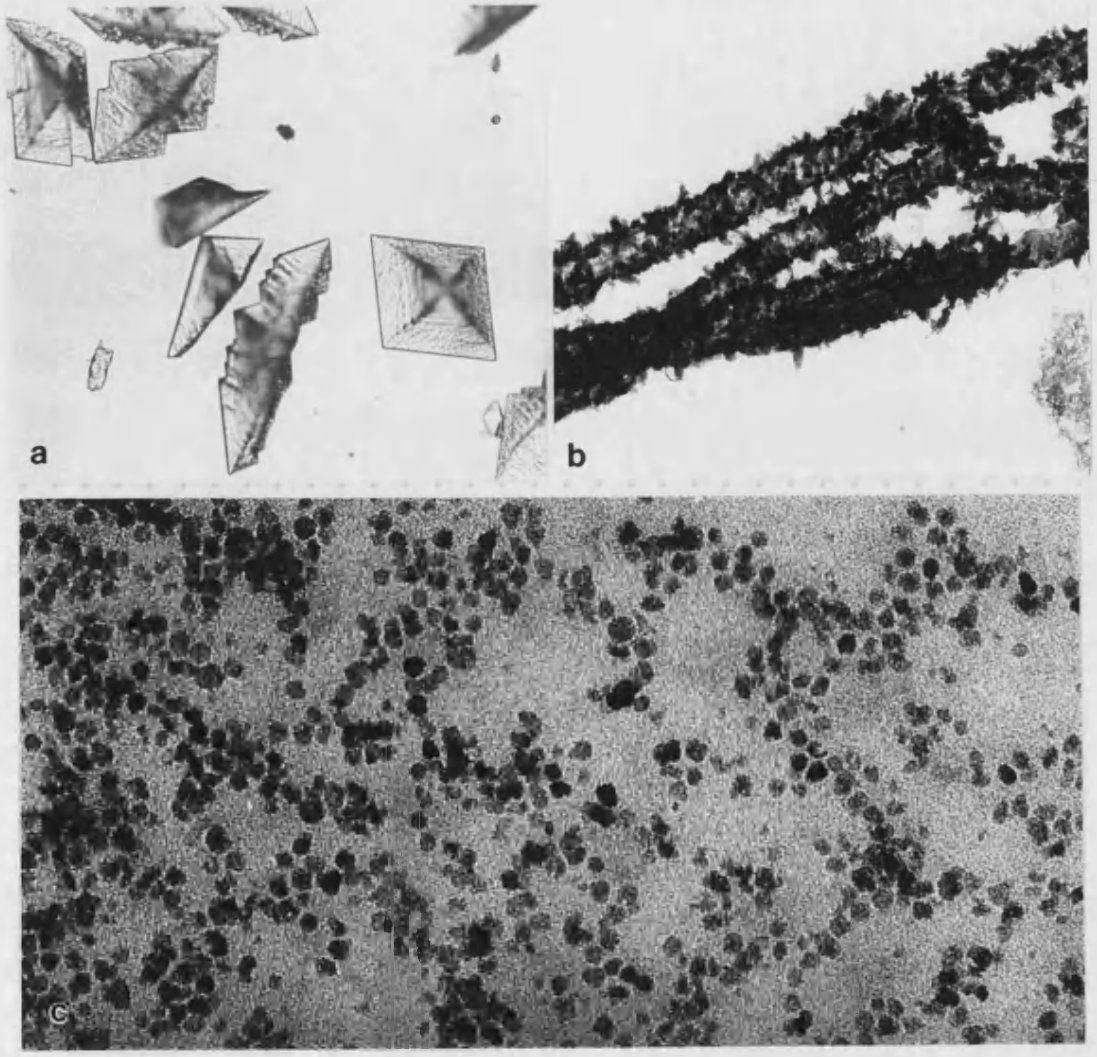

Figure 1.1 Examples of biomimetic inorganic materials. (a) Array of oriented calcite crystals nucleated under a surfactant monolayer formed at the air water interface. (b) Mineralized cylinders of self-assembled tubules formed by template-induced nucleation of iron oxides. (c) Nanoscale magnetite crystals formed within the cavity of individual ferritin protein cages. Micrographs courtesy of S. Mann (a and b) and K. K. W. Wong (c), University of Bath).

1.2 *Complex Inorganic Materials Formed* via *a "Synthesis-with-Construction" Approach* (Mann *et al.*, 1997)

A promising route to more complex nanostructured composites uses the ordered environment of preformed amphiphile-solvent mesophases. Such an approach involves the ordered pre-assembly of organic molecules in the mesophase to partition the solvent and confine the reactive species; thus providing a controlled environment for the formation of the inorganic nanostructures. In initial experiments that attempted to harness the order of the mesophase during the inorganic materials synthesis, precipitates with unique morphology were obtained, including oblong crystallites and macroporous crystalline networks. However, in these instances, large changes in the scale and form of the pattern replicated during mineralization generated architectures that did not resemble the initial organization of the associated reaction medium. For example, the mineralization reactions within the nanoscopic, interconnecting water channels of bicontinuous microemulsions produced microscopic mesh-like architectures of silica (Watzke and Dieschbourg, 1994) or calcium phosphate [Walsh *et al.*, 1994 (Figure 1.2)].

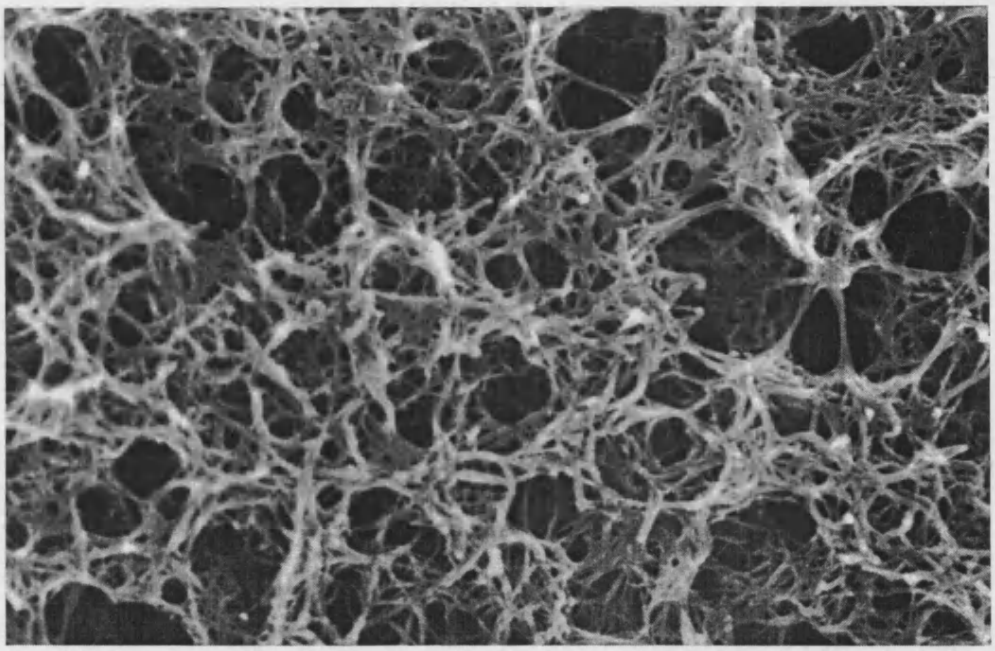

Figure 1.2 Microscopic mesh-like architecture of calcium phosphate mineralized within the nanoscopic, interconnecting water channels of a bicontinuous microemulsion . Photograph courtesy of D. Walsh, University of Bath.

These results suggest that in these instances the microskeletal inorganic form 'evolves' by localized disruption and reordering of the microemulsion due to incipient crystallization. Assembly of the inorganic framework depends on the ability of the self-organized reaction environment to undergo restructuring or 'metamorphosis' during inorganic crystallization. Believed implicit in this transformability is that the

surfactant head groups initially act as boundaries of nanoscale containers and templates but become growth directors as crystallization proceeds (Mann and Ozin, 1996).

In 1992 a new series of molecular sieves, M41S was reported which demonstrated how surfactants could be used in the fabrication of ordered silica mesophases (Kresge *et al.*, 1992). Nanostructured ceramic oxides with high surface areas, and uniform shapes and pore sizes, are obtained by surfactant-assisted hydrothermal synthesis in the presence of quaternary ammonium surfactants (Beck *et al.*, 1992). The cooperative assembly, which involves interactions between silica precursors and ionic surfactants into a siliceous mesophase, is believed to result from charge-density matching and multi-dentate binding of the chelating oligomeric ions (Monnier *et al.*, 1993; Huo *et al.*, 1994). The formation of M41S materials occurs above the critical micelle concentration of the surfactant, but far below the concentration at which a binary surfactant/water mixture would form a lyotropic liquid crystalline phase. However, the resultant precipitate is rich in surfactant and templating occurs in this heterogeneous gel phase. Post-synthesis removal of the organic phase affords mesoporous materials with superstructures which mimic those of a liquid-crystalline mesophase (Figure 1.3).

The reaction pathways affording M41S-type materials show considerable sensitivity to the reaction conditions and the structure of the resultant inorganic solid can only be determined upon analysis of the product. Phase changes during the preparation of mesoporous silicates have even been observed. Whilst the definitive mechanism of formation is still under debate, it is believed to proceed synergistically with the coassembly of the liquid-crystalline array and organized inorganic oxide.

surfactant head groups initially act as boundaries of nanoscale containers and templates but become growth directors as crystallization proceeds (Mann and Ozin, 1996).

In 1992 a new series of molecular sieves, M41S was reported which demonstrated how surfactants could be used in the fabrication of ordered silica mesophases (Kresge *et al.*, 1992). Nanostructured ceramic oxides with high surface areas, and uniform shapes and pore sizes, are obtained by surfactant-assisted hydrothermal synthesis in the presence of quaternary ammonium surfactants (Beck *et al.*, 1992). The cooperative assembly, which involves interactions between silica precursors and ionic surfactants into a siliceous mesophase, is believed to result from charge-density matching and multi-dentate binding of the chelating oligomeric ions (Monnier *et al.*, 1993; Huo *et al.*, 1994). The formation of M41S materials occurs above the critical micelle concentration of the surfactant, but far below the concentration at which a binary surfactant/water mixture would form a lyotropic liquid crystalline phase. However, the resultant precipitate is rich in surfactant and templating occurs in this heterogeneous gel phase. Post-synthesis removal of the organic phase affords mesoporous materials with superstructures which mimic those of a liquid-crystalline mesophase (Figure 1.3).

The reaction pathways affording M41S-type materials show considerable sensitivity to the reaction conditions and the structure of the resultant inorganic solid can only be determined upon analysis the of the product. Phase changes during the preparation of mesoporous silicates have even been observed. Whilst the definitive mechanism of formation is still under debate, it is believed to proceed synergistically with the coassembly of the liquid-crystalline array and organized inorganic oxide.

Since this initial demonstration of surfactant-assisted synthesis, amphiphiles have been used to produce inorganic materials with a variety of mesomorphic structures, including lamellar, hexagonally-packed tubular, and cubic forms. The lamellar phases, however, collapse to an amorphous oxide upon surfactant extraction (Sakata and Kunitake, 1990; Ogawa, 1994). More complex inorganic nanostructures based on M41S-type materials have also been synthesized (Huo *et al.*, 1995),with catalytically active metal ions being incorporated into the framework of the mesoporous structure, e.g. titanium silicates (Zhang *et al.*, 1996; Bagshaw *et al.*, 1996) and vanadium silicates (Reddy *et al.*, 1994). Mesoporous molecular silica sieves have recently been prepared by a neutral templating route based on hydrogen bonding interactions between nonionic surfactants and uncharged silica precursors (Tanev and Pinnavaia, 1995).

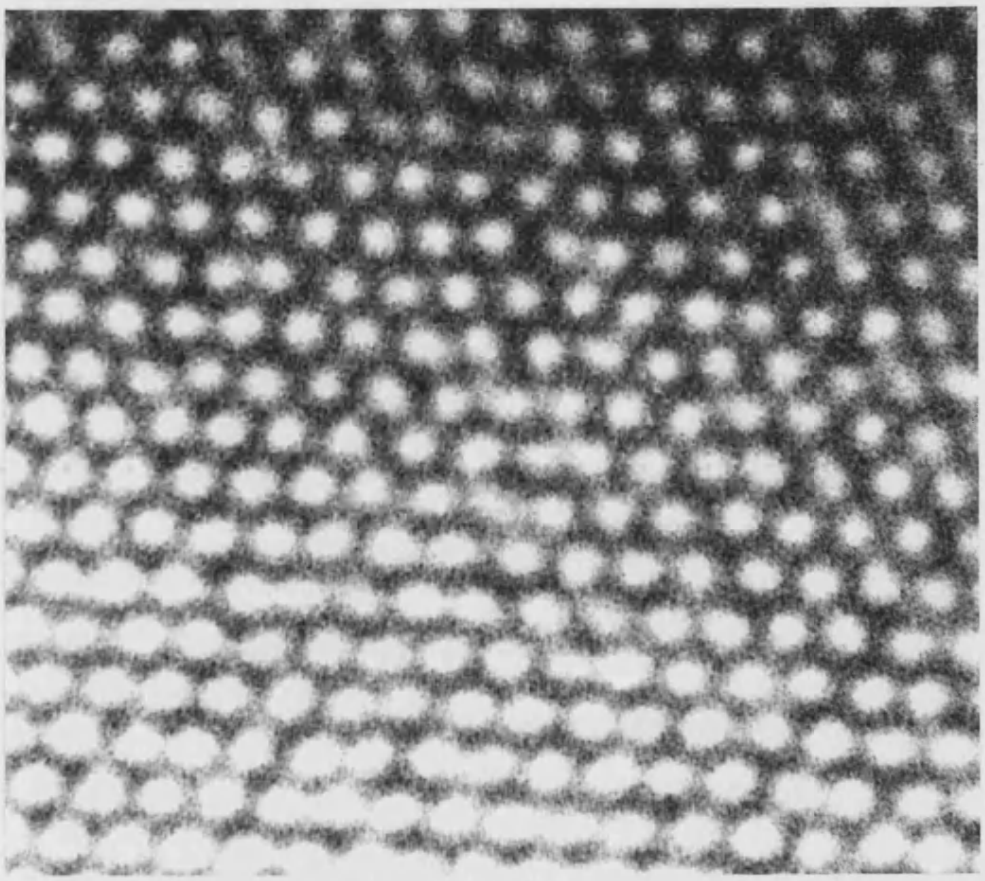

Figure 1.3 Hexagonal morphology of mesoporous silica (MCM41) following removal of surfactant. Photograph courtesy of C. E. Fowler, University of Bath

The synthesis of mesoporous silica has more recently been achieved by a direct templating approach from high surfactant-containing solutions, in which the formation of the bulk liquid-crystalline mesophase is generated before the addition of the inorganic precursors (Attard *et al.*, 1995). A mesoporous ceramic oxide phase can be obtained by solidifying a bulk liquid-crystalline phase within which precipitation of the inorganic phase is spatially confined to the surface of the close-packed rod-like micelles, and thus nanostructured monoliths are available. Removal of the organic component affords materials with a degree of order that is directly correlated to that of the parent liquid crystalline phase. A distinct advantage of this approach is its allowance for the determination of the nanostructure of the inorganic ceramic oxide *a priori* by choosing the binary phase diagram of a surfactant and water as a guideline and applying polarized light optical microscopy during the polycondensation to confirm the nature of the mesophase.

This strategy is not limited to sol-gel chemistry; precipitation and redox processes may also be carried out in such ordered structure-directing media. Attard *et al.* have shown lyotropic phases of nonionic surfactants to be versatile reaction media for the generation of ordered high-surface area platinum (Attard *et al.*, 1997). The growth of stable semiconductor superlattices based on cadmium sulphide and cadmium selenide within the ordered environment of a liquid-crystalline phase has also been accomplished (Braun *et al.*, 1996). In the construction of the hexagonal mesophase, non-ionic block copolymers, possessing hydrophobic and hydrophilic segments which constituted the hydrophobic inner core and hydrophilic external skin of the micelles respectively, are employed. Cadmium ions reside in the external hydrophilic areas of the micelles. Precipitation of the organic-inorganic solid within

the ordered environment of the mesophase is induced upon exposure to sources of sulphur or selenium, and both the symmetry and long-range order of the liquid crystal are preserved.

The utilization of amphiphilic block copolymers in the direct liquid crystalline templating approach to mesoporous ceramic oxides may impart higher stability on the monolithic objects and allow accessibility of larger pore diameters. Complex aggregates, i.e., lyotropic liquid crystalline phases formed from block copolymers, have been employed for the generation of mesoporous nanostructures in the same way as surfactant-based liquid-crystalline phases (Göltner and Antonietti, 1997). The length scale of the mesoporous subunit can be extended significantly by using amphiphilic block copolymer phases as templates and thermal and mechanical stability of the inorganic structure is improved.

Surfactant-induced assembly of inorganic structures is now a recognized way of producing novel nanoporous materials with a larger range of pore sizes than was previously possible. Other complex silicate materials have been prepared transcriptively from pre-assembled microemulsion-based systems. A lyotropic L_3 phase has recently been used as a template to form nanoporous monolithic silicates with continuously adjustable pore sizes. The monoliths have a random, bicontinuous pore structure, the uniform size of which can be adjusted by changing the solvent volume fraction. Characteristic pore size dimensions were measured between six to more than 35 nm (McGrath *et al.*, 1997).

Tanev and Pinnavaia have reported the synthesis of a layered silicate utilizing pre-formed multilamellar surfactant vesicles as biomimetic templates. The approach is based on the hydrolysis and cross-linking of a neutral inorganic alkoxide precursor in

the interlayered regions of stable multilamellar vesicles of a neutral bola-amphiphile surfactant. The close proximity of the layers, and further cross-linking and polymerization of adjacent silica species, leads to the simultaneous growth of parallel silica layers and intergallery pillars. Pore sizes were recorded in the micropore region (Tanev and Pinnavaia, 1996). Previous to this, surfactant-templated lamellar phases were unstable and collapsed upon removal of the organics. Porosity, has previously been introduced into lamellar MCM-50 by a post-synthesis cross-linking treatment with tetraethoxysilane which creates pillars in the gallery region of the layered host (Vartuli *et al.*, 1995). The one-step biomimetic approach, however, eliminates the need for a separate pillaring step.

1.3 *Preformed Inorganic Frameworks and Host-Guest Chemistry*

The most recognised systems with molecularly ordered structures which have been used to organize inorganic reactants are surfactant aggregates such as micelles, Langmuir-Blodgett films, liquid crystals, and inclusion compounds of both organics and inorganics. Among the many ordered or constrained systems utilized to organize organic (and inorganic) species, crystalline inorganic solids such as lamellar materials and zeolites occupy a special position owing to their adsorptive properties, ion-exchange ability and thermal and chemical stability. Zeolites behave as structurally tridimensional systems whilst layered materials display open frameworks which offer two-dimensional expandable interlayer space for organizing guest species.

Intercalation reactions can involve the reversible insertion of guest species into

layered host materials while maintaining the structural features of the host. Various lamellar solids, such as graphite, clay minerals, transition metal dichalcogenides, layered double hydroxides, metal phosphates and phosphonates, and transition metal oxides have been utilized as host materials for intercalation reactions. The incorporation of organic molecules by intercalation into expandable layered materials provides a unique opportunity to orient and assemble the guest species, and to alter, for example, the reactivity, electronic and optical properties of both guest and host (Whittingham, 1982).

Lamellar Inorganic-Organic Hybrids formed by Intercalation into Layered Inorganic Hosts

There are a wide variety of lamellar inorganic compounds that have been utilized as hosts for intercalation reactions of both inorganic and organic guest species. Three of the most studied classes are the smectite 'cationic' clays, the zirconium phosphates and the layered double hydroxides. These will be discussed in structural detail and methods for the intercalation of organic molecules applicable to these compounds will be presented.

Smectites

The smectites belong to the group of 2:1-type layered phyllosilicate clay minerals and consist of negatively charged silicate layers and readily exchangeable interlayer cations. Silicic acid sheets ($Si_2O_5^{2-}$) consist of SiO_4 units in which three oxygens per tetrahedron are shared. The apical oxygen atoms of the silicic acid sheet are commensurate, or nearly so, with $^2/_3$ of the hydroxyl groups of edge-shared sheets of linked $M_{2-3}(OH)_6$ octahedra, where M is either a divalent or trivalent metal cation. The 2:1 phyllosilicate layers are generated through condensation of two silicic acid sheets to a central octahedral sheet resulting in a unit cell formula of $M_{4-6}Si_8O_{20}(OH)_4$.

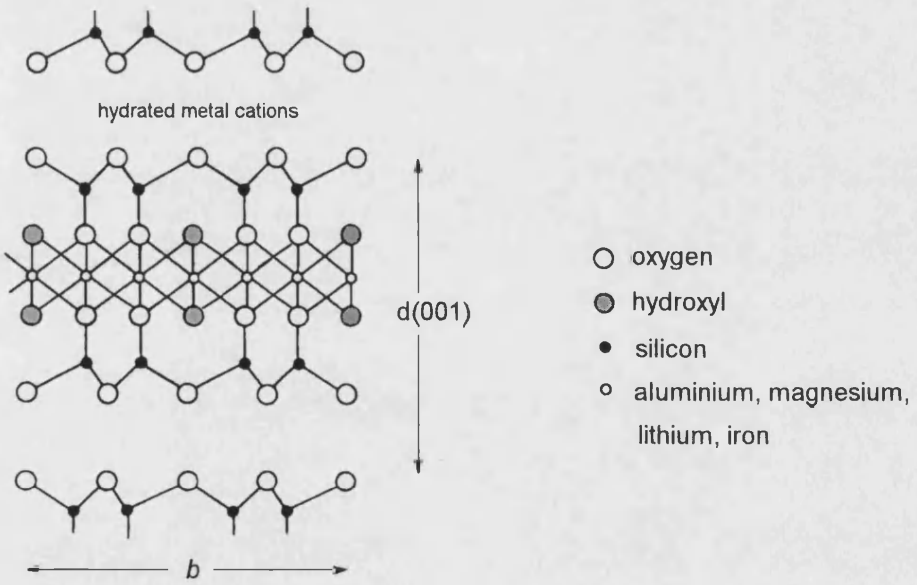

Figure 1.4 Schematic representation of a 2:1 trioctahedral smectite structure.

The members of the smectite group of clays are distinguished by the type and location of cations in the oxygen framework (Table 1.1). In a unit cell formed from 20 oxygens and four hydroxyl groups there are eight tetrahedral sites and six octahedral sites. When two-thirds of the octahedral sites are occupied by cations, the mineral is classified as a dioctahedral 2:1 phyllosilicate. A trioctahedral 2:1 phyllosilicate has all octahedral sites filled by cations (Figure 1.4).

Table 1.1.. Idealized structural formulas for some dioctahedral and trioctahedral 2:1 phyllosilicates.

Mineral group	Dioctahedral	Trioctahedral
Pyrophillite-talc	Pyrophillite: $[Al_{4.0}](Si_{8.0})O_{20}(OH)_4$	Talc: $[Mg_{6.0}](Si_{8.0})O_{20}(OH)_4$
Smectites	Montmorillonite:	Hectorite:
	$Ca_{0.35}[Mg_{0.70}Al_{3.30}](Si_{8.0})O_{20}(OH)_4$	$Na_{0.6}[Li_{0.6}Mg_{5.4}](Si_{8.0})O_{20}(OH,F)_4$
	Beidellite:	Saponite:
	$Na_{0.7}[Al_{4.0}](Si_{7.3}Al_{0.7})O_{20}(OH)_4$	$Na_{0.9}[Mg_{6.0}](Si_{7.1}Al_{0.9})O_{20}(OH)_4$
Micas	Muscovite:	Phlogopite:
	$K_2[Al_{4.0}](Si_{6.0}Al_{2.0})O_{20}(OH)_4$	$K_2[Mg_{6.0}](Si_{6.0}Al_{2.0})O_{20}(OH)_4$

Isomorphous substitution of metal cations of similar size and lower valency, such as Si^{4+} for Al^{3+}, Al^{3+} for Mg^{2+} and Mg^{2+} for Li^{+}, within the tetrahedral or octahedral layers, generates a net negative charge for layers. To compensate for the negative charge, hydrated metal cations (generally Na^{+} or Ca^{2+}) are intercalated in the gallery region between the silicate layers. The amount, as well as the site, of the isomorphous substitution influences the surface and colloidal properties of the layered

silicates, by determining the density of charge and the cation-silicate sheet interactions. The charge per formula unit of a smectite can range between 0.25 to 0.6.

The mechanism of the intercalation of guest species into smectites from aqueous solution is roughly classified into two: one is facile cation exchange with interlayer exchangeable cations, the other is adsorption of polar molecules such as alcohols, ketones , and amides by ion-dipole interactions with interlayer cations and/or hydrogen bonding with the surface oxygen atom of the silicate sheets. Several studies have concentrated on the introduction of organic molecules from aqueous solution into the interlayer region. Organic dye molecules, for example, have been intercalated by ion-exchange. The host-guest interactions in systems such as these are particularly intriguing as they may impart unique structural features and physicochemical properties on the intercalation compound (Carrado *et al.*, 1993).

One of the most unique and attractive properties of smectites is their swelling property (Van Olphen, 1977). Upon dispersion in water the gallery spaces between adjacent inorganic sheets can be expanded to such an extent that stable thixotropic gels form. When the gel is evaporated moderately, the clay particles pile up with their *ab* plane parallel to the substrate to form a transparent self-supporting film. Organic molecules can be introduced into the interlayer spaces by entrapment upon restacking of the sheets. In order to swell smectites in less polar solvents and increase their affinity for such solvents inorganic interlayer cations need to be exchanged with organocations, typically quaternary alkylammonium ions (Pinavaia *et al.*, 1994). Replacement of inorganic exchange cations by larger alkylammonium ions can modify the surface properties of the clays. These ions act as 'pillars' which hold the inorganic sheets permanently apart and render the interlayer region organophilic. This

facilities interaction with organic vapours and organic compounds dissolved in water. 'Organoclays' of this type have been shown to sorb alkanes and aliphatic alcohols, to remove organic contaminants from water, to serve as chromatographic stationary phases and to aid intercalation of organic species from a wide range of solvents (Stul *et al.*, 1978; Boyd *et al.*, 1988; Lee *et al.*, 1989).

A, by far less, common method for intercalation has been observed when transition metal ions are substituted for interlayer cations. Charge transfer between interlayer transition metal ions and neutral organic species in solution can be a driving force for the intercalation of the organic guests. Aromatic compounds can be oxidized by transition metal cations to their cationic form in the interlayer of smectite clay minerals under a dry atmosphere (Soma and Soma, 1988).

Synthetic analogues of smectites, i.e. saponite, hectorite and swelling mica, have attracted increasing interest since natural clay minerals contain impurities, the amounts of which depend on the source of the clay minerals, both within the structure and on the surface.

Zirconium Phosphate

Layered metal phosphates and arsenates have been known to form intercalation compounds. The best known members of this group are zirconium phosphate, $H_2[Zr(PO_4)_2]H_2O$ and other M^{IV} phosphates and arsenates. The α-phase of zirconium hydrogen phosphate, $Zr(O_3POH)_2 \cdot H_2O$ (α-ZrP) has a structure in which zirconium atoms lie in a plane and are bridged by phosphate groups. Three oxygens of

each tetrahedral phosphate are linked to three zirconium atoms so that each zirconium is octahedrally coordinated by six oxygens of six different phosphate groups (Figure 1.5). The fourth oxygen of each phosphate group bears a proton (not shown in Figure 1.5) which can be replaced with another cation.

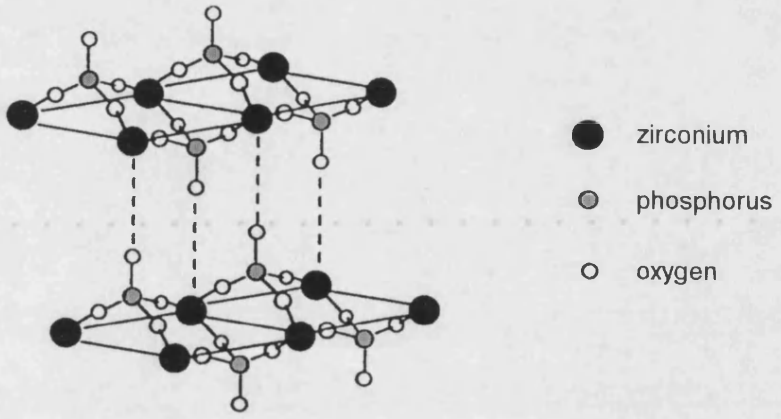

Figure 1.5 Schematic representation of the $Zr(HPO_4)_2 \cdot H_2O$, (α-ZrP). Redrawn from Cao *et al.*, 1992.

Cationic and basic guest species have been intercalated into α-ZrP through ion exchange and acid-base reactions respectively (Alberti, 1978, Bujoli *et al.*, 1993). The protons of the $[HPO_4]^{2-}$ group project into the interlayer region and are exchangeable. ε-aminocaproic acid and acrylamide and caprolactam have been intercalated from aqueous solution although long reaction times and reflux conditions were necessary (Ding *et al.*, 1995). These systems will also undergo swelling behaviour in water and processes in colloidal α-ZrP systems have been investigated

One of the most notable features of this class of materials is that organic substituents can be attached to the phosphate groups to form their organic derivatives. Recently, various tetravalent or divalent metal organophosphonates have been synthesized and the layered structures characterized. These structures will be discussed in a later section.

Layered Double Hydroxides

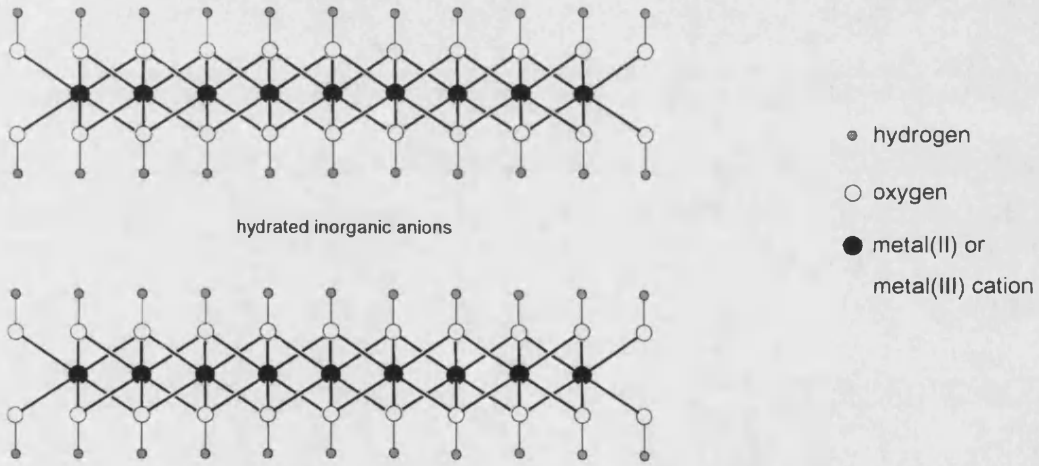

Figure 1.6 Schematic representation of the layered double hydroxide structure.

Layered double hydroxides (LDHs) form a complementary class to the conventional cationic clays and related lamellar systems (e.g. smectite clays, phosphates and phosphonates of tetravalent metals). The structure of these compounds is common to a large number of naturally-occurring minerals (e.g. hydrotalcite and

pyroaurite) and synthetic phases for which the composition can be described by the general formula, $[M^{II}_{1-x}M^{III}_{x}(OH)_2]A_{x/m}.nH_2O$, where M^{II} is a divalent cation such as Ni, Mg, Cu or Zn and M^{III} is a trivalent cation such as Al, Cr, Fe, V or Ga. $A_{x/m}$ is an inorganic anion of charge *m* such as CO_3^{2-}, Cl^-, SO_4^{2-} or NO_3^-. The layered structure is based on that of $Mg(OH)_2$, brucite, and consists of layers of M^{II} and M^{III} cations coordinated octahedrally by six oxygen atoms, as hydroxides. Metal-hydroxide layers are separated by charge-balancing counter-anions and water molecules loosely bound to the hydroxyl groups (Figure 1.6).

Compared with the cation exchange of smectites, the anion exchange reactions involving LDHs are not as facile because of their high selectivity to carbonate anions and large anion exchange capacity. The nature of the anion initially present in the starting LDH plays an important role in controlling the ease of exchange. In general, the more strongly bound anions are those with the smaller radii which result in a decreased spacing between the hydroxide layers (Miyata, 1983, Parker *et al.*, 1995). The exchange facility is generally reported to decrease in the order $NO_3^- > Cl^- > SO_4^{2-} > CO_3^{2-}$. Fatty acid anions, dicarboxylates and alkyl sulphates have, however, been incorporated by ion-exchange into nitrate-containing LDHs.(Meyn *et al.*, 1990)

Alternative methods of intercalation include the rehydration of calcined, amorphous LDH in the presence of an organic anion which can result in the formation of an LDH intercalation compound (Tagaya *et al.*, 1993; Chibwe and Jones, 1989), whilst the reaction between molten mono- (Carlino and Hudson, 1995) and dicarboxylic acids(Carlino and Hudson, 1994) and inorganic-intercalated LDHs results in microcrystalline, polyphasic reaction products thought to contain some residual unreacted LDH host plus organically-intercalated LDH.

pyroaurite) and synthetic phases for which the composition can be described by the general formula, $[M^{II}_{1-x}M^{III}_{x}(OH)_2]A_{x/m}.nH_2O$, where M^{II} is a divalent cation such as Ni, Mg, Cu or Zn and M^{III} is a trivalent cation such as Al, Cr, Fe, V or Ga. $A_{x/m}$ is an inorganic anion of charge *m* such as CO_3^{2-}, Cl^-, SO_4^{2-} or NO_3^-. The layered structure of is based on that of $Mg(OH)_2$, brucite, and consists of layers of M^{II} and M^{III} cations coordinated octahedrally by six oxygen atoms, as hydroxides. Metal-hydroxide layers are separated by charge-balancing counter-anions and water molecules loosely bound to the hydroxyl groups (Figure 1.6).

Compared with the cation exchange of smectites, the anion exchange reactions involving LDHs are not as facile because of their high selectivity to carbonate anions and large anion exchange capacity. The nature of the anion initially present in the starting LDH plays an important role in controlling the ease of exchange. In general, the more strongly bound anions are those with the smaller radii which result in a decreased spacing between the hydroxide layers (Miyata, 1983, Parker *et al.*, 1995). The exchange facility is generally reported to decrease in the order $NO_3>Cl>SO_4^{2-}>CO_3^{2-}$. Fatty acid anions, dicarboxylates and alkyl sulphates have, however, been incorporated by ion-exchange into nitrate-containing LDHs (Meyn *et al.*, 1990).

Alternative methods of intercalation include the rehydration of calcined, amorphous LDH in the presence of an organic anion which can result in the formation of an LDH intercalation compound (Tagaya *et al.*, 1993; Chibwe and Jones, 1989), whilst the reaction between molten mono- (Carlino and Hudson, 1995) and dicarboxylic acids(Carlino and Hudson, 1994) and inorganic-intercalated LDHs results in microcrystalline, polyphasic reaction products thought to contain some residual unreacted LDH host plus organically-intercalated LDH.

Owing, in part, to their anion exchange properties, certain LDH derivatives have been utilized as precursors for the preparation of industrial catalysts. The use of LDH intercalates with properties suitable for the *in situ* remediation of contaminated soils and waste cleanup has also been investigated. Another important feature of LDH compositions is their ionic/protonic conductivity, which makes them potentially useful for sensor and other device applications.

Layered Polymer Nanocomposites formed by Intercalation

The approaches outlined for the intercalation of small organic species within preformed lamellar inorganic solids have been employed for the intercalation of oligomeric and polymeric organic species, with varying degrees of success. Conventionally, organic-inorganic polymeric materials have been regarded as reinforcing systems to improve the mechanical, thermal and chemical resistance of the polymer. More recently, strategies to prepare materials with synergic or complementary behaviour due to interaction between the polymer and inorganic components at the molecular level have been developed. Single-phase nanocomposites may incorporate structural elements as diverse as polymer chains and two-dimensional lattices. The ability of layered inorganic solids to act as host lattices for organic compounds has been applied to obtain polymer intercalation materials exhibiting novel properties. For example, the choice of guest polymer and the electrical characteristics of the host lattice, i.e., insulating, ion-conducting, or

semiconducting, opens a way to new hybrid systems exhibiting behaviour of interest in the development of materials with suitable electrical and optoelectronic properties.

Ion-exchange of polymeric species for interlayer cations is possible although kinetically limited due to the slow diffusion associated with macromolecules. Poly(ethylene oxide)-silicate (Ruiz-Hitzky and Aranda, 1990; Aranda and Ruiz-Hitzky, 1992; Wu and Lerner, 1993) and poly[oxymethylene oligo(oxyethylene)]-silicate (Wu and Lerner, 1993) intercalation compounds have been prepared by virtue of the ability of oxyethylene groups to ligate interlayer cations giving rise to stable complexes, with the release of water molecules of solvation. Dissolution of the uncharged organic polymers in a suitable solvent system allows for polymer adsorption into montmorillonite and hectorite phyllosilicates at ambient temperatures. The poly(ethylene oxide)-silicate compounds formed showed conductivity values lower than conventional poly(ethylene oxide)-salt complexes, but demonstrated better thermal stability and reached good ion conductivity over a broader temperature range. Poly(ethylene oxide) intercalations in hydrated vanadium pentoxide have also been reported (Liu *et al.*, 1991; Ruiz-Hitzky *et al.*, 1992). Laminated intercalation compounds formed from chemically diverse conducting polymers and electrically active host lattices, often show interesting mixed ionic-electronic conducting properties which are under further investigation (for review, see Ruiz-Hitzky, 1993).

In situ polymerization of monomers confined within spaces of molecular dimensions has been studied as a means of synthesizing macromolecules of known stereospecificity. Often the polymerized macromolecules liberated from within host materials exhibit stereospecific sequences not observed in bulk or solution polymerized samples. For example, predominantly isotactic poly(methyl

methacrylate) is obtained from the polymerization of methyl methacrylate intercalated in the galleries of layered silicates (Blumstein *et al.*, 1968).

Recent research suggests that polymer/inorganic nanocomposites resulting from intercalative polymerization of suitable monomers in the galleries of layered solids can also exhibit unique mechanical, thermal and electrical properties. Generally, inorganic adsorption of the appropriate monomer followed by polymerization, which may be induced thermally or chemically, often via a redox process, results in the lamellar polymer/inorganic nanocomposite. Ion-exchange of interlayer metal cations of montmorillonite with 6-aminocaproic acid and induced thermal conversion of the polymer precursors has been shown to result in the formation of a "nylon-6"-intercalated nanocomposite (Kato *et al.*, 1979). Similar treatment of an ε-aminocaproic acid-α-ZrP intercalation compound facilitates the formation of "nylon-6" in the interlayer region (Ding *et al.*, 1995). Acrylamide-intercalated layered polysilicic acids have likewise been thermally converted to polyacrylamide-containing nanocomposites (Yanagisawa *et al.*, 1990) whilst the intercalation of 2,2'-bithiophene in vanadium pentoxide proceeds with *in situ* formation of polythiophene; the result of a redox reaction in which oxidative polymerization occurs with reduction of the V_2O_5 layers, generating V^{4+} centres (Kanatzidis *et al.*, 1990).

Poly(aniline)-(Challier and Slade, 1994) and poly(acrilonitrile)-intercalated (Sugahara *et al.*, 1988) LDHs were prepared by the *in situ* polymerization route. However, in these cases, neutral monomers are co-incorporated into layered double hydroxides already containing organic anions which limits the polymer content of the

product and the factors controlling polymerization and nature of the polymer formed on these occasions are not easily understood.

The aforementioned polymer-clay composites contain alternating inorganic and organic components to give the intercalated layered nanocomposites (Figure 1.7a). Another possibility is the generation of polymer-intercalated composites embedded in polymer matrices. A poly(ε-caprolactone)-silicate composite is prepared by stirring a Cr^{3+}-exchanged fluorohectorite in liquid monomer and initiating thermal polymerization in the presence of excess ε-caprolactone (Messersmith and Giannelis, 1993). Polymerization appears to proceed through acyl-oxygen bond cleavage, catalyzed by the interlayer Cr^{3+} ions and the resulting composite consists of polymer-intercalated silicate particles embedded in a poly(ε-caprolactone) matrix.

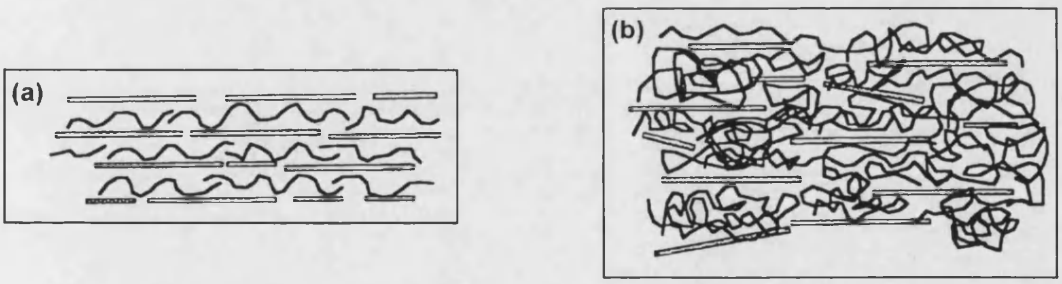

Figure 1.7 (a) Layered intercalated polymer nanocomposite. (b) Exfoliated polymer nanocomposite containing a dispersion of delaminated mineral layers in a continuous polymer matrix. (Redrawn from G. A. Ozin, 1992)

An alternative synthetic approach to intercalated polymer-silicate composites makes use of organically-modified layered silicates and polymer melts. Cation exchange of interlayer metal ions for alkylammonium ions renders the gallery region of silicate clays organophilic, and molten polymer can be intercalated directly into these spaces. Whereas a substantial part of the driving force for polymer intercalation from solution is the entropy gained by desorption of small molecules (e.g. water molecules), direct melt intercalation of polymers in organosilicates is primarily driven by enthalpic polymer-host interactions. By prudent choice of the alkylammonium cation, the interactions between the host layers and the intercalated polymer can be optimized to synthesize new organic-inorganic hybrids. Polystyrene, poly(dimethylsiloxane), poly(vinylidene fluoride), poly(ε-caprolactone) and poly(ethylene oxide) can be intercalated in alkylammonium-exchanged montmorillonite by this method (Vaia *et al.*, 1993). *In situ* polymerization of intercalated organic monomers within alkylammonium-exchanged silicates has also been employed to produce an intercalated polystyrene-clay nanocomposite (Kato *et al.*, 1981). The use of organically-modified silicates has expanded the range of polymers which can be intercalated into ceramic hosts, some of which being more desirable for technological purposes.

Intercalated polymer-clay nanocomposites of the type described above contain inorganic layers separated by the insertion of one or more molecular layers of polymer in the host galleries. The clay content of the intercalates is typically high and the properties usually resemble those of the ceramic host. In contrast, exfoliated polymer-clay nanocomposites have a low clay content, the (~10 Å thick) individual silicate layers are extensively separated and delaminated in a continuous polymer matrix

(Figure 1.7b), and the properties reflect those of the nano-confined polymer. The first hybrid polymer-clay composite with an exfoliated clay structure was a "nylon-6"-montmorillonite hybrid reported by Toyota researchers (Fukushima and Inagaki, 1987). This hybrid material exhibited greatly improved mechanical properties and thermal stability compared to previous composites. Exfoliated polyether-clay nanocomposites have also been prepared by the homopolymerization of an epoxy resin in the galleries of acidic alkylammonium ion exchanged forms of montmorillonite (Wang and Pinnavaia, 1994; Lan *et al.*, 1995) and a layered silicic acid (magadiite) (Wang *et al.*, 1996) with concomitant delamination of the inorganic sheets. Preliminary mechanical experiments carried out on monolithic forms of exfoliated epoxy-montmorillonite nanocomposites show higher tensile moduli than intercalated clay composites.(Lan *et al.*, 1995)

1.4 *Delamination/Relamination and Layer-by-Layer Assembly*

Under appropriate conditions, single-sheet colloids are obtained by chemical oxidation of lithiated metal disulphides. A colloidal suspension of single sheet MoS_2 will incorporate molecular organics, organometallic complexes or other complex cations upon restacking of the single sheets. More recently, the approach has been utilized for the incorporation of polyaniline into MoS_2 (Kanatzidis *et al.*, 1993). Single-phase polymer nanocomposites of poly(ethylene oxide) and poly[oxymethylene oligo(oxyethylene)] with MoS_2 have also been reported (Lemmon and Lerner, 1994). This synthetic approach for the synthesis of polymer

nanocomposites avoids the problem of slow diffusion kinetics of the macromolecule, and avoids polymer infusion into the inorganic lattice.

The swelling nature of the smectite clays and the ability to obtain dispersions of the clay in single-sheet exfoliated form, led to the adoption of the exfoliation/relamination approach to synthesize bulk preparations of polymer-clay nanocomposites. Oriakhi *et al.* (1995) recently reported the synthesis of polymer-montmorillonite nanocomposites synthesized from exfoliated montmorillonite and poly(pyrrole) or poly(thiophene) latex solutions. The reaction proceeds by adsorption of the solubilized polymer onto the colloidal clay particles, by a polymer latex-host colloid interaction, with subsequent flocculation. In clay-rich compositions restacking of the clay platelets results upon formation of the bulk nancomposite.

Dilute 'delaminated' dispersions of organically-modified alkylammonium-hectorite clay complexes can be prepared in organic solvents. Spreading of the colloidal suspension onto the surfaces of water and aqueous electrolyte solutions results in the formation of multilayer films, ranging between of 5-13 intercalated sheets of clay organocomplex platelets (Kotov *et al.*, 1994). Layer-by-layer transfer of the structurally well-defined organoclay platelets to solid substrates affords Langmuir-Blodgett-type structures with linearly variable thicknesses. This demonstration is one of many recently directed towards bridging the gap between molecular self-assembly of monolayer films and nanostructural materials; the goal being the stepwise preparation of thin films having order - i.e. regular modulation of composition - in the direction normal to the film substrate, with lattice spacings of nanometre dimensions. Other chemical approaches reported for the formation of multilayer thin films include the use of self-assembled monolayers in adsorption-activation schemes (Netzer and

Sagiv, 1983; Tilman *et al.*, 1989; Evans *et al.*, 1991; Cao *et al.*, 1992; Bell *et al.*, 1994); sequential adsorption of colloidal particles (e.g. silica, alumina, etc.) having opposite charge (Iler, 1966; Gaines, 1983); and sequential adsorption of organic polyelectrolytes having opposite charge (Lvov *et al.*, 1993; Cheung *et al.*, 1994; Ingersoll *et al.*, 1994).

One strategy for the stepwise formation of multilayered films produces ordered alternating stacks of a cationic organic polymer and anionic sheets of an inorganic mineral (Kleinfeld and Ferguson, 1994; Ferguson and Kleinfeld, 1995). In the first step a cationic polymer, poly(diallyldimethylammonium chloride) (PDDA), is adsorbed on a silicon surface. The second step involves the coulombic attraction of exfoliated anionic sheets of the smectite mineral, hectorite, to the preadsorbed cationic polymer. Since the silicate sheets bear a negative charge, only a single monolayer of 'tiles' can be placed onto the cationic polymer, and repulsion between the like charges on sheets minimizes regions of overlap unless there is an intervening layer of cationic polymer. In this way, growth in each adsorption cycle is limited. The single-sheets have a well-defined thickness (0.96 nm) and average diameters of 25-35 nm. This high aspect ratio minimizes defects in the layer, such as empty spaces at sheet edges, by providing sheet diameters large enough to cover empty spaces between the edges of adjacent platelets in the underlying layer. The multilayer films prepared in this way exhibit excellent structural ordering, can be synthesized quickly, and adapted for a wide range of component materials.

In an almost identical approach Mallouk and coworkers (Keller *et al.*, 1994; Kim *et al.*, 1997) utilized exfoliated sheets of anionic α-ZrP and oligomeric and polymeric cations to construct multilayer films held together by electrostatic

attractions (Figure 1.8). Exfoliation of the zirconium phosphate sheets is achieved by intercalation of sufficient amounts of tetra-*n*-butylammonium (TBA^+), with the formation of an indefinite suspension of single separated layers in water. Placing the suspension in contact with a protonated, amine-modified surface causes displacement of the TBA^+ on one side of the inorganic sheet with NH_3^+ which electrostatically anchors the sheet to the surface. The loosely held TBA^+ cations on the opposite side of the sheet are displaced in the next step by oligomeric/polymeric cationic molecules such as poly(allylamine)hydrochloride (PAH). As in the formation of hectorite-polyelectrolyte multilayer films, the adsorption reactions of both the lamellar polyanion and the polycation are self-limiting. Also demonstrated in this report was the ability to immobilize positively charged proteins (e.g. cytochrome *c*) and inorganic polycations such as $[Al_{13}O_4(OH)_{12}(H_2O)_{24}]^{7+}$, ($Al_{13}^{7+}$).

The beauty of both these approaches for the construction of multilayer films lies in their simplicity. Complex multilayer sequences can be grown quickly and the structural order at the monolayer level easily controlled. In spite of subtle differences, the picture that emerges from these studies is that a multilayer film prepared in this way is essentially a bulk analogue of an intercalation compound.

attractions (Figure 1.8). Exfoliation of the zirconium phosphate sheets is achieved by intercalation of sufficient amounts of tetra-*n*-butylammonium (TBA^+), with the formation of an indefinite suspension of single separated layers in water. Placing the suspension in contact with a protonated, amine-modified surface causes displacement of the TBA^+ on one side of the inorganic sheet with NH_3^+ which electrostatically anchors the sheet to the surface. The loosely held TBA^+ cations on the opposite side of the sheet are displaced in the next step by oligomeric/polymeric cationic molecules such as poly(allylamine)hydrochloride (PAH). As in the formation of hectorite-polyelectrolyte multilayer films, the adsorption reactions of both the lamellar polyanion and the polycation are self-limiting. Also demonstrated in this report was the ability to immobilize positively charged proteins (e.g. cytochrome *c*) and inorganic polycations such as $Al_{13}O_4(OH)_{12}(H_2O)_{24}^{7+}$ (Al_{13}^{7+}).

The beauty of both these approaches for the construction of multilayer films lies in their simplicity. Complex multilayer sequences can be grown quickly and the structural order at the monolayer level easily controlled. In spite of subtle differences, the picture that emerges from these studies is that a multilayer film prepared in this way is essentially a bulk analogue of an intercalation compound.

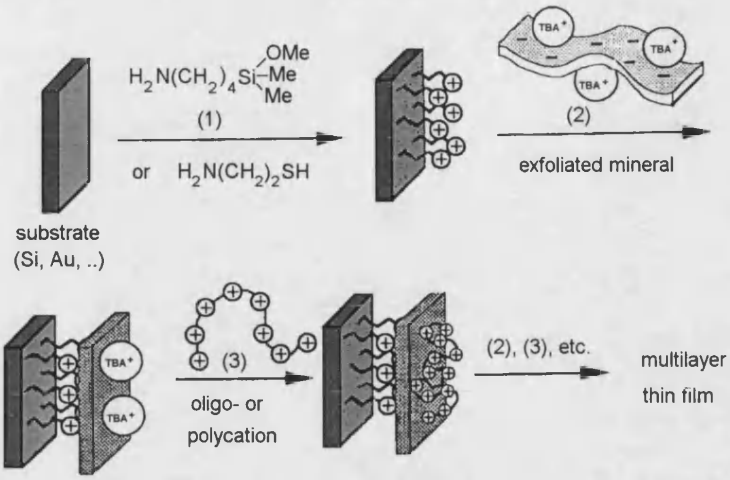

Figure 1.8 Reaction scheme for the sequential adsorption of inorganic two-dimensional polyanions and oligo- or polycations. Redrawn from Keller *et al.*, 1994.

Thus far there have been no reports of exfoliated cationic sheets of layered double hydroxides which would enable complementary multilayer films to be prepared from cationic mineral sheets and polyanions. The high charge density on the LDH sheets is believed to impede exfoliation.

1.5 *Direct Synthesis of Layered Nanocomposites (Inorganic Formation with Organic Intercalation)*

Organic molecules are commonly used as templates in zeolite syntheses, and small organic cations exist in the pores and channels of the resultant zeolite crystallites. In an early report by Barrer and Dicks (1967) synthetic alkylammonium hectorites and montmorillonites were crystallized from precursor reaction gels. This

was one of the first reports of the precipitation of the inorganic sheets of a silicate clay with concomitant intercalation of organic cations into the interlayer spaces.

Water-soluble porphyrins and metalloporphyrins were later employed as flat macrocycles during the hydrothermal crystallization of hectorite clay layers.(Carrado *et al.*, 1991) In this instance, the reaction of porphyrin, silica, $Mg(OH)_2$ (and LiF) in a clay synthesis gel resulted in formation of the layered clay phase intercalated with the organic molecules. This work by Carrado, suggested that the organics play a 'pseudo-templating' role in the formation of the clay structure, but recognised that crystallization mechanisms and organic-inorganic interactions in the systems were not well understood, and the need for further investigation was emphasized. Further work in this area utilized organic phthalocyanine dye molecules during hectorite synthesis with successful incorporation of organics into the clay galleries during clay crystallization (Carrado *et al.*, 1993). The incorporation of poly(vinyl alcohol) during hydrothermal crystallization of a synthetic hectorite clay has more recently been achieved (Carrado *et al.*, 1996)

A direct synthesis approach was concurrently being applied for the formation of organic-intercalated LDHs. The observed difficulties in achieving organic intercalations into preformed LDH structures by ion-exchange and swelling reactions highlighted the need for an alternative approach for nanocomposite synthesis. The direct synthesis method, whereby the inorganic LDH sheets are grown in the presence of the desired organic anion, quickly became the most successful for the preparation of well-ordered organo-intercalated LDH materials (Reichle, 1986; Drezdon, 1988). Organic species so far incorporated include terephthalate dianons (Drezdon; 1988), long-chain fatty acids (Raki *et al.*, 1995), organic dyes (Park *et al.*, 1990) and

phthalocyanine-type molecules (Carrado *et al.*, 1993, Bonnet *et al.*, 1996). Furthermore, the formation of polymer nanocomposites has been achieved using precipitation of the LDH sheets in the presence of a solution containing polyanionic species: poly(acrylate), poly(vinyl sulphonate) and poly(styrene sulphonate) (Oriakhi *et al.*, 1996). The polymer-LDH nanocomposites exhibit sufficiently expanded interlayer spacings to accommodate polymer bilayers and the microstructure of the nanocomposites are significantly altered in comparison with inorganic carbonate-intercalated LDHs.

Prior to the formation of polyanion-LDH nanocomposites a well-ordered layered nanocomposite derived from the LDH, $[Ca_2Al(OH)_6]^+[(OH).3H_2O]^-$, and the neutral polymer, poly(vinyl alcohol) (PVA), was prepared by a similar direct precipitation approach (Messersmith and Stupp, 1992; Messersmith and Stupp, 1995). The structure of the product consists of LDH layers separated by interlayers containing anions, PVA and water. A difference in the microstructural morphological appearance of the 'organoceramic' particles is again observed when compared to materials synthesized in the absence of PVA. Morphological differences could be attributed to a mechanism of polymer intercalation involving nucleation and growth of the calcium aluminate layers by the polymer as well as simple polymer adsorption. The term 'organoceramic' given by the researchers of these-types of materials, is in reference to the synthetic pathway which leads naturally to molecularly dispersed polymer molecules in the inorganic lattice. Analogies between the spontaneous self-assembly of the inorganic and organic phases resulting in the formation of the synthetic layered nanocomposites and the spontaneous aggregation of molecules into stable well-ordered structures in Nature can be made. The application of this approach

in the synthesis of new polymer/ceramic composites which combine the properties of the inorganic and organic components was also suggested (Messersmith and Stupp, 1995).

1.6 *Organically-functionalized Inorganic Solids*

Thus far, interactions between the inorganic and organic components of the hybrid materials have been weak electrostatic, Van der Waals, or hydrogen-bond interactions. The chemistry of layered materials was greatly extended after the observation that organic derivatives could be covalently attached to the phosphate groups of zirconium phosphates to give organophosphonates, $Zr(RPO_3)_2$ (Yamanaka, 1976; Alberti *et al.*, 1978). The synthesis of the organically-functionalized compounds is generally by a simple precipitation reaction in which a source of metal ions is mixed with a solution of organic phosphoric or phosphonic acids. Crystallization of a layered structure similar to that of α-zirconium phosphate results. Each layer consists of a plane of metal atoms linked together by phosphonate groups. The metal atoms are octahedrally coordinated by oxygen atoms, with the three oxygens of each phosphonate tetrahedron bound to three different metal atoms. This arrangement forces the organic groups to lie above and below the inorganic layer (Figure 1.9). A broad range of tetravalent metal phosphonates have been prepared, including $Zr(O_3PC_6H_5)_2$ and $Zr(O_3P(CH_2)_nX)_2$ (n = 1-5; X = H, Cl, SH, SEt, OH, COOH, SO_3H, OC_6H_5). Although zirconium phosphonates have been studied most extensively, isostructural complexes have also been made with the rest of the group 4 elements

(i.e. Ti, Hf). More recently, layered vanadium (IV) phosphonates, divalent metal (Mg, Mn, Zn, Ca, Cd) phosphonates, and trivalent metal (La, Sm, Ce, Fe) phosphonates have been synthesized.

The structure of the layered solid is determined by strong ionic interactions between the metal ions and the phosphate groups, and the organic groups which are "along for the ride" in the structure become geometrically disposed in predictable ways. Control over the structural design of these materials by modulation of both the ionic frameworks and organic constituents allows them to be tailored for purposes other than simple ion-exchange or catalysis. A much wider range of reactivity and device applications, which derive from their structural tunability, chemical and thermal stability, and morphological similarity to well-studied and useful phases are being investigated (For an excellent review of these materials and properties, see Cao *et al.*, 1992).

Analogous structures to multilayer Langmuir-Blodgett films can be constructed by a layer-by-layer assembly process of metal phosphonates. Simple exposure of a suitably prepared surface to solutions of appropriate metal salts and α,ω-bis(phosphonic acid) in alternation results in the growth of stable multilayered films; the stability deriving from the exceptionally strong affinity of metal ions for the RPO_3^{2-} group (Lee *et al.*, 1988a; Lee *et al.*, 1988b). The building blocks of the solid (e.g., zirconyl chloride and phosphonic acids) are individually soluble in water but together form salts that are quite insoluble even in strong mineral acids. Polar zirconium phosphate/phosphonate multilayer films containing oriented azo dye molecules as organic functionalities have been prepared using a modified approach, with a view to studying the second-order nonlinear optical effects of this system (Katz

(i.e. Ti, Hf). More recently, layered vanadium (IV) phosphonates, divalent metal (Mg, Mn, Zn, Ca, Cd) phosphonates, and trivalent metal (La, Sm, Ce, Fe) phosphonates have been synthesized.

The structure of the layered solid is determined by strong ionic interactions between the metal ions and the phosphate groups, and the organic groups which are "along for the ride" in the structure become geometrically disposed in predictable ways. Control over the structural design of these materials by modulation of both the ionic frameworks and organic constituents allows them to be tailored for purposes other than simple ion-exchange or catalysis. A much wider range of reactivity and device applications, which derive from their structural tunability, chemical and thermal stability, and morphological similarity to well-studied and useful phases are being investigated (For an excellent review of these materials and properties, see Cao *et al.*, 1992).

Analogous structures to multilayer Langmuir-Blodgett films can be constructed by a layer-by-layer assembly process of metal phosphonates. Simple exposure of a suitably prepared surface to solutions of appropriate metal salts and α,ω-bis(phosphonic acid) in alternation results in the growth of stable multilayered films; the stability deriving from the exceptionally strong affinity of metal ions for the RPO_3^{2-} group (Lee *et al.*, 1988a; Lee *et al.*, 1988b). The building blocks of the solid (e.g., zirconyl chloride and phosphonic acids) are individually soluble in water but together form salts that are quite insoluble even in strong mineral acids. Polar zirconium phosphate/phosphonate multilayer films containing oriented azo dye molecules as organic functionalities have been prepared using a modified approach, with a view to studying the second-order nonlinear optical effects of this system (Katz

(i.e. Ti, Hf, Ce, Th). More recently, layered vanadium (IV) phosphonates, divalent metal (Mg, Mn, Zn, Ca, Cd) phosphonates, and trivalent metal (La, Sm, Ce, Fe) phosphonates have been synthesized.

The structure of the layered solid is determined by strong ionic interactions between the metal ions and the phosphate groups, and the organic groups which are "along for the ride" in the structure become geometrically disposed in predictable ways. Control over the structural design of these materials by modulation of both the ionic frameworks and organic constituents allows them to be tailored for purposes other than simple ion-exchange or catalysis. A much wider range of reactivity and device applications, which derive from their structural tunability, chemical and thermal stability, and morphological similarity to well-studied and useful phases are being investigated (For an excellent review of these materials and properties, see Cao *et al.*, 1992).

Analogous structures to multilayer Langmuir-Blodgett films can be constructed by a layer-by-layer assembly process of metal phosphonates. Simple exposure of a suitably prepared surface to solutions of appropriate metal salts and α,ω-bis(phosphonic acid) in alternation results in the growth of stable multilayered films; the stability deriving from the exceptionally strong affinity of metal ions for the RPO_3^{2-} group (Lee *et al.*, 1988a; *Lee et al.*, 1988b). The building blocks of the solid (e.g., zirconyl chloride and phosphonic acids) are individually soluble in water but together form salts that are quite insoluble even in strong mineral acids. Polar zirconium phosphate/phosphonate multilayer films containing oriented azo dye molecules as organic functionalities have been prepared using a modified approach, with a view to studying the second-order nonlinear optical effects of this system (Katz

et al., 1991). These experiments illustrated the role of the inorganic superstructure in preserving the orientation of the organic groups from layer to layer in metal phosphonate films. This structure-directing property has also been used to control the juxtaposition of reactive organic groups within layers and prealignment of inorganic layer-bridging diacetylene monomers has been applied to optimize their reactivity towards polymerization [Cao and Mallouk, 1991 (Figure 1.10)].The product of this reaction is an example of a polymer-containing nanocomposite in which the organic polymer phase is covalently linked to the inorganic layers, whilst being molecularly dispersed within the layered structure. Bulk preparations of metal(IV) diphosphonates $M^{IV}(O_3P\text{-}R\text{-}PO_3)$ with specific interlayer porosities are obtained by simple tailoring of the size of the pillaring organic R group (Alberti *et al.*, 1993).

The metal phosphonates are members of a unique class of layered compounds in which organic groups are covalently bound to ordered inorganic structures during synthesis. Another group of materials possessing such connectivity are the layered organosilicon films prepared by sequential adsorption/chemical activation steps. In these multilayer systems the head groups of one organosiloxane layer are covalently bound to the tails of the next. Connectivity in the inorganic layers is provided by the formation of Si-O-Si bonds (Netzer and Sagiv, 1983; Tillman *et al.*, 1989).

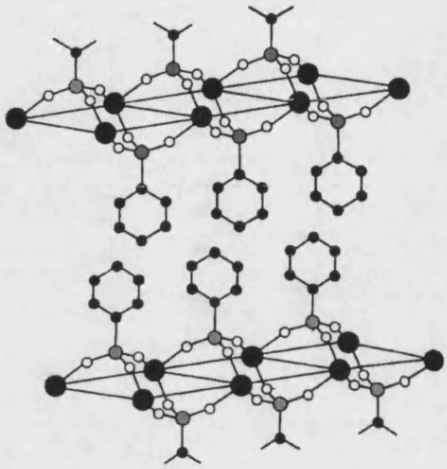

Figure 1.9 Idealized structure of zirconium bis(benzenephosphonate) (cf. Figure 1.5 α-ZrP). Redrawn from Alberti *et al.*, 1978

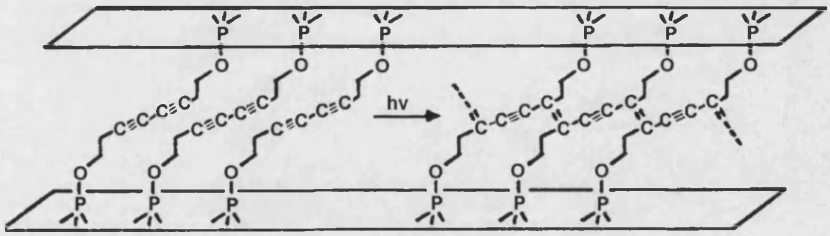

Figure 1.10 Schematic representation of diacetylene polymerization along the *c* axis in phosphate salts of the divalent metals Mn, Mg, and Zn. Redrawn from Cao *et al.*, 1992.

Recently reported have been organically-functionalized, hexagonally-ordered mesoporous silica structures (Burkett *et al.*, 1996, Fowler *et al.*, 1997). Synthesis of these materials employs long-chain surfactants which to a greater or lesser extent facilitate the assembly of the silica superstructure, but do not become an integral part of the inorganic framework. However, combining the usual templating strategy used for the preparation of the M41S-type molecular sieves with one based on the co-condensation of tetraalkoxysilanes [$Si(OR)_4$] and organically-functionalized trialkoxysilanes [$R'Si(OR)_3$], hexagonally-ordered, covalently-linked organo-silica-surfactant mesophases are co-assembled. Removal of the surfactant template post-synthesis affords organo-functionalized hybrid materials with ordered mesoporosity (Figure 1.11). A variety of organic moieties have been introduced into the structure by this approach. It is assumed that a considerable proportion of the organic functional groups occupy the pore regions of the hexagonal structure and that their reactivity may be exploitable for a variety of applications, including ion-sequestration, catalysis and organic reactions.

Recently reported have been organically-functionalized, hexagonally-ordered mesoporous silica structures (Burkett *et al.*, 1996, Fowler *et al.*, 1997). Synthesis of these materials employs long-chain surfactants which to a greater or lesser extent facilitate the assembly of the silica superstructure, but do not become an integral part of the inorganic framework. However, combining the usual templating strategy used for the preparation of the M41S-type molecular sieves with one based on the co-condensation of tetraalkoxysilanes ($SiOR_4$) and organically-functionalized trialkoxysilanes ($R'SiOR_3$), hexagonally-ordered, covalently-linked organo-silica-surfactant mesophases are co-assembled. Removal of the surfactant template post-synthesis affords organo-functionalized hybrid materials with ordered mesoporosity (Figure 1.11). A variety of organic moieties have been introduced into the structure by this approach. It is assumed that a considerable proportion of the organic functional groups occupy the pore regions of the hexagonal structure and that their reactivity may be exploitable for a variety of applications, including ion-sequestration, catalysis and organic reactions.

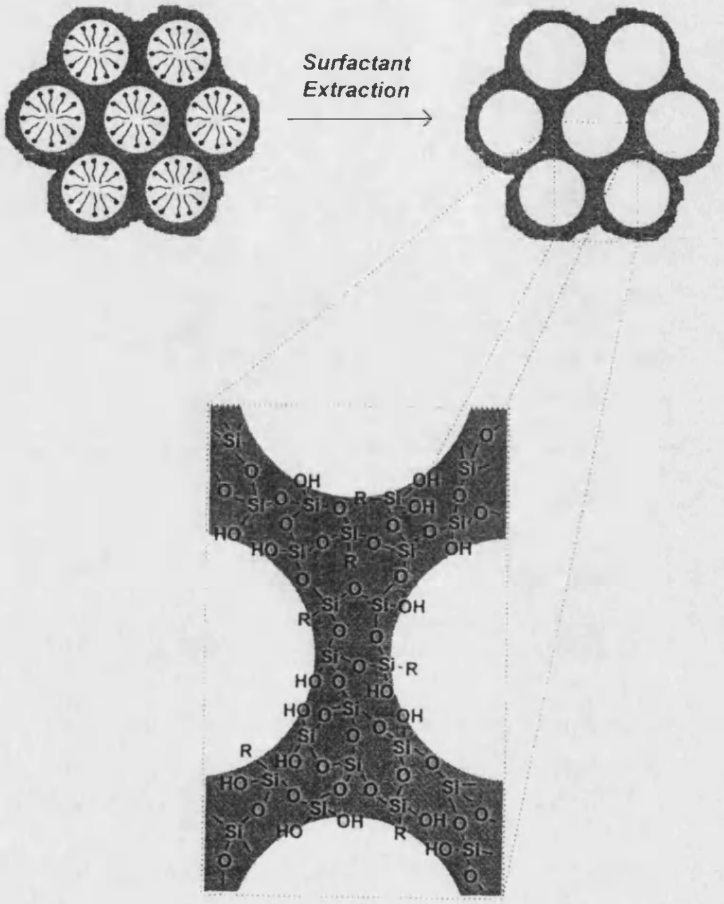

Figure 1.11 Representation of hexagonally-ordered organically-functionalized mesoporous silica formed by a co-condensation approach utilizing tetraalkoxysilanes and organotrialkoxysilanes (Burkett *et al.*, 1996; Fowler *et al.*, 1997). Reproduced courtesy of S. D. Sims, PhD Thesis, University of Bath, 1997.

Organotrialkoxysilanes, in place of tetraalkoxysilanes, have also been employed in the formation of layered smectite-like silicate structures. From reaction mixtures of appropriate compositions, layered organically-functionalized aluminosilicates (pyrophillite) and magnesium silicates (talc) are formed (Fukushima and Tani, 1995; Ukraincyzk *et al.*, 199;, Burkett *et al.*, 1997). The 2:1 silicate sheets are constructed from inorganic lamellae, each of which comprises a sheets of octahedrally-coordinated magnesium oxide/hydroxide (brucite) or aluminium oxide/hydroxide (gibbsite) sheets overlaid on both sides with a tetrahedrally-coordinated silicate layer. Utilization of organotrialkoxysilanes as the silicon source results in the formation of the 2:1 smectite-like sheets with organic functionalities directly-bonded via Si-C bonds to the inorganic layers and occupying the interlayer regions (Figure 1.12). Formation of these layered inorganic-organic nanocomposites most probably occurs by a cooperative synthesis, with the limited coordination of the organosiloxane units, hydrophobicity of the organic moieties and amphiphilic nature of the brucite-/gibbsite-organosiloxane unit each playing a part in facilitating formation of the lamellar architecture. As is the case of the modified MCM-41 materials, it is envisaged that the properties of the organic functionalities may offer a variety of applications for these organic-inorganic hybrids.

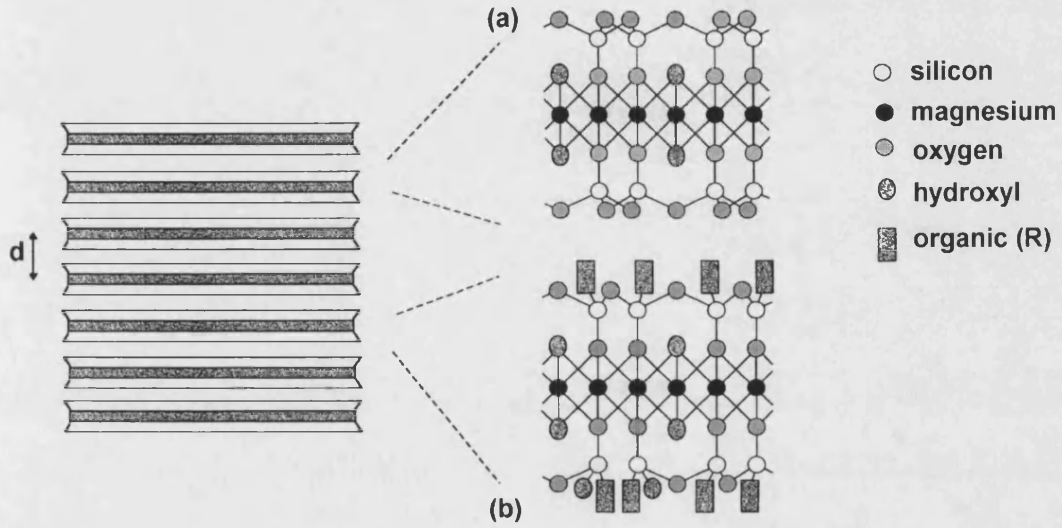

Figure 1.12 Schematic of the idealized structural arrangement of (a) the 2:1 trioctahedral phyllosilicate, talc [$Mg_6Si_8O_{20}(OH)_4$] and (b) magnesium (organo)phyllosilicate [$Mg_6Si_8R_8O_{16-x/2}(OH)_{4+x}$, where x is 2 in this example]. Redrawn from Burkett *et al.*, 1997.

A greater number of reports have been made on the post-synthesis functionalization of silicate-containing structures (Ruiz-Hitzky and Rojo, 1980). Typically, a grafting process is employed whereby organotrialkoxysilanes undergo hydrolysis and condensation with Si-OH groups on exposed surfaces (e.g. pore surfaces) of silicate structures to produce stable organic derivatives. Modification of surface Si-OH groups within the mesopores of an hexagonally-ordered silica recently resulted in a porous material with channels lined with thiol-containing functionalities (Feng *et al.*, 1997). The chemically modified structure exhibits good sequestration of mercury and other heavy metals which presents a possible application in pollution control. The grafting process has also been applied for chemical modification of layered silicates by reaction with functionalized organotrialkoxysilanes (Krysztafkiewicz and Domka, 1997).

The chemical derivatization of ordered inorganic structures during or post synthesis allows for tailoring of the materials for specific functions. New synthetic design strategies aimed at the fabrication of molecularly engineered layered structures (MELS) [Alberti *et al.*, 1993], have the potential to produce materials formed from covalently-linked organic and inorganic components and possessing novel properties, which may lend themselves to applications in hitherto unexplored areas.

1.7 *Overview of Thesis*

The previous sections have outlined some of the recent conceptual approaches and design strategies which have been utilized for the fabrication of ordered

composite materials. The work presented in this thesis focuses on the preparation and investigation into two lamellar nanocomposite systems; namely organically-intercalated layered double hydroxides (Figure 1.6) and organically-functionalized phyllosilicates (Figure 1.12).

Central to the inorganic structural framework of both these systems is the brucitic, $Mg(OH)_2$,edge-shared octahedral sheet. The naturally-occurring brucite mineral consists of an hexagonally close-packed system of hydroxide ions with Mg^{2+} ions occupying all the octahedral holes between alternate pairs of the c.p. layers [analogous to the (*C*6), CdI_2 structure (Figure 1.13)]. The stacked sheets of octahedrons of $Mg(OH)_2$ are uncharged, with the result that adjacent layers are held together by weak residual bonds and are easily cleaved.

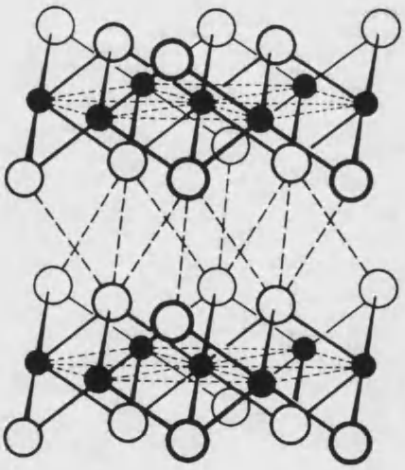

Figure 1.13 Portions of two layers of the (*C6*) CdI_2 structure (analogous to brucite). Black circles represent metal atoms.

In layered double hydroxides, the brucite mineral acts as a framework for metal cation substitution, and part of the Mg^{2+} in a neutral $Mg(OH)_2$ layer is replaced by Al^{3+} (Fe^{3+} or Cr^{3+}), rendering the layer positively charged. Negatively charged anions, $A^{x/m}$, (and water) are incorporated in the interlayer region between adjacent inorganic sheets. Magnesium-aluminium containing layered double hydroxides, $[Mg_{1-x}Al_x(OH)_2]A^{x/m} \cdot nH_2O$, have been synthesized with magnesium/aluminium ratios between 1 and 5, and thus significant variation in layer charge can be obtained (Kooli *et al.*, 1996).

The intercalation chemistry of layered double hydroxides has been previously discussed, and particularly, that involving the incorporation of organic anions in the interlayer spaces. In this thesis, novel organically-intercalated Mg-Al-LDHs are prepared directly *via* coprecipitation involving simultaneous formation of the inorganic layers and intercalation of the anionic species. (Bio)organic amino acid anions and a related, industrially-important polyamino acid derivative, polyaspartate, are intercalated during synthesis resulting in lamellar (bio)organic/inorganic hybrids in which the organic anions are retained between the layers by electrostatic attraction. It is hoped that these bioinorganic hybrid materials will have uses as organoclays with bioactive, biocompatible and biodegradable properties. Furthermore, the *in situ* polycondensation of intercalated aspartate precursors within the gallery region to generate the polymer-containing nanocomposite and the direct intercalation of amphiphilic anionic surfactant-type molecules, with varying hydrophobic chain lengths is investigated.

A second objective of this thesis is to pursue further the synthesis of tailored nanocomposites and, in particular, organically-functionalized 2:1 trioctahedral

phyllosilicates (Figure 1.12). The inorganic structural framework of these hybrid materials is directly related to that of inorganic talc and within this structural arrangement neutral brucite $Mg(OH)_2$ sheets are found sandwiched between sheets of silica tetrahedra; the tetrahedral sheets being generated through the linking of six-membered hexagonal silicate rings in a plane. The generation of the 2:1 (organo)phyllosilicate sheet structure is believed to proceed *via* the condensation of tetrahedral silicate layers on preexisting brucitic sheets and in this mechanism the brucite layers present a templating framework (Fukushima and Tani, 1995; Burkett *et al.*, 1997).

A one-step procedure involving the co-precipitation of the magnesium and organosilicon components to form the 2:1 smectite-like structure is employed to generate a host of organically-functionalized hybrids. The organotrialkoxysilanes used in the synthesis are chosen to contain functional organic substituents, the reactivity, metal-complexing/binding behaviour and hydrophobicity/hydrophilicity of which will impart novel properties to the interlayer regions and be investigated post-synthesis of the layered system. Attempts are also made to generate porosity in the layered structure *via* the incorporation of layer-bridging organic functionalities.

phyllosilicates (Figure 1.12). The inorganic structural framework of these hybrid materials is directly related to that of inorganic talc and within this structural arrangement neutral brucite $Mg(OH)_2$ sheets are found sandwiched between sheets of silica tetrahedra; the tetrahedral sheets being generated through the linking of six-membered hexagonal silicate rings in a plane. The generation of the 2:1 (organo)phyllosilicate sheet structure is believed to be proceed via the condensation of tetrahedral silicate layers on preexisting brucitic sheets and in this mechanism the brucite layers present a templating framework (Fukushima and Tani, 1995; Burkett *et al.*, 1997).

A one-step procedure involving the co-precipitation of the magnesium and organosilicon components to form the 2:1 smectite-like structure is employed to generate a host of organically-functionalized hybrids. The organotrialkoxysilanes used in the synthesis are chosen to contain functional organic substituents, the reactivity, metal-complexing/binding behaviour and hydrophobicity/hydrophilicity of which will impart novel properties to the interlayer regions and be investigated post-synthesis of the layered system. Attempts are also made to generate porosity in the layered structure *via* the incorporation of layer-bridging organic functionalities.

GENERAL METHODS

Water purification

An Aquatron A4D commercial still with dual boilers was used to produce doubly-distilled water from the local mains supply. Further treatment involved feeding the water through a Purite Standard Stillplus™ system containing a 0.2 μm activated carbon bacterial filter and a mixed bed ion-exchange column. The final output from the combined treatment resulted in water of high quality with a typical conductivity of < 0.5 μS cm^{-1}.

pH measurement

pH measurements were performed using Radiometer PHM 84 and PHM 82 Research meters and a Kent Industrial EIL 7045/46 digital pH meter. Combination pH electrodes were used with each machine. Before use, each machine was calibrated using standard buffers covering the pH range of interest [BDH phthalate pH 4.0; Fisons phosphate pH 7.0; BDH borate pH 10.0)].

C,H,N Microanalysis

Carbon, hydrogen and nitrogen analysis was carried out using a Carlo Erba 1106 elemental analyzer. Typically, 5 mg of solid sample was combusted at 1020 °C in oxygen alongside a reference. Products of combustion (e.g., carbon dioxide, water and nitrogen-containing oxides) were passed down a Cr_2O_3 column containing silver-coated mixed-valance cobalt oxide to remove halogens and sulphur. Heated copper was used to remove any remaining oxygen and further reduced nitrogen-containing oxides to nitrogen gas. The outflow from the column was passed through a gas chromatograph utilizing He as the carrier gas.

Atomic absorption spectroscopy (A.A.)

Solutions were prepared in volumetric flasks by dissolution of accurately weighed amounts of sample in dilute nitric acid. Analysis of solutions was performed using a VarianAA-275 spectrophotometer. The light source was a hollow cathode lamp containing the respective element under investigation. Vaporisation of the sample was carried out in air/acetylene or nitrous oxide/acetylene mixtures and the absorbance was detected using an array of photoelectric cells. Results were compared alongside standard elemental solutions.

Fourier transform infrared spectroscopy (FTIR)

Mixtures of ground sample and IR-grade potassium bromide (Aldrich) - approximately 1% by weight of sample - were pressed to form pellets 12 mm in diameter and 1-2 mm thick. Using a Nicolet 510P Fourier transform infrared spectrophotometer with an attached computer interface samples were routinely scanned from 4000 - 400 cm^{-1}, with a resolution of 1 cm^{-1}. Precise locations of absorption peaks were determined using a Nicolet software package.

Transmission electron microscopy (TEM)

Bare 3 mm copper or nickel grids to be used in transmission electron microscopy were coated on one side with a film of polymer (Formvar) and sputtered with carbon. Dilute dispersions of samples to be analyzed were prepared under sonication in ethanol or water and loaded onto the copper or nickel grids. Samples were examined using either a JEOL 1200EX or JEOL 2000FX transmission electron microscope operating at 120 kV and 200 kV respectively. Alignment of the microscopes was performed before and after insertion of the sample in order to optimize the performance at the chosen accelerating voltage. Electron micrographs were routinely taken over a range of magnification values. For both microscopes routine magnification of up to ×200k could be carried out with an absolute limit in point to point resolution of better than 5 Å; with the JEOL 2000FX microscope providing better image resolution at higher magnification values.

Scanning electron microscopy (SEM)

High resolution microscopy was performed using a JEOL 1200EX transmission electron microscope with an attached scanning imaging device (ASID) and operating in scanning mode. Pre-alignment of the microscope in transmission and scanning mode was necessary before insertion of the sample. This set-up allowed for magnification up to ×100k with a typical resolution of 1 - 2 nm. Samples for examination were loaded onto brass plate specimen holders as dilute dispersions in ethanol or water and sputtered with a coating of gold (applied using an Edwards S150B sputter coater) before mounting in the electron microscope. Gold coating was necessary to avoid charging of the sample during scanning.

Energy dispersive X-ray analysis (EDXA)

Energy dispersive X-ray analysis provided a qualitative and semi-quantitative elemental analysis of samples. Analysis was carried out using a JEOL 2000FX transmission electron microscope equipped with a Link lithium-drifted silicon-type EDXA detector cooled with liquid nitrogen. Analysis was performed on samples loaded as dispersions onto copper or nickel TEM-type grids. A Link AN10000 X-ray microanalyser system was used to accumulate and process the data.

X-ray diffraction (XRD)

Powder X-ray diffraction (PXRD) was performed using a Phillips PW 1730 diffractometer with a 4 kW X-ray generator and 2 kW copper target tube, utilizing CuKα radiation ($\lambda(\alpha_1)$ = 1.54050 Å, $\lambda(\alpha_2)$ = 1.54434 Å, weighted mean = 1.5418 Å). The diffractometer was fitted with a PW 1820/00 computer-controlled vertical goniometer capable of scanning 2θ values of 4 - 185° and a PW 1711/10 Xe proportional counter with graphite monochromator. Diffraction patterns were plotted as intensity *v.* 2θ, and peak fitting was performed utilizing a pattern treatment program.The Bragg equation, $n\lambda = 2d \sin\theta$, illustrates the simple relationship between 2θ and the *d*-spacing.

The JPCDS database was also utilized to access diffraction data for known compounds.

^{13}C and ^{29}Si magic angle spinning nuclear magnetic resonance spectroscopy (MAS NMR)

Solid state NMR experiments were performed using a Varian Unityplus-300 MHz spectrometer at the University of Durham using the EPSRC NMR service. ^{13}C and ^{29}Si measurements were performed using a Doty Scientific MAS probe with a zirconia rotor of outer diameter of 7 mm and Kel-F end caps. Referencing was to an external sample of tetramethylsilane and ambient temperatures were employed for all experiments. ^{13}C cross-polarization (CP) MAS NMR spectra were obtained at 75.4

MHz with magic angle spinning (MAS) speeds of 4 - 5 kHz; the magic angle being 54.74°. ^{29}Si MAS NMR spectra were obtained at 59.6 MHz with a MAS speed of ~ 4.5 kHz.

^{13}C NMR spectra were acquired using cross polarization with relaxation delays of 1 or 2 s and cross polarization times of 1 ms. Non-quaternary suppression (NQS) was utilized in some cases which allowed for the differentiation of carbons with directly bonded protons from those carbons without protons in the CP MAS spectrum. In the NQS experiment the decoupler was turned off for a short time (typically 40 μs) before the acquisition was started. In the 'dephasing' delay any carbon strongly interacting with protons was 'dephased' and lost from the eventual spectrum (see Appendix for more details).

^{29}Si MAS NMR data was acquired using single pulse excitation with direct polarization (DP) applied at 90° with a relaxation delay of 300 s. Deconvolution of the spectra using Varian software provided quantitative data on the contributions from individual silicon species.

Thermogravimetric analysis (TGA)

Thermogravimetric analysis was carried out at English China Clays International, St. Austell, using either a Perkin-Elmer Delta Series 7 thermogravimetric analyser or a Netzsch combined TGA/DSC (differential scanning calorimetry) analyser. Experiments were typically run on powdered samples between ambient and 600 °C (Perkin-Elmer) or 1000 °C (Netzsch), at a ramp rate of 5 °C min^{-1}

under flowing nitrogen. Differential plots of the TGA data (DTG) were also recorded when using the Netzsch instrument.

CHAPTER 3

SYNTHESIS AND CHARACTERIZATION OF ORGANIC ANION-INTERCALATED MG-AL-LAYERED DOUBLE HYDROXIDES

SYNTHESIS AND CHARACTERIZATION OF ORGANIC ANION-INTERCALATED MG-AL-LAYERED DOUBLE HYDROXIDES

3.1 *Introduction*

Layered double hydroxides form a complementary class of minerals to the more common smectite clays. Residing on the brucite-like $Mg^{II}(OH)_2$ inorganic sheets are formal positive charges resulting from the partial substitution of framework divalent cations with trivalent metal ions. Overall electrical neutrality is maintained by the presence of anions (and water [Reichle, 1986]) within the gallery spaces between layers. The general composition of these lamellar materials can be represented as $[M^{II}_{1-x}M^{III}_x(OH)_2]^{x+}.[(A^{m-})_{x/m}.nH_2O]$, where M^{II} is a divalent cation such as Mg, Ni, Cu, Zn, M^{III} is a trivalent metal ion such as Al, Cr, Fe, V, or Ga, and $A_{x/m}$ an anion of charge m such as CO_3^{2-}, Cl^-, SO_4^{2-} or NO_3^-. Naturally occurring hydrotalcite has a representative formula unit of $[Mg_6Al_2(OH)_{16}][CO_3].4H_2O$, although the values of x can vary between 0.16 and 0.45 in synthetic derivatives. These inorganic layered materials are often termed 'anionic clays' complementing the more conventional 'cationic smectite clays' and related lamellar compounds (e.g. metal chalcogenides and phosphates and phosphonates of tetravalent metals). As mentioned earlier, interest in clays, inorganic lamellar materials and other intercalation materials stems from their application in host-guest chemistry, and potential utilization in catalysis and ion-exchange, as hosts for optical materials, and more recently as

SYNTHESIS AND CHARACTERIZATION OF ORGANIC ANION-INTERCALATED MG-AL-LAYERED DOUBLE HYDROXIDES

3.1 *Introduction*

Layered double hydroxides form a complementary class of minerals to the more common smectite clays. Residing on the brucite-like $Mg^{II}(OH)_2$ inorganic sheets are formal positive charges resulting from the partial substitution of framework divalent cations with trivalent metal ions. Overall electrical neutrality is maintained by the presence of anions (and water [Reichle, 1986]) within the gallery spaces between layers. The general composition of these lamellar materials can be represented as $[M^{II}_{1-x}M^{III}_x(OH)_2]^{x+}.[(A^{m-})_{x/m}.nH_2O]$, where M^{II} is a divalent cation such as Mg, Ni, Cu, Zn, M^{III} is a trivalent metal ion such as Al, Cr, Fe, V, or Ga, and $A_{x/m}$ an anion of charge m such as CO_3^{2-}, Cl^-, SO_4^{2-} or NO^{3-}. Naturally occurring hydrotalcite has a representative formula unit of $[Mg_6Al_2(OH)_{16}][CO_3].4H_2O$, although the values of x can vary between 0.16 and 0.45 in synthetic derivatives. These inorganic layered materials are often termed 'anionic clays' complementing the more conventional 'cationic smectite clays' and related lamellar compounds (e.g. metal chalcogenides and phosphates and phosphonates of tetravalent metals). As mentioned earlier, interest in clays, inorganic lamellar materials and other intercalation materials stems from their application in host-guest chemistry, and potential utilization in catalysis and ion-exchange, as hosts for optical materials, and more recently as

important components in the fabrication of new ceramic-based materials and nanocomposites (Cavani *et al.*, 1991).

The anion-exchange properties of LDHs can be exploited for the post-synthesis incorporation of small, negatively-charged organic molecules into the gallery spaces between the inorganic layers (Meyn *et al.*, 1990). However, the ion-exchange of small inorganic anions for organic ions is by no means as facile as the analogous process for the smectite clays, in which interlamellar cations are readily displaced by organoammonium cations and other positively-charged species. Of all the charged lamellar materials the charge density on the brucitic LDH sheets is the greatest, resulting in a tenacious electrostatic attraction for the gallery ions and subsequently making exchange difficult. Limited success has also been achieved by reconstitution of calcined, amorphous LDH in the presence of organic anions (Chibwe and Jones, 1989; Tagaya *et al.*, 1993). A recently developed direct synthesis approach has been more successful for the preparation of well-ordered LDH materials containing intercalated organic anions such as terephthalate (Drezdon, 1988), long-chain fatty acids (Raki *et al.*, 1995), organic dyes (Park *et al.*, 1990) and phthalocyanine-type molecules (Carrado *et al.*, 1993; Bonnet *et al.*, 1996).

The fabrication of LDH nanocomposites with polymeric guest molecules has afforded limited success primarily because the methods generally employed for polymer incorporation in other layered inorganic host materials (Krishnamoorti *et al.*, 1996, and references therein) have not been applicable. Most notably, the exfoliation/adsorption approach (Bissessur *et al.*, 1993; Wu and Lerner, 1993; Lemmon and Lerner, 1994), widely utilized for the fabrication of polymer-clay hybrids of the smectite- and MS_2-type, is not a viable synthetic route for polymer-

LDH nanocomposites The high charge density on the LDH layers prevents exfoliation of the sheets.

To date, poly(aniline)-LDH (Challier and Slade, 1994) and poly(acetonitrile)-LDH (Sugahara *et al.*, 1988) nanocomposites have been prepared by *in situ* polymerization of pre-intercalated monomers. For the *in situ* conversion of intercalated aniline molecules to polyaniline the oxidant character of Cu(II) within the Cu-Cr-metal hydroxyl sheets was used to induce oxidative polymerization of aniline.

A direct synthesis approach, similar to that used for the incorporation of small organic molecules, has been used to intercalate poly(vinyl alcohol) into a Ca-Al-derived-LDH with the formation of a well-ordered layered nanocomposite (Messersmith and Stupp, 1992; Messersmith and Stupp, 1995). More recently, nanostructural materials based on $Mg_4Al_2(OH)_{12}CO_3.nH_2O$ and related LDH sheet structures, and the ionomers poly(acrylic acid), poly(vinyl sulphonate) and poly(styrene sulphonate), have been directly synthesized by coprecipitation from solutions containing the desired polymer as co-solute (Oriakhi *et al.*, 1996).

This chapter concerns itself mainly with the unprecedented synthesis of Mg-Al-layered double hydroxides intercalated with amino acids, aspartic and glutamic acid, and a related polyamino acid, poly(α,β-aspartate) (Table 3.1). The bioinorganic hybrid materials are prepared by direct synthesis involving incorporation of the organic molecules from basic solution during the concomitant precipitation of the metal salts and formation of the inorganic brucite-like framework. *In situ* thermal polycondensation of pre-intercalated aspartate monomers and a non-thermal chemical coupling reaction are also presented as two alternative methods for the preparation of a polyaspartate-containing nanocomposite.

LDH nanocomposites The high charge density on the LDH layers prevents exfoliation of the sheets.

To date, poly(aniline)-LDH (Challier and Slade, 1994) and poly(acetontrile)-LDH (Sugahara *et al.*, 1988) nanocomposites have been prepared by *in situ* polymerization of pre-intercalated monomers. For the *in situ* conversion of intercalated aniline molecules to polyaniline the oxidant character of Cu(II) within the Cu-Cr-metal hydroxyl sheets was used to induce oxidative polymerization of aniline.

A direct synthesis approach, similar to that used for the incorporation of small organic molecules, has been used to intercalate poly(vinyl alcohol) into a Ca-Al-derived-LDH with the formation of a well-ordered layered nanocomposite (Messersmith and Stupp, 1992; Messersmith and Stupp, 1995). More recently, nanostructural materials based on $Mg_4Al_2(OH)_{12}CO_3.nH_2O$ and related LDH sheet structures, and the ionomers poly(acrylic acid), poly(vinyl sulphonate) and poly(styrene sulphonate), have been directly synthesized by coprecipitation from solutions containing the desired polymer as co-solute (Oriakhi *et al.*, 1996).

This chapter concerns itself mainly with the unprecedented synthesis of Mg-Al-layered double hydroxides intercalated with amino acids, aspartic and glutamic acid, and a related polyamino acid, poly(α,β-aspartate) (Table 3.1). The bioinorganic hybrid materials are prepared by direct synthesis involving incorporation of the organic molecules from basic solution during the concomitant precipitation of the metal salts and formation of the inorganic brucite-like framework. *In situ* thermal polycondensation of pre-intercalated aspartate monomers and a non-thermal chemical coupling reaction are also presented as two alternative methods for the preparation of a polyaspartate-containing nanocomposite.

In addition, three previously reported samples, terephthalate-LDH, dodecylsulphate-LDH and a control hydrotalcite-like Mg-Al-CO_3-LDH are prepared and characterized. The results of these samples will not be discussed in great detail but will be used for primarily for comparative purposes.

The chapter will also present the results of a study concerned with intercalated Mg-Al-LDHs containing 5-(alkoxy)isophthalate organic dianions (Table 3.1). These organic molecules are of interest since they possess the carboxylic acid arrangement of isophthalate molecules and the fatty acid chain of the alkylsulphates. It is of interest to investigate the intercalation behaviour of these amphiphiles with varying alkoxy-chain lengths.

3.2 *Experimental*

Materials

All inorganic reagents were obtained from Aldrich Chemical Co. of analytical grade and used without further purification. Terephthalic acid, sodium dodecylsulphate, D,L-aspartic acid, D-glutamic acid, and EDC were obtained from Aldrich Chemical Co.. A solution of sodium poly(α,β-aspartate) (27 % w/w in H_2O; M_r~ 7100; *ca.* 62 aspartate residues per molecule) was obtained as a gift from BP International. Isophthalic acid derivatives were provided by Suresh Valiyaveettil formerly of the Max-Planck Institut für Polymerforschung, Mainz, Germany. Doubly-

distilled, deionized water was used throughout the experiments (Chapter 2: ***General Methods***).

Table 3.1 Structures of organic anionic species intercalated in Mg-Al-LDHs.

Anionic structure	Name
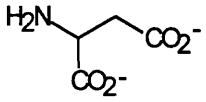	Aspartate
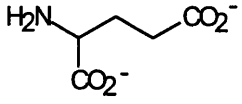	Glutamate
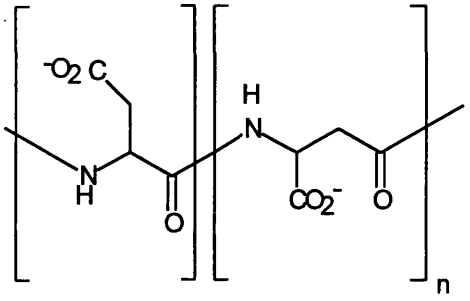	Poly(α,β-aspartate)
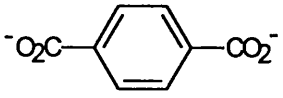	Terephthalate
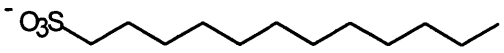	Dodecylsulphate
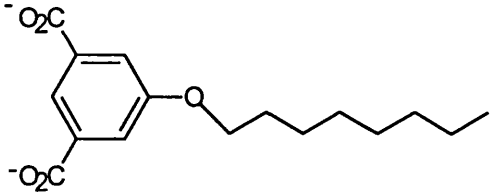	5-(Octyloxy)isophthalate

Preparation of carbonate-containing layered double hydroxide

A layered magnesium/aluminium double hydroxide containing intercalated carbonate (Mg-Al-CO_3-LDH) was prepared using a standard aqueous precipitation and thermal crystallization method (Reichle, 1985). Typically, a solution containing $Mg(NO_3)_2 \cdot 6H_2O$ (0.58 g, 2.3 mmol) and $Al(NO_3)_3 \cdot 9H_2O$ (0.43 g, 1.1 mmol) in 18 ml d.d. water was added dropwise over a one hour period at room temperature to a vigorously stirred solution containing NaOH (0.32 g, 8.0 mmol, pH=12) and Na_2CO_3 (0.24 g, 2.3 mmol) in 10 ml d.d. H_2O. During addition no change in pH was observed. The resultant gel was aged with stirring at 65 °C for 24 h. The white solid was isolated by filtration under suction, washed with copious water (100 ml) and dried in a vacuum oven at 70 °C for 24 h. Elemental analysis gave 2.5% C, 4.0% H, 0.2% N, 62.0% O, 20.0% Mg and 11.3% Al, from which a chemical composition of $Mg_{1.15}Al_{0.4}(OH)_{3.08}[CO_3]_{0.2}[NO_3]_{0.01} \cdot 0.5H_2O$ and a Mg/Al ratio of 2.8 was calculated.

Preparation of terephthalate- and dodecylsulphate-containing LDHs

Preparation of terephthalate and dodecylsulphate-containing LDHs followed the direct synthesis approach of Drezdon (1988). Terephthalic acid (19.01 g, 0.11 mmol) or sodium dodecylsulphate (31.79 g, 0.11 mmol) were dissolved in a basic solution of NaOH (41.0 g, 1.03 mmol, in 42 ml d.d. H_2O). A mixed metal nitrate solution containing $Mg(NO_3)_2 \cdot 6H_2O$ (58.6 g, 0.23 mmol) and $Al(NO_3)_3 \cdot 9H_2O$ (42.9 g, 0.11 mmol) was added dropwise at room temperature to the basic solution under rapid

stirring and the resultant gel-like suspension allowed to age with stirring at 75 °C for 24 h. The products were isolated by filtration under suction, washed with copious water (250 ml) and dried in air at 70 °C for 12 h.

Preparation of aspartate- and glutamate-containing LDHs

Aspartate and glutamate-LDHs were prepared by reacting a mixed metal nitrate solution with a basic solution containing the organic dianion (Drezdon, 1988). The free organic acid (D,L-aspartic acid, D-glutamic acid; 1.1 mmol) was dissolved in a freshly prepared solution of NaOH (10 mmol in 10 ml d.d. H_2O) and the resulting solution stirred under nitrogen. A solution containing $Mg(NO_3)_2 \cdot 6H_2O$ (0.58 g, 2.3 mmol) and $Al(NO_3)_3 \cdot 9H_2O$ (0.43 g, 1.1 mmol) in 18 ml d.d. H_2O was deaerated with nitrogen before slow addition to the organic anion-containing solution. The pH of the reaction mixture remained fairly constant at 11.5-12 during the addition. The resulting precipitate was aged at 65 °C for 24 h, filtered in air under suction and dried at 70 °C under vacuum for a further 24 h. Elemental analysis gave 6.8% C, 4.3% H, 3.5% N, 57.7% O, 17.3% Mg and 10.4% Al for the aspartate-containing LDH, and 7.1% C, 4.7% H, 2.9% N, 59.4% O, 17.0% Mg and 9.3% Al for glutamate-LDH. Respective chemical compositions (and Mg/Al ratios) based on these values were calculated as $Mg_{0.71}Al_{0.38}(OH)_{2.18}[Asp]_{0.14}[NO_3]_{0.10} \cdot 0.6H_2O$ where [Asp] = aspartate dianion (Mg/Al = 1.9), and $Mg_{0.70}Al_{0.34}(OH)_{2.05}[Glu]_{0.12}[NO_3]_{0.10} \cdot 0.9H_2O$ where [Glu] = glutamate dianion (Mg/Al = 1.8).

Preparation of polyaspartate-containing LDHs

The preparation of polyaspartate-intercalated LDHs was accomplished by three synthetic procedures: (a) via direct intercalation of the preformed polymer present as co-solute in the basic reaction solution, (b) by *in situ* thermal polycondensation of an aspartate-containing LDH, and (c) via a chemical coupling reaction with EDC.

(a) Direct intercalation

Polyaspartate solution (0.75 g of a 27 % w/w polymer solution: 1.5 mmol aspartate monomers, [Asp*]) was stirred in a solution of NaOH (7.5 mmol in 10 ml H_2O) under nitrogen. The pH of the resulting solution was ~12. A solution containing $Mg(NO_3)_2.6H_2O$ (0.29 g, 1.2 mmol) and $Al(NO_3)_3 \cdot 9H_2O$ (0.22 g, 0.6 mmol), previously purged with nitrogen, was added dropwise to the vigorously stirred polymer solution. The resulting suspension was aged at 65 °C for 24 h and the tan-coloured product was dried under vacuum at 50 °C for 24 h. Elemental analysis gave 15.3% C, 4.4% H, 4.4% N, 57.0% O, 10.4% Mg and 8.6% Al, which gave a calculated chemical composition $Mg_{0.43}Al_{0.32}(OH)_{2.05}[Asp^*]_{0.32} \cdot 1.1H_2O$, where [Asp*] = aspartate monomer, and Mg/Al = 1.2.

(b) Thermal polycondensation of aspartate-containing LDH

Typically, a sample (0.5-1.0 g) of the dried aspartate-LDH was heated in a furnace at 220 °C for 24 h in air. Upon removal from the furnace the crucible and sample were allowed to cool slowly in a desiccator in air to room temperature. The product was yellow/pale brown in colour. Organic content of the heated materials was calculated as 21-25 % by weight. The heat-treated sample was dispersed in 20 ml d.d. H_2O under an argon purge and the pH of the solution adjusted to ~11.0 by the addition of 10 M NaOH solution. The reaction mixture was stirred at 60 °C for 1 h, during which time the pH was maintained at ~11.0 by further addition of NaOH solution. Upon cooling to room temperature the solution was neutralized by the addition of HCl and the solid product isolated by centrifugation and washed with d.d. H_2O. Elemental analysis of the heated sample gave 7.7%C, 3.8%H, 3.9%N, 57.1%O, 16.9%Mg and 9.9%Al, and after base hydrolysis, 7.3%C, 4.2%H, 1.2%N, 60.5%O, 16.8%Mg and 10.0%Al.

(c) Coupling reaction between intercalated aspartate molecules using the EDC coupling agent

Finely-ground aspartate-LDH (0.15 g; containing approximately 0.23 mmol aspartate residues) was dispersed in deaerated H_2O (20 ml). The pH of the slurry was adjusted to pH 5.0 with 2.0 M hydrochloric acid. Purging of the solution with argon was employed throughout the reaction. To this mixture a 50× excess of 1-ethyl-3-(3-

dimethylaminopropyl)carbodiimide, (EDC), (2.0 g, 11 mmol) was added, resulting in an immediate rise in pH. The pH, readjusted back to 5.0 by the addition of 0.2 M hydrochloric acid, was subsequently monitored over a period of 2 h and buffered back to 5.0 when necessary. After this time the pH had stabilized at 5.0 and underwent no further change. The reaction vessel was sealed and stirring continued for a further 24 h before the product was isolated by filtration in air and thoroughly washed with water. The solid was dried in air at 50 °C for 18 h and a straw-coloured product resulted. Elemental analysis gave 8.4% C, 5.1% H, 2.0% N, 62.3% O, 14.2% Mg, 8.0% Al, from which a chemical composition of $Mg_{0.6}Al_{0.3}(OH)_{1.8}[Asp^*]_{0.16}[CO_3]_{0.07}\cdot 1.4H_2O$ was calculated.

Preparation of 5-(alkoxy)isophthalate layered double hydroxides [ISA(C_n)-LDHs]

5-(Alkoxy)isophthalic acid, ISA(C_n) (5 mmol), was dissolved in a freshly-prepared solution of NaOH (2.8 g, 30 mmol in 12 ml H_2O) and the solution was purged with argon. To this solution a freshly prepared and argon-purged solution containing $Mg(NO_3)_2\cdot 6H_2O$ (2.56 g, 10 mmol) and $Al(NO_3)_3\cdot 9H_2O$ (1.87 g, 5.0 mmol) was added dropwise under rapid stirring. The pH of the solution following addition was 10. The reaction mixture was left stirring at 70 °C for 24 h before the solid product was isolated by filtration in air under suction and washing with copious water. The white solid was dried under vacuum at 60 °C for 12 h.

Characterization

X-ray diffraction, Fourier-transform infra-red (FTIR) and elemental analyses were carried out on powdered solid samples. Atomic absorption spectroscopy was used to determine the Mg and Al contents. Organic contents were calculated from the C:N ratio obtained from microanalyses of the sample performed on a Varian AA-275 Series spectrophotometer. Atomic absorption spectroscopy was used to determine the Mg and Al contents. Solid state ^{13}C CP MAS NMR spectroscopy were obtained using the EPSRC service at Durham University. Electron microscopy was performed using the JEOL 12OO EX transmission electron microscope with attached scanning imaging device (ASID) on ground samples dispersed in ethanol. Thermogravimetric analyses were carried out using a Perkin-Elmer Delta Series 7 instrument at English China Clays International, St. Austell. A ramp rate of 5 °C min^{-1} was applied between ambient and 600 °C in flowing nitrogen. A more detailed discussion of the characterization techniques employed during the study can be found in Chapter 2: **General Methods**.

3.3 *Results and Discussion*

Carbonate-, terephthalate- and dodecylsulphate-LDHs

The samples obtained from the preparations involving carbonate, terephthalate and dodecylsulphate as the anionic intercalated species were characterized and the

data compared with that previously reported in the literature. Powder X-ray diffraction data from each of these samples showed layered materials with sharp reflections implying a high degree of crystallinity (Figures 3.1 and 3.2). The patterns were indexed with reference to the previous paper by Chibwe and Jones (1989) and JCPDS card 22-700 (synthetic hydrotalcite). The Mg-Al-LDH system shows a preference for rhombohedral packing of the LDH unit cell and, as a result, *ABCABC*-type stacking causes (*hkl*) reflections along the *c* axis to occur in increments of (003) (Carrado *et al.*, 1993; Bellotto *et al.*, 1996).

The carbonate-LDH displayed a d_{003}-spacing of 7.6 Å in accordance with previously reported interlayer spacings (Figure 3.1). Higher order harmonics of the (003) reflection were indicative of the good long range ordering within the material. Previously reported interlayer values for vertically-intercalated (with respect to the inorganic sheets) terephthalate-containing LDHs agreed with the measured 14.1 Å *d*-spacing (Figure 3.2a) (Drezdon, 1988), whilst an additional expanded phase with a *d*-spacing of 11.8 Å could be attributed to a second order (00l) reflection from a superstructure ($d = 23$ Å) made up of interstratified layers of vertically-and horizontally-orientated terephthalate anions (Kooli *et al.*, 1996). The observance of the 23 Å reflection was beyond the capabilities of the diffractometer used. A measured d-spacing of 13.1 Å for the dodecylsulphate-LDH was more suggestive of the second order reflection of an approx. 26 Å interlayer separation arising from an interdigitated arrangement of the dodecylsulphate anions within the gallery space (Clearfield *et al.*, 1991)

data compared with that previously reported in the literature. Powder X-ray diffraction data from each of these samples showed layered materials with sharp reflections implying a high degree of crystallinity (Figures 3.1 and 3.2). The patterns were indexed with reference to the previous paper by Chibwe and Jones (1989) and JCPDS card 22-700 (synthetic hydrotalcite). The Mg-Al-LDH system shows a preference for rhombohedral packing of the LDH unit cell and, as a result, *ABCABC*-type stacking causes (*hkl*) reflections along the *c* axis to occur in increments of (003) (Carrado *et al.*, 1993; Bellotto *et al.*, 1996).

The interlayer spacings, d_{003}, for each of the samples were assigned to the lowest angle reflection in the X-ray diffraction pattern. The carbonate-LDH displayed a d_{003}-spacing of 7.6 Å in accordance with previously reported interlayer spacings (Figure 3.1). Higher order harmonics of the (003) reflection were indicative of the good long range ordering within the material. The interlayer spacings exhibited by terephthalate- and dodecylsulphate-intercalated LDH were 14.1 Å (Figures 3.2a) and 13.1 Å (Figure 3.2b) respectively which correlated well with previously reported values (Drezdon, 1988; Chibwe and Jones, 1989). The terephthalate-containing LDH also contained an additional expanded phase with a d_{003}-spacing of 11.8 Å which can be attributed to a tilted mode of intercalation, rather than a vertical which is implied by the 14.1 Å phase. An interlayer spacing of 13.1 Å for the dodecylsulphate-LDH does not indicate a bilayer arrangement for the organic anions, but is more consistent with an interdigitated motif.

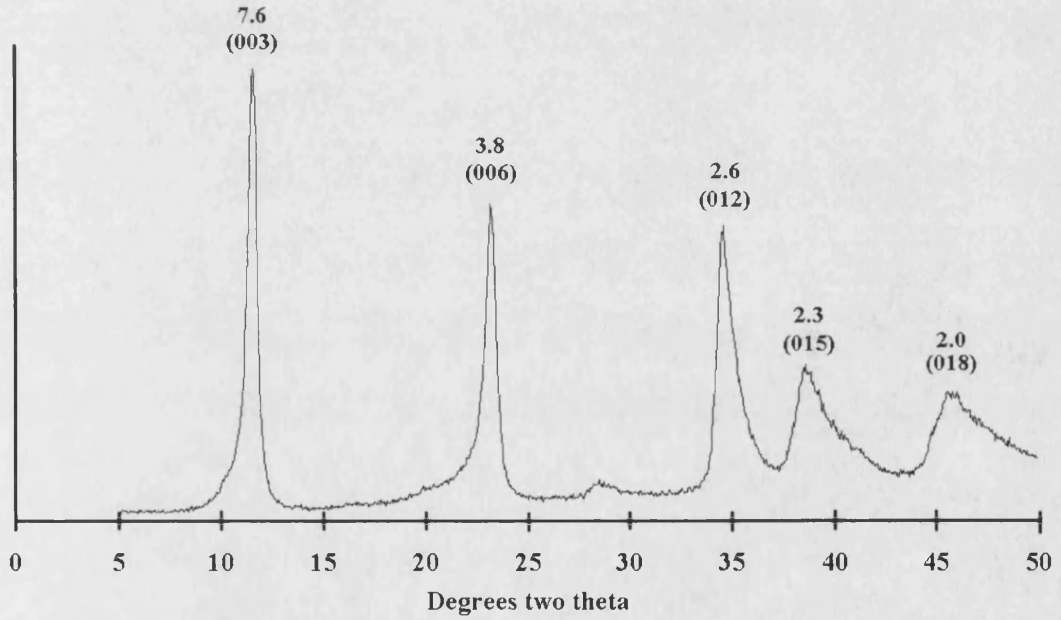

Figure 3.1 PXRD pattern obtained for carbonate-LDH. Miller indices and *d*-spacings in Å are shown

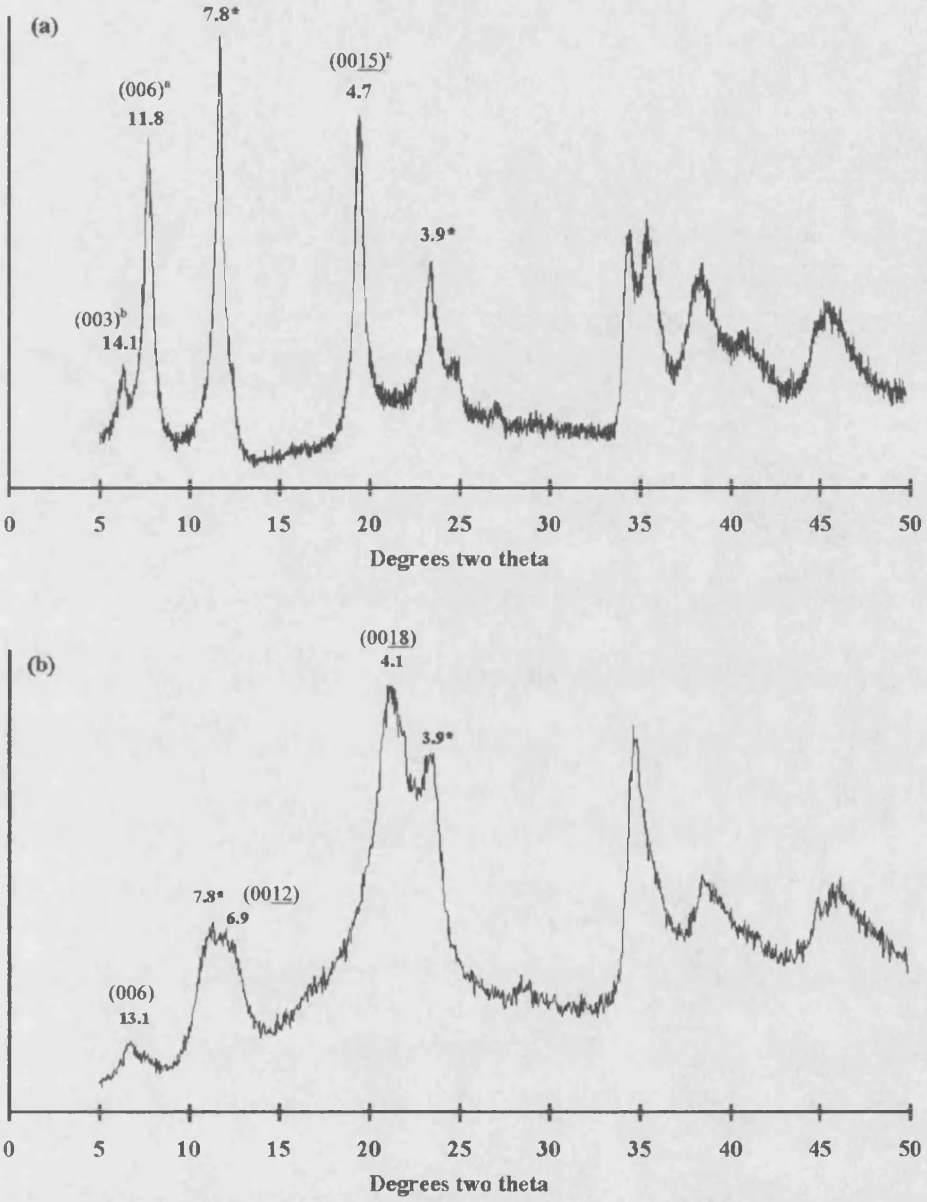

Figure 3.2 PXRD patterns obtained for (a) terephthalate-LDH and (b) dodecylsulphate-LDH (*d*-spacings are shown in Å). * indicates reflections from carbonate/nitrate intercalated phase

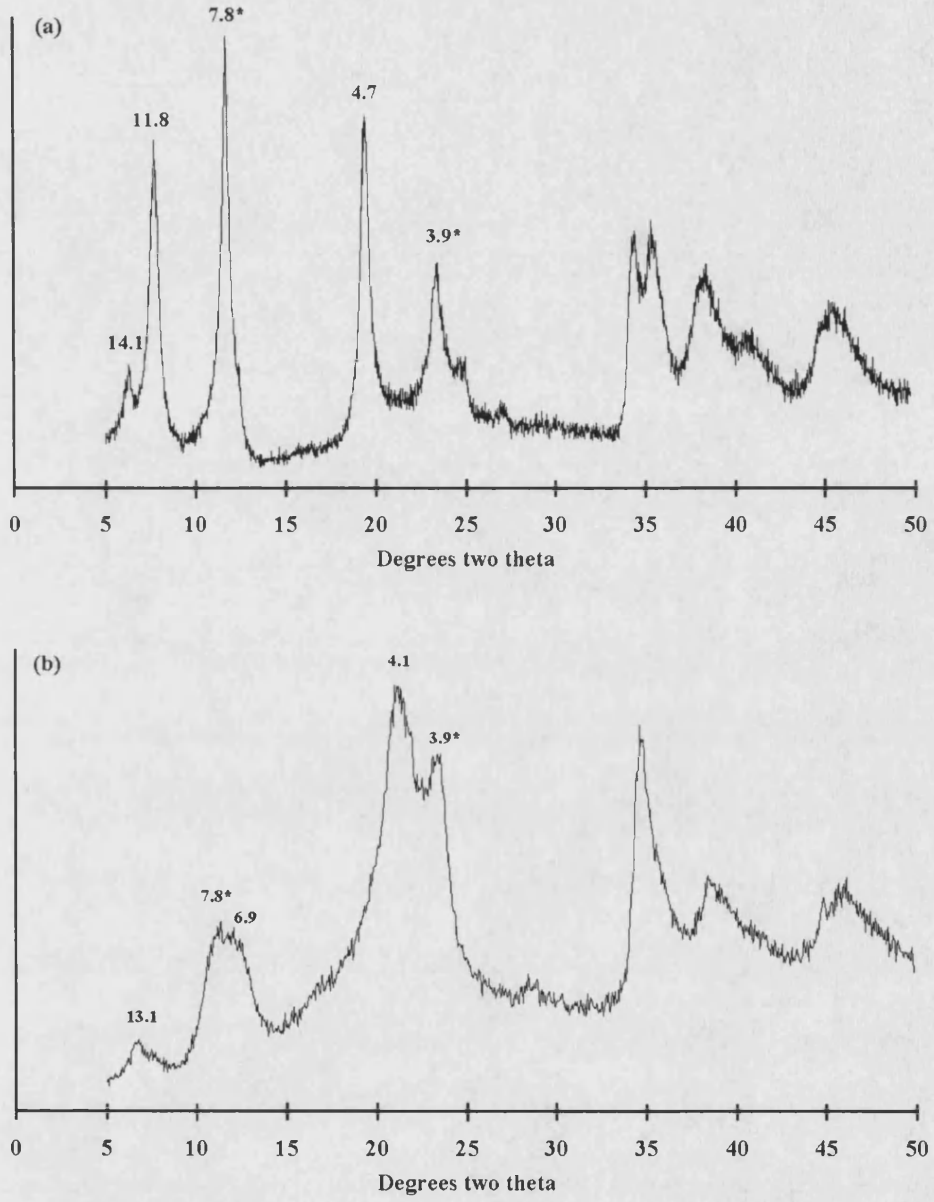

Figure 3.2 PXRD patterns obtained for (a) terephthalate-LDH and (b) dodecylsulphate-LDH (*d*-spacings are shown in Å). * indicates reflections from carbonate/nitrate intercalated phase

The organic-intercalated materials also showed a phase with a 7.8 Å interlamellar spacing, which was assigned to a carbonate-intercalated phase. Preparations were carried out under exposure to the atmosphere, and carbon dioxide was thus able to dissolve in the reaction mixture to become incorporated as inorganic carbonate. Patterns were indexed accordingly with some reflections arising from inorganic phases indicated (Figure 3.2). The presence of organics intercalated into the LDH structure was further confirmed by the presence of respective vibrational modes in the FTIR spectra. Assignments could be made for the terephthalate dianionic species: COO^- (1400 cm^{-1}, 1600 cm^{-1}) and aryl vibrations (1360 cm^{-1}, 1580 cm^{-1}) (Figure 3.3a); and the dodecylsulphate anion: SO_3^- (1300 cm^{-1}) and alkyl vibrations (2850 cm^{-1}, 2960 cm^{-1}, 2980 cm^{-1}) (Figure 3.3b).

Electron microscopy proved a useful tool for observing the microstructure of the materials. Transmission electron microscopy of the carbonate-LDH revealed a homogeneous morphology, bead-like in nature, with regularly-sized particles of approximately 50 nm (Figure 3.4a). Terephthalate-LDH had a similar beady morphology with striations on the particles being observed at higher magnifications and reflecting the turbostratic layered nature of the material (Figure 3.4b). Electron micrographs of the dodecylsulphate-LDH presented a less homogeneous morphology with particles being more random in shape and size (Figure 3.4c) and lattice images observed in certain areas of the sample (Figure 3.4d).

The organic-intercalated materials also showed a phase with a 7.8 Å interlamellar spacing, which was assigned to a carbonate-intercalated phase. Preparations were carried out under exposure to the atmosphere and carbon dioxide was thus able to dissolve in the reaction mixture to become incorporated as inorganic carbonate. Patterns were indexed accordingly with some reflections arising from inorganic phases indicated (Figure 3.2). The presence of organics intercalated into the LDH structure was further confirmed by the presence of respective resonances in the FTIR spectra. Assignments could be made for the terephthalate dianionic species: COO^- (1400 cm^{-1}, 1600 cm^{-1}) and aryl vibrations (1360 cm^{-1}, 1580 cm^{-1}) (Figure 3.3a); and the dodoecylsulphate anion: SO_3^- (1300 cm^{-1}) and alkyl vibrations (2850 cm^{-1}, 2960 cm^{-1}, 2980 cm^{-1}) (Figure 3.3b).

Electron microscopy proved a useful tool for observing the microstructure of the materials. Transmission electron microscopy of the carbonate-LDH revealed a homogeneous morphology, bead-like in nature, with regularly-sized particles of approximately 50 nm (Figure 3.4a). Terephthalate-LDH had a similar beady morphology with striations on the particles being observed at higher magnifications and reflecting the turbostratic layered nature of the material (Figure 3.4b). Electron micrographs of the dodecylsulphate-LDH presented a less homogeneous morphology with particles being more random in shape and size (Figure 3.4c) and lattice images observed in certain areas of the sample (Figure 3.4d).

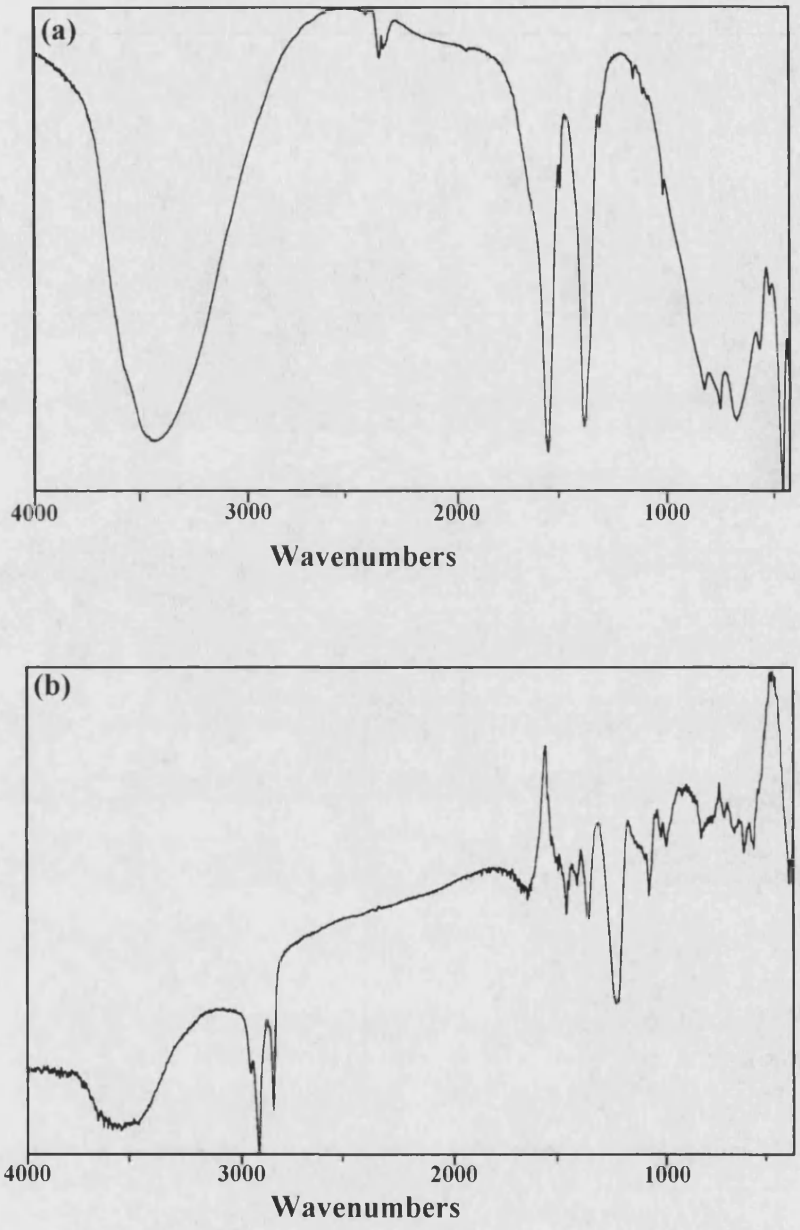

Figure 3.3 FTIR spectra for (a) terephthalate-LDH and (b) dodecylsulphate-LDH

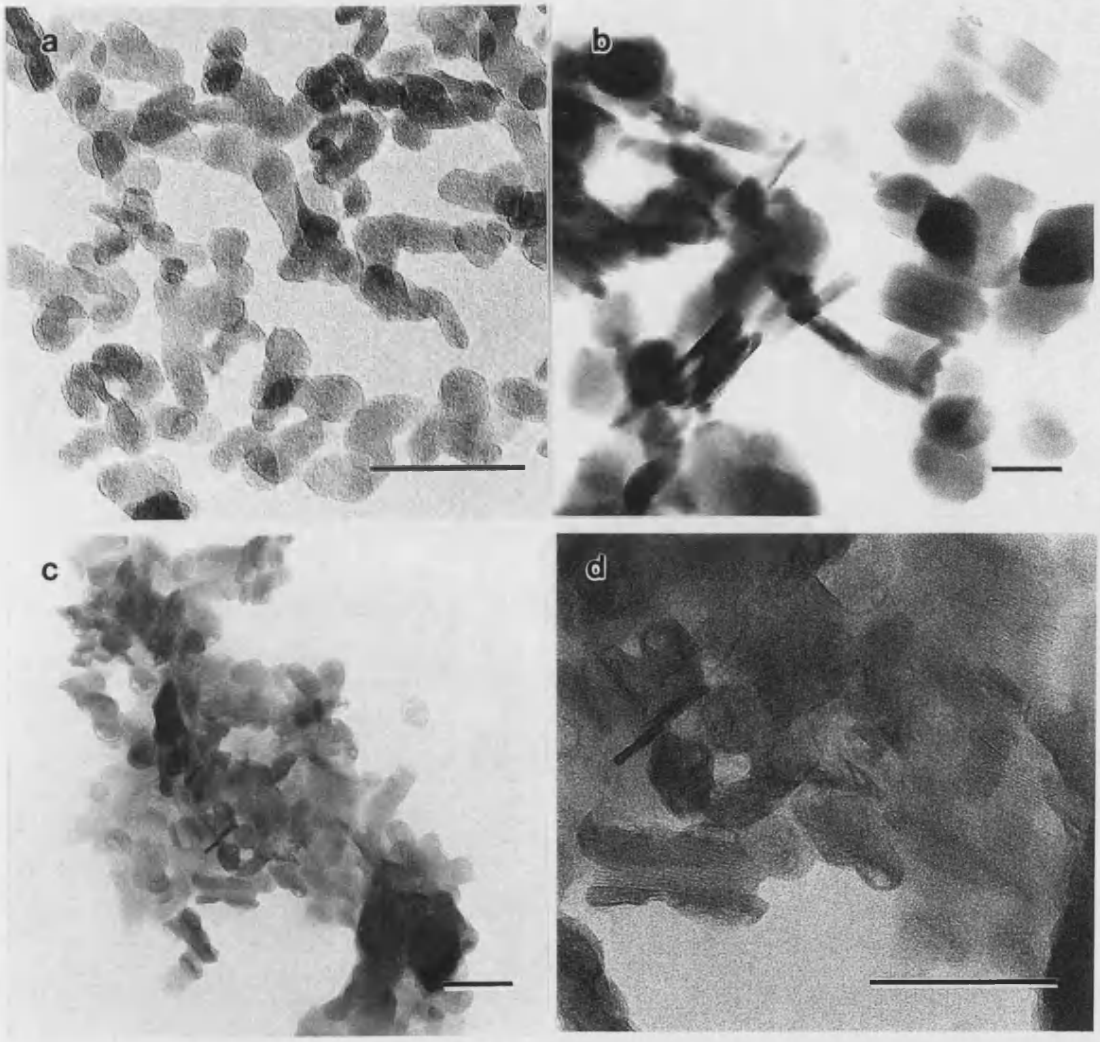

Figure 3.4 Transmission electron micrographs for (a) carbonate-LDH, (b) terephalate-LDH, (c) dodecylsulphate-LDH. Micrograph (d) shows lattice fringes evident in the dodecylsulphate-LDH sample. All scale bars = 100 nm.

Aspartate- and glutamate-LDHs

The synthesis of aspartate- and glutamate-LDH was carried out under an inert nitrogen atmosphere to minimize the competitive intercalation of carbonate anions in LDH arising from adsorption of atmospheric carbon dioxide. As illustrated in the cases of the terephthalate-LDH and dodecylsulphate-LDH preparations carbonate is readily incorporated within the interlayer spaces of LDHs and initial preparations of aspartate- and glutamate-LDH carried out under aerobic conditions resulted solely in the production of a carbonate-containing LDH, with little organic incorporated. This result was not surprising bearing in mind the strong tenacity with which small, highly-charged carbonate anions is held between the hydroxide layers. Amongst the simple inorganic anions the exchange facility is generally reported to decrease in the order $NO_3^- > Cl^- > SO_4^{2-} > CO_3^{2-}$ (Parker et al 1995), with the charge density on LDH layers also believed to play a significant role on the anion-exchange properties (Kooli *et al.*, 1996).

The XRD pattern for the carbonate-LDH showed characteristic reflections which corresponded to an interlayer spacing of 7.6 Å (Figure 3.1; Table 3.2). By contrast, the aspartate-and glutamate-LDHs showed expanded structures with broad (003) diffraction peaks at 11.1 Å and 11.9 Å, respectively (Figure 3.5; Table 3.2). These expanded interlayer separations were consistent with the intercalation of the organic anions within the gallery spaces of the LDH. Weak (006) and (00,12) reflections were also observed, indicating that the amino acid intercalated LDHs were single phases with significant stacking disorder.

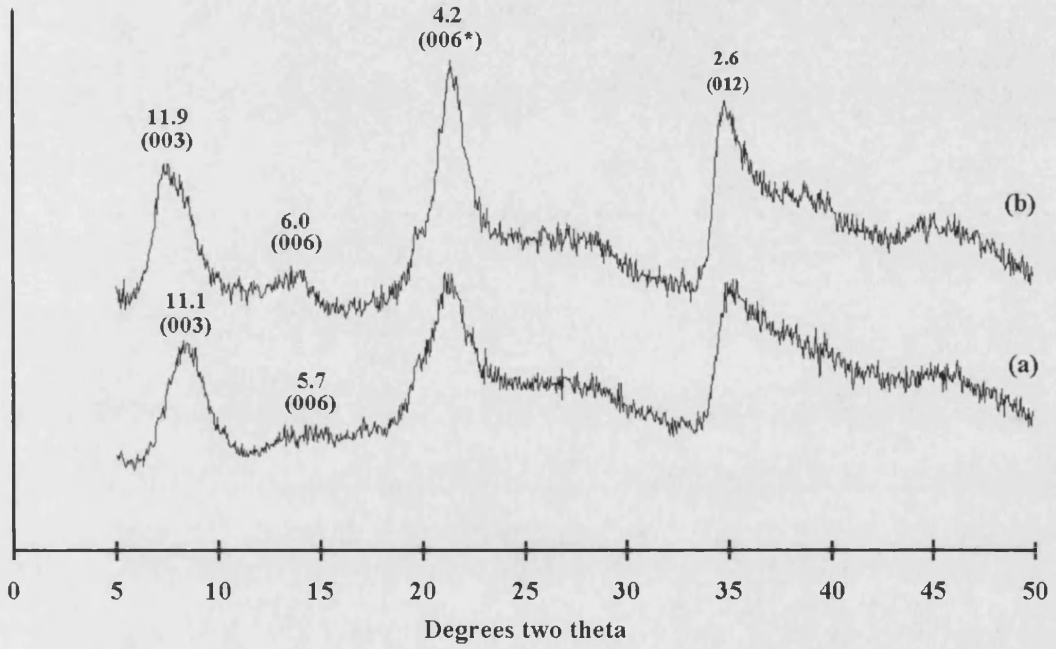

Figure 3.5 PXRD patterns obtained for (a) aspartate-LDH and (b) glutamate-LDH. Miller indices and *d*-spacings in Å are indicated

Assuming a thickness of 4.8 Å for the brucite layer, the gallery spacings were approximately 6.3 Å and 7.1 Å for aspartate- and glutamate-LDHs, respectively, compared with a carbonate-LDH gallery height of 2.8 Å. These values suggested a monolayer arrangement for the intercalated amino acids, with the carboxylates of individual molecules bridging adjacent layers of the inorganic framework.

Table 3.2 PXRD data (*d*/Å) for synthesized amino acid- and polyaspartate-intercalated LDHs

	d_{003}	d_{003}[a]	d_{006}	d_{009}	d_{006}[a]	$d_{00,12}$	d_{012}	gallery height[b]
CO_3-LDH	7.6	-	3.8	-	-	-	2.6	2.8
Glu-LDH	11.9	-	6.0	-	4.2	3.1	2.6	7.1
Asp-LDH	11.1	-	5.7	-	4.2	2.9	2.6	6.3
polyAsp-LDH	15.1	-	7.7	5.8	-	3.9	2.6	10.3
ht-Asp-LDH	9.0	-	4.4	-	4.2	-	2.6	4.2
ht-Asp-LDH+OH	12.1	-	6.3	3.9	-	-	2.6	7.4
ht-CO_3-LDH	6.8	-	3.4	-	-	-	2.6	2.0
Asp-LDH+EDC	12.9	7.6	-	-	3.8	-	2.6	8.1

[a]Values assigned to intercalated nitrate/carbonate. [b]Assumes a thickness for the brucite layer of 4.8 Å. ht = heated.

Elemental analysis and calculated chemical compositions for the as-synthesized intercalated LDHs revealed organic contents for the aspartate and glutamate-containing materials of typically 20 % by weight. Nitrate ions were also co-intercalated within the gallery spaces. This was confirmed by FTIR spectroscopy (see below) and was consistent with a broad XRD peak at 4.2 Å (Figure 3.5) which was attributed to disordered layers of intercalated nitrate anions (d_{006} for pure NO_3-LDH = 4.0 Å) within the amino acid-LDH materials. The compositional data demonstrated

that the amount of organic and inorganic anions incorporated into the LDH materials was stoichiometrically related to the net positive charge generated by Al substitution in the inorganic layers. In addition, the data indicated that the acidic amino acids were incorporated as dianionic species, consistent with the highly alkaline (pH = 12; pK_a ($-NH_3^+$) = 10.0) reaction conditions.

For all synthetic procedures, an initial mole ratio of Mg/Al = 2 was charged to the reaction vessel. The resulting Mg/Al ratios in the precipitated products differed according to the nature of the intercalated anions. For the purely inorganic carbonate-LDH, a ratio of Mg/Al of 2.8 indicated an incomplete precipitation of aluminium ions. In comparison, the corresponding ratios in the aspartate and glutamate samples were slightly lower than the theoretical value at 1.9 and 1.8 respectively, indicating an enrichment of the trivalent cation in the brucite layers. This suggests that the composition of the brucite layer can be influenced by host-guest interactions that are presumably taking place prior to assembly of the double hydroxide layers. For example, differences in the stability constants of Al^{3+} and Mg^{2+} complexes of the amino acid dianions might favour the partial fractionation of the more highly charged cationic species. However it is known that LDH materials with low crystallinity often have low Mg/Al ratios (Albiston *et al.*, 1996) suggesting that the trivalent enrichment could be a general kinetic effect.

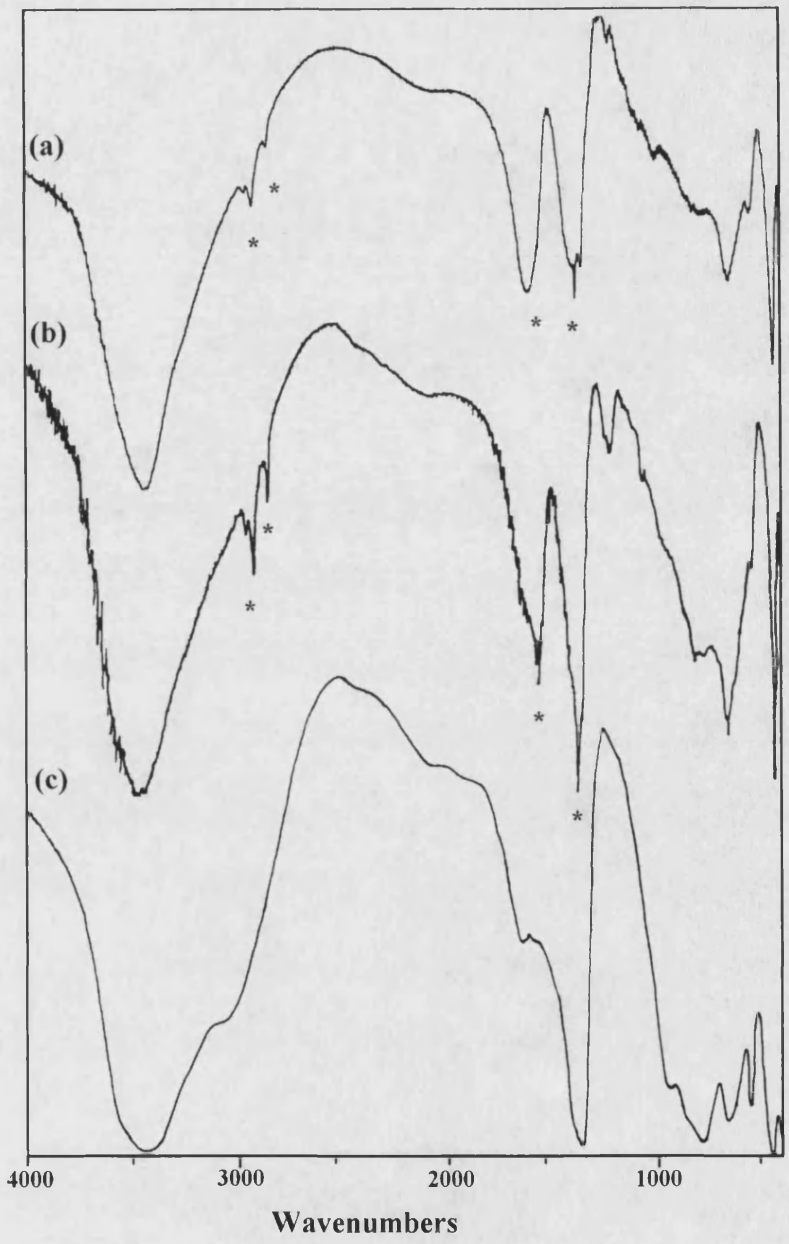

Figure 3.6 FTIR spectra for (a) aspartate-LDH, (b) glutamate-LDH and (c) carbonate-LDH. * indicate assignments for organic group vibrations

FTIR spectra of the aspartate- and glutamate-LDHs showed absorption bands corresponding to the intercalated organic dianions (Figure 3.6a and 3.6b respectively). Characteristic alkyl C-H stretches were observed in the 2800-3000 cm^{-1} region of both spectra and the RCO_2^- asymmetric and symmetric stretches (1590 cm^{-1} and 1400 cm^{-1} respectively), were also evident. Co-intercalated nitrate anions gave a very intense absorption at 1385 cm^{-1}. A broad absorption between 3200 cm^{-1} and 3600 cm^{-1} was associated with the stretching mode of hydrogen-bonded hydroxyl groups from both the hydroxide layers and interlayer water. Peaks at 650 cm^{-1} and 460 cm^{-1} were assigned to the metal-oxygen modes of the LDH sheets.

Solid state ^{13}C NMR spectroscopy gave assignments for the dianionic organic species, with broad resonances implying a low degree of ordering of the organic entities in the gallery spaces (Figure 3.7a and 3.7b) (Table 3.3). Low intensity resonances with narrow line widths present in both cases at 170 ppm were attributable to mobile inorganic carbonate ions. Carbonate may have been incorporated into the sample during synthesis or more likely was absorbed onto the surface of clay particles post synthesis upon exposure to the atmosphere. The corresponding spectrum from carbonate-LDH showed a single sharp resonance at 170 ppm (Figure 3.7c).

Figure 3.7 ^{13}C CP MAS NMR spectra for (a) aspartate-LDH, (b) glutamate-LDH and (c) carbonate-LDH. * indicate spinning sidebands.

Table 3.3 ^{13}C CP MAS NMR assignments for synthesized amino acid- and polyaspartate-intercalated LDHs

	-COO^-	-C(=O)N-	CO_3^{2-}	-CHRN-	-CH_2-	Other peaks
CO_3-LDH	-	-	170	-	-	-
Glu-LDH	180	-	170(*wk*)	55	39,30	-
Asp-LDH	180	-	170(*wk*)	54	41	-
pure polyAsp[a]	180	174	-	54	40	-
polyAsp-LDH	178	173	170	54	40	32,30,23
ht-Asp-LDH	178	175(*sh*)	170(*wk*)	54	42	166,20
ht-Asp-LDH+OH	178	174	170	52	39	60,32,31,21
Asp-LDH+EDC	178	172	170	54	40	-

[a]Assignments made from solution NMR of sodium polyaspartate solution. *wk* = weak. *sh* = shoulder.

Thermogravimetric analysis of the carbonate-LDH (Figure 3.8a) showed a distinctive weight reduction between 80-200 °C (15 wt. %) attributed to loss of surface adsorbed and interlayer water. A major weight loss was observed at 280 °C, continuing up to 500 °C, due to concomitant dehydroxylation of the inorganic layers and decomposition of intercalated carbonate anions (~30 wt. %) (Constantino and Pinnavaia, 1995). In contrast, the aspartate-LDH underwent a more gradual weight loss from room temperature up to ~330 °C (25 wt. %) (Figure 3.8 b) due to both dehydration of the hydroxide layers and polycondensation of the intercalated aspartate monomers. At 330 °C, the onset of a rapid and major weight loss ensued, continuing up to 500 °C as dehydroxylation and partial decomposition of organics occurred (30 wt. % loss). The corresponding DSC trace (data not shown) showed two endotherms centred at 360 °C and 430 °C due to dehydroxylation and organic decomposition respectively.

Electron microscopy revealed significant differences in the morphologies of the carbonate- and amino acid-intercalated LDHs. The bead-like structure of the carbonate-LDH, evident in TEM (Figure 3.4a) was also apparent in the SEM (Figure 3.9b), which showed discrete, regular-sized particles of approximately 0.1μm dimensions. In contrast, the aspartate-LDH afforded non-uniform irregular aggregates (<1.0 μm in size) of plate-like morphology (Figures 3.9a and 3.10a). Layering within the sample was evident and coherent lattice fringes were occasionally imaged (Figure 3.10b). These results indicated that the texture and morphology of LDH materials can be influenced by the nature of the intercalated anion; aspartate, carbonate, terephthalate and dodecylsulphate exerting different effects over the resultant morphology. The insertion of new growth units into a developing crystal surface, as well as the aggregation behaviour of primary particles, can be influenced by properties such as spatial charge distribution, lattice periodicity and the stereochemical disposition of surface groups. Guest anions can therefore make a significant contribution to the interfacial interactions associated with crystallization. For example, the basal (001) face of the LDH structure appears to be preferentially stabilized in the presence of aspartate, with the result that plate-like primary particles are formed.

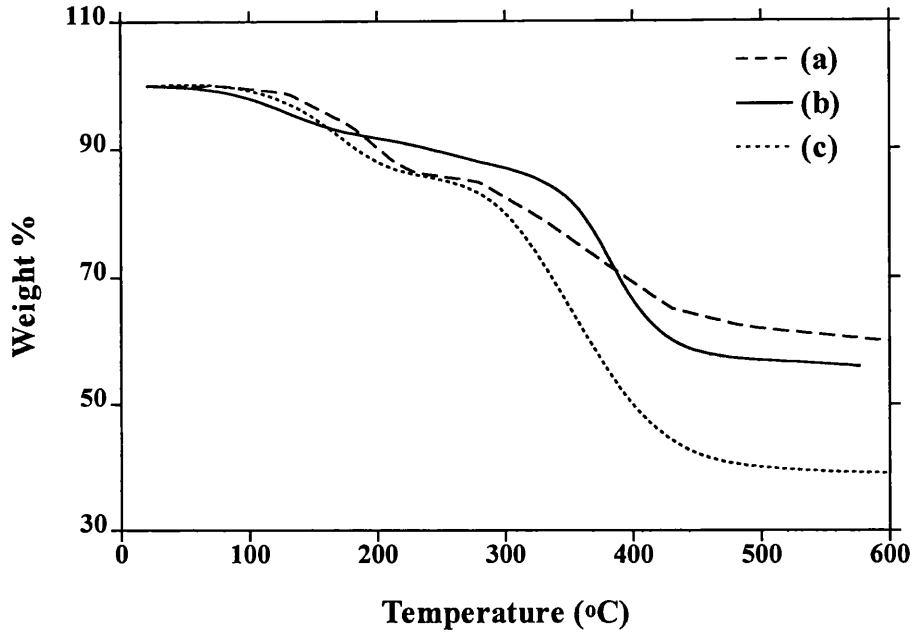

Figure 3.8 Thermogravimetric analysis data for (a) carbonate-LDH, (b) aspartate-LDH and (c) polyaspartate-LDH prepared by direct incorporation

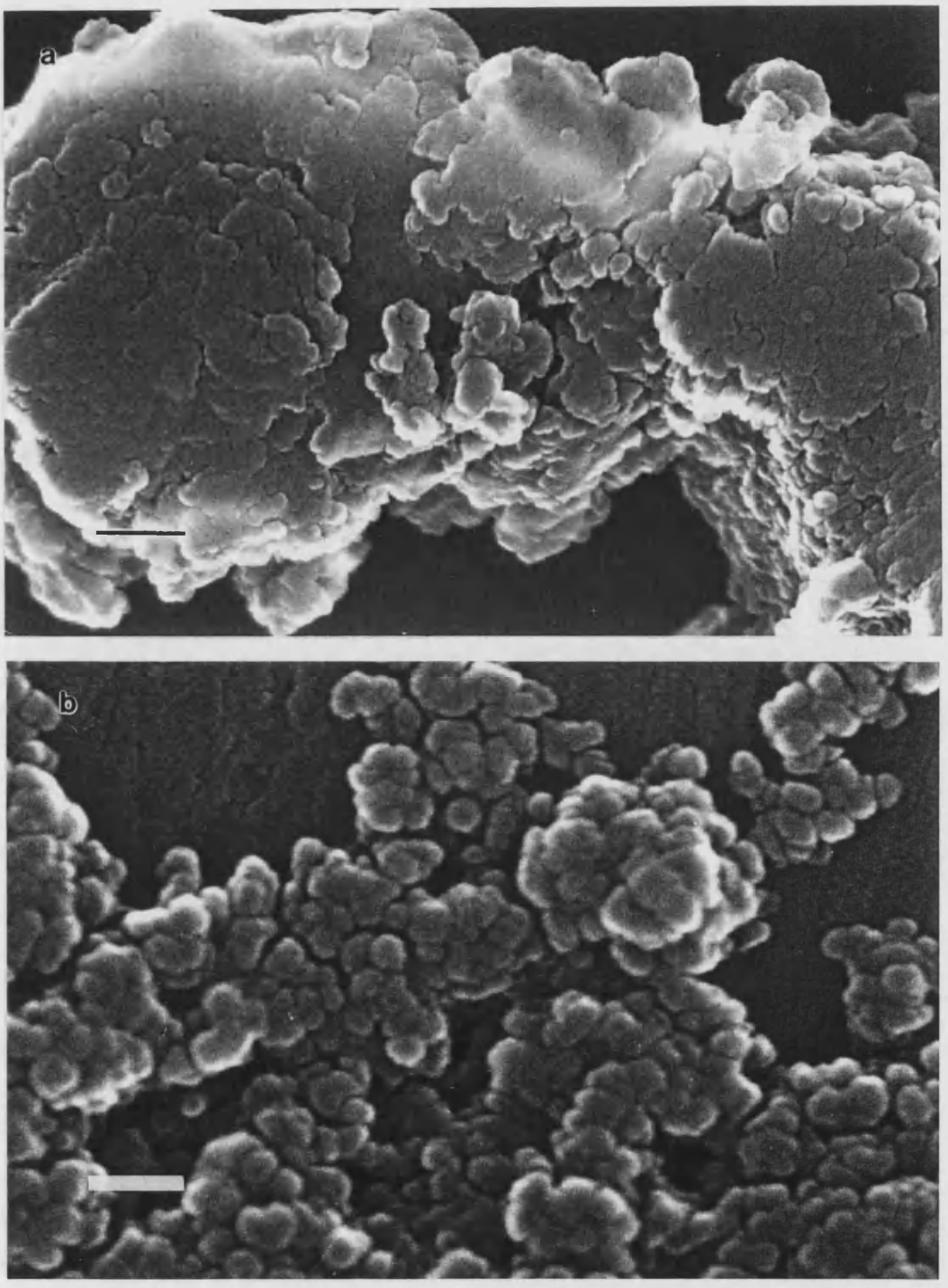

Figure 3.9 Scanning electron micrographs of (a) aspartatete-LDH (scale bar = 200 nm) and (b) carbonate-LDH (scale bar = 500 nm).

Figure 3.10 Transmission electron micrograph for (a) aspartate-LDH and (b) A higher magnification view of an area of (a) showing lattice fringes (d = 10.8 Å). Scale bars = (a) 50 nm, (b) 25 nm.

Polyaspartate-containing LDHs

a) Direct synthesis

Direct intercalation of polyaspartate by co-precipitation afforded an organo-LDH with an average interlayer separation of 15.1 Å, although peaks were extensively broadened (Table 3.2, Figure 3.11). The XRD pattern also showed broad peaks for the d_{006} and d_{009} spacings, and a very broad reflection centred at 3.9 Å which could be $d_{00,12}$ or d_{006} of highly disordered carbonate-intercalated layers, or both. However, elemental analysis of the polymer-LDH gave a typical chemical composition, $Mg_{0.43}Al_{0.31}(OH)_{1.48}[Asp^*]_{0.31}.0.8H_2O$. Assuming 62 [Asp*] monomers per polymer molecule, this gives a molar stoichiometry of $[polyaspartate]_{0.006}$, with an organic content between 20-35 % by weight. The data indicated that the singly charged aspartate side residues of polyaspartate are the charge balancing species, and no evidence for the incorporation of other inorganic anions was observed. The Mg/Al ratio was 1.2, indicating that Al^{3+} incorporation into the inorganic layers was more favourable than in the case of the dianionic aspartate and glutamate LDHs, which again demonstrated a degree of guest-assisted cationic selectivity in the synthesized clay

FTIR spectroscopy showed characteristic frequencies associated with the intercalated polyaspartate macromolecules (Figure 3.12). Major assignments included those for N-H (1520 cm^{-1}, 3500 cm^{-1}), C=O (1650 cm^{-1}), CO_2^- (1410 cm^{-1},1580 cm^{-1}). The clearly resolved absorption peaks arising from the intercalated organic species reflected in part the higher organic content of the preformed polymer intercalation material. No absorptions from intercalated nitrate ions (1385 cm^{-1}) were observed.

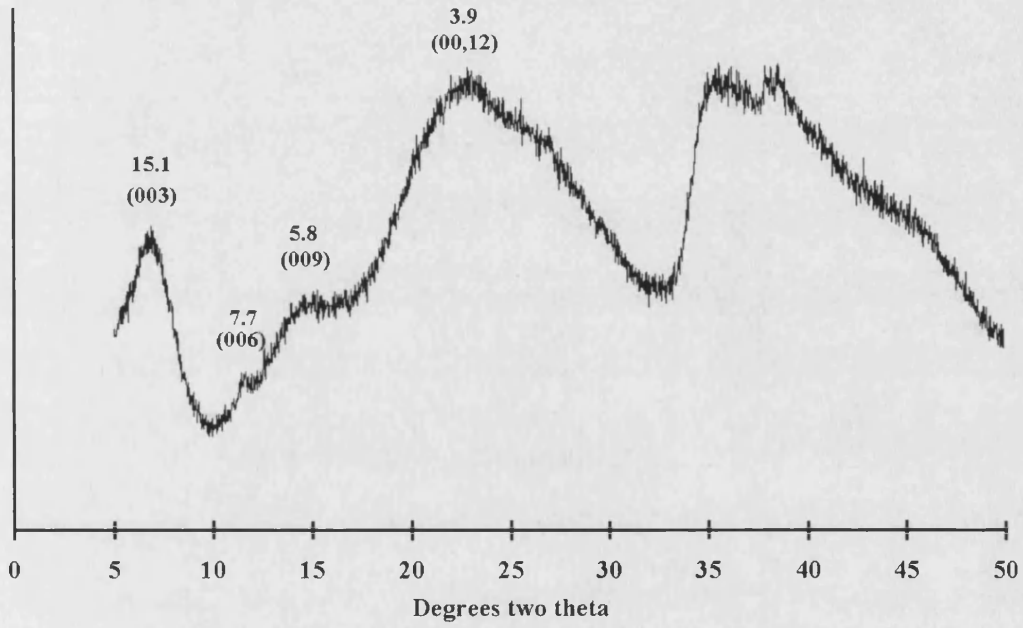

Figure 3.11 PXRD pattern obtained for polyaspartate-LDH prepared by direct intercalation. Miller indices and *d*-spacings in Å are indicated.

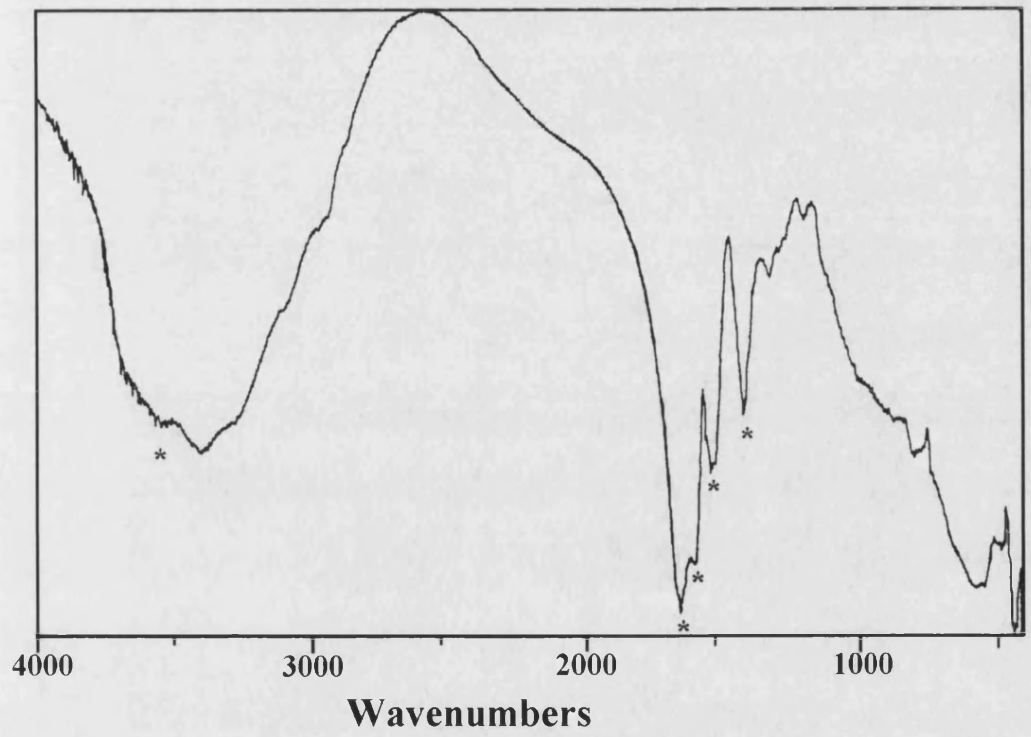

Figure 3.12 FTIR spectrum for polyaspartate-LDH prepared by direct intercalation. * indicate assignments for organic group vibrations.

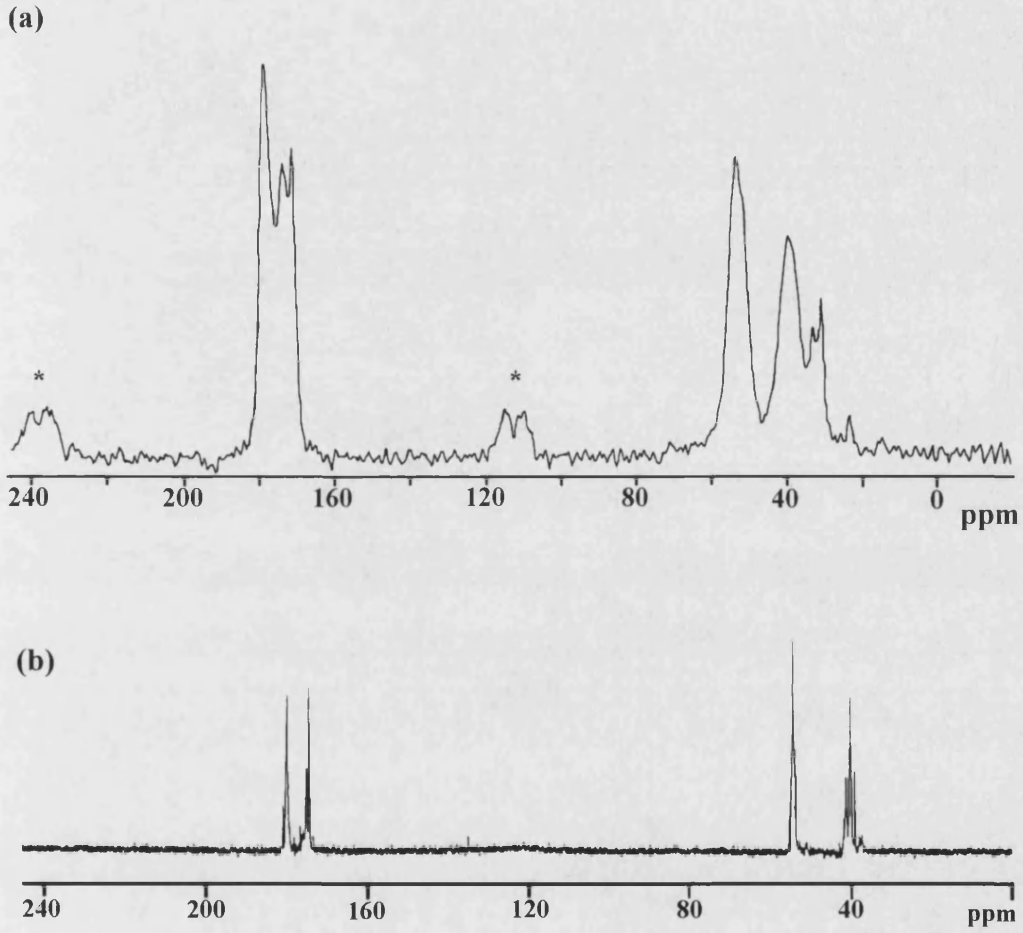

Figure 3.13 (a) ^{13}C CP MAS NMR spectra for polyaspartate-LDH prepared by direct intercalation and (b) solution NMR of sodium polyaspartate

Solid state ^{13}C NMR spectroscopy of the polymer-clay nanocomposite (Figure 3.13a, Table 3.3) exhibited resonances which correlated well with those from a solution NMR of the polyaspartate solution used in the synthesis (Figure 3.13b, Table 3.3). In both cases resonances from the amide (174-175 ppm) and carboxylic (178-180 ppm) were evident. A signal from inorganic carbonate was again present, most likely due to incorporation post-synthesis, since no evidence for carbonate was observed in FTIR of the freshly prepared sample.

TGA profiles showed an almost linear loss in weight of 13% from room temperature up to 280 °C (Figure 3.8c), which was attributed to dehydration of the layered double hydroxide. At 280 °C, a more rapid and sustained decrease in weight began, corresponding to dehydroxylation and loss of intercalated organics (30-50 wt.%), leveling out around 600 °C. It was impossible to distinguish between the onset of these two events. However, the onset of decomposition of a pristine sodium polyaspartate sample was found by TGA and DSC to be around 420 °C.

The polyaspartate-LDH formed by direct intercalation consisted of irregularly shaped aggregates of plate-like particles, often exceeding 1.0 μm in size, and with very smooth surface textures (Figure 3.14). TEM images showed crystals often with well-defined edges (Figure 3.14b).

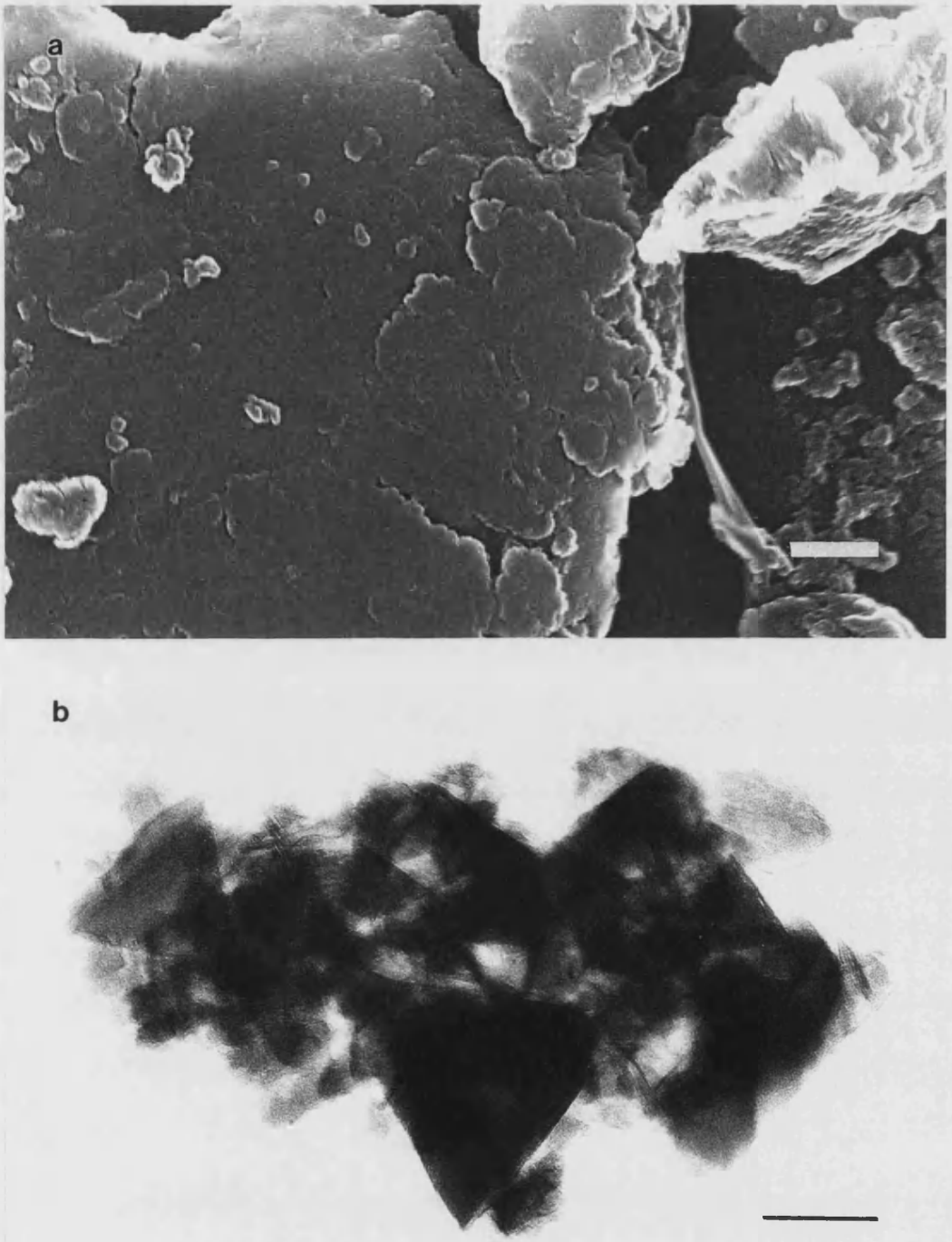

Figure 3.14 (a) Scanning electron micrograph for polyaspartate-LDH prepared by direct synthesis (scale bar = 1 μm). (b) Transmission electron micrograph for the same sample (scale bar = 100 nm).

(b) In situ *thermal polymerization*

The thermal polymerization of aspartic acid at 200 °C followed by treatment with base is a well-documented method of forming poly(α,β-aspartate). The reaction proceeds via a polysuccinimide intermediate which rearranges to give polyaspartate (Donachy and Sikes, 1994) [Scheme 3.1]. This reaction is commonly employed in industry to obtain polyaspartic acids which are biodegradable polymers of industrial importance. Polyaspartates have found medical, cosmetic and fabric applications as metal-absorbent-materials, as well as being used in water treatment as inhibitors of scale growth.

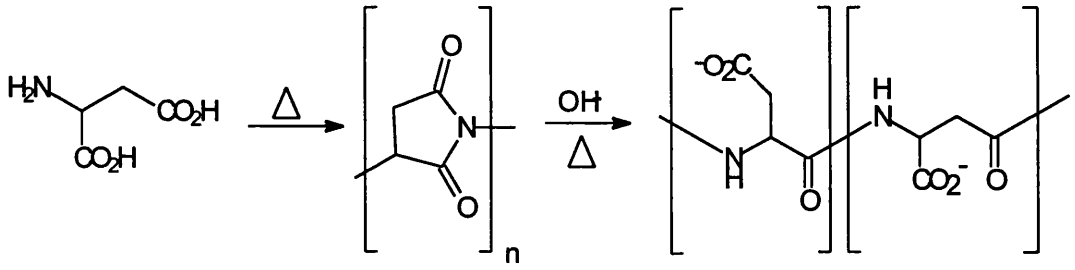

aspartic acid polysuccinimide poly(α,β-aspartate)

Scheme 3.1 Thermal polycondensation of aspartic acid to poly(α,β-aspartate)

Thermal treatment of the white aspartate-LDH (d_{003}=11.1 Å) at 200 °C for 48 h resulted in a single-phase yellow material with a decreased d_{003} spacing of 9.0 Å, corresponding to a reduction in the interlayer separation of 2.1 Å (Table 3.2, Figure 3.15a). The d_{003} peak width was comparable with that of the aspartate-LDH material before heating, but no d_{006} reflection was observed. By comparison, a heated sample of

carbonate-LDH showed only a small contraction in d_{003} from 7.6 Å to 6.8 Å and the d_{006} reflection was still present. The decreases in basal spacing and structural order can be attributed to the loss of intercalated water molecules and, in the case of aspartate-LDH, also to the polymerization of the organic monomers within the gallery spaces of the LDH. The organic content of the heated samples remained between 20-25 wt. % indicating no significant deintercalation of the organic molecules.

Electron microscopy of aspartate-LDH following thermal treatment showed little change in morphology of the clay particles with the turbostratic nature of the material being retained (Figure 3.16 compared with Figure 3.9). Surface cracking could be observed in the SEM (Figure 3.16a), presumably due to loss of water during dehydration, but the overall plate-like shape and aggregated texture remained.

Subsequent treatment of the heat-treated sample with sodium hydroxide yielded a material which exhibited a broad (003) reflection (Table 3.2, Figure 3.15b) corresponding to an interlayer spacing at the peak maximum at 12.2 Å, and the reappearance of the (006) reflection, suggesting further rearrangement/conversion of the intercalated organic species. In addition, the 4.2 Å reflection attributed to intercalated nitrate was no longer observed, and a new peak at 3.9 Å was assigned to the presence of disordered brucite layers containing carbonate anions. Thus, treatment with NaOH resulted in facile exchange of intercalated nitrate for carbonate, presumably by rehydration in the presence of high concentrations of dissolved CO_2. This interpretation is consistent with the NMR and FTIR data described below.

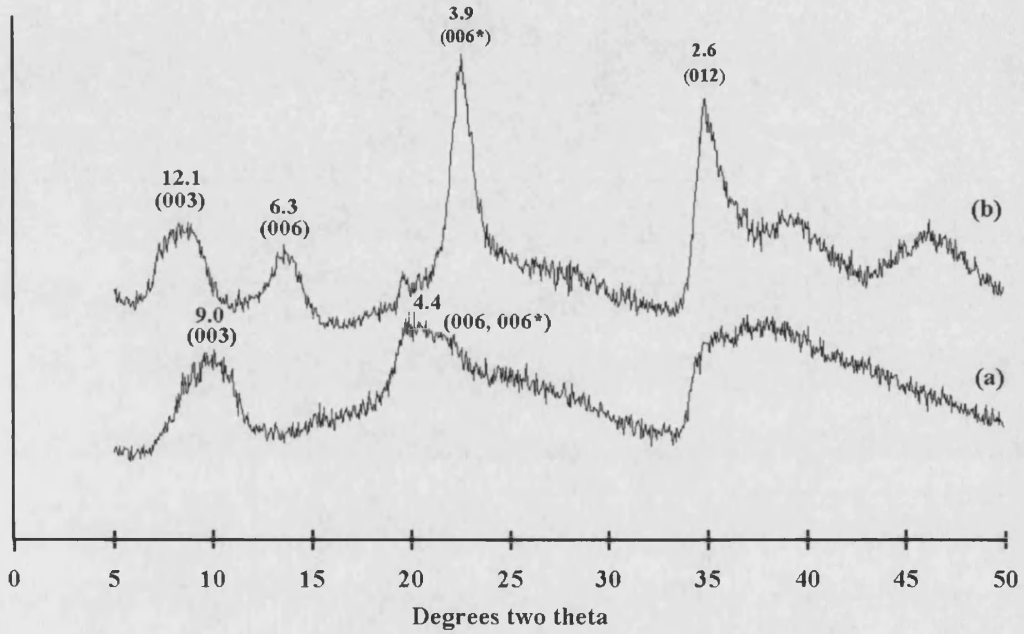

Figure 3.15 PXRD patterns obtained for (a) heated aspartate-LDH and (b) heated and base-treated aspartate-LDH. Miller indices and *d*-spacings in Å are indicated

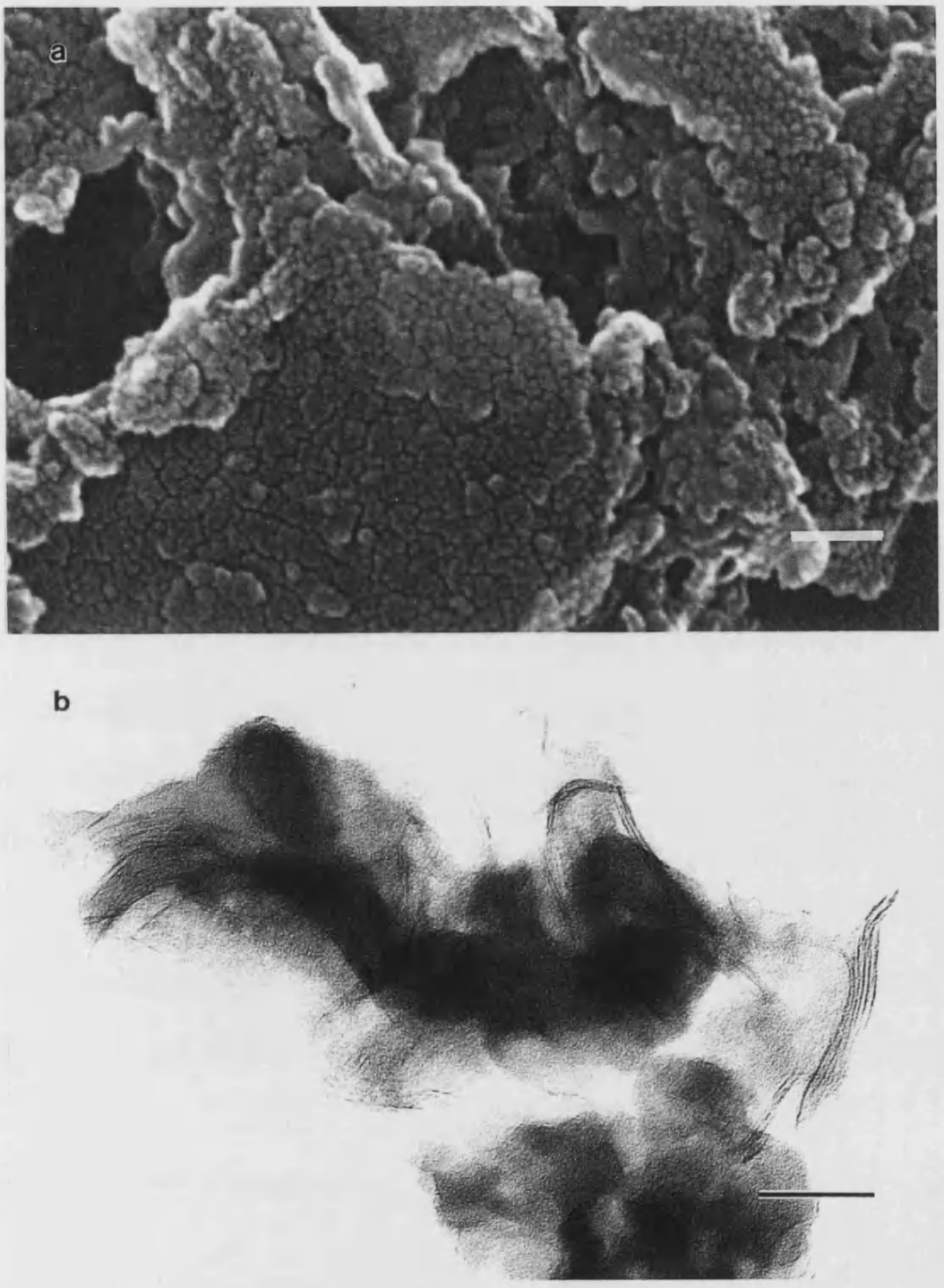

Figure 3.16 (a) Scanning electron micrograph obtained for aspartate-LDH following thermal treatment (scale bar = 200 nm). (b) Transmission electron micrograph of the same sample (scale bar = 50 nm).

The decrease in the interlayer spacing after dry thermal treatment, and subsequent expansion following reaction with aqueous NaOH supported the implication that initial heating of the organo-LDH brought about *in situ* polymerization of the aspartate monomers to produce intercalated polyimides, which subsequently underwent ring-opening by hydrolysis.

Supporting evidence for polycondensation of the intercalated monomers was provided by solid state ^{13}C NMR spectroscopy. Following heat treatment, a new resonance at 175 ppm was observed in the aspartate-LDH spectrum in the form of a shoulder to the 180 ppm peak (Figure 3.17a, Table 3.3); this peak was characteristic of an amide linkage (-C(=O)-N-). However, an additional resonance at 166 ppm suggested the presence also of an imide (-(C=O)-NR-(C=O)), although this peak is not reported in the NMR spectrum for polysuccinimide (Wolk *et al.*, 1994). Subsequent treatment with NaOH gave a spectrum consistent with further reaction of the imide intermediate; in particular, the 174 ppm resonance (amide linkage) was now well resolved against the 178 ppm carboxylate peak, and the 166 ppm (imide) resonance was absent (Figure 3.17b, Table 3.3). The spectrum also contained several new resonances between 15 ppm and 60 ppm, suggesting that a number of species were formed in the hydrolysis reaction. A sharp resonance at 170 ppm due to inorganic carbonate, which was small in the heated aspartate-containing LDH prior to base hydrolysis, was also observed and was consistent with nitrate ions having undergone exchange with carbonate ions.

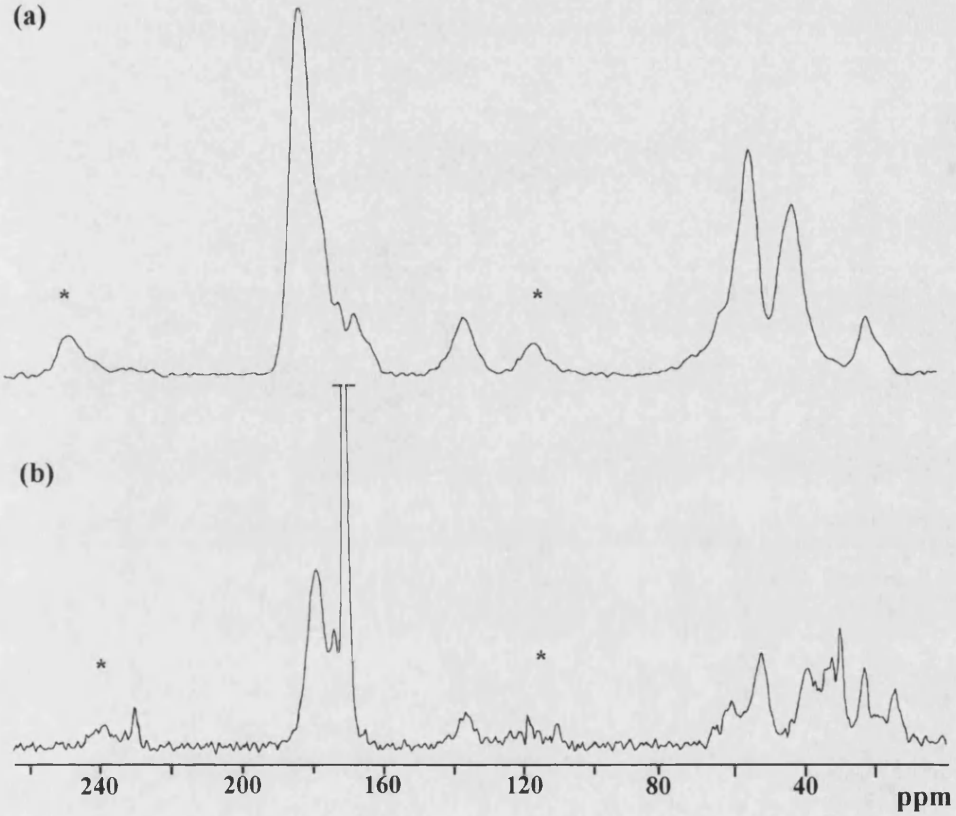

Figure 3.17 ^{13}C CP MAS NMR spectra for (a) heated aspartate-LDH and (b) heated and base-treated aspartate-LDH. * indicate spinning sidebands.

No attempt was made to calculate an overall chemical composition on the basis of the elemental analyses of the sample following heat treatment and following subsequent treatment with base. The calculation was complicated due to the ion-exchange reactions occurring between nitrate and carbonate ions and the side reactions to the polymerization reaction which evidenced themselves in the form of additional, unassigned peaks in the NMR spectra (Table 3.2). There was, however, no change in the Mg/Al ratio throughout the polycondensation reaction, suggesting no decomposition of the inorganic framework structure.

There was little change in the FTIR spectrum of the sample after heating (Figure 3.18a), when compared to the as-synthesized aspartate-LDH (Figure 3.6a). Absorptions due to alkyl C-H groups were still evident between 2800 cm^{-1} and 2950 cm^{-1}, but the unambiguous assignment of polymer residues was not possible. Other assignments could be made for intercalated nitrate ions (1385 cm^{-1}), and the metal-oxygen stretching modes (460 cm^{-1} and 650 cm^{-1}). Following base hydrolysis an intense but broad absorption peak at 1500-1700 cm^{-1} was attributed to carbonyl resonances from amide (1650 cm^{-1}) and carboxylate groups (~1580 cm^{-1}) of polyaspartate, whilst a broad peak of comparable intensity (1380 - 1450 cm^{-1}) was consistent with the symmetric stretching mode of carboxylate groups (1410 cm^{-1}), and inorganic carbonate (1390 cm^{-1}) (Figure 3.18b). Metal-oxygen stretching absorptions were also observed (480 cm^{-1}).

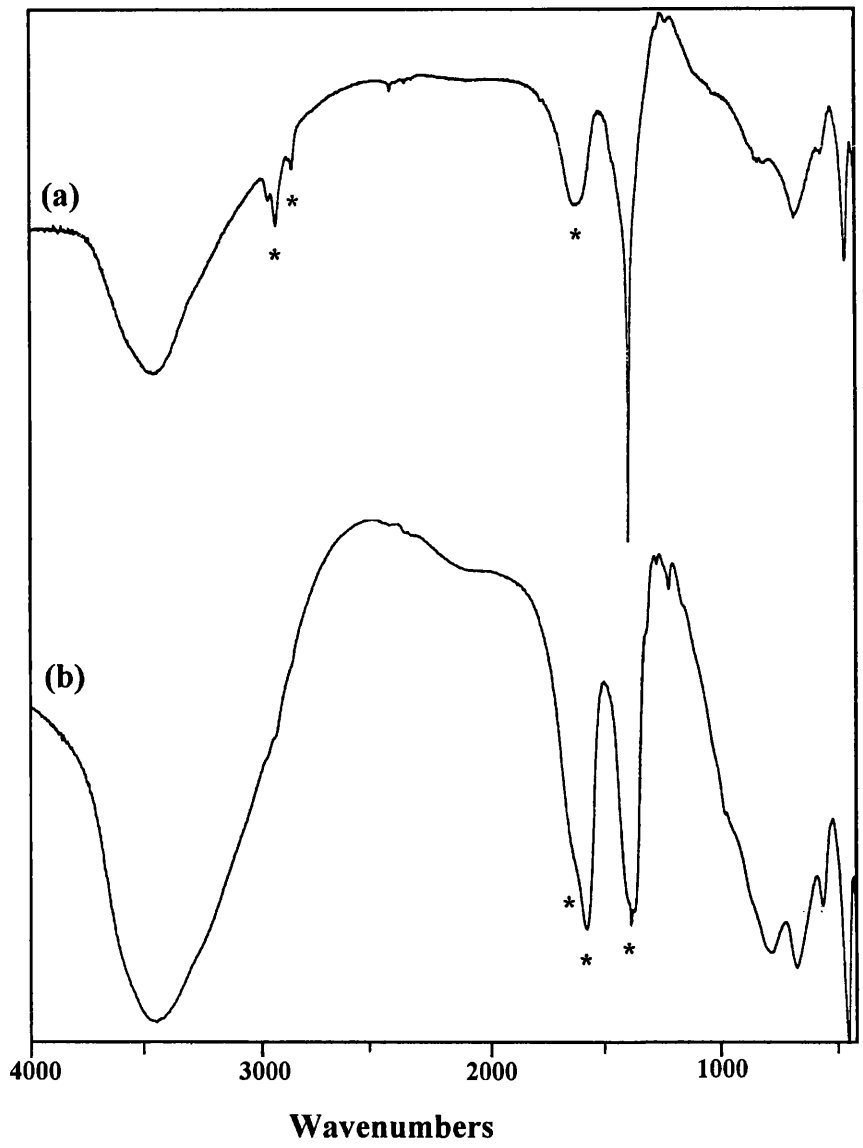

Figure 3.18 FTIR spectra obtained for (a) heated aspartate-LDH and (b) heated and base-treated aspartate-LDH. * indicate assignments for organic group vibrations.

(c) Chemical coupling reaction

The coupling of peptide amine and carboxylate groups with the formation of an amide linkage has been a widely used reaction among peptide chemists (Sheehan and Hess, 1955; Merrifield, 1963). The procedure makes use of a water soluble diimide which serves as the coupling agent forming a reaction intermediate by reacting at the carboxylate group and activating this group to further attack by the amino group (Scheme 3.2). The chemical modification of carboxylate groups of protein by employment of this reaction has also proved useful for the elucidation of the number of acidic residues present (Paus, 1978; Burkey and Gross, 1981; Woodhead and Malcolm, 1981). More recently the reaction has been adapted to incorporate hydrocarbon chains onto the external surface of the iron-storage protein ferritin and modify the external surface of the macromolecule (Wong *et al.*, 1997).

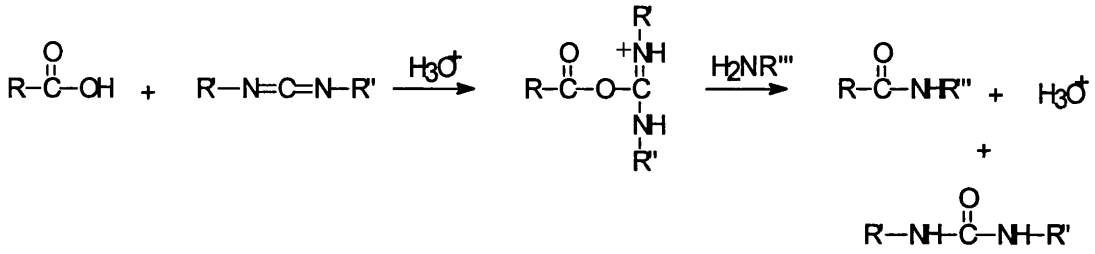

Scheme 3.2 Reaction between a carboxyl group and a nucleophile mediated by a carbodiimide

This reaction was therefore employed as an alternative way of achieving oligomerization of the intercalated aspartate monomers within an LDH.

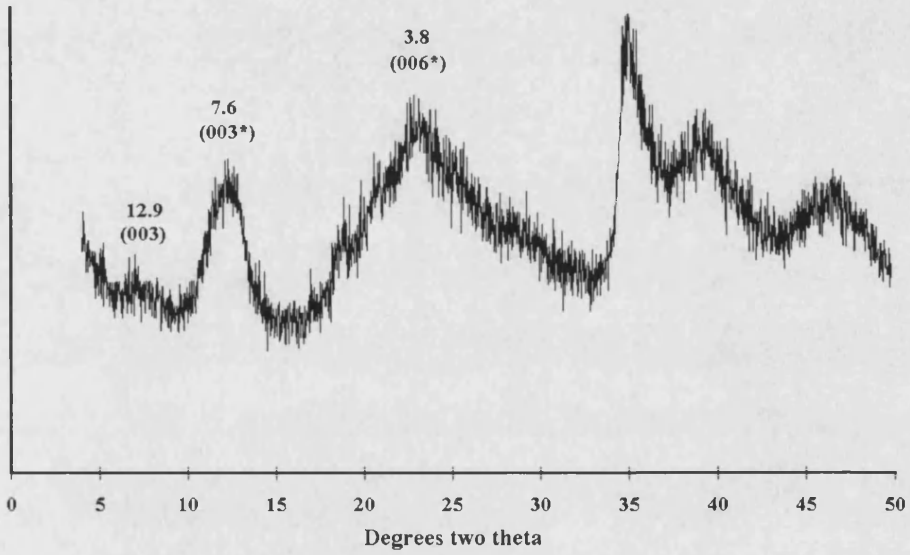

Figure 3.19 PXRD pattern obtained for LDH product of EDC-activated coupling reaction. Miller indices and *d*-spacings in Å are indicated.

Characterization of the reaction product confirmed coupling of the amino acids had taken place. From the XRD pattern the d_{003} peak was broad with a value for the interlayer spacing at the peak maximum of 12.9 Å (Figure 3.19). This was comparable to the results obtained for both the direct intercalation and thermal polymerization approach to polymer-clay nanocomposite synthesis and represented a 1.8 Å expansion in d-spacing from the 11.1 Å of the aspartate-LDH before reaction. No higher order harmonics of this phase were observed and from this the ordering within this face was deemed to be low. A second phase present in the XRD pattern had a basal d_{003}-spacing of 7.6 Å indicating the formation of a dominant carbonate-containing phase which reflected the observation in the thermal polycondensation reaction in which intercalated nitrate was replaced by carbonate under conditions of high amounts of dissolved CO_2.

The spectrum provided by the ^{13}C CP MAS NMR on the product of the reaction (Figure 3.20) revealed resonances strongly suggestive of amide bond formation. Most convincingly, the replacement of the single carboxylate peak at 180 ppm with peaks at 178 ppm (-COO-) and 173 ppm (-NH-C(O)-) (close to an inorganic carbonate peak at 171 ppm of similar intensity) correlated well with the changes in NMR spectrum reported during thermal polymerization of intercalated aspartate monomers (Figure 3.17) and may be compared with the spectrum obtained from the direct synthesis of polyaspartate-LDH (Figure 3.13a).

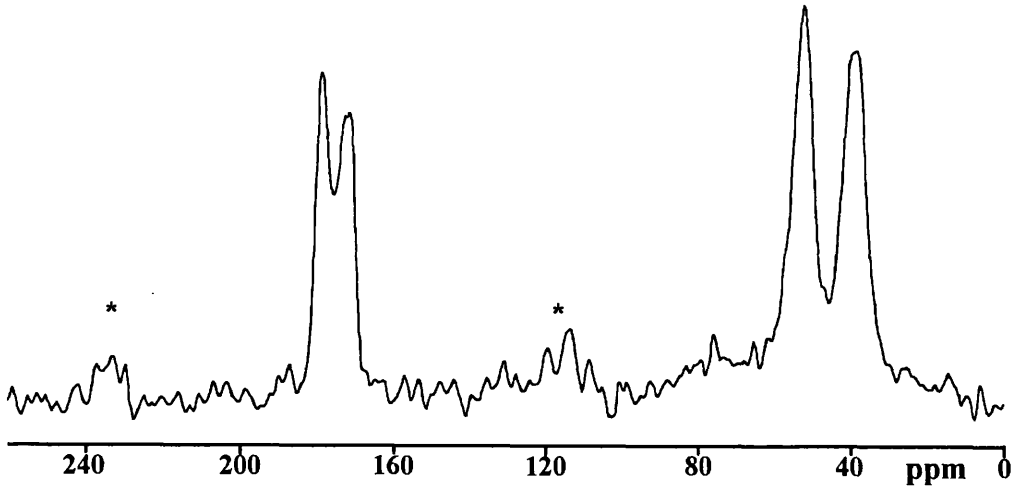

Figure 3.20 ^{13}C CP MAS NMR data for LDH product of EDC-activated coupling reaction. * indicate spinning sidebands.

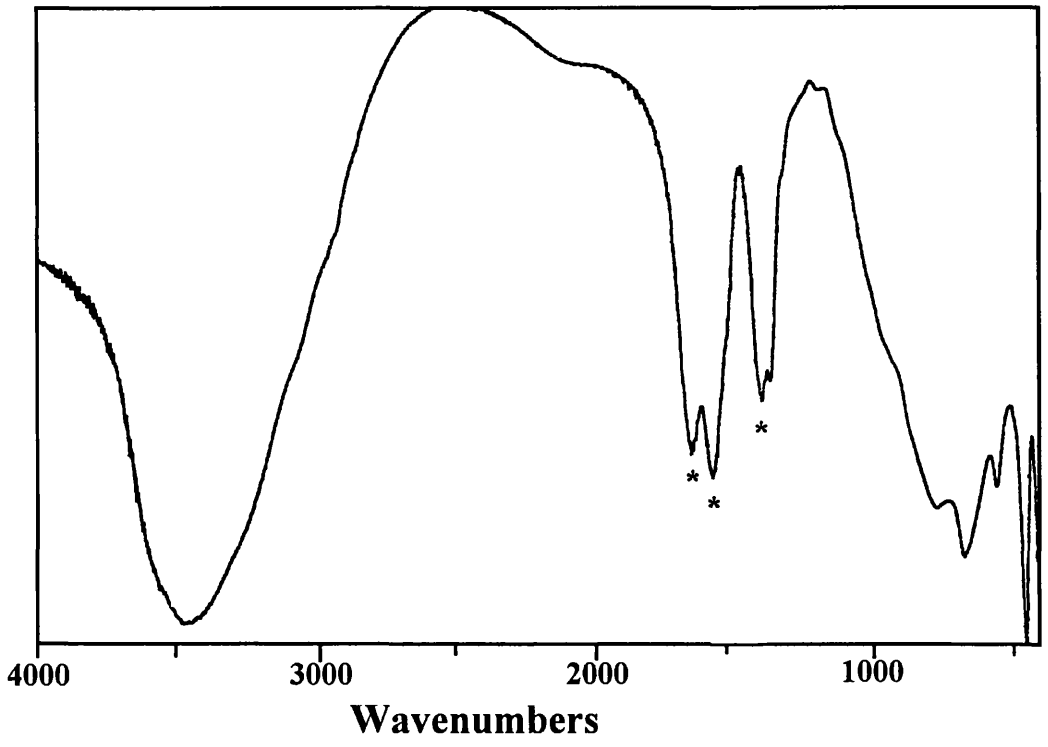

Figure 3.21 FTIR data for LDH product of EDC-activated coupling reaction. * indicate assignments for organic group vibrations.

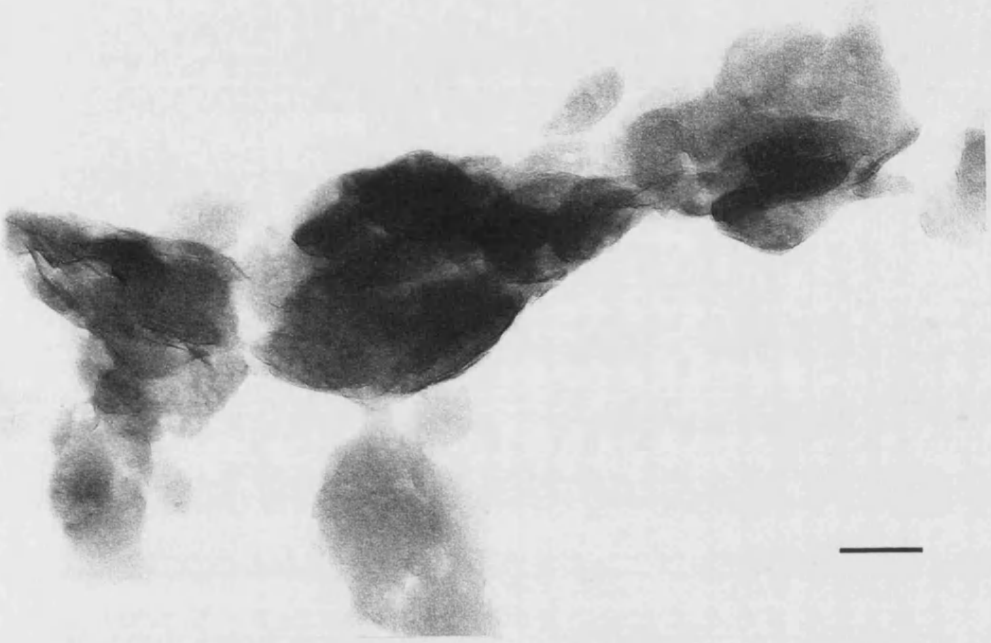

Figure 3.22 Transmission electron micrograph for the product of the EDC-activated coupling reaction. Scale bar = 50 nm.

FTIR spectroscopy showed a spectrum comparable with that obtained following thermal and base treatment of aspartate-LDH and polymer assignments could be made: carboxylate (1410 cm^{-1}, 1580 cm^{-1}) and amide (1650 cm^{-1}) (Figure 3.21). A chemical composition could be assigned on the basis of elemental analysis, NMR and FTIR data and allows for the co-intercalation of polycondensed aspartate monomers and inorganic carbonate ions.

A tentative chemical composition of $Mg_{0.6}Al_{0.3}(OH)_{1.8}[Asp^*]_{0.16}[CO_3]_{0.07}.4H_2O$ was calculated, based on the assumptions that all nitrate ions within the initial aspartate-LDH are exchanged for carbonate during the reaction and dianionic aspartate molecules undergoing coupling to yield monoanionic aspartate monomers The extent of coupling and the oligomeric/polymeric nature of the intercalated organics was not determined. It is, however, unlikely that the intercalated polymer was high in molecular weight.

Transmission electron micrographs of the sample revealed ovoid-shaped particles between 150-200 nm in size (Figure 3.22). Certain areas showed evidence of layering within the sample.

5-(Alkoxy)isophthalate-LDHs [ISA(C_n)-LDHs]

5-(Alkoxy)isophthalic acid amphiphiles have been recently studied as models for biomembranes (Van Genderen et al., 1996). Specifically, their behaviour as model compounds to study the structure and dynamics of high-temperature membrane structures was under investigation in these studies. The intercalation of these anionic

species within LDHs offered the possibility of creating similar bilayer membrane-type arrangements within the gallery spaces. ISA(C_n)-LDHs were prepared from basic solutions containing 5-(octyloxy)-, 5-(dodecyloxy)- and 5-(pentadecyloxy)isophthalate.

It was of interest to observe the effect of increasing chain length on the mode of intercalation of the organic dianionic species. However, from the XRD patterns it was immediately evident that the intercalation mode was not one in which the alkyloxy chains were oriented perpendicular to the inorganic sheets. The observed d_{003}-spacings for all three samples were between 12.9 Å and 13.1 Å (Figure 3.23 shows a representative pattern) with the slight increase in d-spacing being observed with increased alkoxy chain length. The expanded gallery height of 8.1-8.3 Å and knowledge of the dimensions of the isophthalate dianion implies an orientation whereby the carboxylate groups are directed towards the inorganic sheets, as in the earlier cases of aspartate and glutamate dianions, with the plane of the aromatic ring tilted perpendicular (or almost) to the layers. The alkoxy chains are positioned parallel to the hydroxyl layers and consequently increasing the length of the ether linkage did not significantly influence the interlayer separation. The broadness of the d_{003} peak indicated disorder within the system and no other (00*l*) reflections for an organic-intercalated phase were observed. However, there was evidence for a nitrate/carbonate intercalated phase due to a broad peak between 11-12 degrees 2θ. A reflection at 2.6Å, indexed to the (012) reflection was observed in the pattern, as previously in data from other intercalated-LDHs reported in this study.

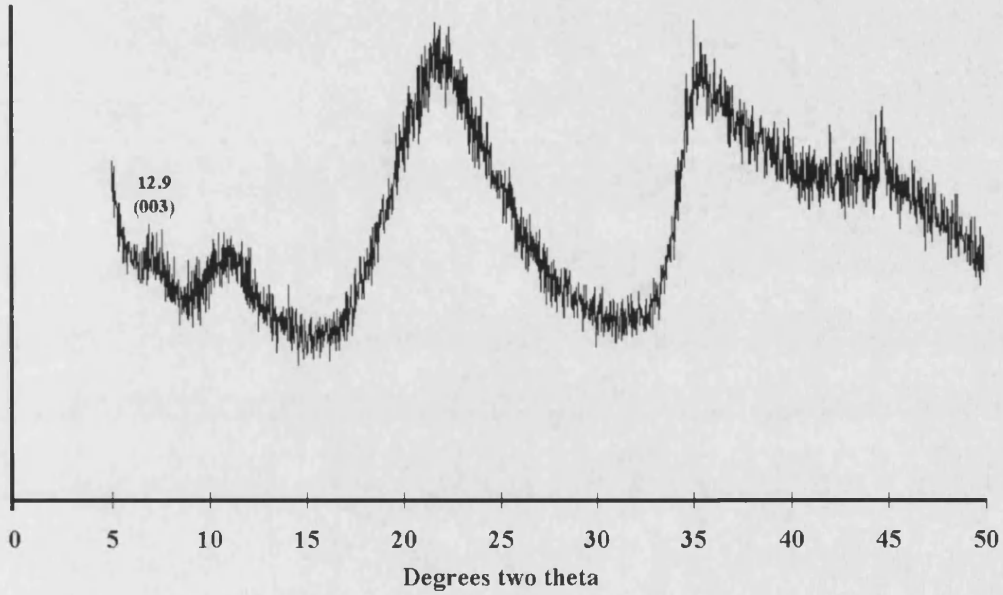

Figure 3.23 PXRD pattern for ISA(C_8)-LDH. Miller indices and *d*-spacing in Å shown.

Assignments in the FTIR could be made for the alkyloxyisophthalate dianion and co-intercalated nitrate/carbonate ions (Figure 3.24): C-O-C (1310 cm^{-1}), alkyl (1370 cm^{-1}, 2850-2980 cm^{-1}), CO_2^- (1420 cm^{-1}, 1550 cm^{-1}), aryl (1460 cm^{-1}, 1620 cm^{-1}), nitrate/carbonate (1385-1400 cm^{-1}).

^{13}C CP MAS NMR spectroscopy on ISA(C_8)-LDH afforded resonances from the intercalated organic species (Figure 3.25). The broadness of the aryl ring and carboxylate resonances suggests a lower mobility of these carbons in comparison to the sharper resonances from alkyloxy group carbons. It was concluded that carbonate was either absent or present in only small amounts due to the lack of a typically sharp carbonate signal around 170 ppm.

From transmission electron micrographs Moiré fringes were evident with spacings around 51 Å (Figure 3.26).

The adopted mode of intercalation of guest anions is non-trivial and is dependent on a number of factors, including the charge density on the metal hydroxyl layers, the degree of hydration (Kooli *et al.*, 1996), and the alkyl chain length, (Meyn *et al.*, 1990), electron density (Tagaya *et al.*, 1993) and relative positions of anionic groups (if more than one) on the guest (Bonnet *et al.*, 1996) species. Results of the intercalation experiments reveal that vertical alignment of the organic dianions within the interlayer for the alkyloxyisophthalate system under the synthesis conditions employed was disfavoured

Assignments in the FTIR could be made for the alkyloxyisophthalate dianion and co-intercalated nitrate/carbonate ions (Figure 3.24): C-O-C (1310 cm^{-1}), alkyl (1370 cm^{-1}, 2850-2980 cm^{-1}), CO_2^- (1420 cm^{-1}, 1550 cm^{-1}), aryl (1460 cm^{-1}, 1620 cm^{-1}), nitrate/carbonate (1385-1400 cm^{-1}).

^{13}C CP MAS NMR spectroscopy on ISA(C_8)-LDH afforded resonances from the intercalated organic species (Figure 3.25). The broadness of the aryl ring and carboxylate resonances suggests a lower mobility of these carbons in comparison to the sharper resonances from alkyloxy group carbons. It was concluded that carbonate was either absent or present in only small amounts due to the lack of a typically sharp carbonate signal around 170 ppm.

From transmission electron micrographs Moiré fringes were evident with spacings around 51 nm (Figure 3.26).

The adopted mode of intercalation of guest anions is non-trivial and is dependent on a number of factors, including the charge density on the metal hydroxyl layers, the degree of hydration (Kooli *et al.*, 1996), and the alkyl chain length, (Meyn *et al.*, 1990), electron density (Tagaya *et al.*, 1993) and relative positions of anionic groups (if more than one) on the guest (Bonnet *et al.*, 1996) species. Results of the intercalation experiments reveal that vertical alignment of the organic dianions within the interlayer for the alkyloxyisophthalate system under the synthesis conditions employed was disfavoured

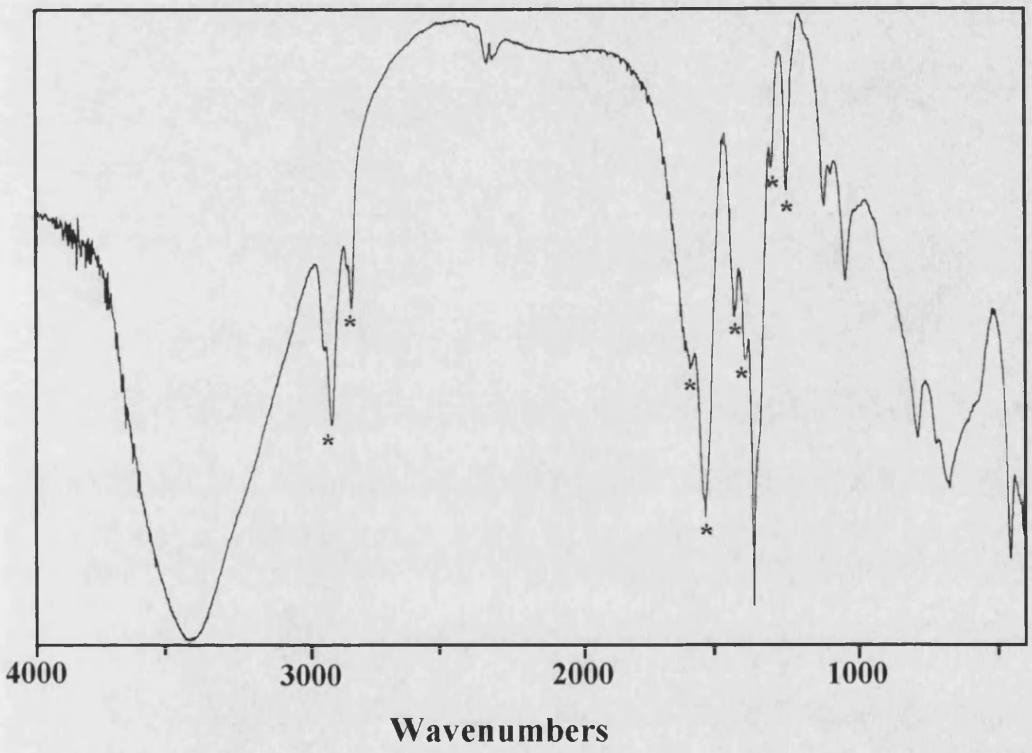

Figure 3.24 FTIR spectrum obtained for ISA(C_8)-LDH. * indicate assignments for organic group vibrations.

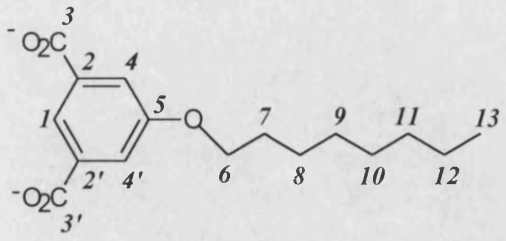

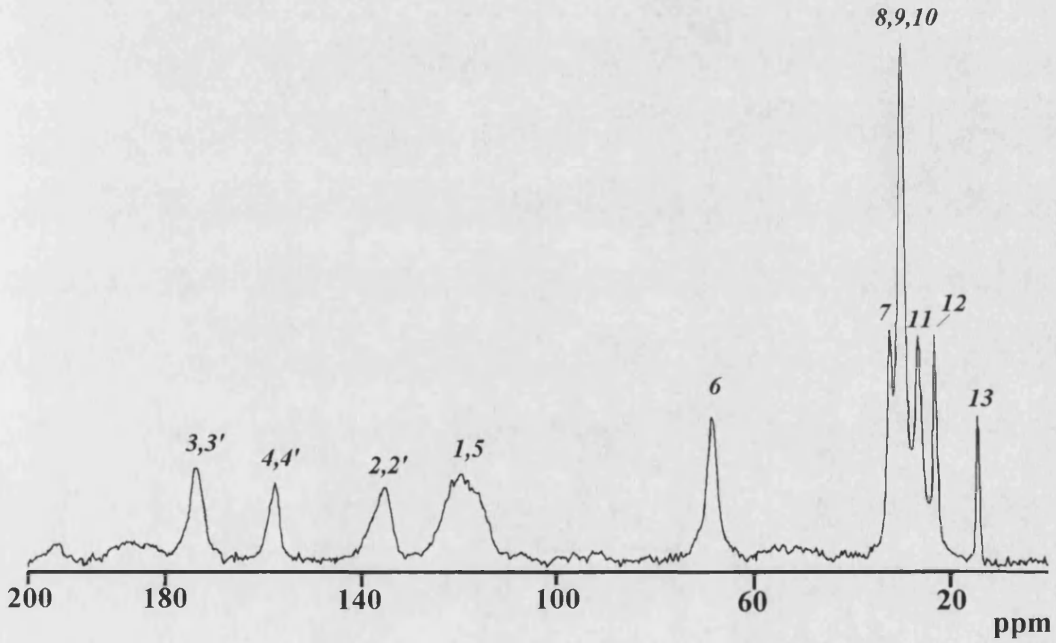

Figure 3.25 ^{13}C CP MAS NMR spectrum of ISA(C_8)-LDH.

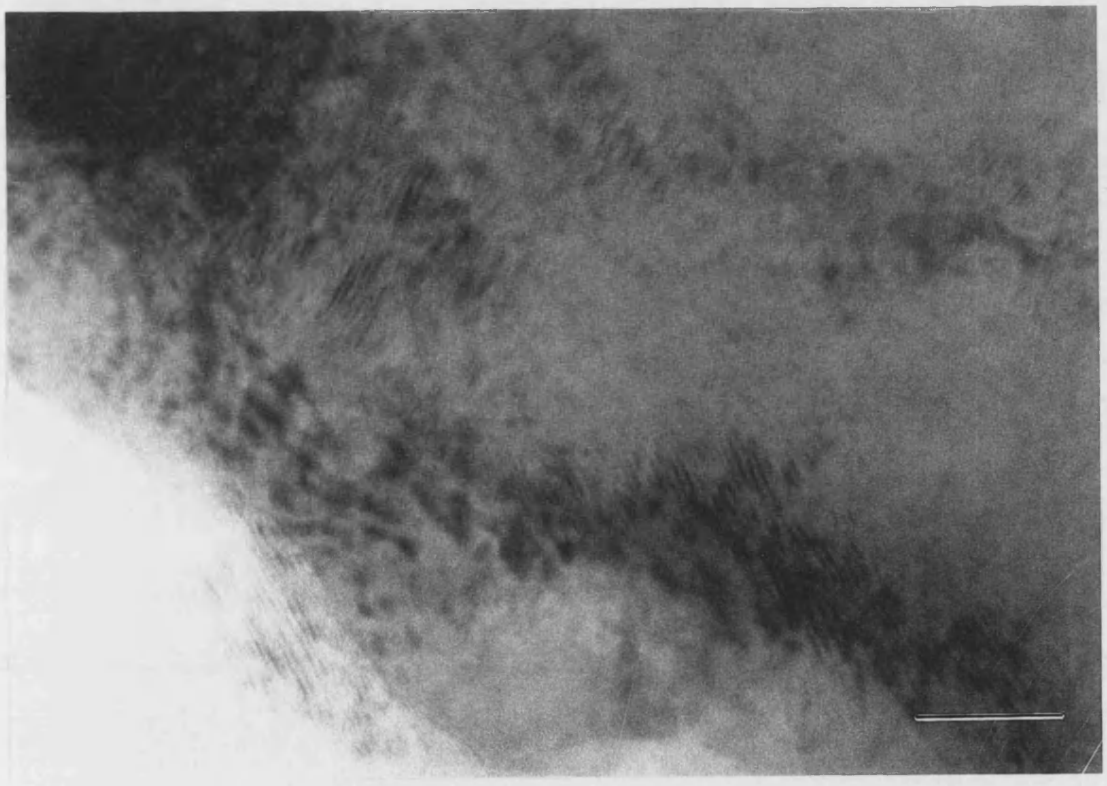

Figure 3.26 Transmission electron micrograph for ISA(C_8)-LDH. Scale bar = 100 nm.

3.4 *Conclusions*

The results of this study indicated the capability of accommodating acidic amino acids and polyamino acids within the interlayers of LDH materials by direct synthesis. Aspartate and glutamate monomers can be intercalated at 20 wt. % to produce expanded interlayer spacings and modified texture. Previous work has shown how basic amino acids; histidine, lysine and arginine; may be incorporated within acidic α- and γ- zirconium phosphates (Kijima et al., 1982; Kijima and Ueno, 1986). As such, the intercalation of acidic aspartate and glutamate amino acids provides a complementary system to the zirconium phosphate intercalates.

A biologically-relevant macromolecule, poly(α,β-aspartate), could be intercalated between LDH layers to form a laminated nanocomposite with *ca.* 15 Å repeat spacing. The synthesis of the polymer-LDH nanocomposite is one of only a few to be reported. The direct coprecipitation method surmounts the problems of high layer charge density which makes exfoliation and ion-exchange processes unsuitable and allows for a templating approach whereby the inorganic sheets are grown in the presence of the desired polyanion. The strong binding of the polymer in the interlayer, derived from the electrostatic attraction between itself and the metal hydroxyl sheets, is also believed to provide important kinetic stability against ion exchange (Oriakhi *et al.*, 1996).

In addition, a well-documented approach for the synthesis of polyaspartate, involving thermal treatment followed by base synthesis of aspartic acid, can be utilized to synthesize polymer-LDH nanocomposites *via* polycondensation of pre-intercalated aspartate monomers within the interlamellar spaces. A coupling reaction

usually employed by peptide chemists may also provide a route to oligomerisation of intercalated monomers and formation of an ordered layered nanocomposite.

It is hoped that the preparation of such bioinorganic hybrid materials may have uses arising from their potential bioactivity, biocompatibility and biodegradability. Polyaspartate is a biodegradable polymer, with good dispersing and sequestering properties (Donachy and Sikes, 1994). Its inclusion within clay host frameworks provides an interesting system which may afford further application possibilities.

Finally, it has been demonstrated that intercalated LDHs containing 5-(alkyloxy)isophthalate species can be prepared by the direct synthesis approach. Variation of the alkyloxy chain length of isophthalic acid derivatives had little effect on the resultant interlayer spacings of the intercalated LDHs. In all cases, the factor apparently dictating the intercalation mode was for the carboxylate groups on the isophthalate molecules to be directed towards adjacent brucite sheets.

CHAPTER 4

SYNTHESIS AND CHARACTERIZATION OF LAMELLAR MAGNESIUM (ORGANO)PHYLLOSILICATES BASED ON A 2:1 TRIOCTAHEDRAL TALC STRUCTURE

SYNTHESIS AND CHARACTERIZATION OF LAMELLAR MAGNESIUM (ORGANO)PHYLLOSILICATES BASED ON THE 2:1 TRIOCTAHEDRAL TALC STRUCTURE

4.1 *Introduction*

Silicate clay formation in nature is known to be dependent on silica concentration, pH and the nature of the metal ion which will constitute the octahedral sheet. Early synthetic studies showed how clay minerals would form from some (but not all) hydroxide-silica precipitates after only a few days aging at low temperatures (Harder, 1977). The importance of understanding the copolymerization processes between silicic acid and aqua metal ions, which are known to crystallize out as a variety of minerals at low temperatures, was recognized (Mizutani *et al.*, 1990a). Most importantly, the initiation of silicate gel formation could be accounted for in terms of the acid-base equilibria of silicic acid and aqua-metal ions [Equations (1) and (2) respectively] and relationship to the hydrolysis constants, [pK_a] and [pK_1*] respectively. (Mizutani *et al.*, 1990a).

$$\equiv Si\text{-}OH + OH^- \longleftrightarrow \equiv Si\text{-}O^- + H_2O \qquad [pK_a] \qquad (1)$$

$$M(OH_2)^{n+} + OH^- \longleftrightarrow M(OH)^{(n-1)+} + H_2O \qquad [pK_1^*] \qquad (2)$$

Different copolymerization mechanisms were proposed depending on whether the hydrolysis constant of the aqua-metal cation was of lower or higher pH than that of silicic acid ($pK_a = 9.8$). In general, increasing the pH of a solution causes M^{n+} gelation and formation of hydroxides. Under appropriate pH conditions, however, Si-O-M bonds as well as Si-O-Si and M-O-M bonds will form when Si^{4+} cations are combined in solution with M^{n+} cations.

A related study on the selective precipitation of 1:1 and 2:1 nickel and magnesium phyllosilicates (Mizutani *et al.*, 1990b) illustrated how in the case of the more highly acidic nickel ions ($pK_1^* = 6.5 - 10.6$) (Burgress 1978) crystallization of the phyllosilicate was faster than with the less acidic magnesium ion ($pK_1^* = 12.2 - 12.8$) (Burgress, 1978). The stronger tendency of nickel ions to bond oxygen atoms and form octahedral nickel oxide layers was tentatively proposed as resulting in faster nucleation of phyllosilicate crystals. The aquamagnesium ion is less acidic and slow to form the octahedral magnesium oxide sheet. Moreover, the silicate anion, which is more quickly formed, can condense with silicic acid as well as aquamagnesium ions and these competitive reactions result in the formation of a poorly crystalline phyllosilicate.

The 2:1 trioctahedral phyllosilicate, talc, with an ideal structural formula of $Mg_3Si_4O_{10}(OH)_2$, and consisting of uncharged inorganic layers, each constructed from an octahedrally-coordinated magnesium oxide/hydroxide (brucite) sheet overlaid on both sides with a sheet of silica tetrahedra, can be prepared under hydrothermal conditions. In a synthesis involving the reaction between soluble silica and powdered magnesium hydroxide, well-crystallized talc was formed with a layered serpentine mineral, $Mg_3Si_2O_5(OH)_4$, being identified as a reaction intermediate. The

serpentinization of $Mg(OH)_2$ involved the linking of SiO_4 tetrahedra to Mg-(O,OH) octahedral sheets (Muraishi, 1981).

Recent publications have employed organofunctional trialkoxysilanes, $RSi(OEt/Me)_3$, to produce lamellar organically-functionalized magnesium, nickel and aluminium silicate clays with structures analogous to the inorganic 2:1 phyllosilicates (Fukushima and Tani, 1995; Ukrainczyk *et al.*, 1997; Burkett *et al.*, 1997). The sol-gel based synthetic method involved the precipitation of the inorganic smectite-like framework from mixed alcohol/water solutions containing organotrialkoxysilane, metal salts and sodium hydroxide. Prepared magnesium organosilicates had the same inorganic structural arrangement as the parent 2:1 trioctahedral phyllosilicate, talc, with an Si-C bond on each silicon providing a covalent linkage between the inorganic framework and the organic functionalities (Figure 1.12). The organic substituents occupied the interlamellar spaces between adjacent inorganic sheets. Studies on the formation of inorganic 2:1 trioctahedral phyllosilicates had postulated that the central octahedrally-coordinated brucite sheet forms first in solution, then acts as an incipient template for the condensation of the tetrahedral silica sheets (Carrado, 1992). This proposal, one in which the preferred octahedral coordination of the magnesium ion is the primary structural determinant, was similarly suggested for the generation of organically-functionalized magnesium (and nickel) phyllosilicates (Fukushima and Tani, 1995; Burkett *et al.*, 1997). An analogy was drawn between the self-assembly of layered zirconium organophosphonates in that structure formation is directed by the coordination geometry of the inorganic components.(Cao *et al.*, 1992) Additional contributing factors such as the limited coordination of the organotrialkoxysilane units, the hydrophobicity of the organic moieties and the resulting microphase

segregation may also facilitate the formation of the lamellar structures. In the case of the organically-functionalized aluminium silicates a 2:1 dioctahedral phyllosilicate structure resulted. More interesting was the proposed template synthesis of the layered inorganic framework, which proceeds *via* the self-assembly of lamellar micelles of silane triols to direct the condensation and generation of the inorganic framework, implying a more biomimetic approach to synthesis (Ukrainczyk *et al.*, 1997).

In principle, it seemed reasonable to propose that the use of organotrialkoxysilanes in this one-step approach could be of general use for the fabrication of chemically-functionalized hybrid 2:1 trioctahedral phyllosilicates. In the following chapter a selection of functionalized trialkoxysilanes are employed in the synthesis of magnesium organosilicates with a view to characterizing the reaction products and utilizing the characterization data to elucidate further information into the formation mechanism. Organotrialkoxysilanes, however, exhibit a more varied hydrolysis/condensation behaviour than silicic acid, being sensitive to a number of reaction conditions including pH, catalyst, solvent, $Si:H_2O$ molar ratio and the nature of the organic R group (Brinker and Scherer, 1990). It was therefore envisaged that, in practice, optimization of reaction conditions may be necessary as the nature of the organic substituent was varied.

4.2 *Experimental*

Materials

Magnesium chloride hexahydrate (99 %) was obtained from Aldrich Chem. Co. Sodium hydroxide solutions were freshly prepared using NaOH pellets (97 %) from Aldrich Chem. Co. Methyltriethoxysilane (99 %) and aminopropyltriethoxysilane (99 %) were obtained from Aldrich Chemical Co. Octyltriethoxysilane (> 97 %) was obtained from Fluka. Hexadecyltrimethoxysilane, (3-(2-aminoethyl-3-aminopropyl)trimethoxysilane, dihydro-triethoxysilylpropyl-1H-imidazole, 1-propenyltrimethoxysilane, 3-methacryloxypropyltrimethoxysilane and 3-glycidyloxypropyltrimethoxysilane were obtained from Apollo Scientific Ltd. and were of unknown purity. All materials were used without further purification. Doubly-distilled and deionized water was used during preparation and washing stages (Chapter 2: ***General Methods***). Bench ethanol (94-96 %) was employed during preparation and washing stages.

Standard synthesis of magnesium (organo)phyllosilicates

The standard synthetic procedure employed a direct one-step approach, in which products were precipitated from basic ethanolic solutions.(Fukushima and Tani, 1995) Typically, magnesium chloride hexahydrate, $MgCl_2 \cdot 6H_2O$, (1.68 g, 8.3 mmol) was charged to a reaction vessel and ethanol (50 ml) was added. Stirring was

employed to dissolve the magnesium salt. Organotrialkoxysilane, $RSi(OR')_3$, (11.1 mmol) was added, under rapid stirring, followed immediately by the addition of sodium hydroxide solution (200 ml, 0.05 M, 10 mmol). The resultant reaction mixture was stirred at room temperature for 24 h. The product of the reaction was isolated by filtration or centrifugation, washed with copious water (200 ml) and ethanol (50 ml), and dried in air at 50 °C for 24 h.

The amount of organotrialkoxysilane added in each case was equal to the stoichiometric amount required to synthesize materials with the empirical formula $Mg_6Si_8R_8O_{16}(OH)_4$, Si/Mg = 1.33. This procedure was employed for syntheses using the following organosiloxanes (Table 4.1): the aliphatic organofunctional trialkoxysilanes: methyltriethoxysilane, (MTES), octyltriethoxysilane, (OTES), hexadecyltrimethoxysilane, (HDTMS); and the functionalized organotrialkoxysilanes, 1-aminopropyltriethoxysilane, (ATES), (3-(2-aminoethyl-3-aminopropyl)trimethoxysilane, 'ethylenediamine'-containing, (EDTMS), dihydro-triethoxysilylpropyl-1H-imidazole, (ITES), 1-propenyltrimethoxysilane (allyl-containng, ALTMS), 3-methacryloxypropyltrimethoxysilane, (MPTMS), 3-glycidyloxypropyltrimethoxysilane (epoxide-containing, EPTMS). The products of the standard syntheses employing the respective organotrialkoxysilanes were given the prefix Mg-.

Ethanolic, base-free synthesis of magnesium aminopropyl- and ethylenediamine-containing (organo)phyllosilicates

An alternative method for preparation of Mg-ATES and Mg-EDTMS employed base-free, ethanolic conditions. Magnesium chloride hexahydrate, $MgCl_2 \cdot 6H_2O$,(1.68 g, 8.3 mmol) was dissolved in ethanol (50 ml) and organotrialkoxysilane (ATES or EDTMS) (11.1 mmol) was added with rapid stirring. Immediate clouding of the solution followed by copious precipitation ensued after 5 min stirring. The reaction mixture was left stirring at room temperature for 24 h. The product of reaction, pale yellow in coloration, was isolated by filtration and washed thoroughly with ethanol (200 ml) and water (50 ml) and dried in air at 70 °C for 48 h.

The products of the base-free syntheses were given the abbreviated names Mg-H^+EDTMS and Mg-H^+ATES for reasons which will be explained in the ***Results and Discussion*** section.

Synthesis of (organo)phyllosilicates using mixed organotrialkoxysilanes systems

(a) Standard synthesis

Magnesium chloride hexahydrate, $MgCl_2 \cdot 6H_2O$,(1.68 g, 8.3 mmol) was dissolved in ethanol (50 ml). A stoichiometric molar amount of organotrialkoxysilane (11.1 mmol) was added containing molar ratios of octyltriethoxysilane: methyltriethoxysilane of O20%:M80%, O25%:M75%, O50%:M50%, O80%:M20%

and hexadecyltrimethoxysilane:methyltriethoxysilane of H30%:M70%. Sodium hydroxide solution (200 ml, 0.05 M, 10 mmol) was added with rapid stirring and the reaction mixture left stirring for 48 h at room temperature. Products were isolated by centrifugation, washed with copious water (200 ml) and ethanol (50 ml), and dried at 50 °C in air for 24 h.

(b) Synthesis in ethanolic conditions using solid NaOH

An alternative synthesis approach employed mixed organotrialkoxysilane ratios and solid sodium hydroxide pellets as the source of base. Typically, magnesium chloride hexahydrate, $MgCl_2 \cdot 6H_2O$, (1.68 g, 8.3 mmol) was dissolved in bench ethanol (50 ml) A stoichiometric amount of organotrialkoxysilane, (11.1 mmol), was added under rapid stirring in molar ratios: O20%:M80%, O25%:M75%, O50%:M50% and H30%:M70%. The colourless solution was allowed to mix for a short time before the addition of NaOH pellets (0.4 g, 0.1 mol). With stirring, the pellets were allowed to dissolve slowly in the reaction mixture. After a short period of time (5 min) clouding to the mixture was apparent and the precipitation became more copious with time. Stirring was continued at room temperature for 24 h. Solid products were isolated by filtration and washed thoroughly with water (200 ml) to remove excess NaOH and magnesium salts and finally with ethanol (100 ml). The solids were dried at 60 °C in air for 48 h.

Characterization

Powder XRD, microanalysis and FTIR data was routinely collected for all samples. Solid state ^{13}C NMR and ^{29}Si NMR was carried out using the EPSRC service at Durham University. Thermal analysis data was recorded at English China Clays International, St. Austell. Electron microscopy and energy dispersive X-ray analysis (EDXA) was performed using JEOL 1200 EX and JEOL 200 FX transmission electron microscopes. Unless stated otherwise samples for TEM were prepared as dilute dispersions in ethanol. Thin sections for TEM were prepared by stirring dried and ground magnesium (organo)phyllosilicate samples in a TAAB/T02BH resin mix overnight. Aliquots of resin/clay samples were transferred to moulds and heated in an oven at 60 °C for 24h. Thin sections of 2-10 nm thickness were microtomed from the hardened samples. Further details of the characterization procedures employed are given in Chapter 2: ***General Methods***.

Table 3.1 Organically-functionalized trialkoxysilanes used in the syntheses of layered magnesium (organo)phyllosilicates

Abbreviated Name	Structure
MTES	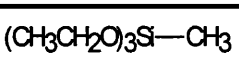
OTES	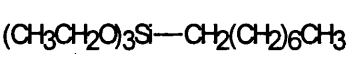
HDTMS	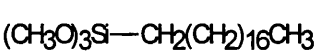
ATES	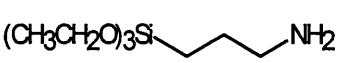
EDTMS	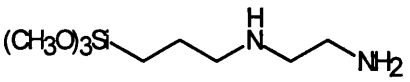
ITES	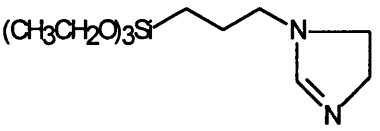
ALTMS	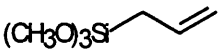
MPTMS	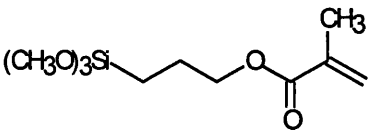
EPTMS	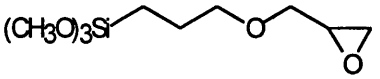

4.3 *Results and Discussion*

Magnesium was employed as the metal ion to constitute the octahedral sheet of the 2:1 structure in all syntheses. Magnesium(II) has an ideal ionic radius (0.65 Å) for 6-fold coordination in an octahedral site, whilst difficulties have been observed for the installation of other ions, eg. Al(III) (0.57 Å), in such positions during low temperature silicate synthesis (Harder, 1977). A reportedly good epitaxial match at the brucite Mg(O,OH) - tetrahedral silica interface also facilitates the formation of the layered 2:1 silicate structure (Carrado, 1992). Moreover the decision to synthesize magnesium (organo)phyllosilicates was due, in part, to the slow hydrolysis kinetics of the aqua magnesium ion which, it was hoped, would complement the hydrolysis/condensation kinetics of the organotrialkoxysilane and limit phase separation

Ethanol was employed in the preparations due to its ability to solubilize organotrialkoxysilanes, magnesium chloride and aqueous catalysts alike. It is the preferred solvent used in sol-gel preparations and is less toxic than methanol.

Standard syntheses of magnesium (organo)phyllosilicates

Synthesis of the desired layered organosilicate structure was primarily confirmed by a typical powder X-ray diffraction pattern (Figure 4.1). Despite reflections being broadened in the functionalized silicate pattern compared to those of the parent inorganic talc (JCPDS card 13-0558), assignments could be made based on

the 2:1 trioctahedral phyllosilicate smectite structure (MacEwan, 1961). Reflections from clays are generally broad since the crystals are thin and layer stacking is frequently turbostratically disordered (Brown and Brindley, 1980). In the case of the hybrid materials the incorporation of the organic functionalities in the structure was expected to further increase the disorder. The intralayer reflection at ~59° 2θ ($d_{060,330}$ = 1.56-1.57 Å) is characteristic of the 2:1 trioctahedral phyllosilicate structure (Carrado *et al.*, 1991) and was observed in the XRD patterns of all the magnesium (organo)phyllosilicates synthesized. The presence of this reflection indicated not only the successful formation of the smectite-like structure, but also the ability of the layered inorganic framework to accommodate a range of pendent organic functionalities without losing long-range periodicity.

Table 4.2 Interlayer spacings for as-synthesized magnesium (organo)phyllosilicates.

Magnesium (Organo)phyllosilicate	Interlayer d_{001}-spacing (Å)
talc [JCPDS card 13-0558]	9.34†
Mg-MTES	8.9
Mg-ALTMS	11
Mg-ITES	13.1
Mg-MPTMS	13.7
Mg-ATES	14.2
Mg-EDTMS	15.3
Mg-EPTMS	15.9

†Value for d_{002}, with two 2:1 trioctahedral phyllosilicate sheets per unit cell.

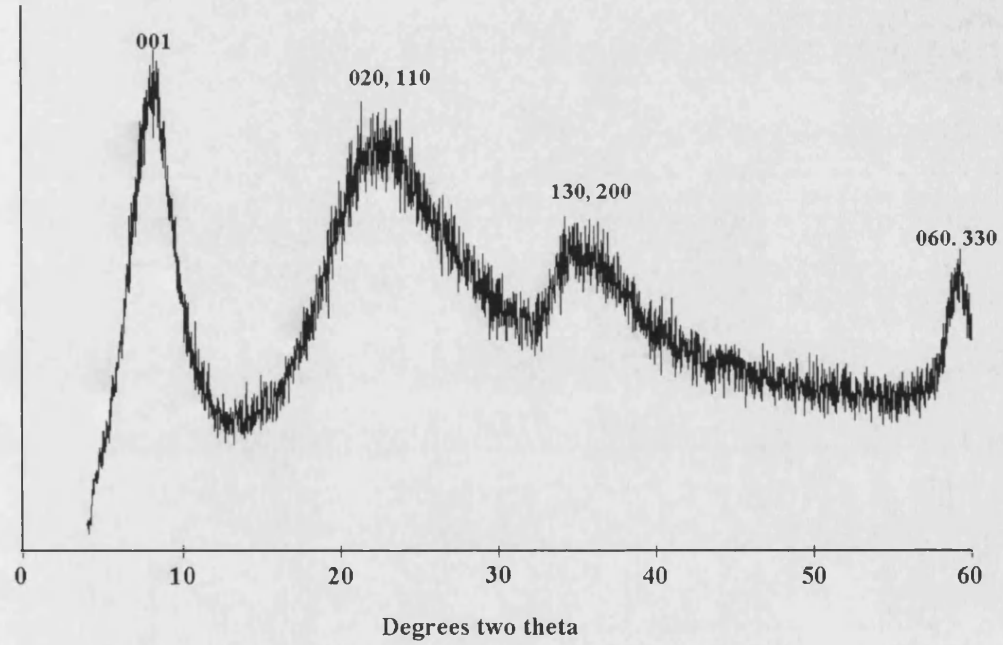

Figure 4.1 PXRD pattern for Mg-ALTMS, typical for as-synthesized magnesium (organo)phyllosilicates. Reflections from the 2:1 trioctahedral phyllosilicate structure are indicated.

The interlayer spacings, d_{001}, were measured directly from the position of the diffraction peak at the lowest angle of 2θ on the patterns. The high intensity and broadness of this peak indicated short-range ordered stacking of the adjacent organic/inorganic layers. Table 4.2 shows the expanded interlayer spacings (with the exception of Mg-MTES) observed compared to talc; the expansion due to the necessary accommodation of the organic functionalities in the gallery regions between adjacent inorganic sheets. The thickness of a 2:1 tetrahedral-octahedral-tetrahedral sheet in talc is approximately 9Å and gallery spaces for the magnesium organosilicates of between 2.0 Å and 6.9 Å were observed. These heights were too small to be consistent with a bilayer motif considering the dimensions of the fully-extended organic moieties, and instead suggested possible interdigitation or a disordered arrangement of the organic moieties.

In the case of octyl-containing Mg-OTES and hexadecyl-containing Mg-HDTMS materials the XRD patterns were not indexable to the 2:1 trioctahedral phyllosilicate structure. Instead the pattern consisted of reflections assignable to synthetic brucite ($Mg(OH)_2$) (JCPDS card 7-239) and an additional peak at approximately 22° 2θ assignable to amorphous silica (Figure 4.2). In this instance phase separation of the magnesium and silicon components had occurred and the results of this observation will be discussed later in the chapter.

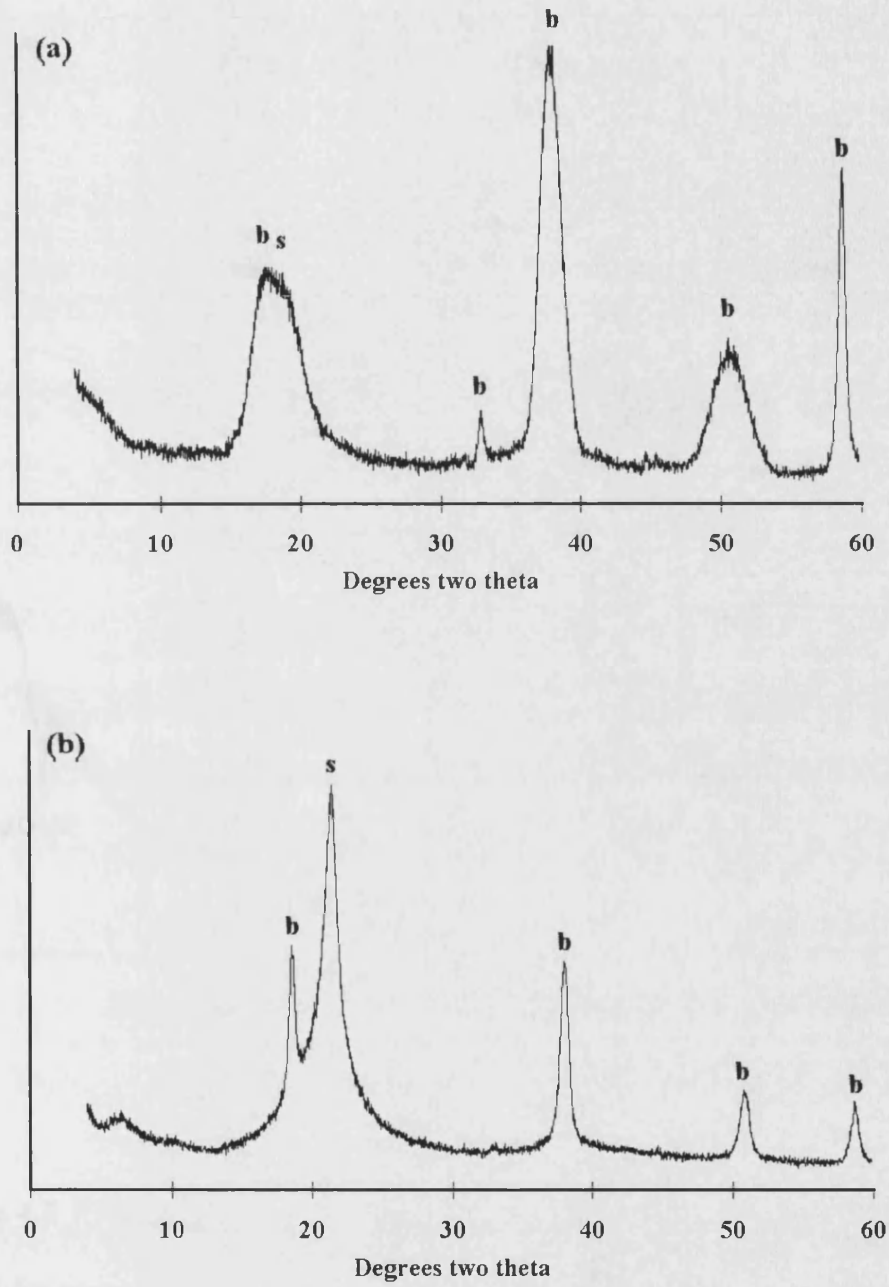

Figure 4.2 PXRD patterns for the products of the standard syntheses employing (a) octyltriethoxysilane and (b) hexadecyltrimethoxysilane. **b** indicates reflections from a brucite phase (JCPDS card 7-239). **s** indicates reflections from an amorphous silica phase.

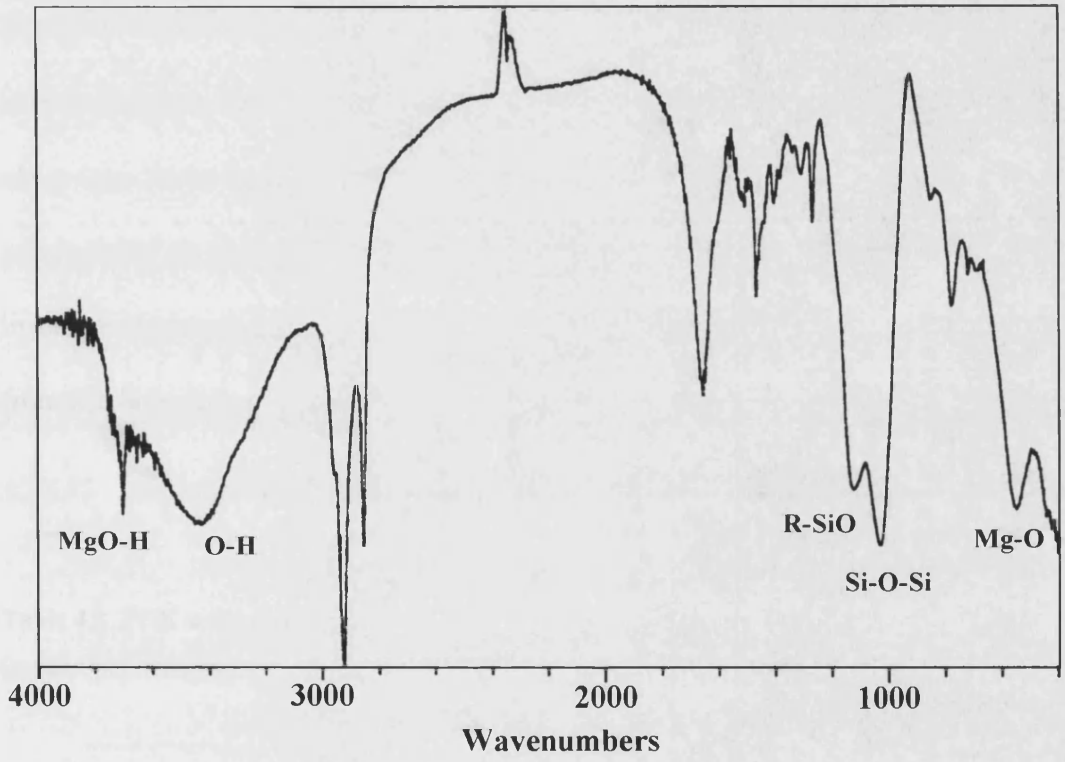

Figure 4.3 FTIR spectrum for Mg-ITES showing inorganic framework absorptions typical for as-synthesized magneium (organo)phyllosilicates.

Those organosilicates exhibiting the 2:1 trioctahedral phyllosilicate structure, showed characteristic framework vibrational modes in the infra-red spectra (Figure 4.3). Assignments included the Mg-O stretch (500-550 cm^{-1}), Si-O-Si within a 2:1 phyllosilicate (1015-1040 cm^{-1}) (Kermarec *et al.*, 1994), Si-C (1120-1200 cm^{-1}), O-H from adsorbed water and silanol groups (3400-3450 cm^{-1}) and MgO-H (3700 cm^{-1}) (Kermarec *et al.*, 1994). In addition, resonances from organic vibrational modes indicated the presence of the organic entities within the layered structures and observed vibrations at 1120-1200 cm^{-1} showed the retention of the Si-C bond. Major assignments for the organic vibrational modes are given in Table 4.3; in some instances, however, functional group vibrations were obscured by broad absorptions from the inorganic framework.

Table 4.3 FTIR assignments for organic vibrational modes within as-synthesized magnesium (organo)phyllosilicates.

	Organic Assignments (cm^{-1})
Mg-MTES	2975, 2880, 1470, 1380 ($-CH_3$), 1200 (Si-C)
Mg-ATES	3600-3200 ($-NH_2$), 2935,2840 ($-CH_2-$), 1600 ($-NH_2$), 1450 ($-CH_2-$), 1150 (Si-C), 800 ($-CH_2-$)
Mg-EDTMS	3600-3200 ($-NH_2$), 2935,2850 ($-CH_2-$), 1597 (1°-NH_2), 1510 (2° -NH-), 1460 ($-CH_2-$), 1100 (Si-C), 800 ($-CH_2-$)
Mg-ITES	2920, 2850 ($-CH_2-$), 1655 (C=N), 1470 ($-CH_2-$), 1125 (Si-C), 780 ($-CH_2-$)
Mg-EPTMS	3100 (epoxide $-CH_2-$), 3000 (epoxide -CH-), 2937,2850 ($-CH_2-$), 1450-1400 ($-CH_2-$), 1345 (epoxide -CH-), 1201 (Si-C)
Mg-MPTMS	3100 ($=CH_2$), 2900-2850 ($-CH_2-$), 1720 (C=O), 1610 (C=C), 1430 ($-CH_2-$), 1380 ($=CH_2$), 800 ($-CH_2$)
Mg-ALTMS	3050 (=CH), 2950-2850 ($=CH_2$, $-CH_2-$), 1620 (C=C), 1400 ($-CH_2-$), 1380 ($=CH_2$), 900 (H-C=), 880 ($-CH_2-$)

Solid state ^{13}C CP MAS NMR spectroscopy was essential for proof of the integrity of the organic components to the synthesis conditions employed. Figures 4.4 to 4.9 show spectral data and assignments for the organic species present. In all cases the ^{13}C CP MAS NMR spectra could be assigned to complete and unreacted functionalities. On occasions rogue peaks were observed (30 ppm, 33 ppm and 166 ppm) which, due to their recurrence in spectra of different samples, were attributed to impurities within the sample. In general, the magnesium organosilicates showed broad linewidth resonances (3-10 ppm), with the exception of the epoxide-containing Mg-EPTMS (Figure 4.5), which displayed resonances with very narrow line widths (~ 1 ppm). Linewidth broadening in the ^{13}C NMR spectra was indicative of disordered arrangements for the organic functionalities occupying the interlayer region, which result in dispersions of isotropic chemical shifts, and incomplete averaging of the signals from chemically-alike carbons by the MAS technique. Broadening of signals may also be a reflection of the rigidity of the environment in which the carbon centres are held whereby suppression of molecular tumbling generates static disorder within a sample. Where broad peaks were observed exact assignments were often difficult due to overlapping of signals. This was the case in the data from the Mg-ITES sample (Figure 4.4), whilst an additional broadening of the spectral lines may have arisen from ^{13}C-^{14}N dipolar coupling (Naito *et al.*, 1981). The narrow linewidths shown in the spectrum of Mg-EPTMS implied a greater ordering and/or mobility of the epoxide-containing functionalities in the interlayer region (Figure 4.5). The Mg-MPTMS spectrum (Figure 4.9) exhibited resonances with varying linewidths which indicated varying degrees of success of magic angle sample spinning in resolving the chemical shift anisotropies of "like" carbons to single isotropic signals which may be

due to a variation in the mobilities of different organic groups. For example, the methyl signal in the Mg-MPTMS structure was intense and narrow, most probably a reflection of the high mobility and unique relaxation characteristics of this organic group.

Solid state ^{29}Si direct polarization (DP) MAS NMR spectroscopy provided information on the condensed state of the two-dimensional polysiloxane network within the (organo)phyllosilicate structure (Figures 4.10 to 4.15). Three distinct peaks for silicon atoms with different degrees of condensation are possible which are given the notation T^n; where T refers to the oxo trifunctional R'-SiO_3 units, and n is the number of Si-O-Si/Si-O-Mg bridging oxygens attached to each central unit. For example, a T^1 peak represents a silicon atom with one siloxane-type bond and two hydroxy (or ethoxy) substituents. For all organosilicates the NMR data showed that the condensation (the relative number of siloxane bonds to each silicon atom) in the network polysiloxanes was incomplete. Evidence for this was illustrated by resonances from T^1 (-49 to -50 ppm) and T^2 (-55 to -61 ppm) species in addition to the fully-condensed T^3 (-65 to -71 ppm). The single pulse technique used to acquire the ^{29}Si NMR data allowed for deconvolution of the spectra and the provision of quantitative data on the contributory percentages from each T^n species (data given in tables in Figs 4.10 to 4.15). Incomplete condensation was predictable due to the imposed geometric constraints as the silanols pack and slow condensation kinetics of the silanol derivatives. Interestingly, the less-condensed T^2 and T^1 species only were observed in both the Mg-ATES and Mg-EDTMS (Figure 4.12 and 4.13, respectively), whilst in the case of the 'imidazole'-containing Mg-ITES sample (Figure 4.10) the amount of T^3 in the sample was very low. By comparison, for other magnesium

organosilicates, the relative amounts of condensation species observed was generally $T^3 > T^2 > T^1$. Amine-containing organofunctional trialkoxysilanes have a disfavoured condensation chemistry, which results from a stabilization of the silanol-containing hydrolysis product through hydrogen-bonding with the amine functionality (Ishida *et al.*, 1982). This may be a contributing factor for the lack of fully-condensed T^3 in the amino-containing samples.

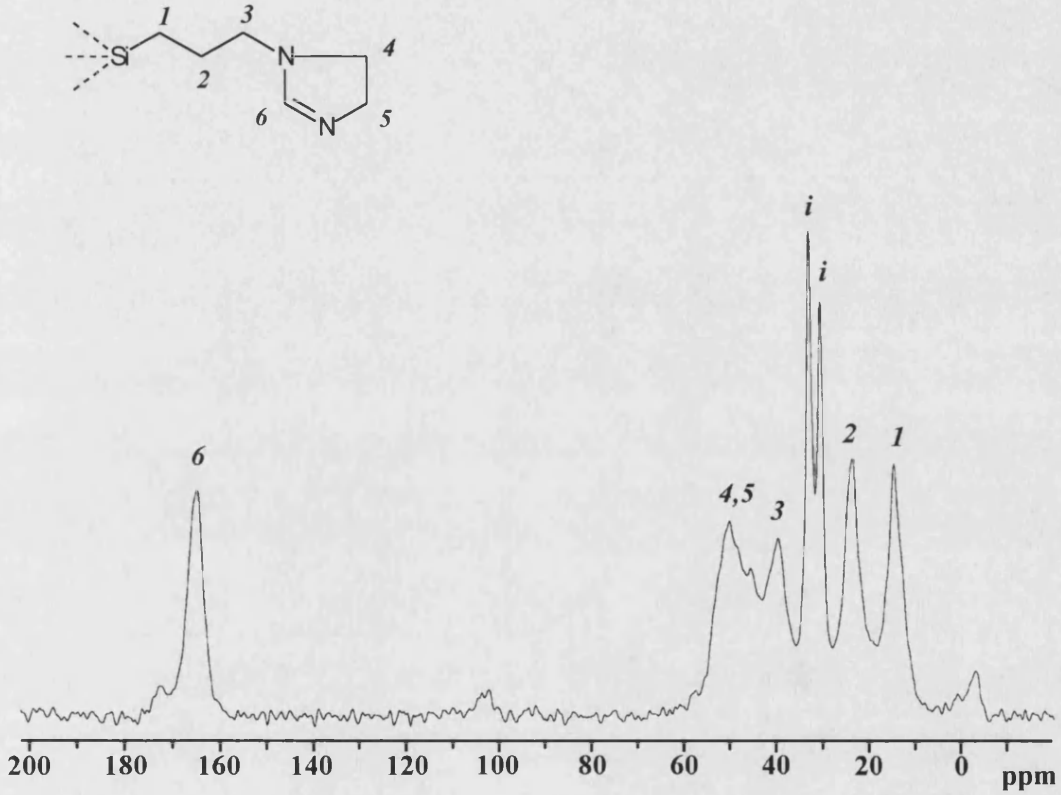

Figure 4.4 ^{13}C CP MAS NMR spectrum of Mg-ITES. ***i*** = impurity.

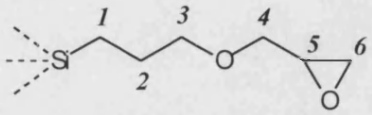

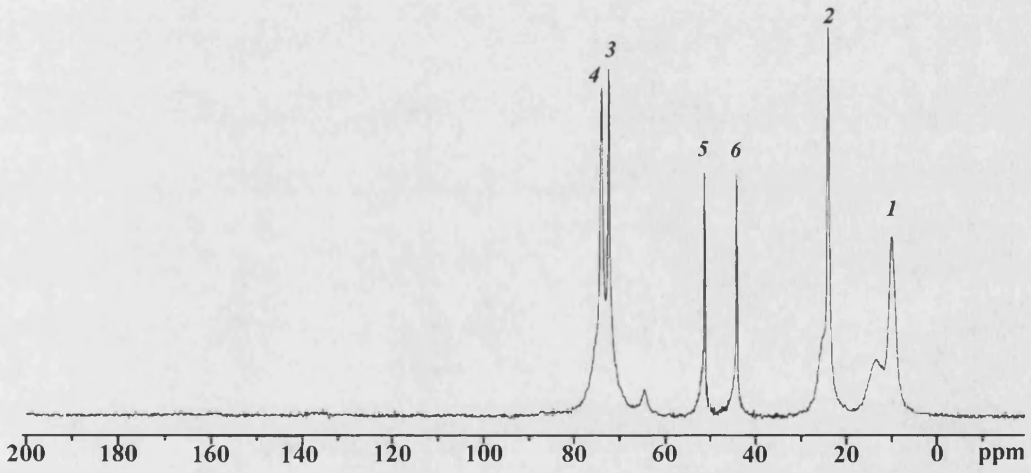

Figure 4.5 ^{13}C CP MAS NMR spectrum for Mg-EPTMS

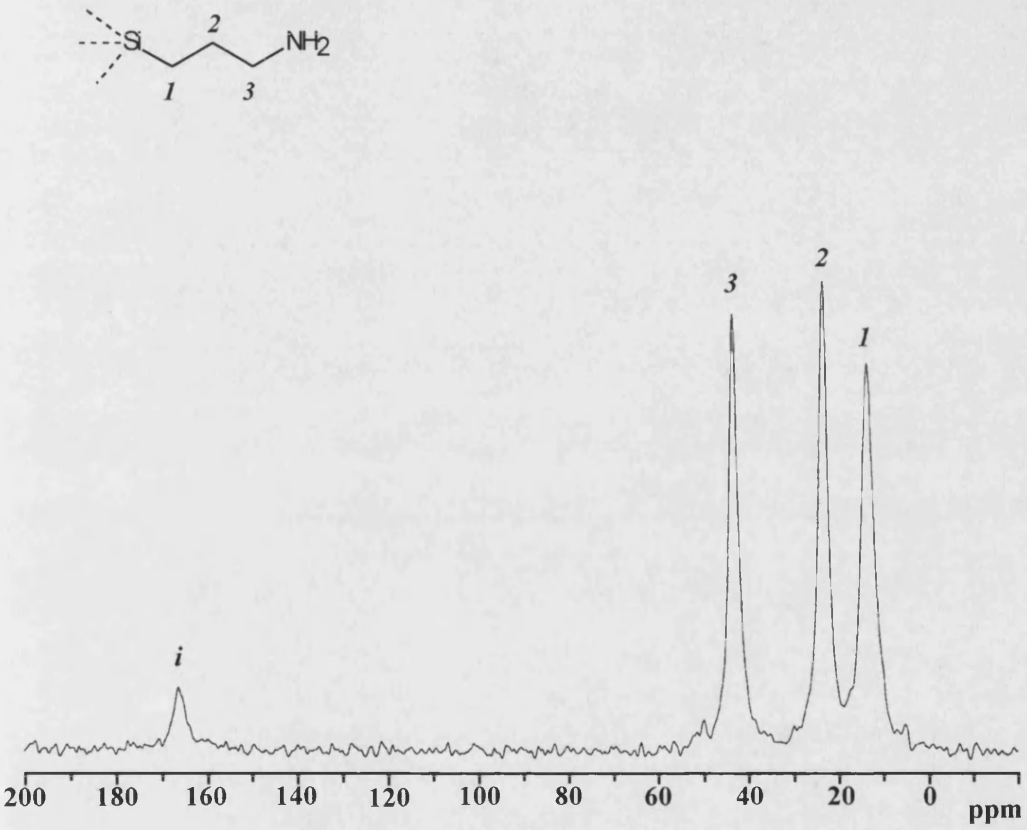

Figure 4.6 ^{13}C CP MAS NMR spectrum for Mg-ATES. ***i*** = impurity.

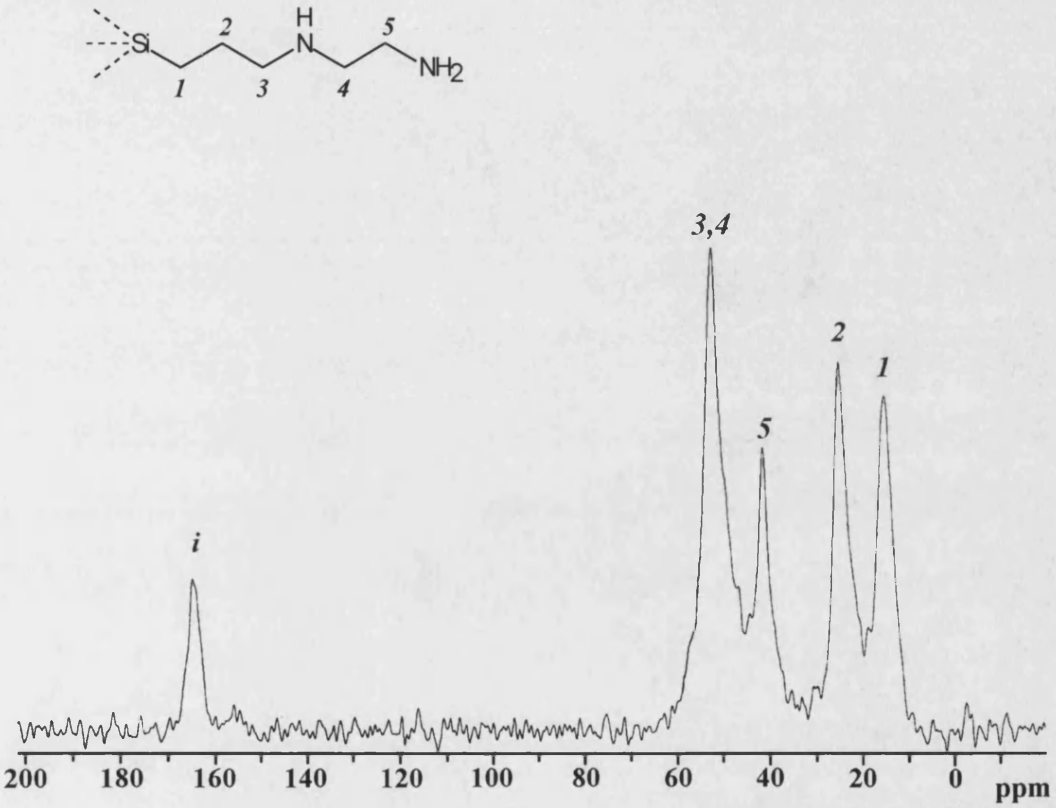

Figure 4.7 ^{13}C CP MAS NMR spectrum for Mg-EDTMS. ***i*** = impurity

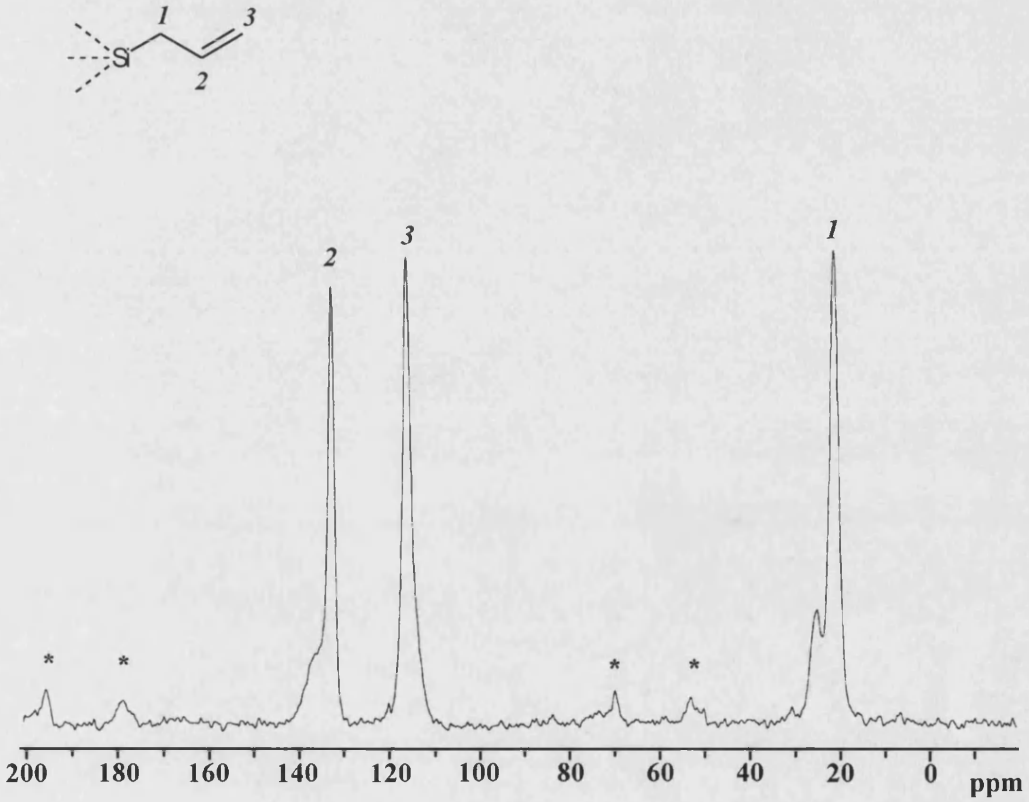

Figure 4.8 ^{13}C CP MAS NMR spectrum for Mg-ALTMS. * indicate spinning sidebands.

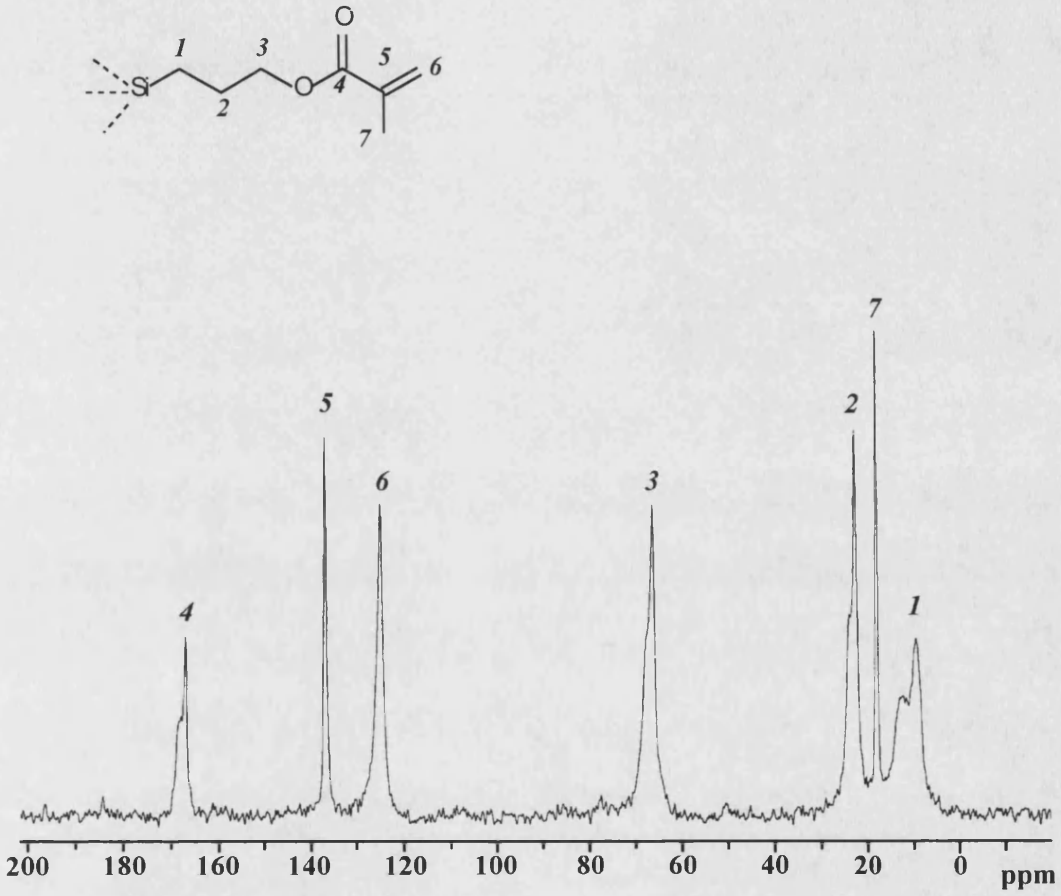

Figure 4.9 ^{13}C CP MAS NMR spectrum for Mg-MPTMS

	Chemical Shift (ppm)	%
T^1	-49	43.6
T^2	-56	34.5
T^3	-66	21.9

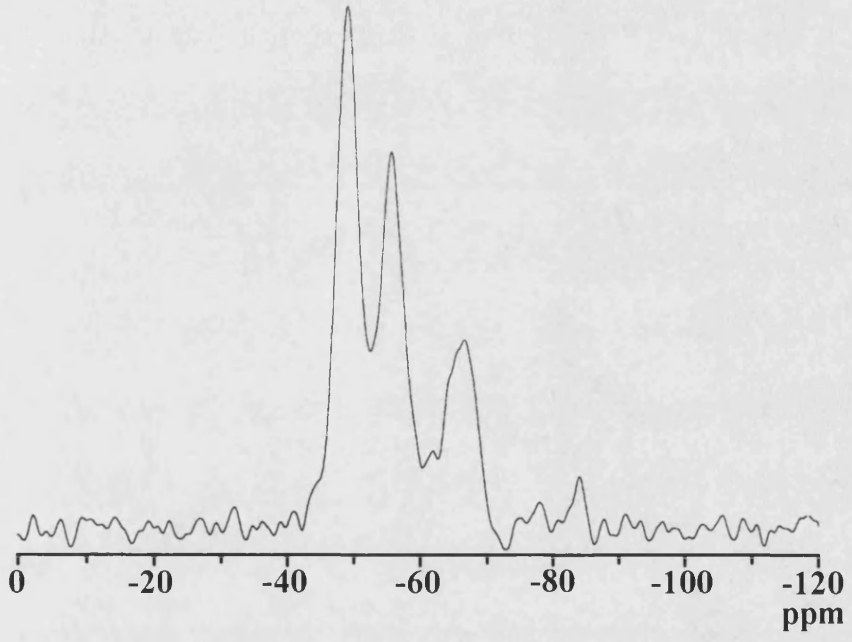

Figure 4.10 ^{29}Si DP MAS NMR spectrum for Mg-ITES.

	Chemical Shift (ppm)	%
T^1	-49	13.6
T^2	-56 to -60	18.5
T^3	-65 to -68	67.9

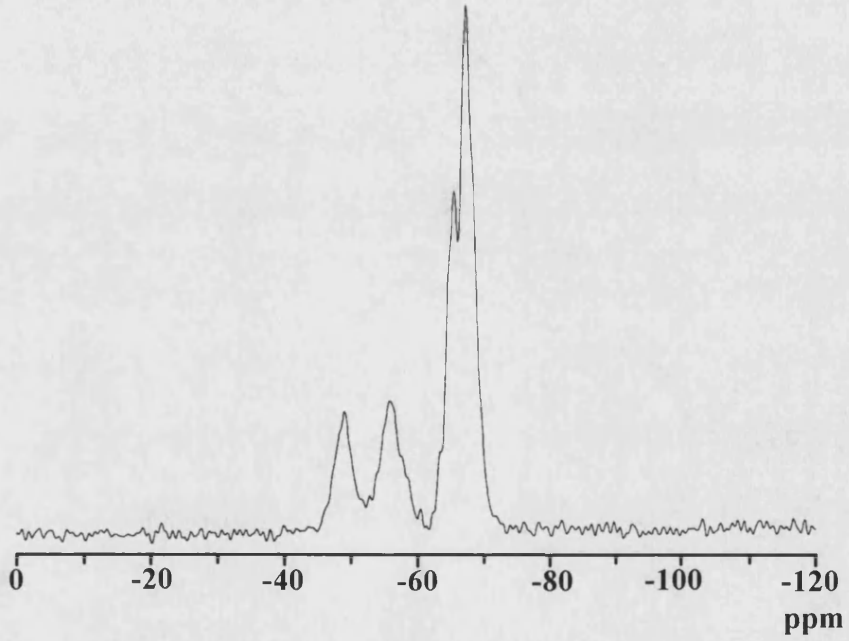

Figure 4.11 ^{29}Si DP MAS NMR spectrum for Mg-EPTMS.

	Chemical Shift (ppm)	%
T^1	-49	60.2
T^2	-55	39.8

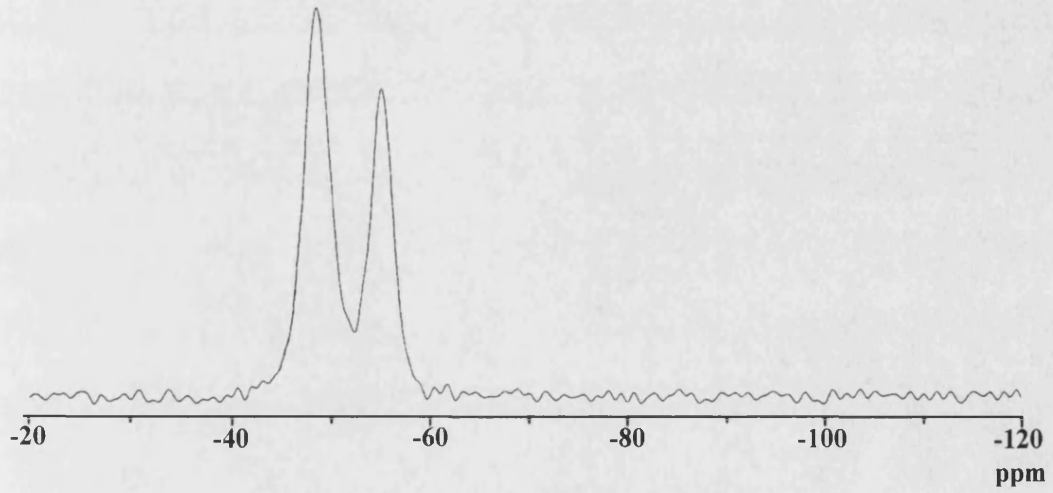

Figure 4.12 ^{29}Si DP MAS NMR spectrum for Mg-ATES.

	Chemical Shift (ppm)	%
T^1	-49	58.2
T^2	-56	41.8

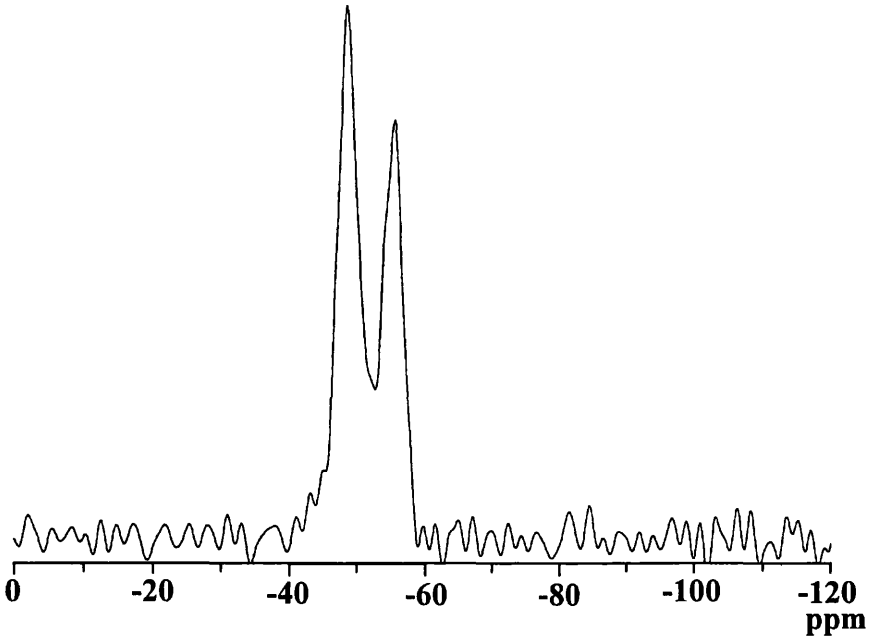

Figure 4.13 ^{29}Si DP MAS NMR spectrum for Mg-EDTMS.

	Chemical Shift (ppm)	%
T^1	-52	8.0
T^2	-61	21.5
T^3	-72	70.5

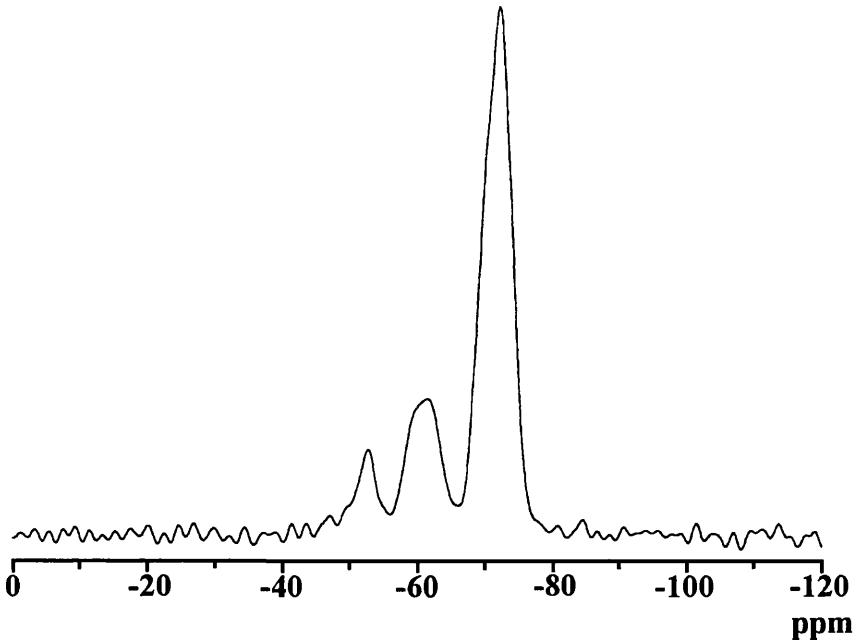

Figure 4.14 ^{29}Si DP MAS NMR spectrum for Mg-ALTMS.

	Chemical Shift (ppm)	%
T^1	-50	15.1
T^2	-57	32.1
T^3	-66 to -68	52.8

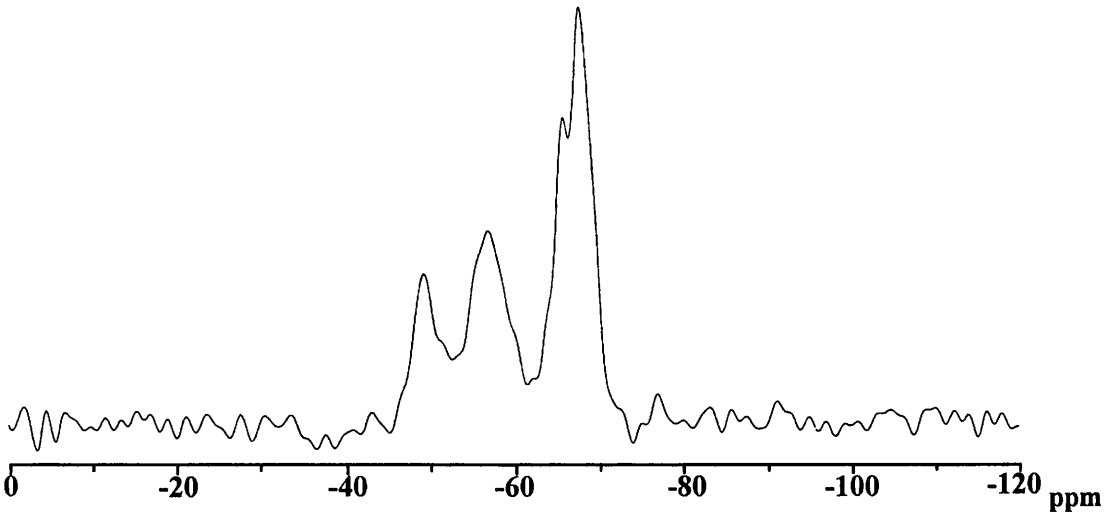

Figure 4.15 ^{29}Si DP MAS NMR spectrum for Mg-MPTMS.

No quantitative evaluation of the amount of amorphous material present in the final products was made. Whilst thorough washing of the samples removed unreacted alkoxy groups, any disordered amorphous silica-containing material was unremoved, and was difficult to identify using the characterization techniques available. In XRD a reflection due to an amorphous silica phase would usually be observed at just above 20 degrees 2θ. However, 2:1 trioctahedral phyllosilicate reflections, (020) and (110), occur in this region of the XRD pattern, and their broad unresolved nature made additional assignment of an amorphous phase reflection non-trivial. Due to the intractable nature of the materials, microanalysis provided an indication only of the total amount carbon, nitrogen and hydrogen present in each sample (Table 4.4).

Table 4.4 C, H, N microanalysis data for as-synthesized magnesium (organo)phyllosilicates

	C_{calc} %	C_{obs} %	H_{calc} %	H_{obs} %	N_{calc} %	N_{obs} %
Mg-MTES	11.8	**10.2**	3.4	**4.3**	-	-
Mg-ATES	24.9	**13.7**	5.9	**5.3**	9.7	**4.3**
Mg-EDTMS	32.4	**16.8**	7.0	**5.8**	14.2	**6.54**
Mg-ITES	36.4	**22.1**	5.6	**5.9**	14.2	**5.0**
Mg-EPTMS	35.7	**33.3**	5.7	**6.0**	-	-
Mg-ALTMS	28.2	**25.8**	4.3	**5.0**	-	-
Mg-MPTMS	39.3	**32.7**	5.4	**5.3**	-	-
Mg-H^+EDTMS	32.4	**26.1**	7.0	**7.0**	14.2	**10.9**
Mg-H^+ATES	24.9	**17.5**	5.9	**5.9**	9.7	**6.5**

Assuming the amount of amorphous material to be low or absent in all samples then the analyses show that for Mg-EDTMS and Mg-ATES the empirical amount of carbon and silicon within the samples is roughly half of that expected for a

2:1 trioctahedral phyllosilicate of formula, $Si_8R_8Mg_6O_{16}(OH)_4$, whilst other magnesium (organo)phyllosilicates showed reasonably good correlation with the calculated values, allowing for defects in the complex structure.

Thermogravimetric analysis curves for Mg-EPTMS and Mg-EDTMS are shown in Figure 4.16. Most striking was the endotherm between 20 °C and 150 °C in the data for Mg-EPTMS (Figure 4.16b) which was absent in that of Mg-EPTMS (Figure 4.16a). The endotherm corresponded to a loss in surface adsorbed water and was accompanied by a 14 % weight loss for the ethylenediamine-containing organosilicate. In contrast, only a minor weight loss (1 %) in this temperature range was recorded for the epoxide-containing sample. These results served to assess the hydrophobic/hydrophilic nature of the two organosilicates, and demonstrated the increased 'wettability' of Mg-EDTMS compared to Mg-EPTMS. The next major weight loss for both samples was centred at just under 400 °C and extended to 600 °C before leveling out and was attributed mainly to the decomposition of the organic functionalities. The respective losses for Mg-EPTMS and Mg-EDTMS of 48 % and 28 % over this temperature range correlated well with the total organic percentages estimated from the microanalysis data.

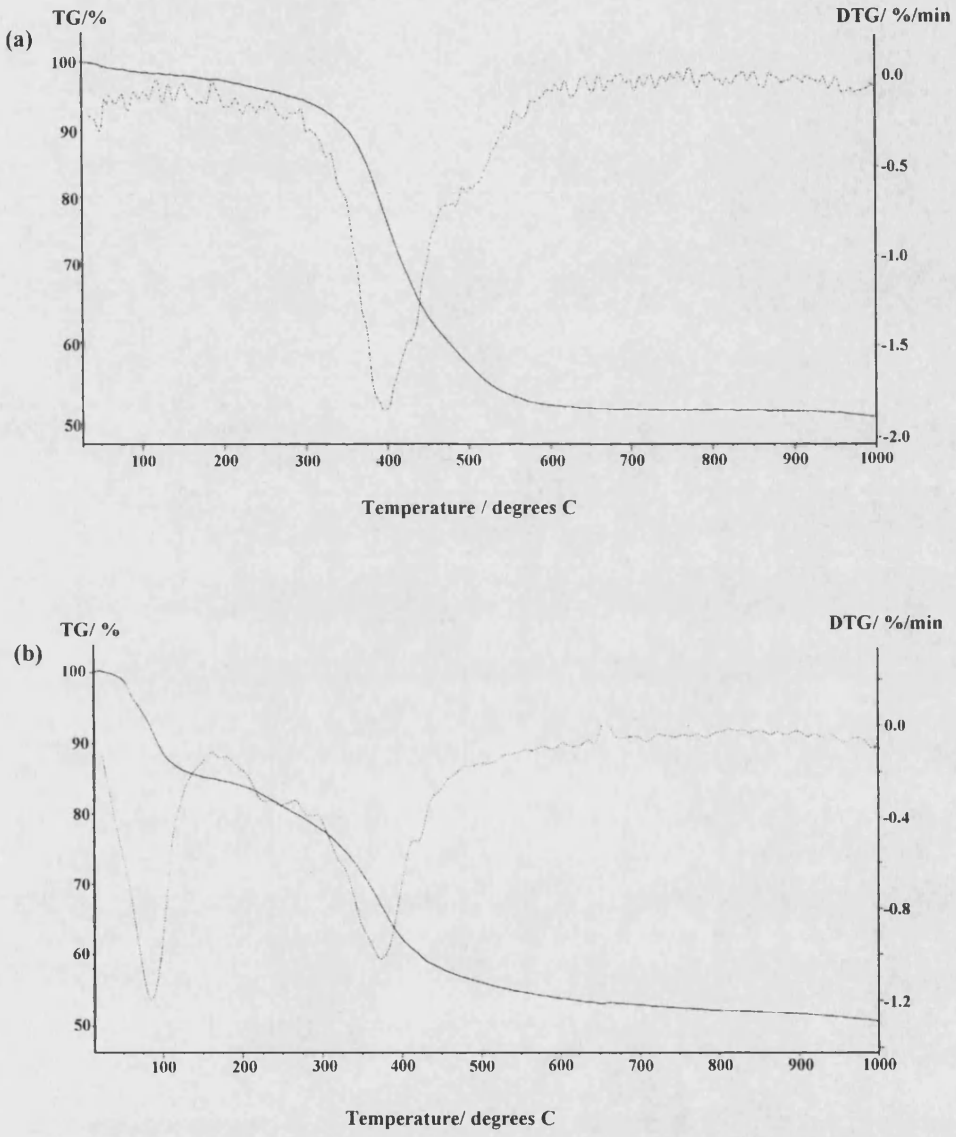

Figure 4.16 Thermogravimetric analysis data for (a) Mg-EPTMS and (b) Mg-EDTMS. Dotted trace shows differential (DTG) trace.

The results of the characterizations illustrated the potential of preparing a wide range of layered inorganic/organic hybrid structures containing organic functionalities covalently bound to the inorganic sheets and occupying the interlayer spaces. Under the basic reaction conditions employed (pH=11-12), hydrolysis of aquamagnesium ions is facile (Burgess, 1978), whilst that of organotrialkoxysilanes is reported to be slow relative to condensation (Glaser *et al.*, 1989). Bulky organic substituents on the silicon centre sterically hinder the rate of hydrolysis which under basic conditions proceeds either by a conventional S_N2-type mechanism with inversion of the centre (Schaefer and Keefer, 1984) or *via* a 5-coordinate stable negatively-charged intermediate (Pohl and Osterholtz, 1985) [Equations (3) and (4)].

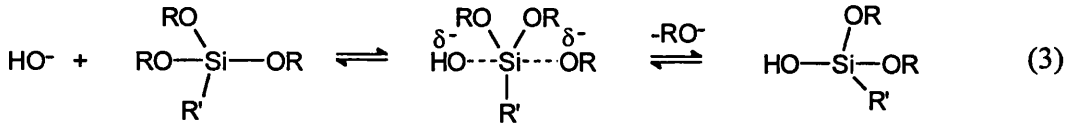

(3)

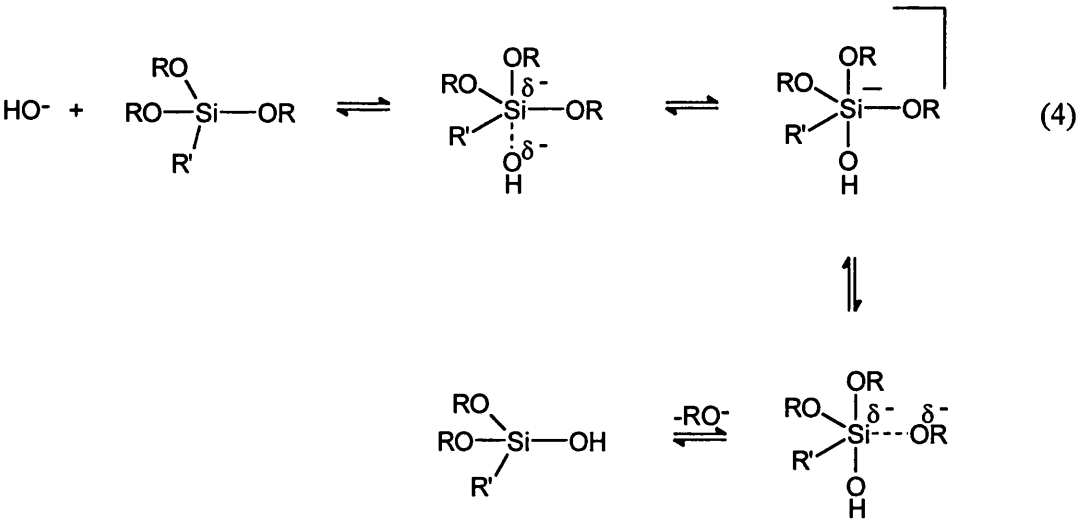

(4)

Facile condensation between negatively-charged ≡SiO$^-$ units and neutral alkoxysilanes is prevented due to the bulkiness of the organic substituents, and

condensation is likely to occur initially between silicate and rapidly hydrolyzing magnesia species. Indeed, at high pH the favourable formation of Si-O-Mg and Mg-O-Mg bonds has previously been observed (Mizutani, 1990b). The limited coordination of the silicon centres (able to form only three siloxane-type bonds rather than four due to the organic substituents) and steric constraints, which required for the disposition of the organic moieties in energetically favourable positions, inevitably led to puckering of the disordered tetrahedral sheets (Fukushima and Tani, 1995). Microanalysis and ^{29}Si NMR data for Mg-ATES, Mg-EDTMS and Mg-ITES indicated that, as well as poor condensation of the silicon centres, very incomplete tetrahedral sheets with a number of vacancies and defects were produced, which nevertheless indexed to the 2:1 trioctahedral phyllosilicate structure.

With no evidence from the XRD data for a bilayer arrangement of organic groups within the gallery regions, and little from the ^{13}C CP MAS NMR to suggest close-packed ordering of the functionalities, it appeared unlikely that the generation of the 2:1 trioctahedral phyllosilicate involved a lamellar micelle templating mechanism (although other micellar structures may be contributing to the formation [Ukrainczyk *et al.*, 1997]). Formation of the materials was instead most likely driven by the preorganization of the octahedral brucite sheets. Reactive hydroxyl sites on the $Mg(OH)_2$ layers are then presented for rapid condensation with silanol derivatives and nucleation and epitaxial growth of the tetrahedral sheets on either side of the central octahedral sheet proceeds in this way. It seems likely that the hydrolysis and condensation kinetics involved in the syntheses were suitably complemented to allow for formation of the layered structures without induction of phase separation of magnesium and silicon components. The influence of the organic functionalities on

directing primary structure formation appeared incidental although previous studies have demonstrated that favourable hydrophobic interactions facilitate and generate ordering in the stacking direction. An earlier study, however, reported that reactions carried out under identical reaction conditions and utilizing tetraalkoxysilane or triethoxysilane (i.e., alkoxysilanes with no R groups) did not produce a layered structure (Burkett *et al.*, 1997).

Transmission electron microscopy revealed a variety of morphologies for the magnesium (organo)phyllosilicates (Figures 4.17 and 4.18). Thin sections of the samples, Figures 4.17a and 4.18b illustrated the textural differences between the methyl-containing and epoxide-containing organosilicate. Mg-MTES showed a granular morphology, whilst Mg-EPTMS consisted of aggregates of larger particles. On occasions, imaging of the samples revealed direct evidence for a layered material. In Figure 4.18b lattice images can be discerned on close observation. In general, however, the clay particles tended to fall onto the microscope grid with their stacking planes perpendicular to the electron beam and the layered structure could not be discerned. Figure 4.17b shows a sample of Mg-EDTMS prepared by placing a drop of the dispersed clay in ethanol onto the grid and in this instance then aggregated irregular-sized particles were evident but there was no suggestion of layering, even though from the corresponding XRD pattern the layered phyllosilicate structure was revealed. Attempts to obtain selected area electron diffraction data on the samples were unsuccessful

directing primary structure formation appeared incidental although previous studies have demonstrated that favourable hydrophobic interactions facilitate and generate ordering in the stacking direction. An earlier study, however, reported that reactions carried out under identical reaction conditions and utilizing tetraalkoxysilane or triethoxysilane (i.e., alkoxysilanes with no R groups) did not produce a layered structure (Burkett *et al.*, 1997).

Transmission electron microscopy revealed a variety of morphologies for the magnesium (organo)phyllosilicates (Figures 4.17 and 4.18). Thin sections of the samples, Figures 4.17a and 4.18b illustrated the textural differences between the methyl-containing and epoxide-containing organosilicate. Mg-MTES showed a granular morphology, whilst Mg-EPTMS consisted of aggregates of larger particles. On occasion, imaging of the samples revealed direct evidence for a layered material. In Figure 4.18b lattice images can be discerned on close observation. In general, however, the clay particles tended to fall onto the microscope grid with their stacking planes perpendicular to the electron beam and the layered structure could not be discerned. Figure 4.17b shows a sample of Mg-EDTMS prepared by placing a drop of the dispersed clay in ethanol onto the grid and in this instance then aggregated irregular-sized particles were evident but there was no suggestion of layering, even though from the corresponding XRD pattern the layered phyllosilicate structure was revealed. Attempts to obtain selected area electron diffraction data on the samples were unsuccessful

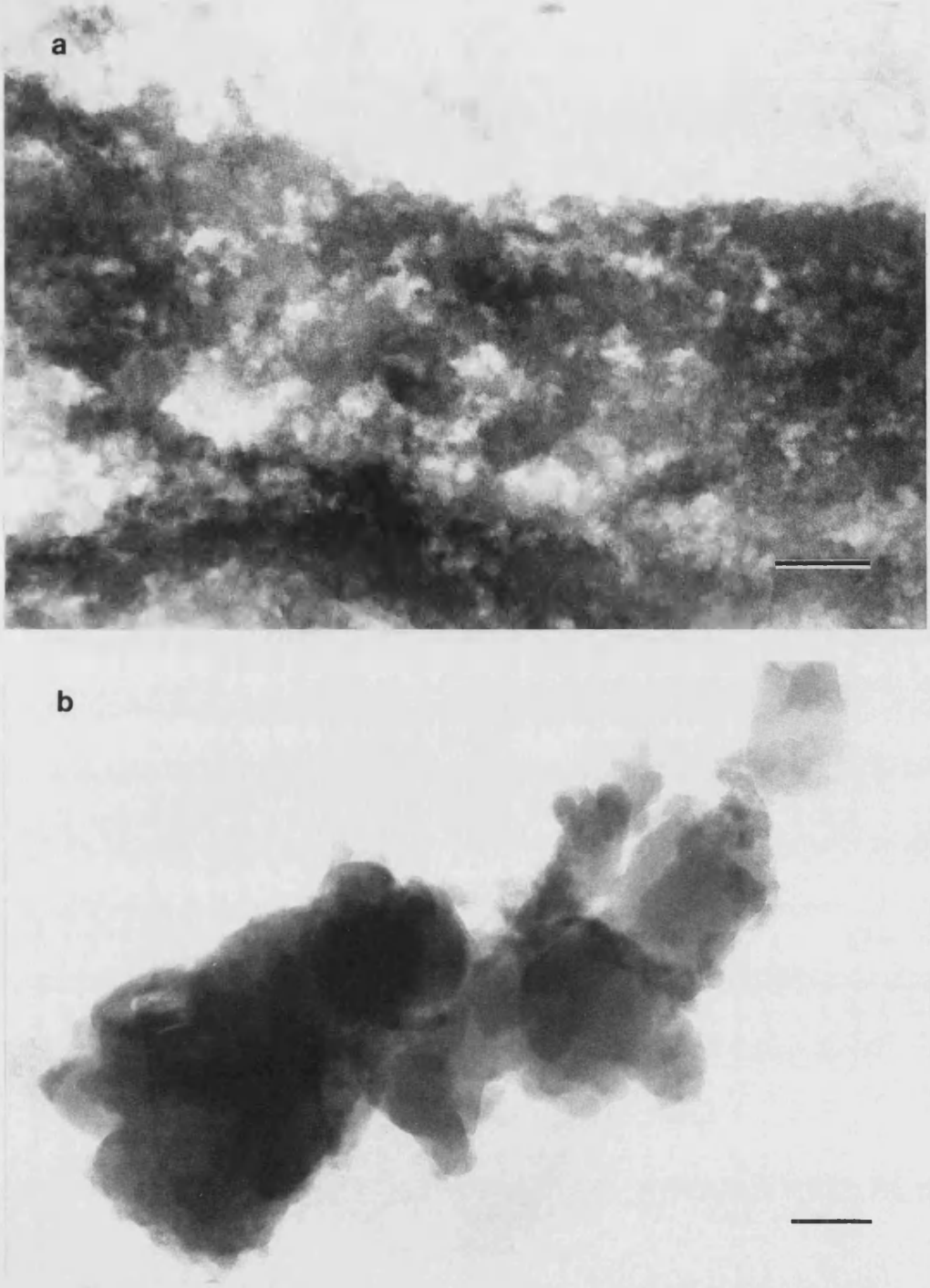

Figure 4.17 Transmission electron micrographs of (a) Mg-MTMS (thin section) and (b) Mg-EDTMS. Scale bars = 100 nm.

Figure 4.18 Transmission electron micrographs of Mg-EPTMS (thin section). (b) shows layering within the sample. Scale bars = (a) 100 nm, (b) 25 nm.

Ethanolic, base-free synthesis of amine-functionalized magnesium phyllosilicates

The decision to isolate the products of syntheses involving only magnesium chloride, ethanol and EDTMS/ATES, came from the observation during standard syntheses that clouding of the reaction mixture occurred following addition of the organotrialkoxysilane and before the addition of base. Amine-containing organotrialkoxysilanes are known to have self-catalyzing hydrolysis behaviour and thus reaction mixtures without base were allowed to stir for 24 h at room temperature. The result in both cases was a copious precipitation, slightly yellow in coloration. Due to the reaction being carried out at pH values close to neutral (pH during reaction = 7.5) it was anticipated that the acid-base equilibria of both the primary and secondary amine group functionalities would tend towards the protonated states [pK_a (-NH_3^+/-NH_2^+ = ~ 10)] and isolated products were given the names Mg-H^+EDTMS and Mg-H^+ATES, in reference to this.

Resultant XRD patterns exhibited broad reflections attributable to the 2:1 trioctahedral phyllosilicate structure, but the d_{001}-spacings differed to those of the complementary organosilicates prepared by the standard procedures. Mg-H^+EDTMS exhibited an interlayer spacing of 18.4 Å; 3.1 Å greater than that of the sample prepared under standard reaction conditions, Mg-EDTMS (Figure 4.19). However Mg-H^+ATES exhibited a smaller d_{001}-spacing than Mg-ATES; 13.0 Å compared to 14.2 Å (data not shown). The differences in the interlayer spacings could be attributed to different arrangements of organic species in the gallery regions.

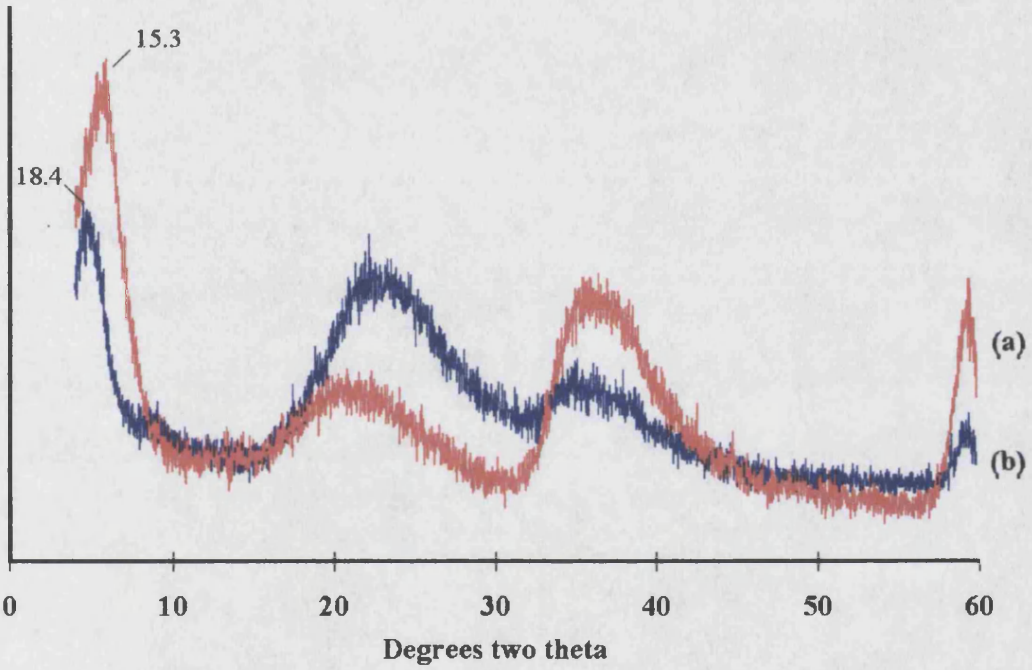

Figure 4.19 PXRD patterns for (a) Mg-EDTMS prepared under standard synthesis conditions and (b) Mg-H^{+}EDTMS prepared under ethanolic, base-free conditions. Interlayer spacings are indicated in Å.

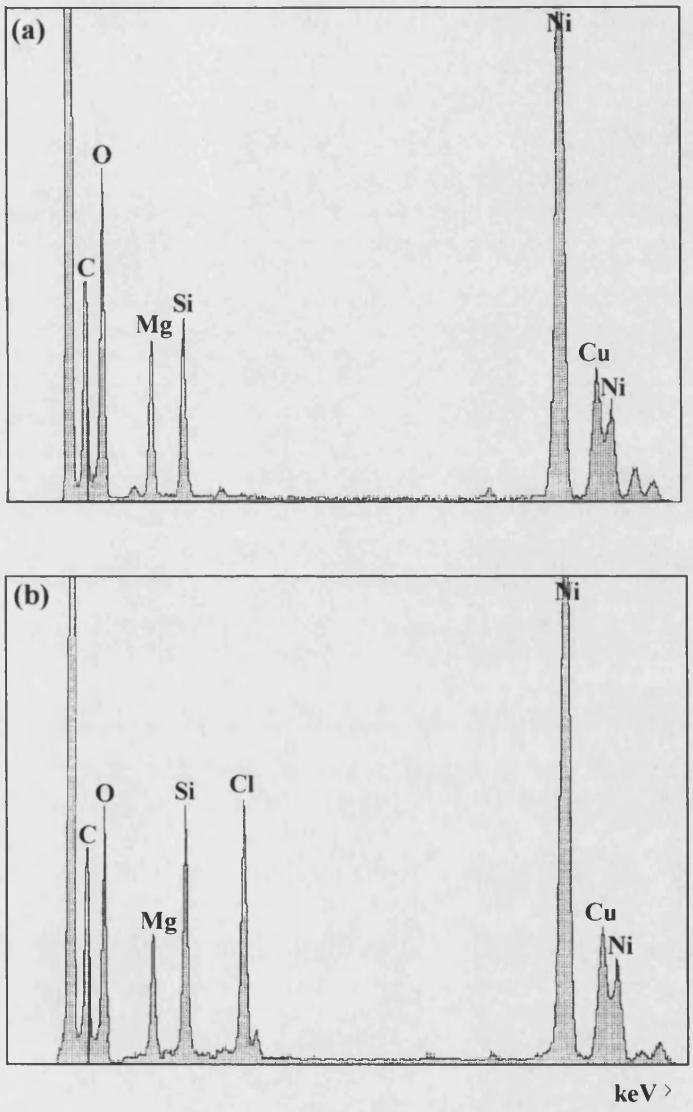

Figure 4.20 EDXA data for (a) Mg-ATES and (b) Mg-H^{+}ATES. Bare nickel grids used to mount samples for analysis.

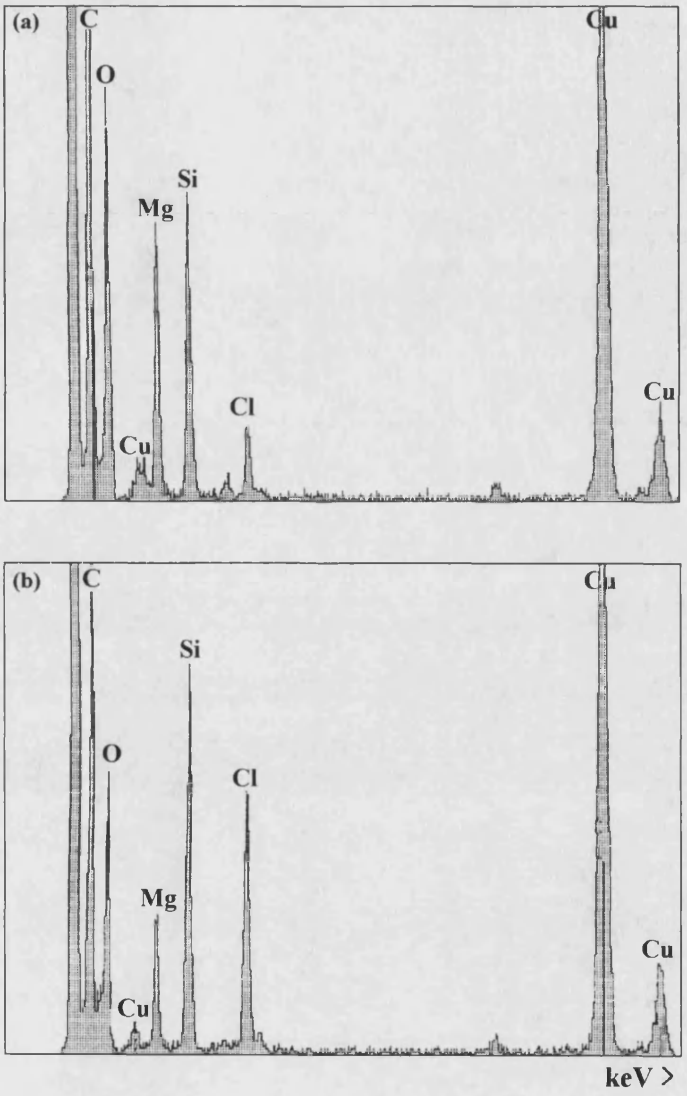

Figure 4.21 EDXA data for (a) Mg-EDTMS and (b)=Mg-H^{+}EDTMS. Bare copper grids used to mount samples for analysis.

FTIR spectra of the base-free synthesized products displayed absorptions clearly assignable to protonated primary (3600-3400 cm^{-1}, 2100-1900 cm^{-1}, 1600 cm^{-1}) and secondary (3200-3000 cm^{-1}, 2400 cm^{-1}) (for Mg-H^+EDTMS only) amine groups (Cross and Jones, 1969). Peaks attributable to Si-C bond vibrations were also observed, indicating no bond hydrolysis. The presence of charged organic functionalities in the otherwise neutrally-charged interlayers of the lamellar solid necessitated the incorporation of charge-balancing counter anions. Consideration of the composition of the reaction mixtures highlighted the chloride ion and implied the formation of an organoammonium chloride salt. Significant amounts of chlorine were detected in Mg-H^+ATES and Mg-H^+EDTMS by energy dispersive X-ray analysis (EDXA). This was in contrast to the products of the standard syntheses which displayed little or no chlorine (Figures 4.20 and 4.21).

The accommodation and subsequent arrangement of the organoammonium chloride functionalities in the interlayer region of Mg-H^+ATES resulted in a smaller d_{001}-spacing than observed for Mg-ATES. However, protonation of both amine groups in Mg-H^+EDTMS required the incorporation of two chloride ions per 'ethylenediamine' functionality to balance the excess charge and an increased *d*-spacing compared to Mg-EDTMS resulted in this case.

The ratio of the elemental peak heights obtained during EDXA could only be used semi-quantitatively as an indicator of the relative elemental amounts within a sample. It was interesting, however, to observe the Si/Mg peak height ratios for the products of the standard and ethanolic, base-free syntheses for comparative purposes. Products synthesized from ethanol/water mixtures in the presence of base displayed magnesium and silicon signals of roughly comparable intensity; those prepared from

ethanolic solutions in the absence of base gave an increased silicon signal compared to that of magnesium; Si/Mg ratios of approximately 1.75 and 2.5 were observed in the EDXA data shown for Mg-H^+ATES and Mg-H^+EDTMS respectively.

Microanalysis data for Mg-ATES and Mg-EDTMS afforded lower carbon and nitrogen percentages than calculated for the 2:1 trioctahedral phyllosilicate empirical formulae (Table 4.4). Assuming no Si-C bond hydrolysis, a reduced silicon content would also be anticipated. For a tri-octahedral (organo)phyllosilicate structure a Si/Mg ratio of 1.33 is quantitatively expected. Thus a reduced silicon content within Mg-ATES and Mg-EDTMS could be implied from the Si/Mg ratio of ~1 displayed in the EDXA data. Within the structure this diminution in the amount of silicon would be evidenced as vacancies in the tetrahedral sheets. A 1:1 phyllosilicate structure for these samples was ruled out by analysis of the XRD patterns (Brown and Brindley, 1980). In contrast, microanalysis data obtained for the products of the ethanolic, base-free syntheses, Mg-H^+ATES and Mg-H^+EDTMS, gave carbon and nitrogen percentages more closely comparable to calculated empirical values. The semi-quantitative EDXA data showed the expected excess of silicon over magnesium. A greater degree of condensation and more complete structure formation could be tentatively proposed for these samples. The semi-quantitative nature of the EDXA technique and intractability of the samples, however, made it impossible to eliminate the possibility of a contribution from amorphous silica to the silicon signal.

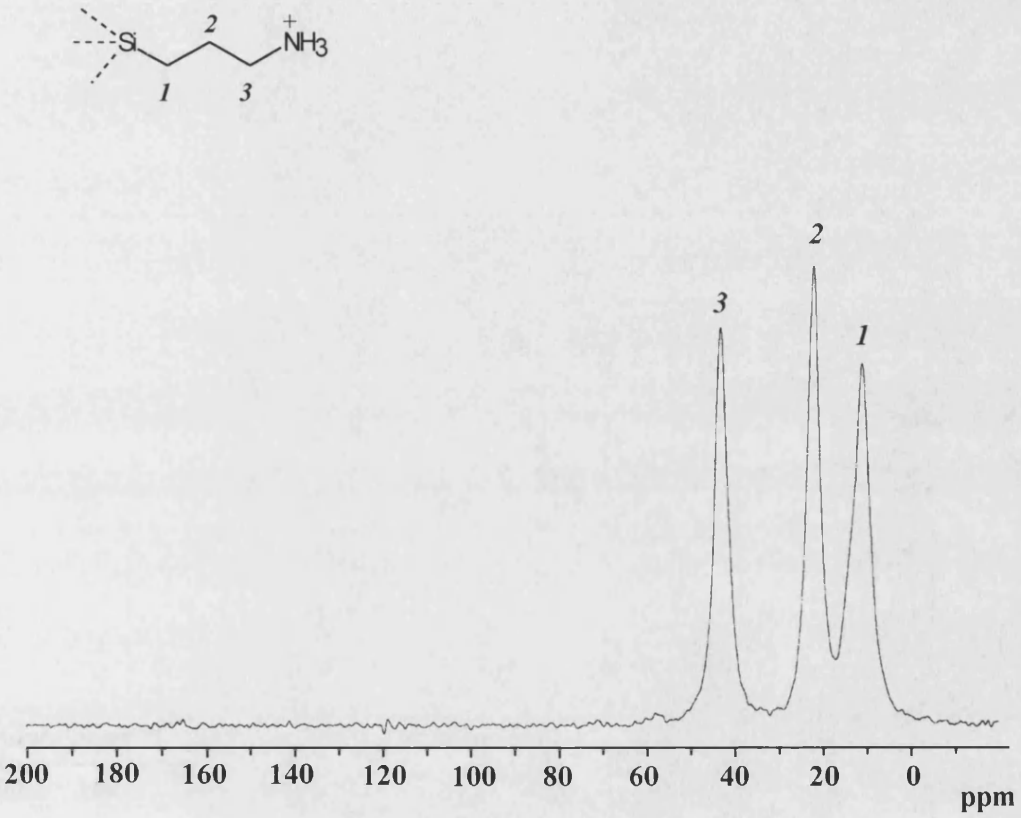

Figure 4.22 ^{13}C CP MAS NMR spectrum for Mg-H^+ATES.

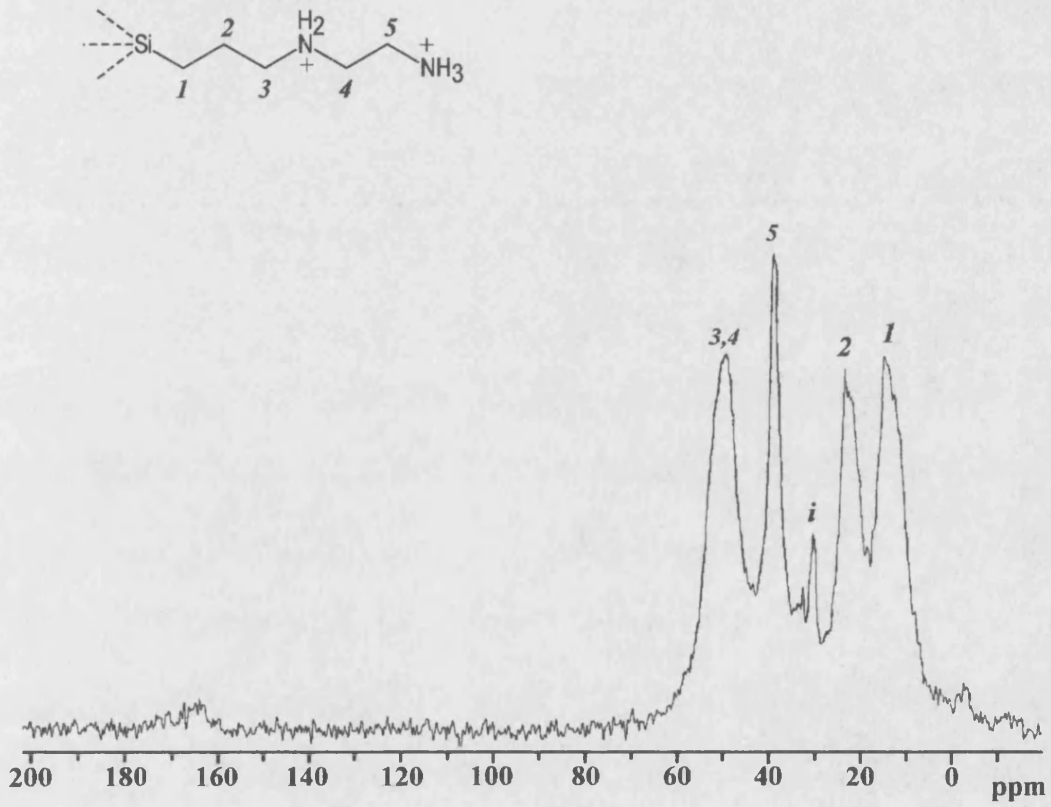

Figure 4.23 ^{13}C CP MAS NMR spectrum for Mg-H^+EDTMS. ***i*** = impurity.

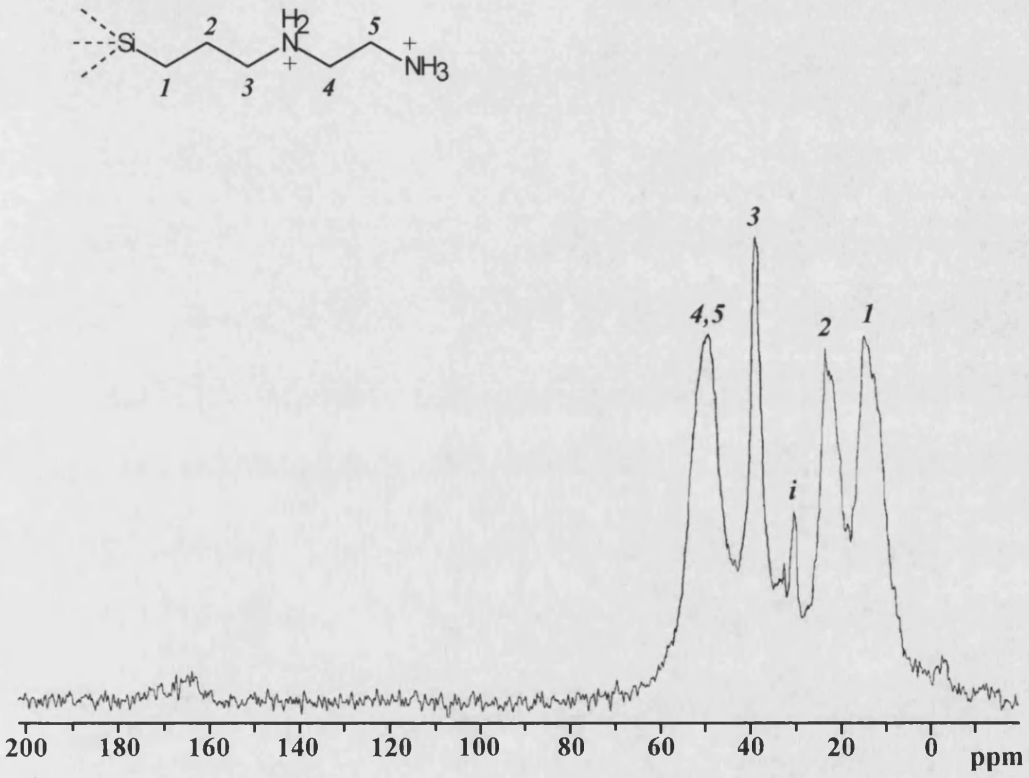

Figure 4.23 ^{13}C CP MAS NMR spectrum for Mg-H^{+}EDTMS. ***i*** = impurity.

Solid state ^{13}C CP MAS NMR spectra and assignments for Mg-H^+ATES and Mg-H^+EDTMS are shown in Figures 4.22 and 4.23 respectively. Assignments were made for complete aminopropyl and 'ethylenediamine' functionalities. The chemical shift values were slightly upfield-shifted from those of Mg-ATES and Mg-EDTMS, in accordance with protonation of the amine groups. For example, non-protonated Mg-EDTMS afforded resonances: 15 ppm, 24 ppm, 41 ppm and 52 ppm (Figure 4.7); whilst corresponding signals for Mg-H^+EDTMS were 14 ppm, 23 ppm, 38 ppm and 49 ppm respectively (Figure 4.23).

^{29}Si DP MAS NMR spectroscopy on Mg-H^+ATES (Figure 4.24) and Mg-H^+EDTMS (Figure 4.25) revealed a high percentage of fully-condensed T^3 silicon species. This was in contrast to NMR data for the corresponding standard syntheses which revealed only T^1 and T^2 silicon centres. The amine substituents were not expected during the ethanolic, base-free synthesis to participate in stabilization of silanol species through hydrogen bonding, since the amine groups are protonated, and this may account for the highly-condensed nature of the materials, along with better condensation of the silicon centres under the reaction condition employed.

	Chemical Shift (ppm)	%
T^1	-49	15.3
T^2	-56 to -60	15.2
T^3	-66 to -68	69.5

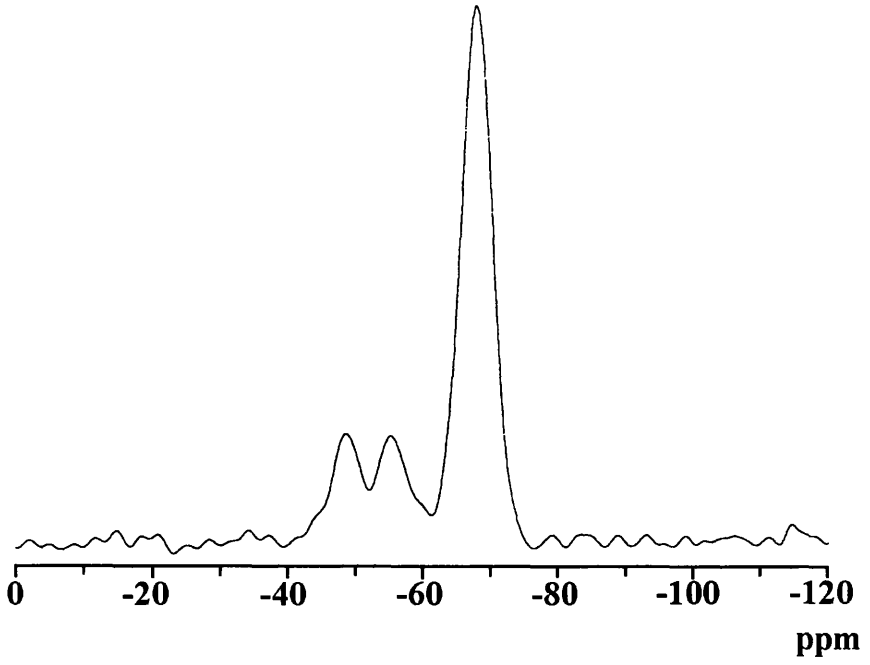

Figure 4.24 ^{29}Si DP MAS NMR spectrum for Mg-H$^+$ATES.

	Chemical Shift (ppm)	%
T^1	-49	58.2
T^2	-56	41.8

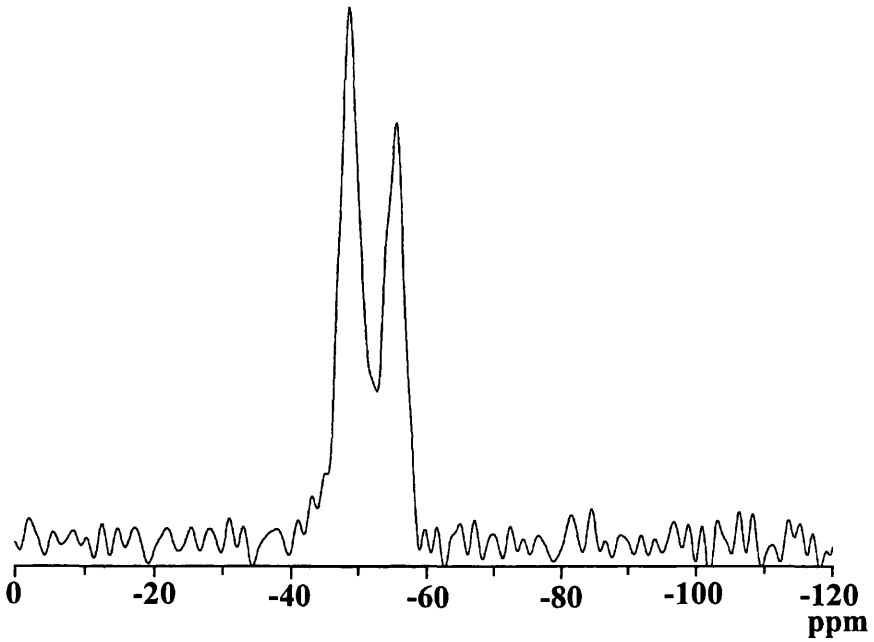

Figure 4.13 ^{29}Si DP MAS NMR spectrum for Mg-EDTMS.

As was the case for magnesium (organo)phyllosilicates prepared under standard synthesis conditions, a complex interplay of factors makes elucidation of the structure formation non-trivial. Leaving aside the effects of $Si:H_2O$ ratio and solvent, at pH values close to 7 the rate of hydrolysis of alkoxysilanes passes through a minimum, whilst that of condensation is favoured due to there being significant concentrations of both protonated and deprotonated silanol groups available for reaction [Equation (5)] (Iler, 1979).

(5)

A low water content to the system often serves to make the hydrolysis reaction the rate-limiting step, but ethanol as cosolvent will facilitate both hydrolysis and condensation, particularly of silanes containing bulky organic or akoxyl ligands, at or near neutral pH, thus favouring Si-O-Si bond formation. The hydrolysis of the aqua magnesium ion is, however, retarded under neutral pH conditions.

A complex interplay of influential factors appears to combine to generate the 2:1 smectite-like sheets. The extent of in-plane condensation is observed to be high presumably because the formation of the brucite sheet is retarded such that a significant degree of intermolecular condensation occurs prior to coupling onto the inorganic framework. Depending on the rates of these two processes, formation of the layered hybrid could be dominated by self-organization of partially condensed organotrialkoxysilane molecules that act as organic templates for brucite assembly. Alternatively the process could involve the cooperative assembly of inorganic and

As was the case for magnesium (organo)phyllosilicates prepared under standard synthesis conditions, a complex of interplay of factors make elucidation of the structure formation non-trivial. Leaving aside the effects of $Si:H_2O$ ratio and solvent, at pH values close to 7 the rate of hydrolysis of alkoxysilanes passes through a minimum, whilst that of condensation is favoured due to there being significant concentrations of both protonated and deprotonated silanol groups available for reaction [Equation (5)] (Iler, 1979).

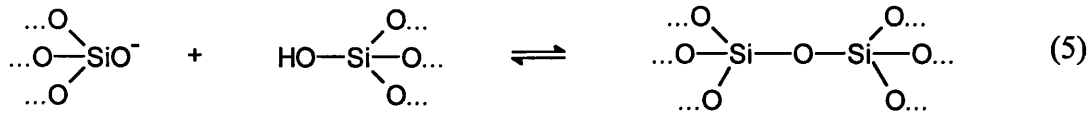

(5)

A low water content to the system often serves to make the hydrolysis reaction the rate-limiting step, but ethanol as cosolvent will facilitate both hydrolysis and condensation, particularly of silanes containing bulky organic or akoxyl ligands, at or near neutral pH, thus favouring Si-O-Si bond formation. The hydrolysis of the aqua magnesium ion is, however, retarded under neutral pH conditions.

A complex interplay of influential factors appear to combine to generate the 2:1 smectite-like sheets. The extent of in-plane condensation is observed to be high presumably because the formation of the brucite sheet is retarded such that a significant degree of intermolecular condensation occurs prior to coupling onto the inorganic framework. Depending on the rates of these two processes, formation of the layered hybrid could be dominated by self-organization of partially condensed organotrialkoxysilane molecules that act as organic templates for brucite assembly. Alternatively the process could involve the cooperative assembly of inorganic and

organic components similar to that described for the synthesis of silica-surfactant mesophases. In each case, hydrophobic interactions between organic functionalities are likely to be a key aspect in the assembly process, as well as playing an important role in the stabilization of the highly disordered structure of the lamellar nanocomposite.

Mixed organosiloxane preparations used to prepare magnesium (organo)phyllosilicates

Before presenting the results from the mixed organotrialkoxysilane preparations attention is drawn to the resultant XRD patterns from the standard syntheses carried out using HDTMS and OTES (Figure 4.2). The patterns exhibited reflections assignable to a brucite, $Mg(OH)_2$, phase and a disordered amorphous silica-containing phase, and not the expected 2:1 trioctahedral phyllosilicate structure. Phase separation of the magnesium and silicon components was evident with the standard synthesis conditions being unsuitable for formation of the layered smectite-like structure.

Octyl and hexadecyl substituents of the organotrialkoxysilane present steric factors which retard the hydrolysis rate significantly. Steric crowding around the five-coordinate hydrolysis intermediate complicates the mechanism (Equation 4) and the inductive electron-donating effects of these substituents serve to further decrease the hydrolysis rate under basic conditions, by disfavouring the generation of the negatively-charged silanol intermediate. The rate of hydrolysis of the aqua

magnesium ion under these conditions would, however, be facile and formation of the brucite sheets was most likely rapid. Phase separation of the magnesium components most likely occurred quickly before condensation of silica tetrahedra onto the octahedral layers could take place.

It has been previously observed that dilution of an organic functionality within the interlayer space can be achieved using mixtures of organotrialkoxysilane with the desired organic substituent and methyltrialkoxysilane. Mixtures of phenyltrimethoxysilane and methyltriethoxysilane were employed in varying molar ratios and resulted in the formation of the layered hybrid structures with expanded d-spacings of dimensions intermediate between those observed for a methyl-containing organosilicate and a phenyl-containing organosilicate. To a certain extent the observed interlayer dimensions reflected the molar ratio of phenyl- and methyl-containing organotrialkoxysilanes employed. (Burkett *et al.*, 1997)

To this end, and bearing in mind the slower reaction kinetics of OTES and HDTMS compared to MTES, mixed organotrialkoxysilane syntheses were carried out in an attempt to fabricate magnesium organosilicates accommodating a random mix of organic substituents within an interlayer region. It was hoped, that the faster-reacting MTES would hydrolyze first and condense rapidly onto preformed octahedral $Mg(OH)_2$ sheets to form partial layers of tetrahedra. Favourable hydrophobic interactions between MTES and OTES/HDTMS would retain the slower reacting OTES and HDTMS molecules in the vicinity of free hydroxyl groups on the brucite sheet allowing for slower condensation and completion of the tetrahedral layer. Moreover, crowding of the interlayer space with bulky organics would be alleviated, and strain in the layered structure would be lessened.

(a) Standard syntheses

XRD data obtained for the isolated products of the O50%:M50% and H30%:M70% preparations are shown in Figure 4.26a and 4.26b respectively. The major reflections in this data were attributable to brucite. In contrast, the product of the O20%:M80% preparation (Figure 4.27) afforded an XRD pattern exhibiting some evidence for the (organo)phyllosilicate structure. Weak brucite peaks were observed alongside broad clay reflections. The position of a peak assignable to the d_{001} reflection gave an interlayer spacing of 8.8 Å. The reflection at 59.5° usually observed in smectite-like structures was also present. A previous synthesis utilizing MTES alone yielded a d-spacing of 8.9 Å which suggested that the layered organosilicate phase formed from the O20%:M80% preparation had arisen primarily from condensation of the faster reacting methyltriethoxysilane onto the brucite octahedral sheet. Under standard synthesis conditions water content was high in the reaction mixture and considering the organophilicity of octyltriethoxysilane it is possible that dissolution was low. Mixing of the reaction components may not have been thorough and rate of hydrolysis of OTES slow.

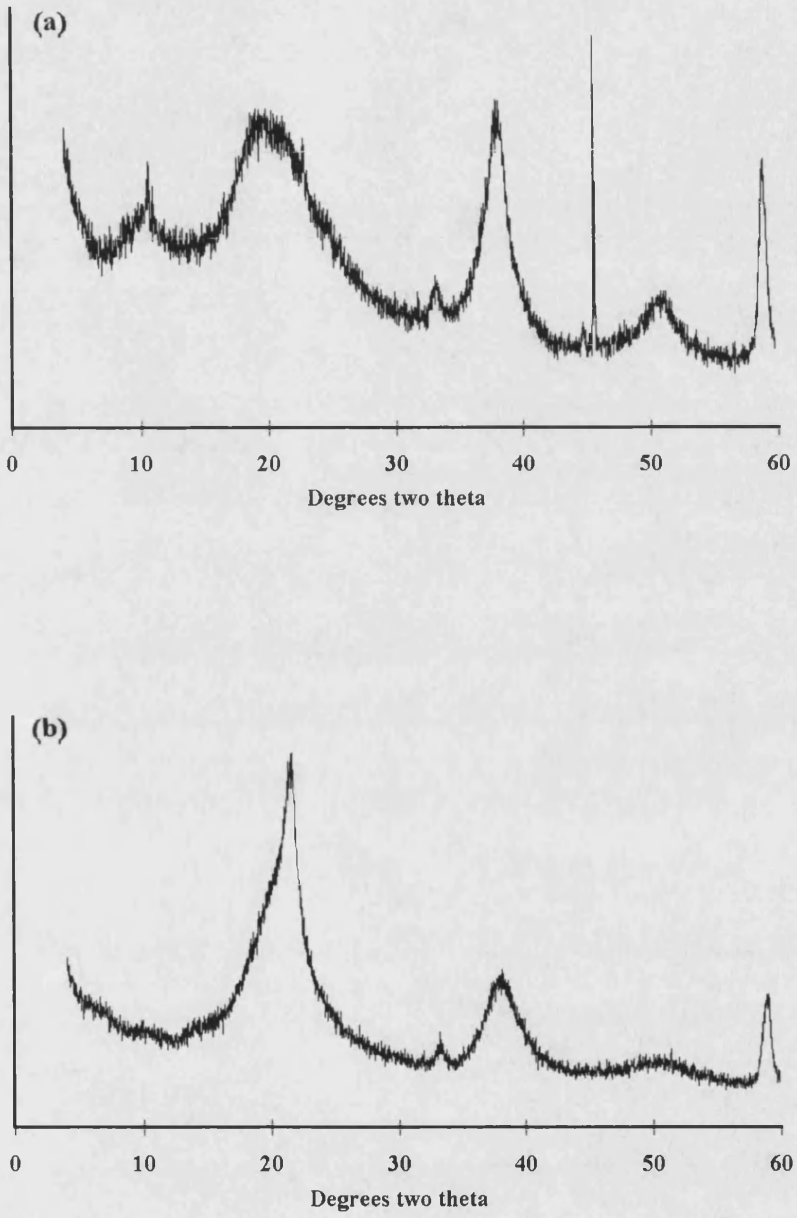

Figure 4.26 PXRD patterns for the products of standard mixed organotrialkoxysilane syntheses employing (a) O50%:M50% and (b) O30%:M70%.

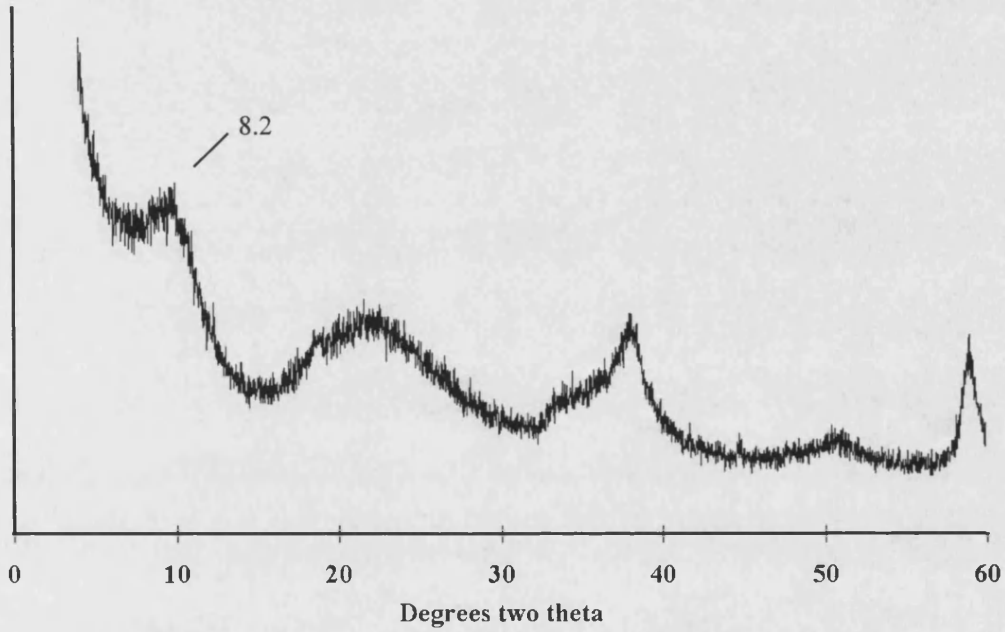

Figure 4.27 PXRD pattern for the product of the standard synthesis employing O20%:M80%.

(b) Solid NaOH, ethanolic syntheses

Bench ethanol (~5 % water) was employed as the solvent in syntheses utilizing magnesium chloride hexahydrate, mixtures of MTES and OTES/HDTMS and solid sodium hydroxide pellets. The magnesium salt and organotrialkoxysilanes dissolved readily in ethanol, whilst the NaOH pellets dissolved slowly in the reaction mixture. Characterization of the isolated products of these syntheses afforded interesting results. XRD data for the O20%:M80% and O50%:M50% preparations are presented in Figures 4.28a and Figure 4.28b respectively, and show patterns consisting of a series of broad reflections which can be indexed to the 2:1 trioctahedral phyllosilicate structure. O20%:M80%, O25%:M75% and O50%:M50% yielded d_{001}-spacings of 12.2 Å, 10.8 Å and 11.0 Å respectively. These values were in better accordance with interlayers accommodating mixed organic moieties, with dimensions intermediate between those expected for a pure methyl-containing silicate and pure octyl-containing silicate. The most expanded d_{001}-spacing resulted from the O20%:M80% preparation, but the stacking dimension was not large enough to correspond to a bilayer arrangement. For an extended octyl chain length of approximately 10 Å and consideration of the Van der Waals thickness of a 2:1 clay layer (~ 9 Å), a basal spacing of approximately 30 Å would be expected for a bilayer motif. This was clearly not the case and instead a spacing of only 12.2 Å corresponded to a disordered arrangement of octyl chains.

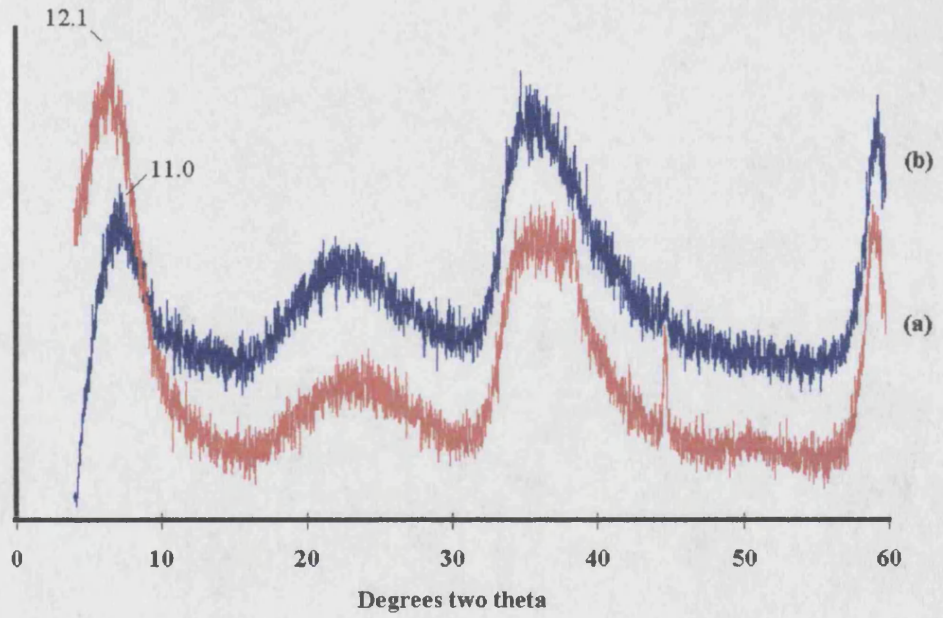

Figure 4.28 PXRD patterns for the products of ethanolic, solid NaOH syntheses employing mixed organotrialkoxysilanes (a) O20%:M80% and (b) O50%:M50%. Interlayer spacings are indicated in Å.

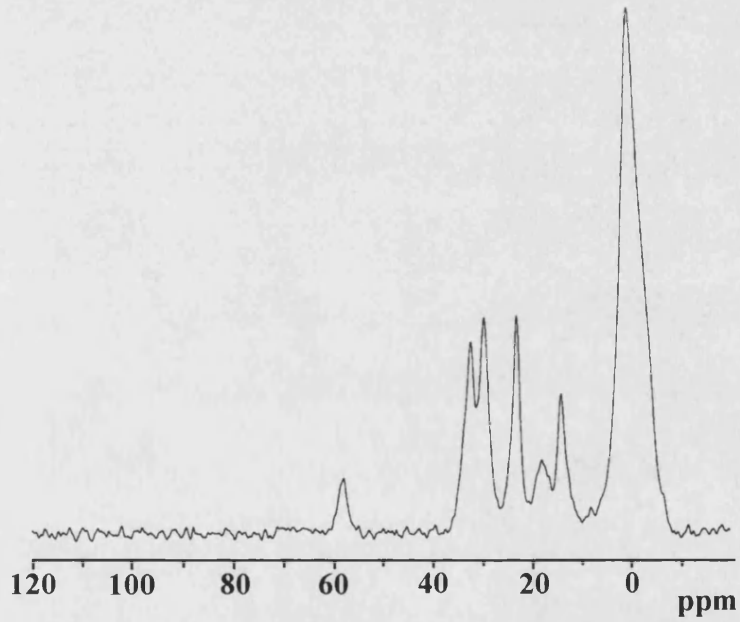

Figure 4.29 ^{13}C CP MAS NMR spectrum for the product of the ethanolic, solid NaOH synthesis employing O20%: M80%.

	Chemical Shift (ppm)	%
T^1	-44 to -47	31.4
T^2	-54	51.1
T^3	-65	17.5

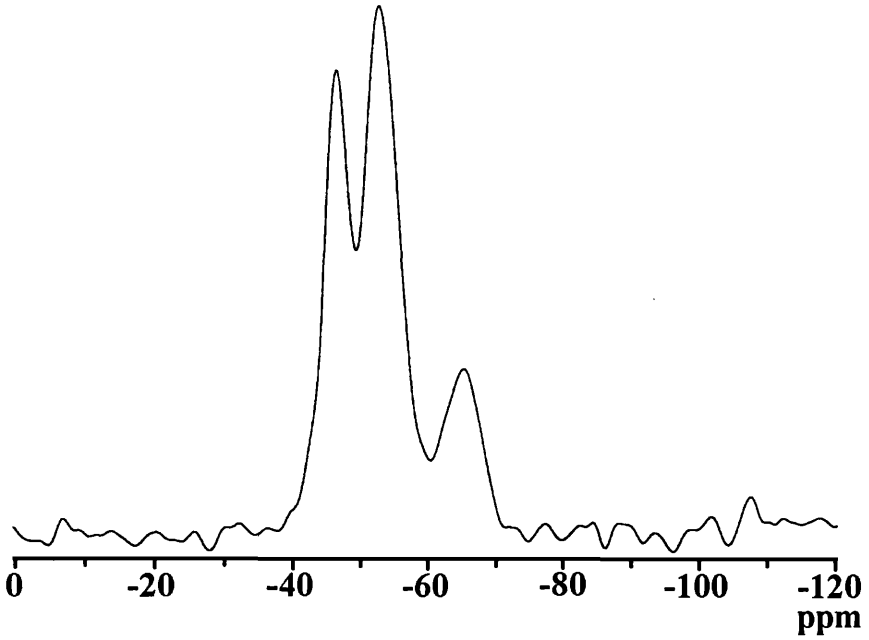

Figure 4.30 29Si DP MAS NMR spectrum for the product of the ethanolic, solid NaOH synthesis employing O20%:M80%.

FTIR spectroscopy on the product of the O20%:M80% preparation showed the presence of the Si-C deformation at 1270 cm^{-1} and other absorptions attributable to alkyl chain vibrations (1380-1470 cm^{-1}, 2860 cm^{-1}, 2970 cm^{-1}).

The solid state ^{13}C CP MAS NMR spectrum for this product (Figure 4.29) showed resonances in the alkyl region which could be assigned to the octyl hydrocarbon chain (4 ppm, 14 ppm, 24 ppm, 29 ppm and 33 ppm). A resonance from pendent methyl ($Si-CH_3$) functionalities was assumed to be obscured by the broad C1 resonance (~ 4 ppm) of the octyl group. Weak signals at 19 ppm and 58 ppm indicated the possibility of unhydrolyzed ethoxysilyl ($SiOCH_2CH_3$) species or bound (adsorbed) ethanol.

Deconvolution of the ^{29}Si MAS NMR (Figure 4.30) showed a poorly condensed sample in which T^1 and T^2 species were dominant, contributing 31.4 % and 51.1 % of the total silicon species respectively. In contrast, the percentage of fully condensed silicon centres was only 17.5 %. A disordered arrangement of bulky organic substituents within the interlayer most probably presented steric barriers to condensation between silanol species during structure formation whilst the organic groups also served to space out the silicon centres further and make Si-O-Si bond formation difficult. Due to the poor resolution of the signals the deconvolution data does not distinguish between unhydrolyzed (ethoxysilyl-containing) and partially-hydrolyzed (hydroxysilyl- and ethoxysilyl-containing) centres. The downfield shift in the assigned T^1 signal (-44 to -47 ppm) compared to other magnesium (organo)phyllosilicates (-49 ppm) could arise from contributions to this peak from unhydrolyzed T^0 and partially-hydrolyzed T^1 centres (Oviatt *et al.*, 1993). Similarly,

contributions from only partially hydrolyzed monomers may contribute to the assigned T^2 and T^3 signals.

The reaction conditions employed are likened to those employed in the ethanolic, base-free synthesis of the amine-containing organosilicates, with the difference being the use of solid sodium hydroxide as the source of base which dissolves slowly in the ethanol-rich reaction mixture to gradually raise the pH. Hydrolysis and condensation of organofunctional trialkoxysilanes are facilitated by ethanol. The rate of hydrolysis of the aqua magnesium ions is, however, slow at neutral pH but rapid at higher pH values. It seems probable that raising the pH of the reaction mixture gradually, allows for the more slowly hydrolyzing organotrialkoxysilanes to get a 'head start' on the hydrolysis of the magnesium cations with the result that copolymerization proceeds cooperatively with the formation of Si-O-Mg bonds as well as Si-O-Si and Mg-O-Mg with increasing pH and phase separation is avoided. Favourable hydrophobic interactions between organic functionalities most likely aids generation of the layered structure, but rapid condensation between silicon centres may be sterically hindered as a result. Unhydrolyzed or partially hydrolyzed monomers trapped within microscopic hydrophobic aliphatic domains may not be accessible for further condensation.

Preparations employing a H30%:M70% mixture and 100 % HDTMS, ethanol-rich conditions and solid NaOH pellets afforded solid products exhibiting XRD patterns shown in Figure 4.31. XRD data from the H30%:M70% preparation exhibited reflections attributable to the 2:1 trioctahedral phyllosilicate structure (Figure 4.31a). Taking the reflection at the lowest degree of 2θ as the d_{001}-spacing a value of ~13 Å was estimated. Again, a disordered arrangement of the organic entities within the interlayer space was assumed, but the expanded interlayer spacing indicated the accommodation of hexadecyl and presumably methyl functionalities. A significant contribution to the disorder is likely to arise from the bulk of the hexadecyl functionalities creating steric hindrances to an ideal packing arrangement of the tetrahedral sheets. The peak at 59.6°, indicative of the 2:1 trioctahedral phyllosilicate structure was evident, but no reflections from a brucite phase were observed.

The ^{13}C CP MAS NMR data (Figure 4.32) revealed chemical shift values which were assigned to the hexadecyl hydrocarbon chain. The asymmetric nature of each signal was indicative of a mixture of amorphous and ordered phases within the sample (Fyfe, 1983). High-field narrow components to each peak signal were attributed to more mobile regions of the sample, whilst broad and tapering lower-field components of each peak were due to disordered amorphous components of the material. Due to clay reflections occurring in the 20-25° region of the XRD pattern, it was not possible to assign a definitive reflection in the pattern to an amorphous silica-containing phase. However, the intensity and broadness of the diffraction peak supported the ^{13}C CP MAS NMR evidence for an amorphous component to the material.

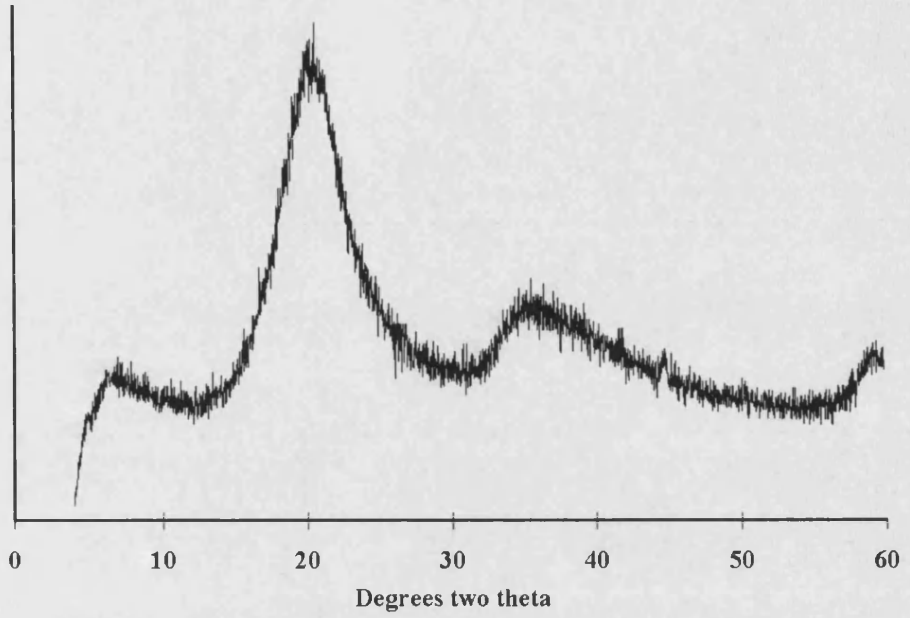

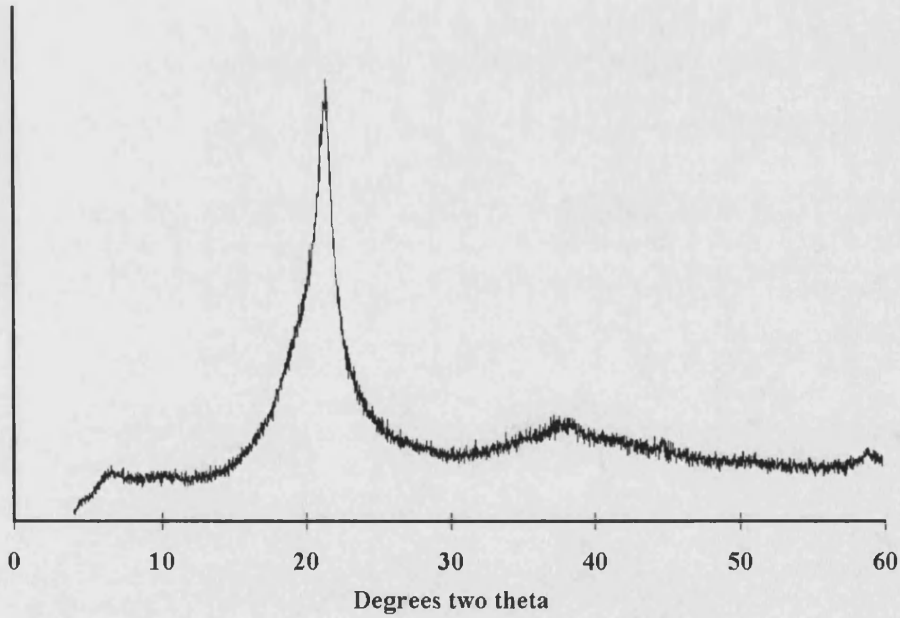

Figure 4.31 PXRD patterns for the products of ethanolic, solid NaOH synthese employing (a)H30%:M70% and (b) 100% hexadecyltrimethosysilane.

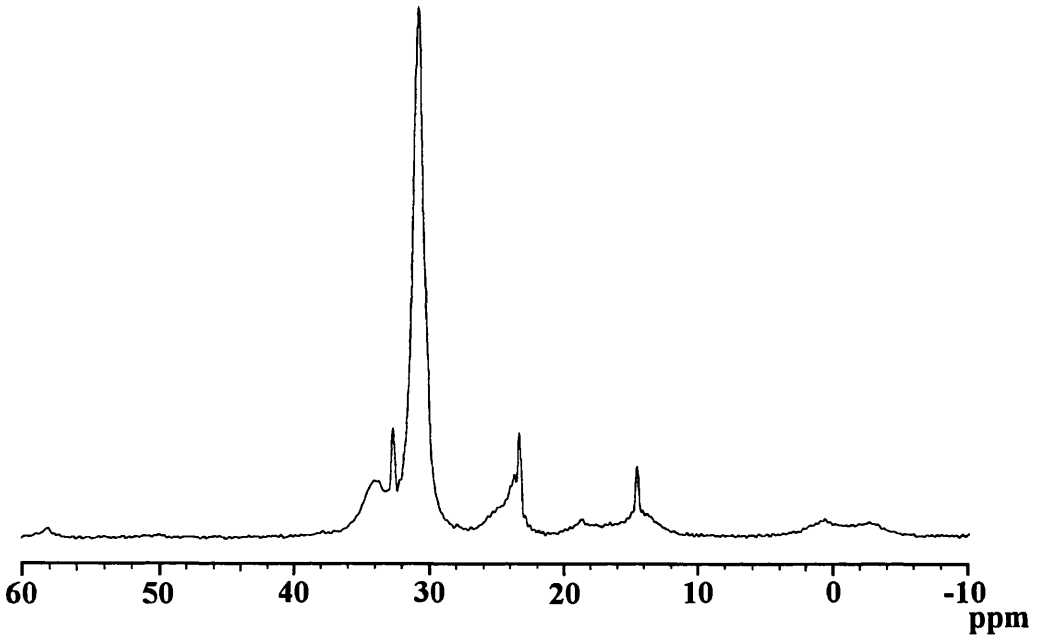

Figure 4.32 ^{13}C CP MAS NMR spectrum for the product of the ethanolic, solid NaOH synthesis employing H30%:M70%.

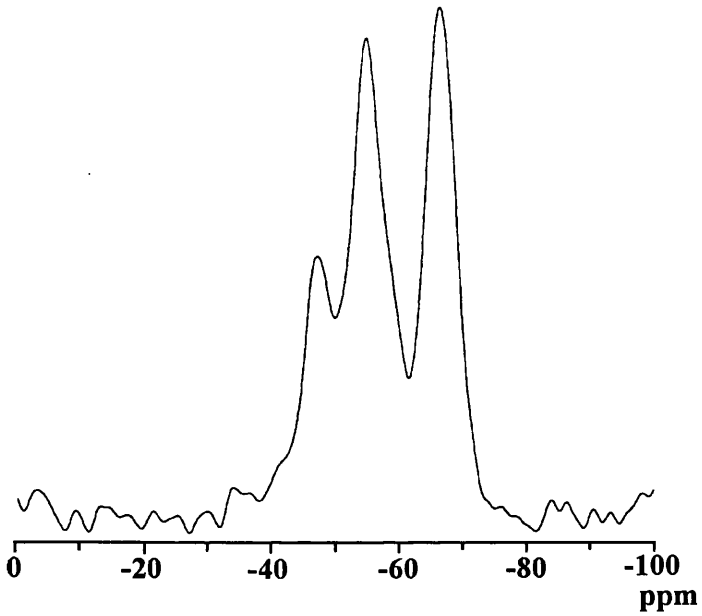

Figure 4.33 ^{29}Si DP MAS NMR spectrum for the product of the ethanolic, solid NaOH synthesis involving H30%:M70%.

Solid state ^{29}Si MAS NMR data (Figure 4.33) showed good condensation within the mixed phase product. Fully condensed T^3 centres were observed in comparable percentages to T^2 centres. Poorly-condensed T^1 silanol derivatives contributed the smallest percentage to the sample. Quantitative determination of the percentage contributions from the amorphous and ordered phyllosilicate components separately was, however, not possible.

Limitations to the usefulness of the characterization data arise when mixed-phase materials are produced, and interpretations must often be made tentatively. It does, however, seem likely that steric factors imposed by the bulk of the hexadecyl functionalities were primarily responsible for the coprecipitation of an amorphous component from the reaction mixture alongside a disordered layered organosilicate phase.

Preliminary XRD data obtained for the product of the preparation involving 100 % HDTMS indicated little ordering within the sample (Figure 4.31b). Diffraction peaks of very low intensity in the XRD pattern possibly arising from an ordered phyllosilicate structure could be discerned, but a surprisingly narrow and intense reflection at 20-25° dominated the pattern and was evidence for a predominantly amorphous phase. No further characterization was carried out on the reaction product, as it was clear that reaction conditions were not ideal for formation of the layered 2:1 trioctahedral phyllosilicate structure.

4.4 *Conclusions*

A variety of 2:1 trioctahedral (organo)phyllosilicates have been prepared from water/ethanol mixtures containing magnesium chloride, organotrialkoxysilane and base. In general, conditions of high pH favoured the formation of the silicate structure. There was evidence to suggest that in most cases generation of the layered structure occurs *via* the pre-formation of the central brucitic sheet acting as an incipient template for silanol condensation.

Amine-containing (organo)phyllosilicates were also prepared from ethanolic, base free conditions at near neutral pH. Magnesium (organo)phyllosilicates prepared by this method contained positively-charged organic moieties. Modification of the reaction conditions appeared to necessitate a modification of the mechanism by which the layered structures formed, and a more cooperative assembly between the inorganic and organic components was implied.

The employment of further modified reaction conditions was necessary in order to prepare (organo)phyllosilicates incorporating lengthy hydrocarbon chain substituents. However, it was clear from the results that there may be limitation to the types of organic functionality which can be incorporated in the interlayer region owing to the bulk of the organic moiety or unsuitable reaction kinetics of the organofunctional alkoxysilane which leads to phase separation of the magnesium and silicon components.

4.4 *Conclusions*

A variety of 2:1 trioctahedral (organo)phyllosilicates have been prepared from water/ethanol mixtures containing magnesium chloride, organotrialkoxysilane and base. In general, conditions of high pH favoured the formation of the silicate structure. There was evidence to suggest that in most cases generation of the layered structure occurs *via* the pre-formation of the central brucitic sheet acting as an incipient template for silanol condensation.

Amine-containing (organo)phyllosilicates were also prepared from ethanolic, base free conditions at near neutral pH. Magnesium (organo)phyllosilicates prepared by this method contained positively-charged organic moieties. Modification of the reaction conditions appeared to necessitate a modification of the mechanism by which the layered structures formed, and a more cooperative assembly between the inorganic and organic components was implied.

The employment of further modified reaction conditions were necessary in order to prepare (organo)phyllosilicates incorporating lengthy hydrocarbon chain substituents. However, it was clear from the results that there may be limitation to the types of organic functionality which can be incorporated in the interlayer region owing to the bulk of the organic moiety or unsuitable reaction kinetics of the organofunctional alkoxysilane which leads to phase separation of the magnesium and silicon components.

CHAPTER 5

EXPLORING THE PRACTICAL APPLICATIONS OF MAGNESIUM (ORGANO)PHYLLOSILICATES

EXPLORING THE PRACTICAL APPLICATIONS OF MAGNESIUM (ORGANO)PHYLLOSILICATES

5.1 *Introduction*

In Chapter 4 the preparations of a selection of magnesium (organo)phyllosilicates were presented. Earlier reports have also been made on the synthesis of magnesium organosilicates utilizing a one-step synthetic approach (Fukushima and Tani, 1995; Ukraincyzk *et al.*, 1997; Burkett *et al.*, 1997). These inorganic/organic hybrid materials are members of an exclusive class of layered compounds containing organic entities chemically connected to the inorganic mineral framework. The layered metal(IV) organophosphonates and organophosphates also belong to this group of materials and may likewise be generated utilizing a one-step synthetic approach (Yamanaka, 1976; Alberti *et al.*, 1978). An analogy has been drawn between the formation mechanisms of the metal(IV) organophosphonates and phosphates and magnesium (organo)phyllosilicates; namely, that the generation of the structure is primarily directed by the coordination requirements of the inorganic components (Cao *et al.*, 1992). The widely-synthesized metal(IV) organophosphonates and organophosphates were quick to arouse interest since they provided an ordered array of organic moieties within a stable inorganic matrix. Tailoring of the organic components has allowed for a variety of applications in ion-exchange, catalysis and in the construction of nanoscale assemblies. The magnesium (organo)phyllosilicates contain a similar structural arrangement of alternating

inorganic and organic moieties and thus have extensive applicability. Thus far, however, little investigation into the properties of these materials has been reported.

Catalytic conversions involving organic compounds immobilized on clay surfaces or intercalated between the silicate sheets have been known for some time (Laszlo, 1987). *In situ* reactivity of magnesium (organo)phyllosilicates containing phenyl and thiol functionalities was recently investigated by Burkett *et al.* (1997). Thiol functionalities were oxidized to disulphides, and phenyl groups were reacted with organometallic $Mo(CH_3CN)_3(CO)_3$ compounds to form molybdenum arene carbonyl complexes. It is clear, however, that the number of bimolecular reactions possible between clay-bound organic groups and guest molecular species are numerous, and a variety of conversions are possible in order to assess the accessibility of the interlayer regions and reactivity of the pendent functionalities.

In the preparation of layered polymer-containing nanocomposites intercalation of the organic polymer or *in situ* polymerization of monomeric species in a pre-formed inorganic host is usually necessary (Vaia *et al.*, 1993, and references therein). Retention of the organic polymer within the inorganic host generally involves physical interactions such as weak electrostatic, Van der Waals or hydrogen-bonding. Copolymerizations involving tetralkoxysilanes and organofunctional alkoxysilanes have been utilized in sol-gel chemistry for the fabrication of organically-modified ceramics (ORMOCERS); hybrid systems consisting of organic networks covalently connected to inorganic silica matrices. The organofunctional alkoxysilanes contain polymerizable functionalities which lead to the formation of highly cross-linked composite systems (Phillip and Schmidt, 1984). There is, however, little ordering of the organic and inorganic components within these systems. Magnesium

(organo)phyllosilicates have been prepared which contain polymerizable organic functionalities (e.g., epoxide, methacrylate) in the interlayer spaces between the inorganic sheets. Controlled polymerization of the pendent organic functionalities offers the possibility of preparing ordered inorganic-organic polymer composites in which the polymer is molecularly dispersed in, but covalently bound to, the layered inorganic framework. A composite of this type was realized recently with the solid state polymerization of layer-bridging diacetylene monomers predisposed in a Mn(IV) organophosphonate [Cao and Mallouk, 1991 (Figure 1.10)].

Post-synthesis modifications of the internal pore surfaces of hexagonally-ordered silica structures (MCM-41) recently allowed for the attachment of organic functionalities with ion-binding and metal sequestering properties (Feng *et al.*, 1997; Díaz *et al.*, 1997). Rational design strategies applied for the fabrication of similar materials will, it is hoped, lead to applications in a variety of areas including environmental clean-up and separation processes. Metal sequestration in the interlayer region of magnesium (organo)phyllosilicates is equally possible through selection of suitable organic functionalities. Gold nanoparticles have been prepared within the organothiol-derivatized interlayer spaces of a magnesium (organo)phyllosilicate (Burkett *et al.*, 1997). It is envisaged that 2-D molecular arrays of inorganic and organometallic guest species may be prepared within the layered inorganic-organic hybrid structures.

Porosity has been created in layered inorganic systems through the insertion of organic or inorganic pillars between adjacent sheets (Pinnavaia, 1983; Behrens, 1993). The swelling of smectite clays and substitution of the small interlayer cations with larger oligomeric cations leads to the establishment of stable inorganic links between

the clay layers and pillars upon calcination. Silica pillars have been inserted in alkylammonium-cation exchanged silicates, by diffusion and reaction of tetraethoxysilane within the interlayer regions (Landis *et al.* 1991, Galarneau *et al.*, 1995) creating porosity in the lamellar structure. Layered double hydroxides have also been pillared by inorganic isopolymetalate cationic pillars with a view to extending the catalytic applications of these materials (Drezdon, 1988). Pillared zirconium diphosphonates, $Zr^{IV}(O_3P\text{-}R\text{-}PO_3)$, have been prepared directly utilizing bisphosphinic acids in a similar synthetic approach to the synthesis of metal(IV) organophosphonates (Alberti *et al.*, 1993). In the pillared structures, adjacent inorganic layers are joined covalently by organic R groups, and materials with specific interlayer porosity can be prepared by simply changing the length of the organic R group. Through suitable choice of organofunctional silicon source it may be equally feasible to introduce porosity into the magnesium (organo)phyllosilicates.

This chapter outlines some preliminary work focused on investigating the practical potential of magnesium (organo)phyllosilicates. In particular, the reactivity of the organic functionalities towards bimolecular intra- and intermolecular reactions will be explored with a view to generating novel organic polymer composites and tailoring the organic functionalities within the solid for a specific purpose. Preliminary results from cobalt and gold sequestration investigations and syntheses involving organically- bridged bis(trialkoxysilyl) monomers in an attempt to generate "pillared" (organo)phyllosilicates with porosity will be presented.

5.2 *Experimental*

Materials

Magnesium (organo)phyllosilicates prepared as reported in Chapter 4 were utilized. Methyl thioglycolate, magnesium chloride hexahydrate, cobalt chloride hexahydrate, *m*-phenylenediamine flakes and hydrogentetrachloroaurate(III) trihydrate were obtained from Aldrich Chemical Co. and used without further purification. Potassium carbonate from Aldrich was dried in an oven at 100 °C for 12 h to remove water. α-Azo-*iso*-butyronitrile was obtained from BDH. 1,6-Bis(trimethoxysilyl)hexane and 1,4-bis(trimethoxysilylethyl)benzene of unknown purity were obtained from Apollo Scientific Ltd and used without further purification. Sodium hydroxide pellets (99 %) were obtained from Aldrich and used in the preparation of sodium hydroxide solutions. Dry tetrahydrofuran, methanol (99 %), ethanol (94 - 96%), and doubly distilled, deionized water were utilized as solvents and in the washing stages.

Ring-opening of clay-bound epoxides by reaction with guest thiols

Epoxy-containing Mg-EPTMS (0.22 g, approx. 1.0 mmol epoxide residues) was charged to a reaction vessel with anhydrous potassium carbonate (1.40 g, 10 mmol). The vessel was placed under vacuum and back-filled three times before leaving under nitrogen for the duration of the reaction. Nitrogen-purged THF (80 ml)

was added to the solid reagents before the addition of methyl thioglycolate (0.4 ml, 4.0 mmol). The temperature was raised to 70 °C and reflux conditions employed for 24 h after which time the reaction vessel was allowed to cool to room temperature. The reaction mixture was filtered and the solid material isolated stirred for 30 min in 200 ml water in order to redissolve any residual potassium carbonate and filtered and washed with a further 100 ml of water. Finally the solid product was washed with THF (50ml) to remove residual organics. The product was dried at 45 °C for 18 h resulting in a pale yellow solid.

Crosslinking of clay-bound epoxides upon thermal treatment in the presence of an m-PDA curing agent

Thermal treatment of Mg-EPTMS in the presence of an amine curing agent was employed to achieve crosslinking of epoxide residues. Typically, a sample of Mg-EPTMS (0.3g; containing 0.15g organic residues) was ground with *m*-phenylenediamine, *m*-PDA (0.02g; ~14 wt.% of clay organics), and stirred for 30 min. The solid mixture was placed under vacuum and degassed at 75 °C for 30 min before the temperature was raised to 125 °C under vacuum for 4 h. The resultant solids were washed thoroughly with water and ethanol to remove *m*-phenylenediamine.

A control sample of Mg-EPTMS was thermally-treated in an identical way in the absence of *m*-phenylenediamine.

Polymerization of clay-bound methacrylate residues utilizing a free-radical initiator

The free-radical polymerization of methacrylate monomers initiated by α-azo-*iso*-butyronitrile [2,2'-azo-bis(2-methylpropionitrile) (AIBN)] is a well-known reaction. This synthetic approach was employed to react adjacent pendent methacrylate groups within the interlayer region of Mg-MPTMS.

A reaction vessel was charged with Mg-MPTMS (0.24 g, ~0.14 g methacrylate residues), AIBN (0.005 g, equivalent to 4 wt. % of the methacrylate residues) and THF (60 ml). The reaction mixture was heated at 70 °C for 20 h under reflux conditions. The solid was isolated by filtration and thoroughly washed with THF (50 ml). The solid product was dried at 40 °C for 12 h.

Incubation of Mg-EDTMS in Co(II)-containing solution

The ethylenediamine residues within the interlayers of the Mg-EDTMS are available for metal ion binding. A 0.2 M solution of cobalt(II) was prepared by dissolving cobalt(II) chloride hexahydrate, $CoCl_2 \cdot 6H_2O$, (0.476 g, 2.0 mmol) in 10 ml of freshly doubly distilled water. The metal ion solution was purged for a short period with nitrogen before addition of Mg-EDTMS (0.2 g, approx. 0.5 mmol ethylenediamine residues). Upon addition of the clay to the red-coloured solution the solution quickly darkened to a purple coloration. The mixture was left stirring in a sealed vessel for 12 h at room temperature. The solid products were washed with

deionized water and methanol using centrifugation. The products were dried in air at 50 °C for 24 h. The final product was pale mauve in colour.

An identical incubation was carried out using Mg-H^+EDTMS, the product of the synthesis carried out in Chapter 4 under ethanolic, base-free conditions. A pale pink-coloured solid was isolated.

Gold binding in the interlayer spaces of amine-containing magnesium (organo)phyllosilicates

(a) In situ *reduction of $HAuCl_4$ during standard synthesis of Mg-ATES*

The procedure involved the concomitant reduction of $HAuCl_4$ and formation of Mg-ATES under methanolic, basic conditions. A flask was charged with magnesium chloride hexahydrate, $MgCl_2 \cdot 6H_2O$, (O.42 g, 2.07 mmol), hydrogentetrachloroaurate(III) trihydrate, $HAuCl_4 \cdot 3H_2O$, (0.02 g, 0.055mmol), and methanol (12 ml). To the pale yellow solution, 1-aminopropyltriethoxysilane [(ATES) (0.65 ml, 2.78 mmol)], was added. $[Au]/[NH_2] = 0.02$. The solution underwent a rapid colour change to vibrant red. Upon addition of NaOH solution (50 ml, 0.05 M) a clouding of the solution was observed and the reaction mixture became canary yellow in colour. The reaction mixture was left stirring for 72 h at room temperature. Solid products were isolated by centrifugation and thorough washing with methanol (50 ml) and water (100 ml). After drying for 12 h at 50 °C in air the solid product was deep red/purple in colour.

(b) In situ *reduction of $HAuCl_4$ during ethanolic, base-free synthesis of Mg-ATES*

A second preparation was carried out using base-free conditions. To a flask charged with $MgCl_2 \cdot 6H_2O$ (0.42 g, 2.1 mmol), $HAuCl_4 \cdot 3H_2O$ (0.02 g, 0.055 mmol) and methanol (12 ml), ATES (0.65 ml, 2.8 mmol) was added. An immediate colour change of the reaction mixture from yellow to red was observed. With time the reaction mixture returned to a yellow colour and stirring continued at room temperature for 24 h. The solid product was isolated by centrifugation and thorough washing with methanol (50 ml) and water (25 ml), before it was dried in air at 50 °C for 12 h. A straw-coloured product resulted.

(c) Reduction of $HAuCl_4$ in the presence of pre-formed Mg-EDTMS

The preparative procedure of Burkett *et al.* (1997) was employed in an attempt to utilize the gold-binding affinity of the ethylenediamine groups and immobilize gold particles within the interlayers of the hybrid material upon reduction of $HAuCl_4$.

Finely-ground Mg-EDTMS (0.1 g, approx. 1.0 mmol ethylenediamine residues) was dispersed in 10 ml water. To the clay solution a freshly-prepared solution of hydrogentetrachloroaurate(III) trihydrate, $HAuCl_4 \cdot 3H_2O$, (0.024 g in 1.5 ml methanol) was added. The resultant reaction mixture adopted an initial red coloration before changing to yellow. The mixture was left stirring for 12 h at room temperature. The solid product was isolated by centrifugation and washed with water (50 ml) and methanol (20 ml). The dried sample was indigo in colour.

Synthesis of magnesium (organo)phyllosilicates containing layer-bridging organic aryl and alkyl functionalities

1,6-Bis(trimethoxysilyl)hexane and 1,4-bis(trimethoxysilylethyl)benzene (Scheme 5.1) were employed as the silicon sources in an adapted synthetic approach for the preparation of magnesium (organo)phyllosilicates containing layer-bridging pendant organic groups. Typically $MgCl_2 \cdot 6H_2O$ (0.84 g, 4.15 mmol) was dissolved in ethanol (25 ml) before addition of the bis(trimethoxysilyl) monomers (2.83 mmol) under rapid stirring. Sodium hydroxide solution (100 ml, 0.2 M) was then added and the reaction mixture stirred for 24 h at room temperature. Solid products were isolated by centrifugation, washed with ethanol (3 × 50 ml) and water (2 × 50 ml), and dried at 50 °C in air.

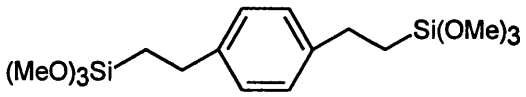

1,4-bis(trimethoxysilylethyl)benzene

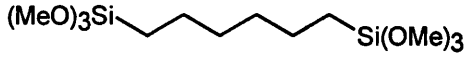

1,6-bis(trimethoxysilyl)hexane

Scheme 5.1 Structures of the organo-bridged ethoxysilyl species utilized in the synthesis of pillared magnesium (organo)phyllosilicates

Characterization

Solid state ^{13}C CP MAS and ^{29}Si MAS NMR spectroscopy was carried out by the EPSRC service at Durham University. Carbon, hydrogen and nitrogen microanalyses, FTIR spectroscopy, X-ray diffraction and electron microscopy were carried out at the University of Bath, using the procedures and equipment outlined in Chapter 2: **General Methods**. Thermal analysis data was collected at English China Clays International, St. Austell.

5.3 *Results and Discussion*

Epoxide ring-opening by guest thiol species

Epoxide ring-opening by reaction with thiol-containing nucleophiles has been recognized and utilized in organic synthesis for some time (Pirkle and Rinaldi, 1978). The reaction typically proceeds to give the 'normal' ring-opened derivative. In an attempt to probe the interlayer accessibility and reactivity of clay-bound organic functional groups, an epoxide ring-opening reaction was attempted using methyl thioglycolate (Scheme 5.2). A 5× excess of nucleophile was utilized in order to compensate for possible slow rates of diffusion into the organophilic interlayers of the (organo)phyllosilicate.

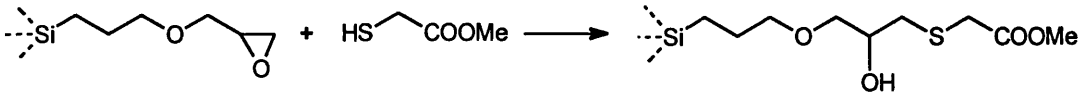

Scheme 5.2.. Reaction between clay-bound epoxide groups and nucleophilic methyl thioglycolate.

The success of the ring-opening reaction was primarily shown by solid state ^{13}C CP MAS NMR spectroscopy carried out on the solid product of reaction (Figure 5.1). Comparison with the corresponding ^{13}C NMR spectrum for as-synthesized Mg-EPTMS (Figure 4.5) showed the disappearance of those signals assigned to the epoxide functionality; namely those at 44 and 52 ppm. Broadened resonances were assigned for the expected product of the reaction with the increased linewidths of resonances compared to those from the unreacted organosilicate indicating a significant increase in the disorder of the organic moieties within the interlayer regions. Their broadness, however, made it difficult to make definitive assignments for those carbons which display signals occurring within a close frequency range. Solution ^{13}C NMR data of the unreacted nucleophile, methyl thioglycolate, gave resonances at chemical shift values of 26 ppm, 52 ppm and 171 ppm, which indicated no residual starting thiol in the reacted magnesium (organo)phyllosilicate.

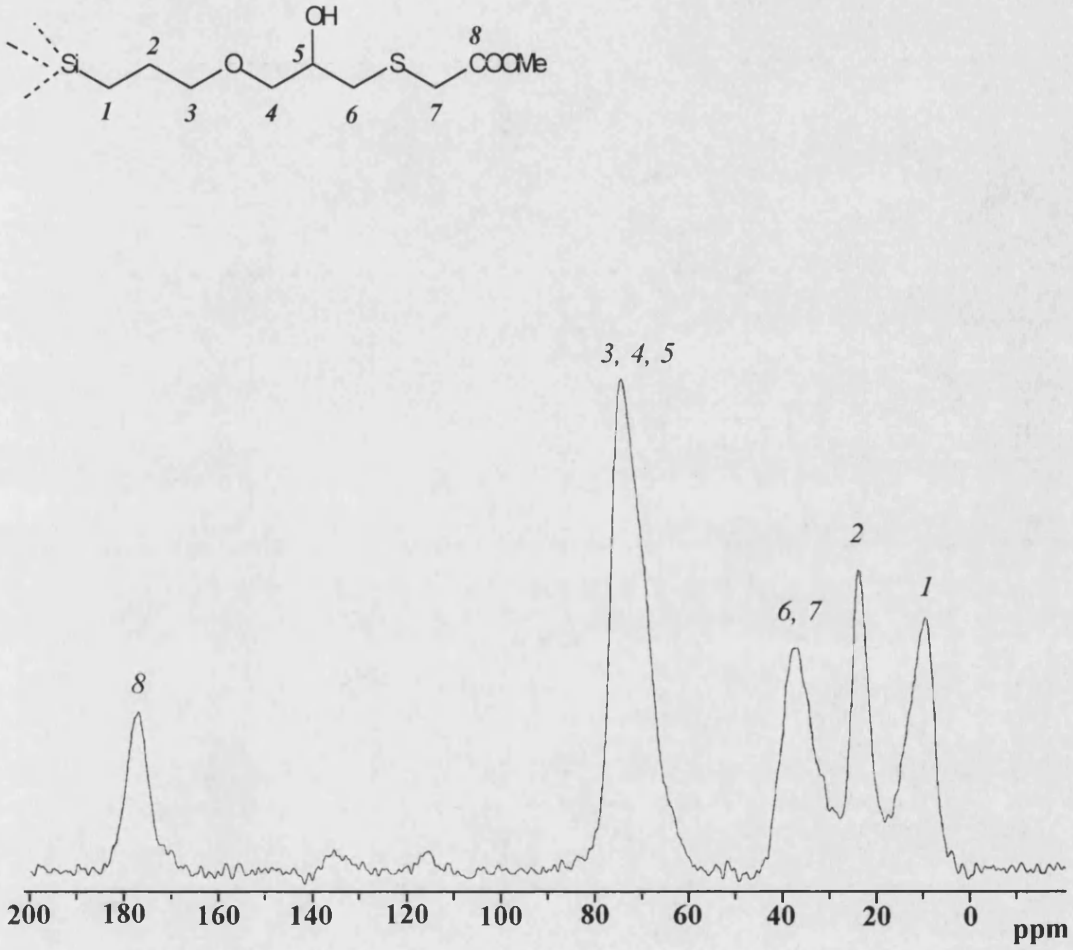

Figure 5.1 ^{13}C CP MAS NMR spectrum for the product of reaction between methyl thioglycolate and Mg-EPTMS

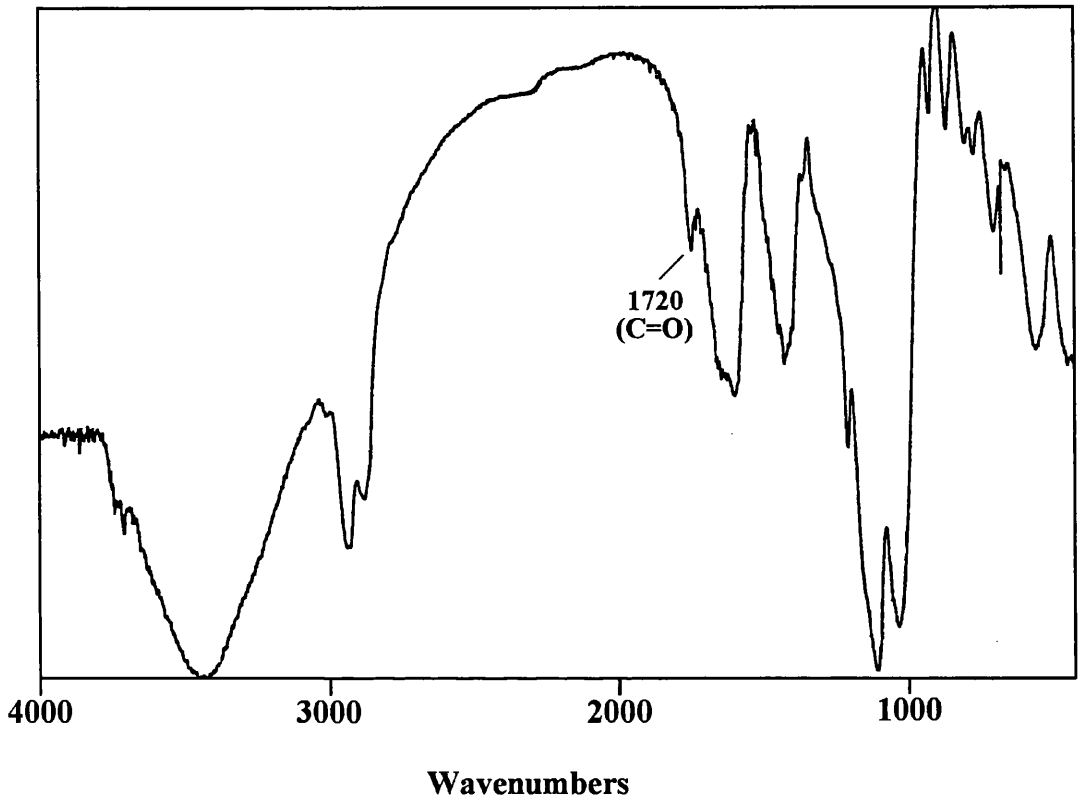

Figure 5.2 FTIR spectrum for the product of reaction between methyl thioglycolate and Mg-EPTMS

In the FTIR spectrum assignments could be made for the inorganic framework modes of the (organo)phyllosilicate: Mg-O (520 cm^{-1}), Si-O-Si (1015-1040 cm^{-1}), O-H (3400-3450 cm^{-1}), MgO-H (3700 cm^{-1}) (Figure 5.2). The Si-C absorption at 1200 cm^{-1} indicated no hydrolysis of these bonds during the hydrothermal reaction conditions employed for ring-opening. Characteristic alkyl absorptions were still evident at 2850 cm^{-1}, 2980 cm^{-1} and 1390-1440 cm^{-1} in addition to a well-resolved peak at 1720 cm^{-1} indicative of a carbonyl (C=O) group vibration. Under the basic reaction conditions employed (pH > 10) it is possible that saponification of the ester group took place. The position of the carboxyl peak at 1720 cm^{-1} could be assigned to either a carboxylic acid or ester functionality. Vibrational modes of the sulphide group are, however, weak and are frequently unresolved in the infra-red (Colthup *et al.*, 1964) and this appeared to be the case in data obtained for the ring-opened Mg-EPTMS derivative, with no discernible vibrations assignable to this group. Energy dispersive X-ray analysis (EDXA) on the reaction product clearly indicated the presence of sulphur (Figure 5.3) which is absent in the starting material.

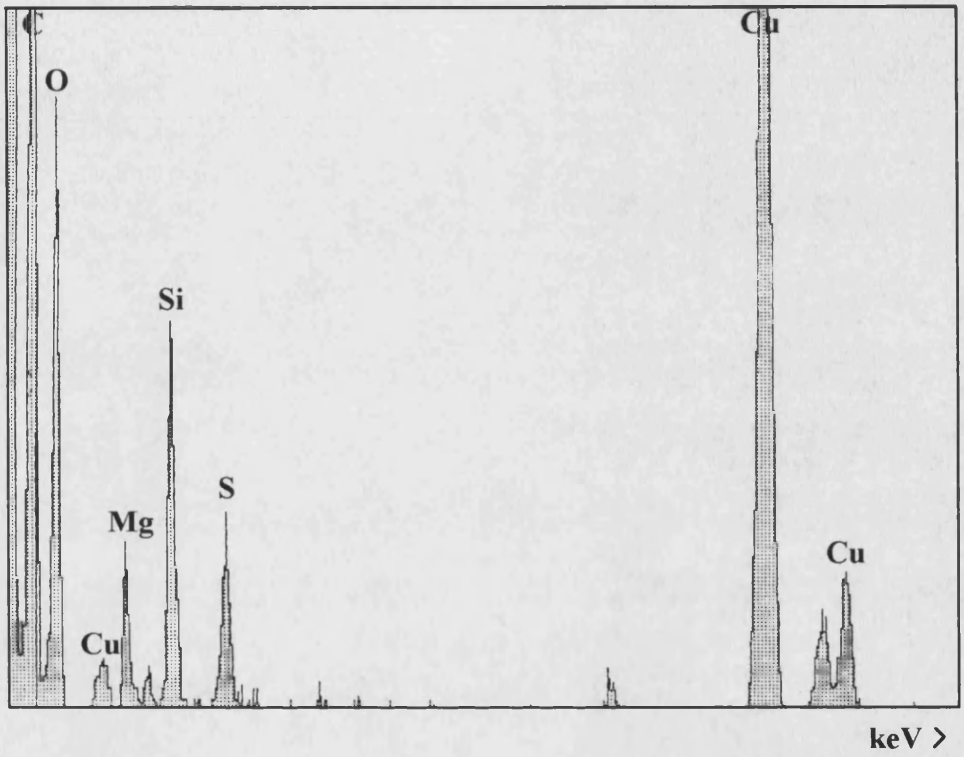

Figure 5.3 EDXA data for the product of reaction between methyl thioglycolate and Mg-EPTMS. Bare copper grids used to mount sample for analysis.

An increase in the disorder in the interlayers of the (organo)phyllosilicate was also apparent from the powder X-ray diffraction pattern (Figure 5.4). The (001) reflection was broadened and of weaker intensity, which indicated a decrease in the short range ordering of the inorganic sheets relative to each other. Moreover, a contraction of the interlayer separation (to 11.2 Å) was implied by the observed increased 2θ value at which (001) peak occurred. The diffusion of the guest thiol species into the interlayer region during the reaction was expected to create a certain degree of disruption to the organization of the inorganic layers relative to each other and increase the extent of turbostratic disorder. Furthermore, the accommodation of reacted thiol derivatives in the gallery region would necessitate rearrangement of the organic functionalities in these spaces. Without knowing the arrangement of the epoxide moieties prior to reaction it is impossible to predict whether the incorporation of increased organic matter would lead to an expansion or contraction in the interlayer spacing. It appeared that in the case of the reaction between the clay-bound epoxide functionalities and guest thiol nucleophiles, the reorganization resulted in a decreased *d*-spacing in the stacking direction. Other intraclay reflections; $d_{020,110}$, $d_{130,200}$ and $d_{060,330}$; were still evident and of comparable broadness to unreacted Mg-EPTMS, which signified no further disruption within the inorganic sheets.

Deconvolution of the well-resolved ^{29}Si MAS NMR spectra showed little change in the relative percentages contributed by individual condensed silicon centres in the sample. Values of T^1 (12.7%), T^2 (24.1%) and T^3 (63.2%) (Figure 5.5) compared with T^1 (13.6%), T^2 (18.5%) and T^3 (67.9%) for as-synthesized Mg-EPTMS (Figure 4.11), indicated a small amount of hydrolysis of the T^3 centres.

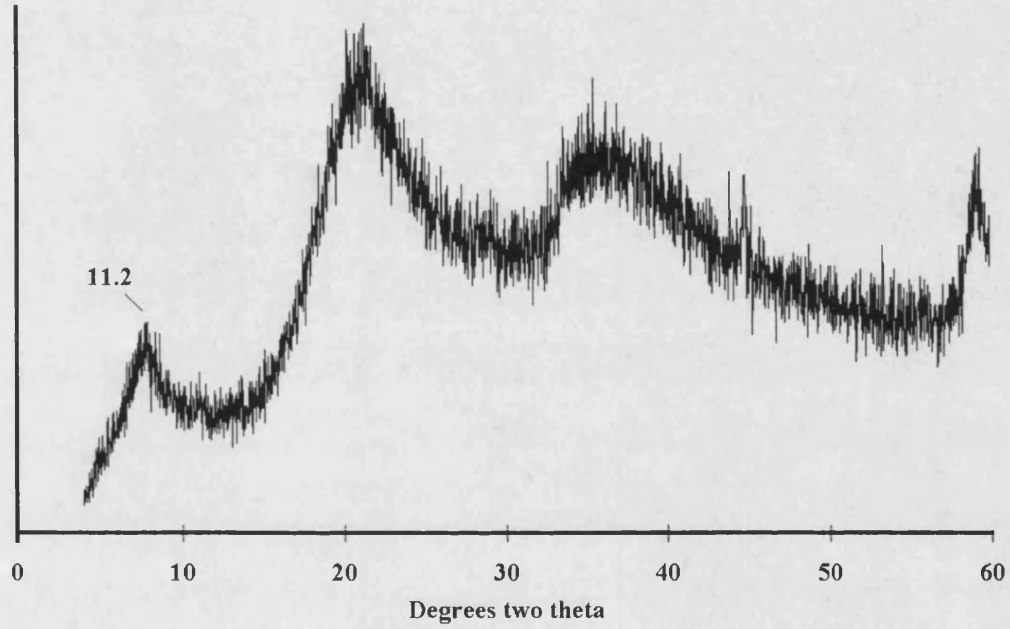

Figure 5.4 PXRD data for product of reaction between methyl thioglycolate and Mg-EPTMS. Interlayer spacing indicated in Å.

	Chemical Shift (ppm)	%
T^1	-49	12.7
T^2	-56	24.1
T^3	-67	63.2

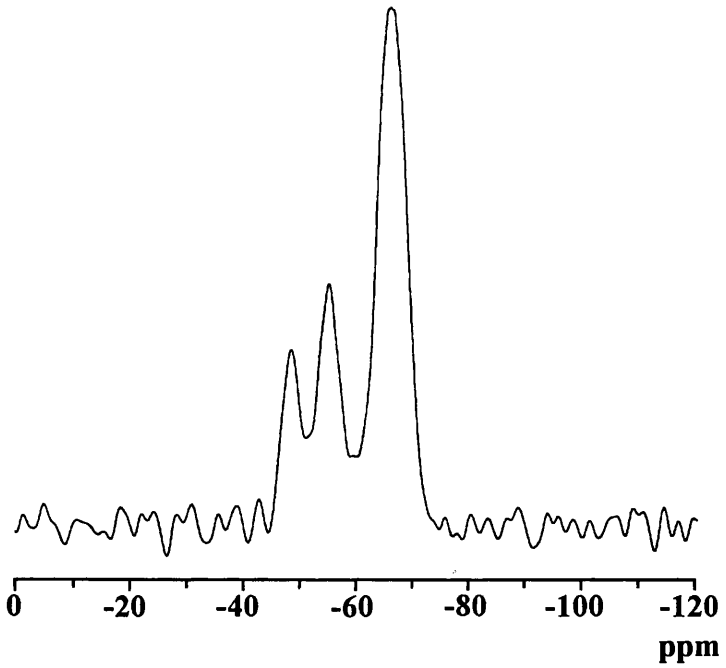

Figure 5.5 ^{29}Si DP MAS NMR data for the product of reaction between methyl thioglycolate and Mg-EPTMS

Thermal analysis of the magnesium (organo)phyllosilicate ring-opened derivative highlighted differences in the thermal behaviour compared to Mg-EPTMS. Firstly, a weight loss of 10% between ambient and 150 °C for the reacted material (Figure 5.6) compared to only 2% for Mg-EPTMS (Figure 4.16a) was attributed to an increase in 'wettability' or hydrophilicity of the sample. Over this temperature range water molecules surface-sorbed on the material were removed from the sample. Since the ring-opening reaction was carried out in organic solvents and, following washing of the sample, drying of the product employed identical conditions to those utilized for drying Mg-EPTMS it seemed likely that adsorption of water from the atmosphere had occurred post-drying. The reaction involving the pendent epoxide functionalities resulted in the generation of more hydrophilic ester (or carboxylic acid) groups which may account for the increased amount of adsorbed water recorded in the thermal analysis. The decomposition of epoxide functionalities within Mg-EPTMS took place at just below 400 °C (Figure 4.16a) with the corresponding endotherm in the differential trace (DTG) maximizing at 400 °C. The weight loss continued up to 600 °C. For the ring-opened derivative the onset of organic decomposition was recorded at 250 °C with a well-resolved endotherm centred at this temperature, and a second broadened endotherm ensued at 325 °C and was centred at 425 °C. Weight losses were 20% and 22% for the 250 °C and 425 °C endotherms respectively. These results implied a lower thermal stability for the ring-opened derivative than the epoxide moiety.

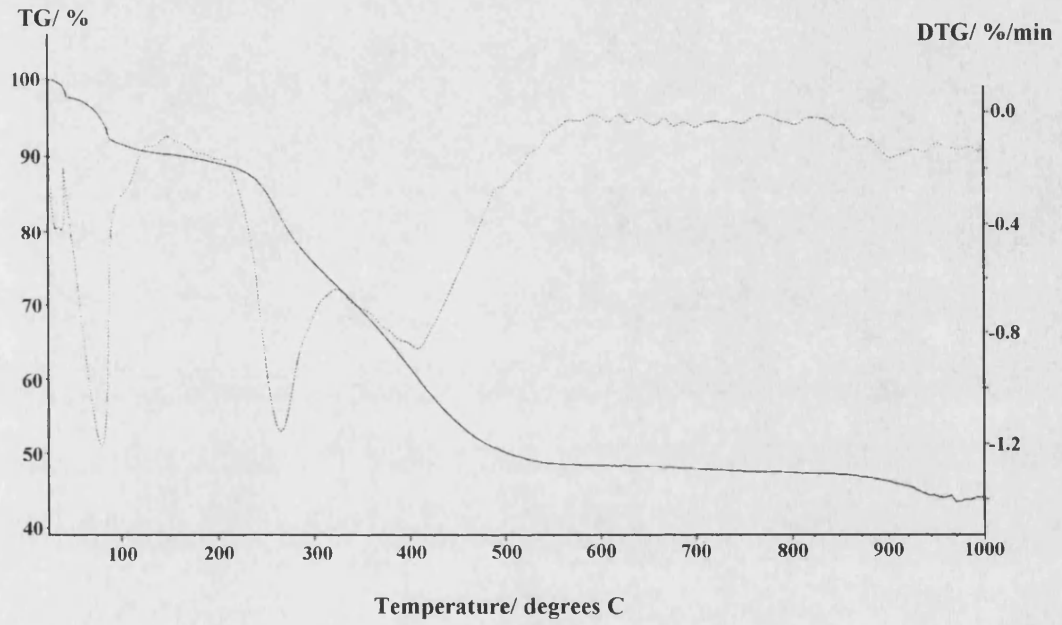

Figure 5.6 Thermogravimetric analysis data for the product of reaction between methyl thioglycolate and Mg-EPTMS. Dotted line indicates differential (DTG) trace.

This study illustrated how the reactivity of the pendent organic groups may be exploited to achieve intercalation of guest molecular species via chemical reaction. Under suitable conditions the interlayer functionalities of pre-formed (organo)phyllosilicates may be readily accessed and available for organic intermolecular conversions which will introduce new functional groups into the interlamellar region. Post-synthesis modifications afford the possibility to incorporate functional groups that are unobtainable, for example, as organofunctional trialkoxysilanes or which in the form of organotrialkoxysilanes have unsuitable hydrolysis/condensation kinetics for the formation of the magnesium (organo)phyllosilicate. In addition, the nature of the interlayer environment, e.g., reactivity, hydrophobicity, hydrophilicity, may be tailored for a specific purpose.

Thermal treatment of Mg-EPTMS in presence of* m-*PDA

The polymerization of epoxides to form crosslinked polymeric materials is employed industrially for the manufacture of commercial resins and ultimately in the synthesis of epoxy-based composite materials. Uncatalyzed self-polymerization of epoxides will occur spontaneously at elevated temperatures, however, the addition of a suitable curing agent serves to lower the reaction temperature required and affords better control over the polymerization process. Curing agents are frequently amine-containing species which react with epoxy groups to produce hydroxyl groups which (1) catalyze the reaction that produces them and (2) can themselves react with epoxy

rings to form ether linkages. Scheme 5.3 outlines the main reaction involved in the cure of epoxy resins with primary amine curing agents (Cole, 1991).

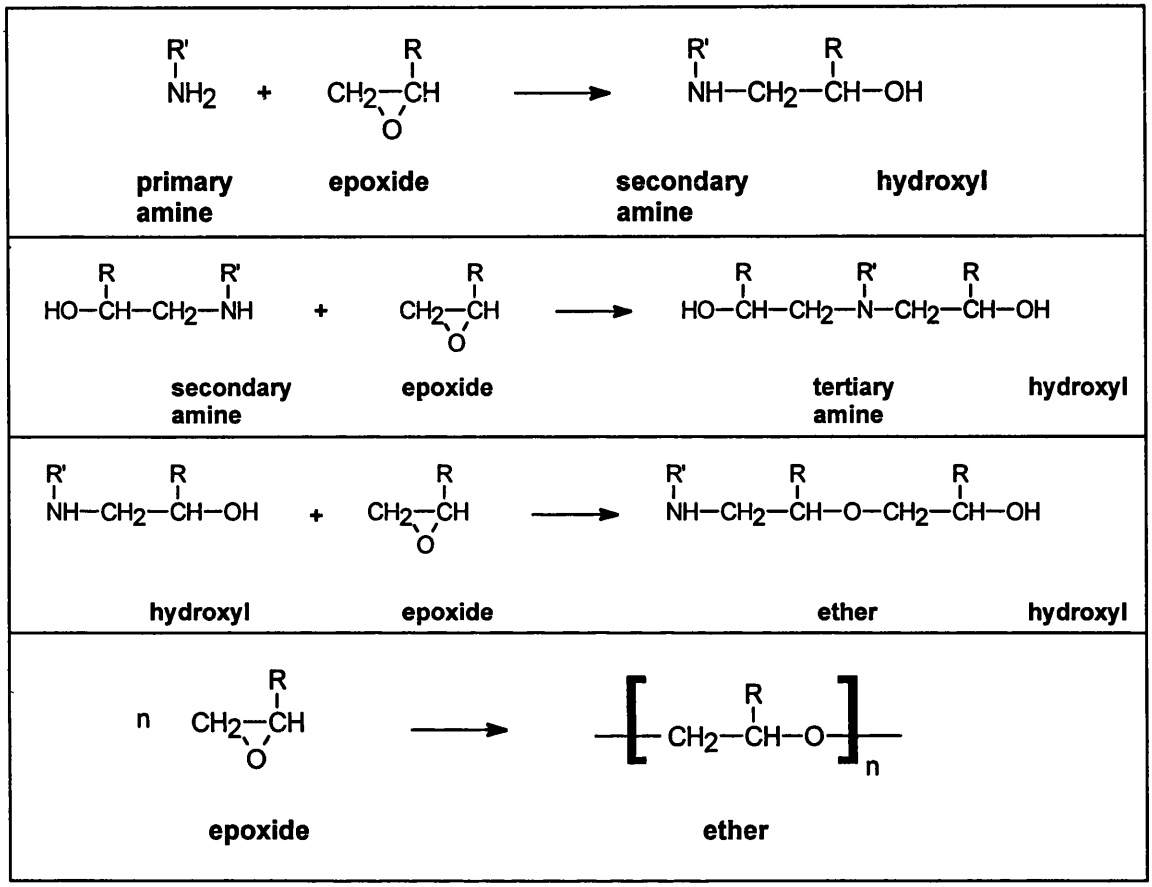

Scheme 5.3 Main reactions involved in the cure of epoxy resins with primary amine curing agents.

Homopolymerization of epoxy resin monomers in the galleries of acidic alkylammonium ion-exchanged forms of montmorillonite has previously been achieved; the polymerization proceeding with concomitant delamination of the inorganic sheets (Wang and Pinnavaia, 1994; Lan *et al.*, 1995). The resultant exfoliated clay-polymer nanocomposites contain individual silicate sheets delaminated in a continuous polymer matrix. Polymerization of epoxy resin monomers within the gallery spaces (intragallery) was facilitated by the catalytic

action of the quaternary alkylammonium ions, whilst extragallery polymerization of the resin was induced by the action of a curing agent and application of suitable curing temperatures and times. One of the curing agents selected for these experiments was *m*-phenylenediamine (*m*-PDA) (Lan *et al.*, 1995):

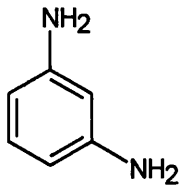

m-PDA

The exfoliated clay-polymer nanocomposite generated by this reaction contained individual silicate layers physically held in a polymer matrix. It was of interest to investigate the possibility of cross-linking the epoxide functionalities of the magnesium (organo)phyllosilicate, Mg-EPTMS, with a view to generating a well-ordered chemically-linked nanocomposite. Within this material the cross-linked organic polymer would be molecularly dispersed in the interlayer regions between adjacent inorganic sheets and in turn be bound to the layered inorganic framework by virtue of Si-C linkages. The hydrophobic interlayer environment of epoxy-functionalized Mg-EPTMS was expected to be suitable to allow for *m*-PDA migration into it at elevated temperatures. The temperature employed for the reaction (125 °C) was, however, considerably lower than that at which self-polymerization of epoxide residues would occur.

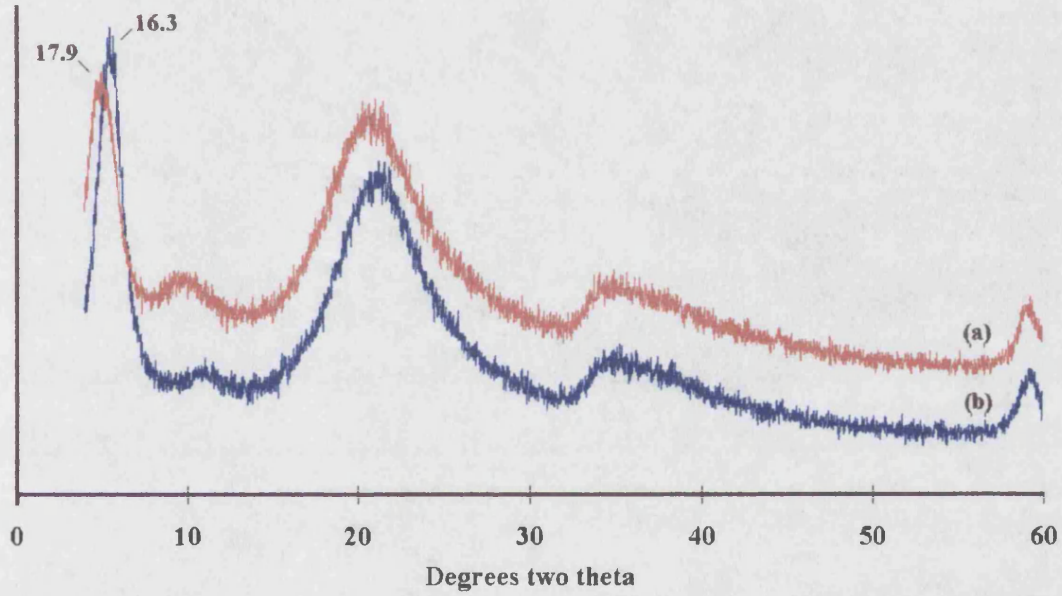

Figure 5.7 PXRD patterns for (a) Mg-EPTMS heated in presence of mPDA and (b) control Mg-EPTMS heated alone. Interlayer spacings indicated in Å.

Promising results indicating the cross-linking of epoxide functionalities were obtained upon analysis of the product of the thermal treatment of Mg-EPTMS in the presence of *m*-PDA. Powder XRD data showed an increase in the d_{001}-spacing from 15.9 Å to 17.9 Å (Figure 5.7a). In contrast a sample of Mg-EPTMS exposed to an identical thermal treatment, but in the absence of m-PDA showed an increase to 16.3 Å; 0.4 Å greater than prior to heating (Figure 5.7b). The change in *d*-spacing in both cases could be attributed to a reorganization of the organic arrangements within the interlayer region. The anticipated cross-linking of the residues under the action of a curing agent appeared to lead to a greater degree of re-ordering than in the control sample. The broadness of the diffraction peaks in both cases were comparable to those of as-synthesized Mg-EPTMS indicating no loss of order within the system and intraclay reflections were still observed.

Solid state ^{13}C CP MAS NMR spectroscopy provided further evidence for a certain degree of cross-linking between epoxide residues. Figure 5.8a shows the spectrum of Mg-EPTMS following thermal treatment in the presence of *m*-PDA. Most notable is the broadening of the signals compared to that of the control sample (Figure 5.8b), which may be attributed to the increased disorder generated in the system upon crosslinking of epoxide residues. Solid state ^{13}C NMR experiments on highly crosslinked polymeric samples are known to exhibit broad linewidths (Komoroski. 1986; Fyfe, 1983). In the disordered bulk of a crosslinked polymer sample the nonregularity of the molecular packing and conformations lead to dispersions of isotropic chemical shifts. Furthermore, in highly crosslinked samples suppression of the molecular tumbling may occur and incomplete averaging of the anisotropic spin interactions is observed which also becomes evidenced as broadened linewidths.

Results from a non-quaternary suppression (NQS) study (Appendix 1) on the reacted Mg-EPTMS sample confirmed there to be a mixture of mobile (ordered) and disordered (rigid) carbon environments within the sample (Figure 5.9). The NQS experiment generates a spectrum in which signals from CH_2 and CH species are removed. However, mobile carbons within the sample (i.e not held in a rigid lattice) are able to overcome the strong C-H dipolar coupling effects and are unremoved. In the NQS spectrum for Mg-EPTMS heated in the presence of *m*-PDA signals were assignable to all carbons of the organic substituent, which was surprising since this indicated the presence of unreacted, mobile groups (Figure 5.9, labeled "non-protonated"). However, in the difference spectrum (CP MAS - NQS) [Figure 5.9 labeled "protonated (difference)"], contributions from more rigid (disordered) carbons were revealed. Interestingly, this spectrum contained no signals from epoxide group carbons, whilst broadened signals for ether and alkyl carbons were observed. Thus, it seemed reasonable to assume that the difference spectrum contained signals arising solely from cross-linked material, since the curing process involved opening of the epoxide rings to generate ether functionalities, with an anticipated downfield chemical shift for the epoxide signals to the ether region of the spectrum.

It was not possible from the data shown, to calculate the quantitative conversion of epoxide to ether functionalities. A decrease in the overall intensity of the epoxide signals relative to those from ether groups was observed, but further studies would be necessary which would take into account different magnetization rates for individual carbon species in order to treat the data quantitatively.

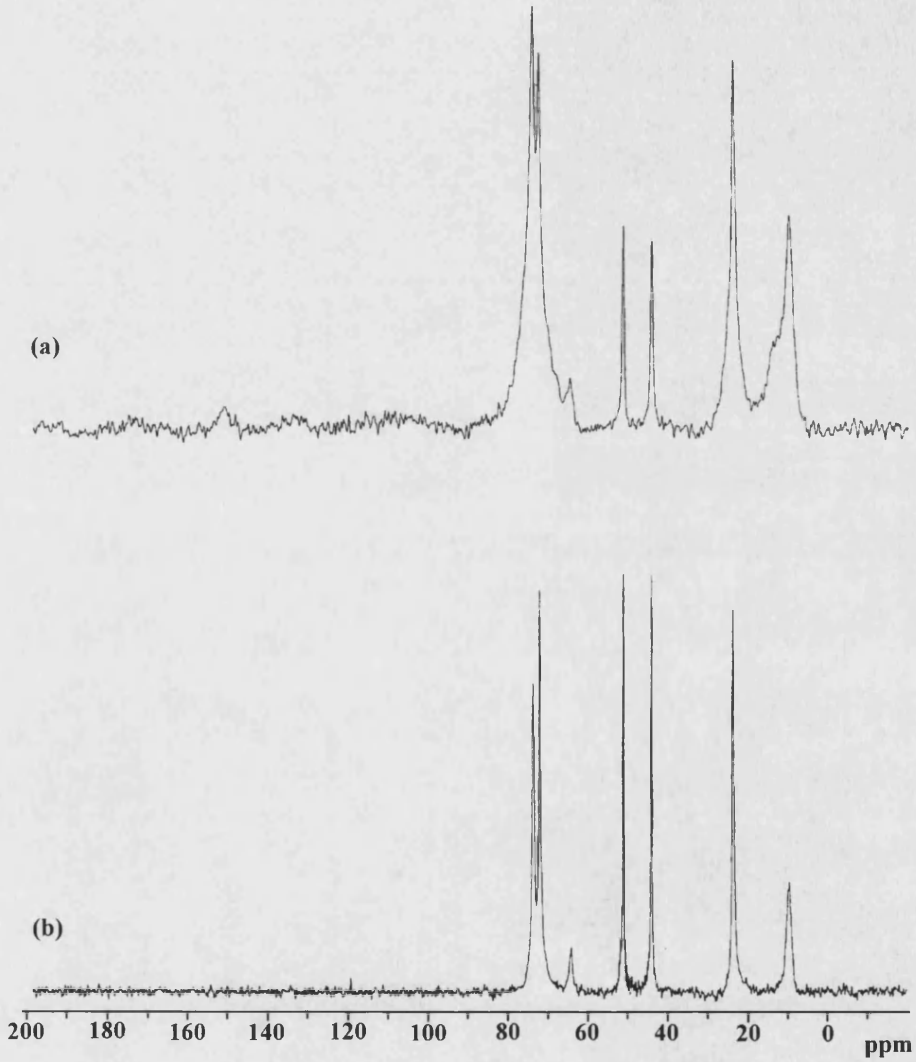

Figure 5.8 ^{13}C CP MAS NMR spectra for Mg-EPTMS following thermal treament

(a) in the presence of mPDA and (b) in the absence of mPDA

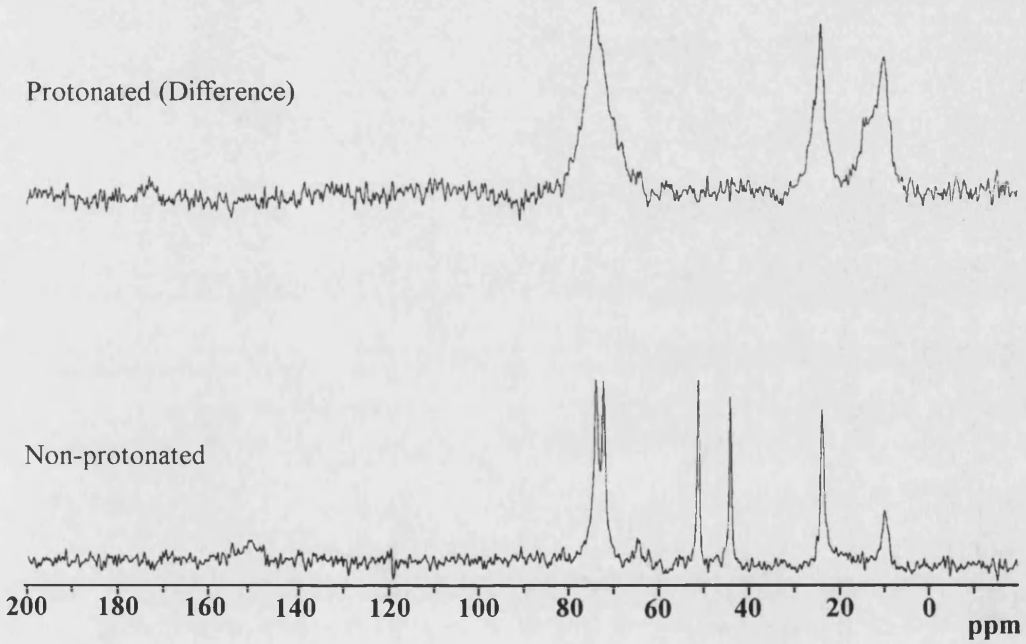

Figure 5.9 Non-quaternary suppression spectrum (bottom) and difference spectrum (top) for Mg-EPTMS following thermal treatment in the presence of *m*-PDA.

FTIR spectroscopy for the sample yielded vibrational absorptions due to the clay framework and absorptions from alkyl groups were still evident at 2850-2900 cm^{-1} and 1400 cm^{-1}. Peaks arising from epoxy methine (CH) and methylene (CH_2) vibrations (3100 cm^{-1} and 3000 cm^{-1} respectively), which were poorly resolved in the unreacted Mg-EPTMS, could not be discerned in the crosslinked sample. Unfortunately, due to both the epoxy and ether C-O-C stretches occurring at frequencies obscured beneath the broad Si-O-Si absorption (950-1200 cm^{-1}) it was not possible to quantitatively assess the degree of conversion from the FTIR data.

^{29}Si MAS NMR data (Figure 5.10) for the reacted sample showed little change compared with that prior to heating. Deconvoluted data suggested a slight increase in the percentage of fully-condensed T^3 silicon centres following the crosslinking treatment: 70 % compared to 67.9 % for as-synthesized Mg-EPTMS, which may have resulted from further condensation of the silicon centres during heating.

Thermal analysis was carried out on the solid sample following thermal treatment in the presence of *m*-PDA (Figure 5.11b) and the data compared with that obtained for as-synthesized Mg-EPTMS (Figure 5.11a). Again, only a 1-2 % weight loss was recorded between ambient and 150 °C, indicating a small amount of water surface-sorbed on the reacted sample. The onset of a steady weight loss occurred just below 400 °C and gradually leveled out around 600 °C. A corresponding broad endotherm observed in the DTG trace could be resolved into two by virtue of two peak maxima corresponding to maximum rates of weight loss at 390 °C and 440 °C. In contrast, as-synthesized Mg-EPTMS exhibited one endotherm which was clearly resolved in this temperature range, with a maximum at 400 °C (Figure 5.11a). From these sets of data it was assumed that the lower temperature endotherm at just below

400 °C corresponded to decomposition of unreacted pendant epoxide functionalities on the clay, due to its comparable location with the endotherm maximum of Mg-EPTMS. The higher temperature endotherm (440 °C) could be attributed to decomposition of cross-linked organic residues and indicated a slight increase in the thermal stability of the product following polymerization of the epoxide moieties. In short, thermal analysis indicated the probability of a mixture of unreacted and cross-linked organic functionalities within the sample following heat treatment with *m*-PDA, and that the thermal stability of the sample could be improved upon cross-linking.

It is also possible that during thermal analysis of Mg-EPTMS, self-polymerization of pendant epoxide residues occurred in the 400 °C temperature region, although for uncatalyzed reactions the polymerization rate is slow. Nevertheless, the DTG trace for Mg-EPTMS showed small unresolved features on the higher temperature side of the major isotherm which may have arisen from decomposition of small amounts of self cross-linked material.

Electron microscopy carried out in scanning mode showed only slight changes to the bulk morphology of the clay material following the cross-linking treatment in the presence of *m*-PDA (Figure 5.12). In transmission mode 'fibrous' regions were observed and illustrated the layered nature of the material (Figure 5.13)

	Chemical Shift (ppm)	%
T^1	-49	13.4
T^2	-56	16.9
T^3	-66 to -68	69.7

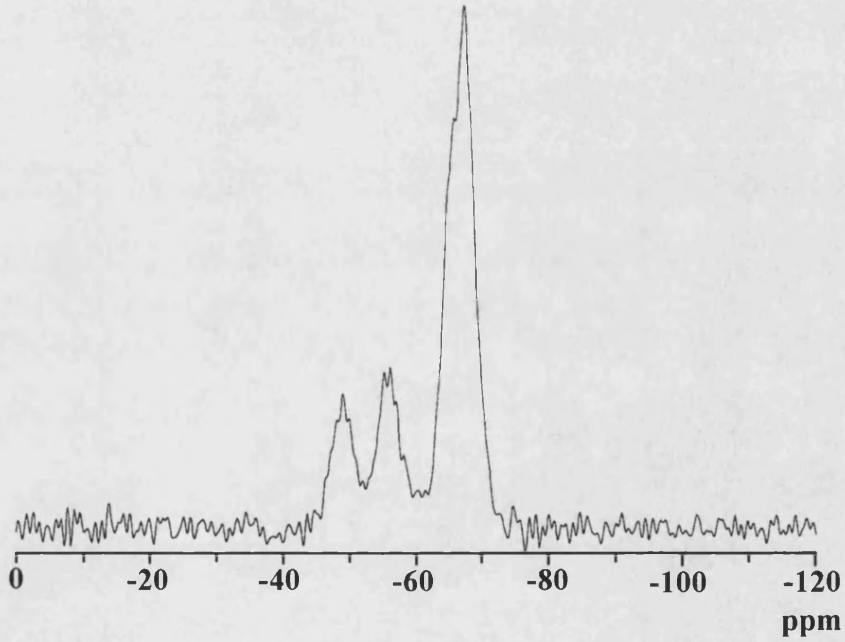

Figure 5.10 ^{29}Si DP MAS NMR spectrum for Mg-EPTMS following thermal treatment in the presence of *m*-PDA.

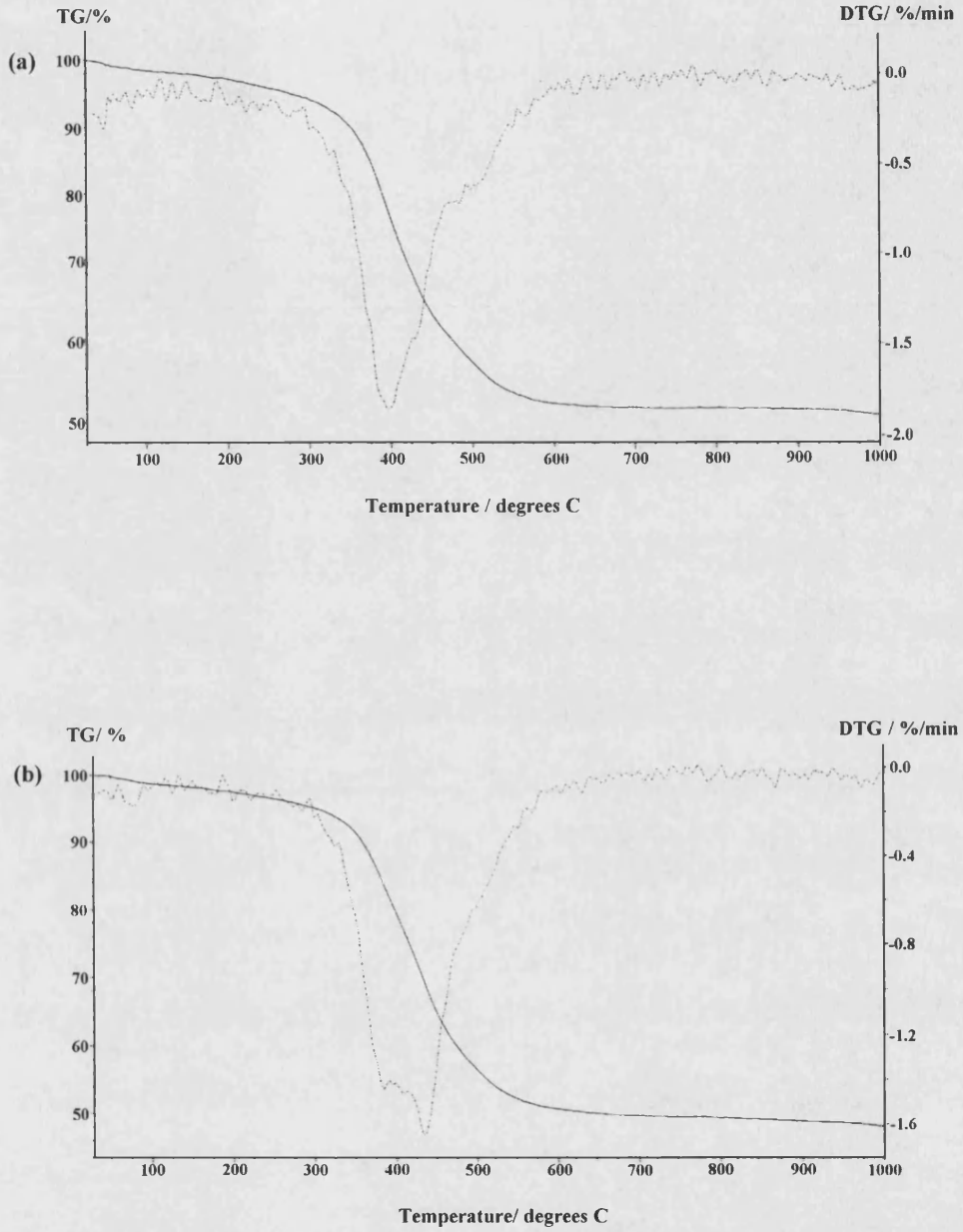

Figure 5.11 Thermogravimetric analysis data for (a) as-synthesized Mg-EPTMS and (b) Mg-EPTMS following thermal treatment in the presence of *m*-PDA.

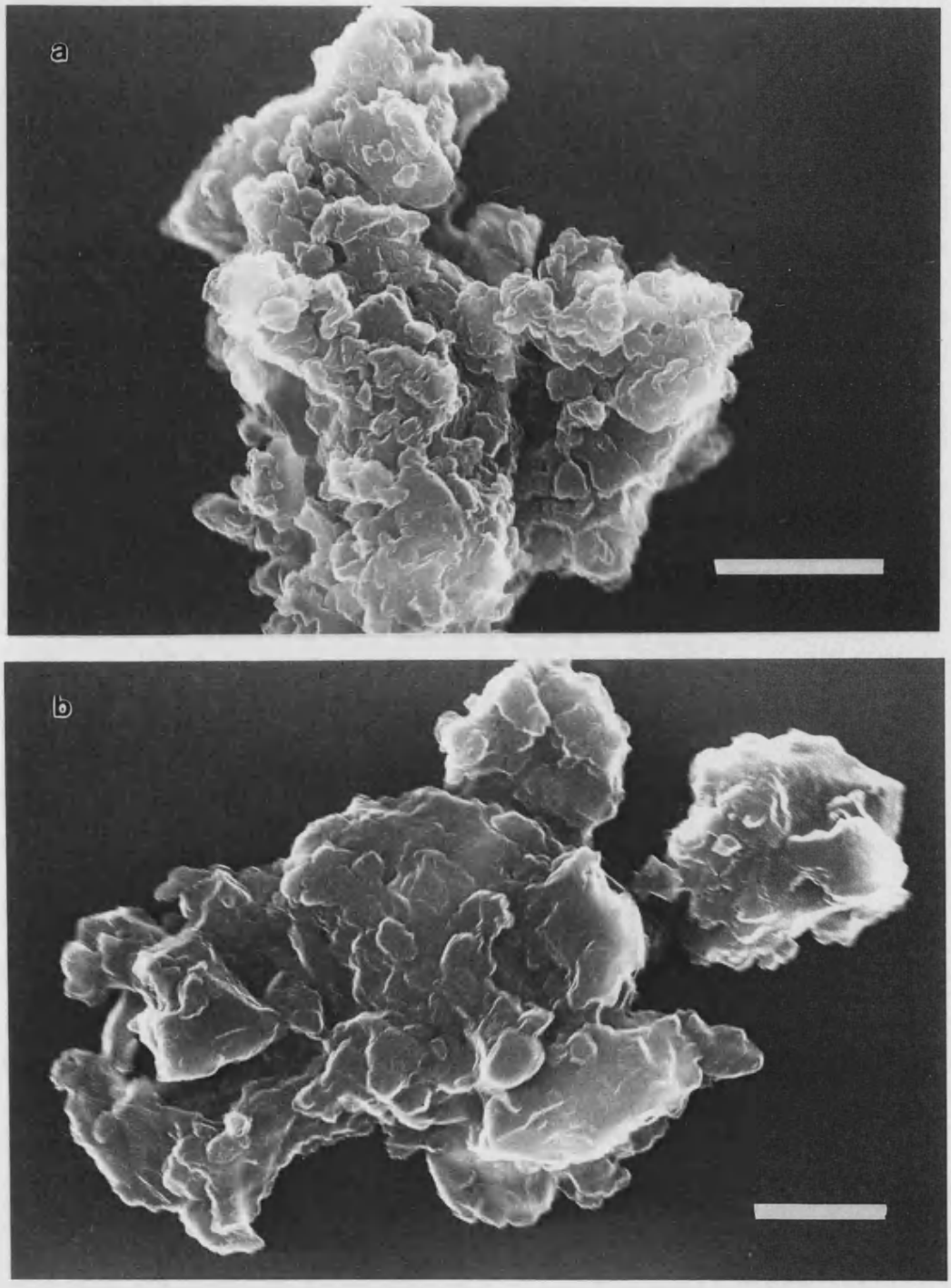

Figure 5.12 Scanning electron micrographs for (a) as-synthesized Mg-EPTMS and (b) Mg-EPTMS following thermal treatment in the presence of *m*-PDA. Scale bars = 5 μm.

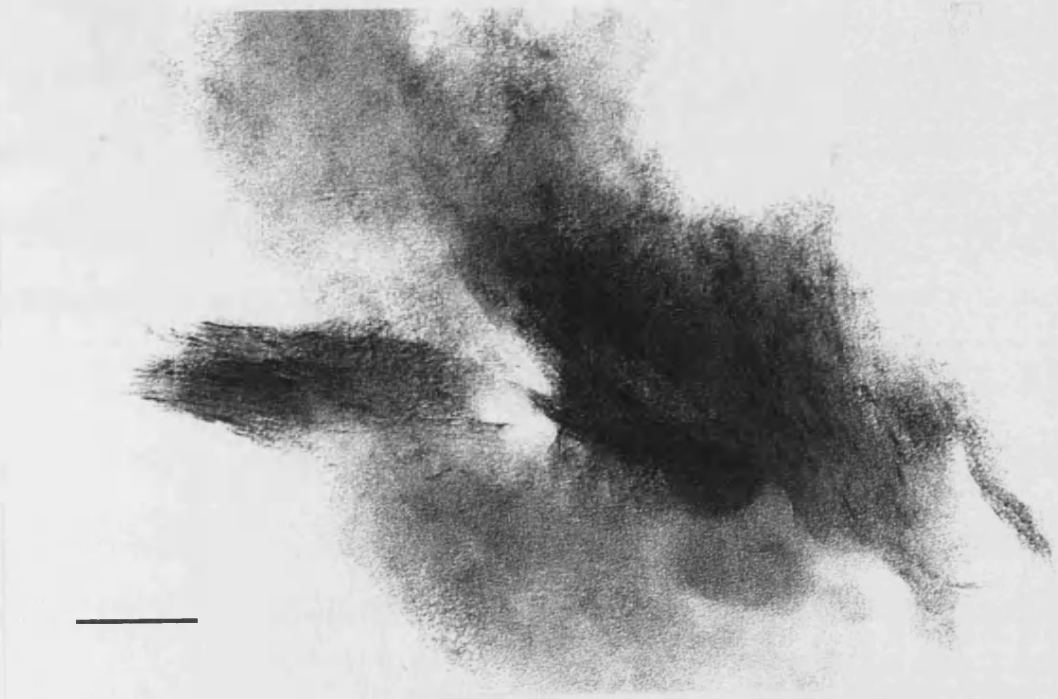

Figure 5.13 Transmission electron micrograph for Mg-EPTMS following thermal treatment in the presence of *m*-PDA (scale bar = 50 nm).

Polymerization of pendent clay-bound methacrylate functional groups

Many substituted ethylenes undergo radical chain polymerization: styrene can be converted to poly(styrene), propylene to poly(propylene) and methyl methacrylate to poly(methyl methacrylate). Polymerization is initiated by the decomposition (often upon heating) of a catalyst to generate a small number of radicals. α-Azo-*iso*-butyronitrile (AIBN) (see below) can be employed as a catalyst, i.e. source of radicals, in the polymerization reaction between methyl methacrylate monomers.

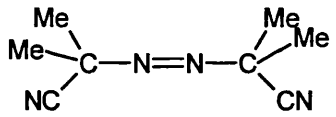

AIBN

Using AIBN as the reaction initiator the polymerization of adjacent clay-bound methacrylate residues in the interlayer regions of Mg-MPTMS was carried out under reflux conditions in THF.

Polymerization across the double bond of the pendent methacrylate groups of Mg-MPTMS was illustrated by ^{13}C CP MAS NMR spectroscopy. Alkenyl carbon signals at 127 ppm and 138 ppm were absent from the spectrum for the reaction product and the appearance of new signals upfield in the alkyl region of the spectrum (39 ppm and 44 ppm) indicated double bond conversion to the single bond form (Figure 5.14). Moreover, the application of a non-quaternary suppression (NQS) technique (data not shown) indicated two quaternary carbons at 44 ppm and 178 ppm corresponding to a reaction-generated quaternary alkyl carbon and the carbonyl

carbon respectively. Other resonances were absent in the NQS experiment indicating there to be no highly mobile species within the solid. Signal broadening further implied a lack of mobility which was in accordance with a disordered rigid arrangement of the oligomerized/polymerized organic material within the interlamellar regions.

FTIR spectroscopy (Figure 5.15) showed the disappearance of organic vibrations from the alkenyl functionality of the methacrylate precursor (880 cm^{-1}, 1410 cm^{-1}, 1640 cm^{-1}, 1800 cm^{-1} and 3090 cm^{-1}). A new alkyl vibration was observed at 1380 cm^{-1}, whilst the absorption at 1650 cm^{-1} was attributed to water within the sample due to the poorly resolved nature of the peak (and on the basis of thermal analysis data discussed below).

Extensive oligomerization/polymerization, as indicated by the NMR and FTIR data, resulted in significant disruption to the ordering of the layered material in the stacking direction. The obtained XRD pattern showed a replacement of the d_{001} peak at 13.7 Å with an unresolved broadened peak spanning *d*-values between 6 Å and 13.6 Å (Figure 5.16b). A low intensity (001) diffraction peak, observed in the XRD pattern of Mg-MPTMS (Figure 5.16a) indicated a certain degree of disorder in the structure prior to reaction and this appeared to increase further upon crosslinking of methacrylate groups. Whilst intra-clay reflections are still evident indicating order to be retained in the 2:1 silicate sheets, a definitive value for the interlayer spacing could not be made.

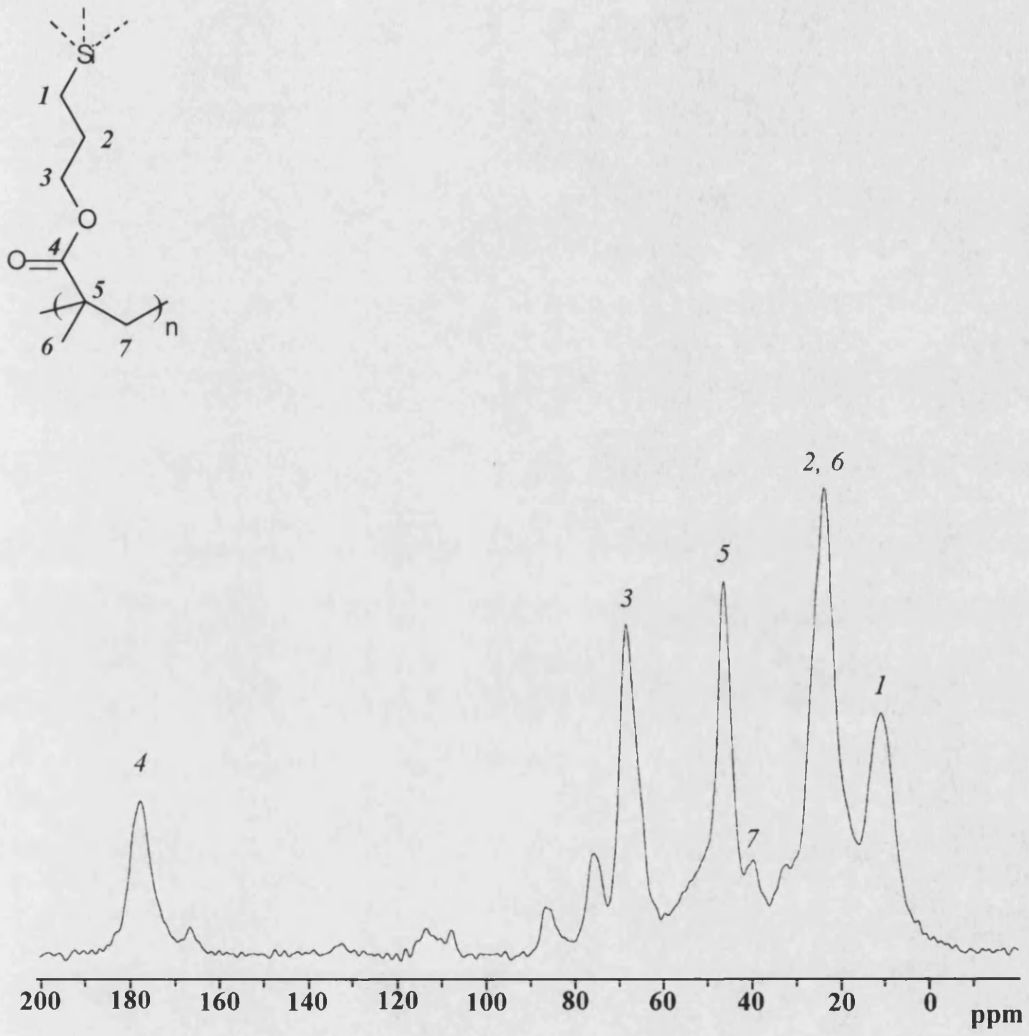

Figure 5.14 ^{13}C CP MAS NMR spectrum for the product of the polymerization reaction involving clay-bound methacrylate residues.

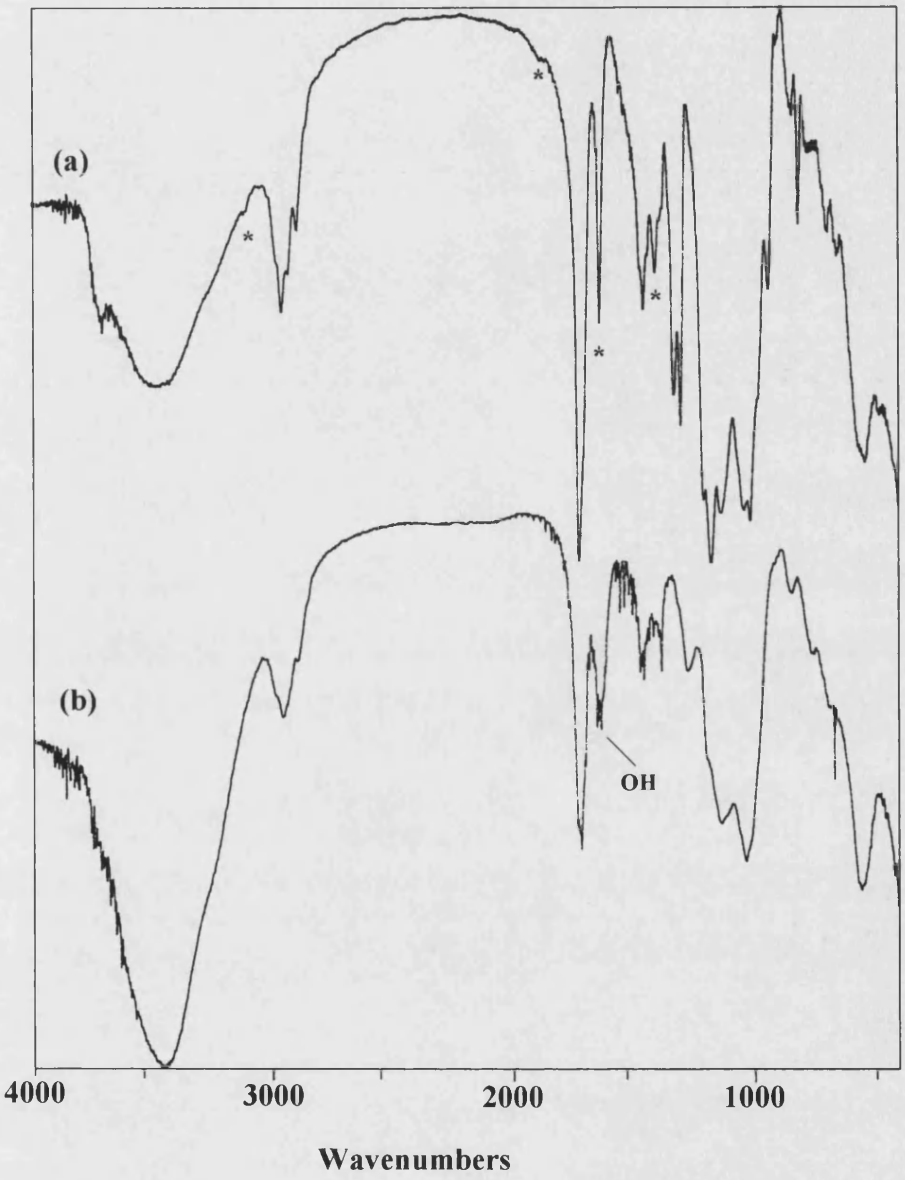

Figure 5.15 FTIR spectra for (a) as-synthesized Mg-MPTMS and (b) the product of the polymerization reaction involving clay-bound methacrylate residues. * indicate assignments for ethylene group vibrational modes.

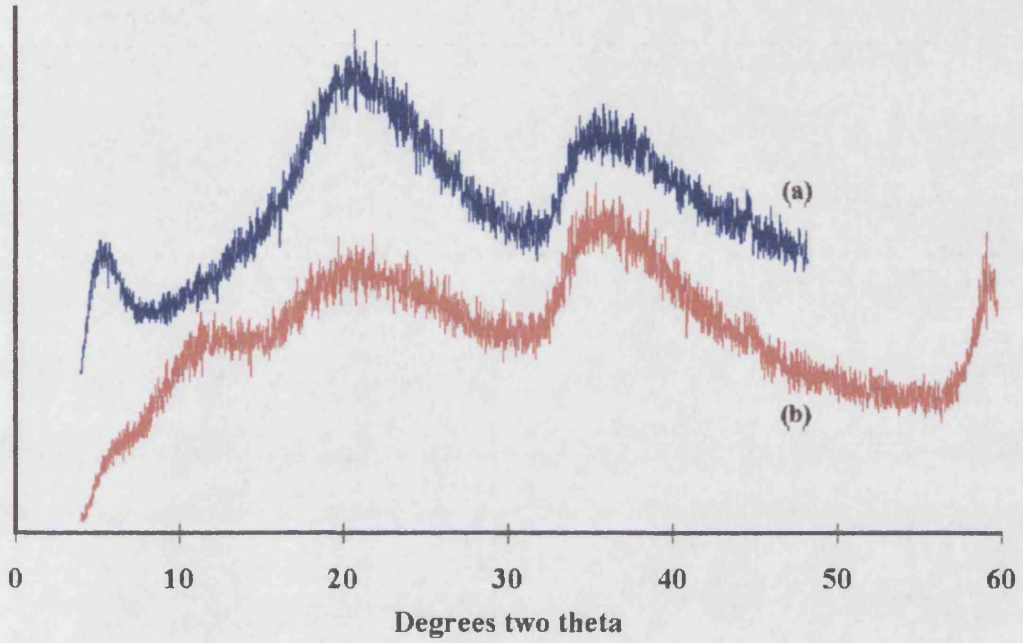

Figure 5.16 PXRD data for (a) Mg-MPTMS and (b) the product of the polymerization reaction involving clay-bound methacrylate groups.

In the thermogravimetric analysis trace a 15 % weight loss below 150 °C indicated a significant amount of water associated with the polymerized (organo)phyllosilicate (Figure 5.17a). Unreacted Mg-MPTMS, on the other hand, showed only a 4 % reduction in weight which was attributable to water (Figure 5.17b). This observation suggested an increased hydrophilicity of the sample upon polymerization of the organic substituents. The thermal behaviour of the polymerized and unreacted samples for the remainder of the analyses appeared, for the most part, identical. The onset of a major weight loss occurred at approximately 370 °C and continued up to 600 °C for both samples. The overall 45 % weight loss over this temperature range appeared to be the result of two endothermic organic decomposition events, centred at 375 °C and 475 °C. From these results it seemed that the thermal stability of the organic moieties was unaltered by polymerization.

Both Mg-MPTMS and AIBN-treated Mg-MPTMS showed a plate-like morphology as revealed by transmission electron microscopy (TEM). Figure 5.18a shows how the plates of the (organo)phyllosilicate fall onto the grid with their stacking dimension perpendicular to the direction of the electron beam, and hence the layered nature is hidden. In the micrograph obtained for AIBN-treated Mg-MPTMS layering was evident in some areas of the sample during TEM analysis (Figure 5.18b).

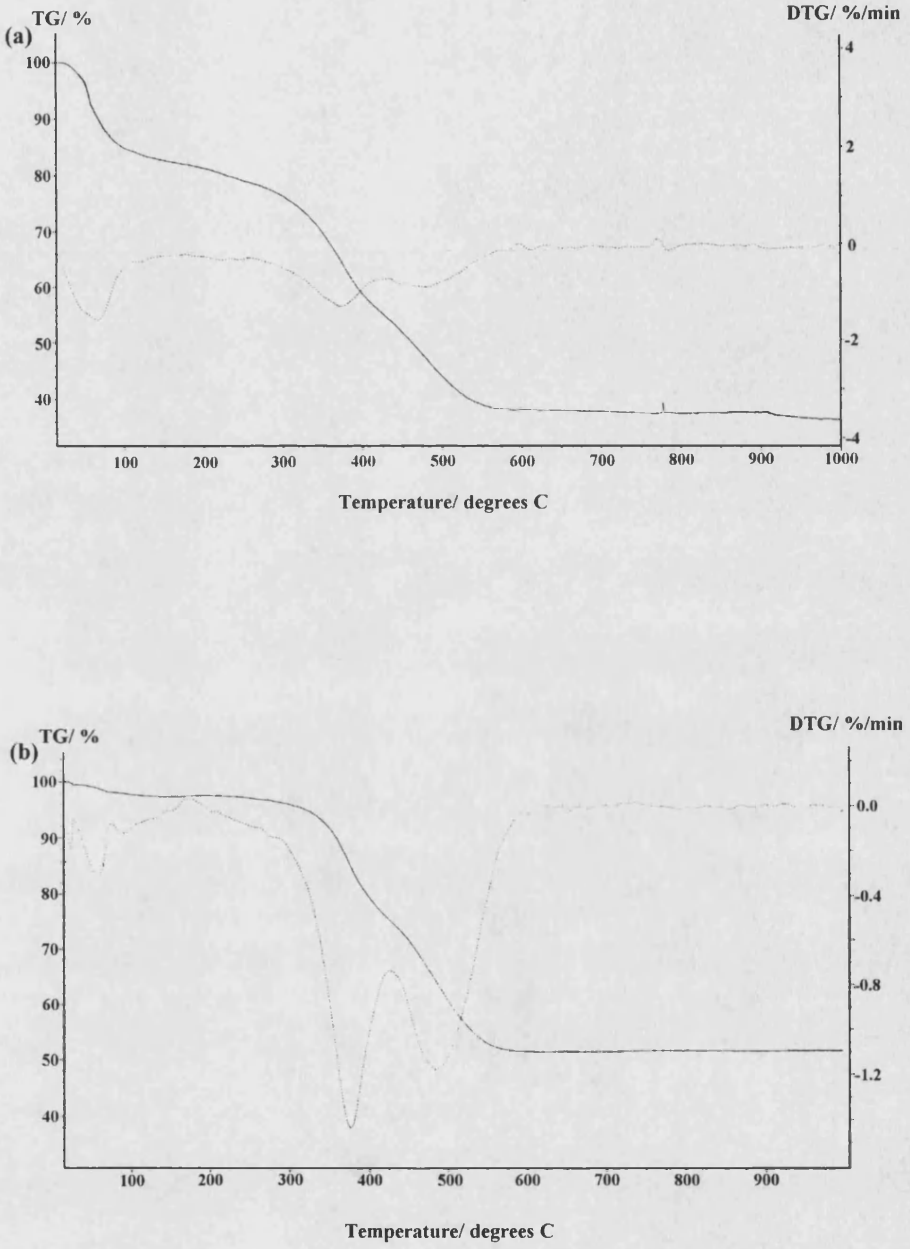

Figure 5.17 Thermogravimetric analysis data for (a) product of the polymerization reaction involving Mg-MPTMS and (b) as-synthesized Mg-MPTMS

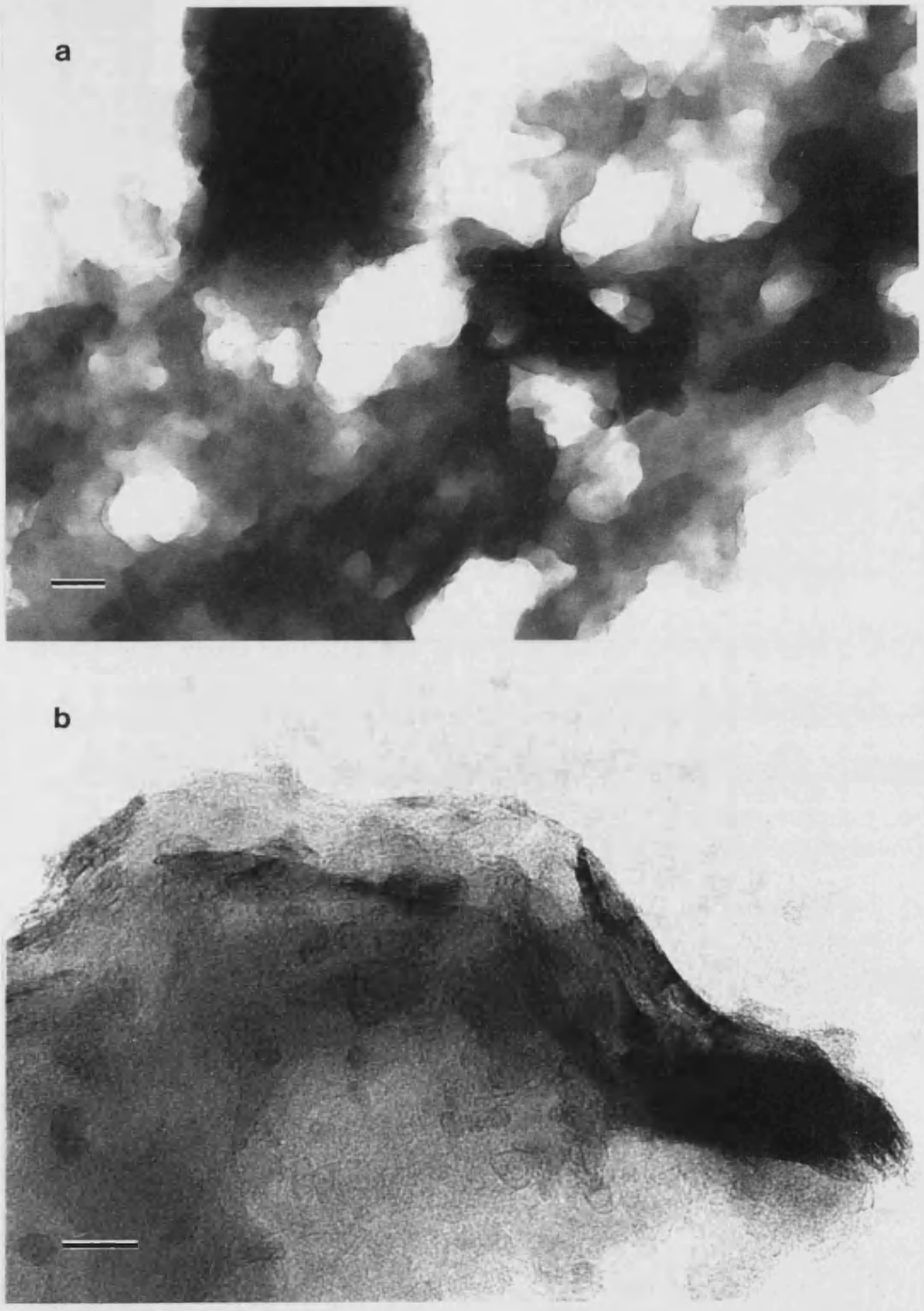

Figure 5.18 Transmission electron micrographs for (a) as-synthesized Mg-MPTMS (scale bar = 50 nm) and (b) the product of the polymerization reaction involving Mg-MPTMS (scale bar = 20 nm).

Cobalt sequestration within ethylenediamine-functionalized magnesium (organo)phyllosilicates

Cobalt complexes exhibit a very rich chemistry in its interactions with dioxygen in solution. Cobalt(II) ethylenediamine complexes have been successfully immobilized on a hectorite-clay surface (Schoonheydt and Pelgrims, 1983) and formed within zeolite X and Y cages. The cages of zeolites provide a unique environment for synthesizing these complexes stemming from the unusual steric and electrostatic constraints that can be imposed and a considerable amount of work has been done on the study of cobalt(II)-dioxygen complexes in zeolites (Howe and Lunsford, 1975; Dutta and Zaykoski, 1989). Recently, a series of MCM-41 grafted metal-amine complexes, including ligands based on ethylenediamine, diethylenetriamine, and ethylenediaminetriacetic acid have been successfully prepared (Díaz and Balkus, 1997). Since the ethylenediamine-functionalized phyllosilicates possess an array of metal-ion binding sites within the gallery spaces it was of interest to investigate the possibility of forming clay-bound cobalt(II)-ethylenediamine complexes in the constrained interlayer environment of Mg-EDTMS and Mg-H^+EDTMS (organo)phyllosilicates, with a view to future investigation into the dioxygen binding affinities of the complexes formed.

To this end, a simple incubation approach, similar to the one employed in the preparation of MCM-41 grafted cobalt(II)-amine complexes (Díaz and Balkus, 1997) was adapted. The initial indication of cobalt becoming bound in association with the clay samples was a visual colour change of the samples from white to pale mauve in

the case of Mg-EDTMS and pale yellow to pink in the case of Mg-H^+EDTMS. The high coloration remained even after thorough washing to remove residual $CoCl_2$.

EDXA showed the presence of cobalt in both samples (Figure 5.19). Chlorine was also indicated in both sets of data. Prior to reaction Mg-EDTMS contained no chlorine (Figure 4.23a) whilst, by virtue of its protonated nature, Mg-H^+EDTMS contained chloride counteranions (Figure 4.21b). It is likely that in the case of both Mg-EDTMS and Mg-H^+EDTMS exposure to $CoCl_2$ resulted in the generation of a cobalt-ethylenediamine species some or all of which had an associated indeterminate amount of chloride. No evidence for crystalline $CoCl_2$ particles could be found upon observation of the samples in the transmission electron microscope; instead aggregates of clay particles were imaged much the same as those observed for the unreacted magnesium (organo)phyllosilicate.

Since the exclusion of oxygen from the reaction mixture was not rigorously imposed it was possible for cobalt(II) to undergo oxidation in the presence of strongly complexing ethylenediamine ligands to form cobalt(III)-(ethylenediamine)-type complexes and dioxygen may also be incorporated in the complex during formation. Moreover, ethylenediamine complexes of Co(II) in solution are known to coordinate O_2 to form diamagnetic dimeric species which are best represented as μ-peroxo adducts, $[Co(III)O_2^{2-}Co(III)]^{4+}$ (Davis *et al.*, 1977). These possibilities served to further complicate the elucidation of the complexes formed within the interlayer of the (organo)phyllosilicates.

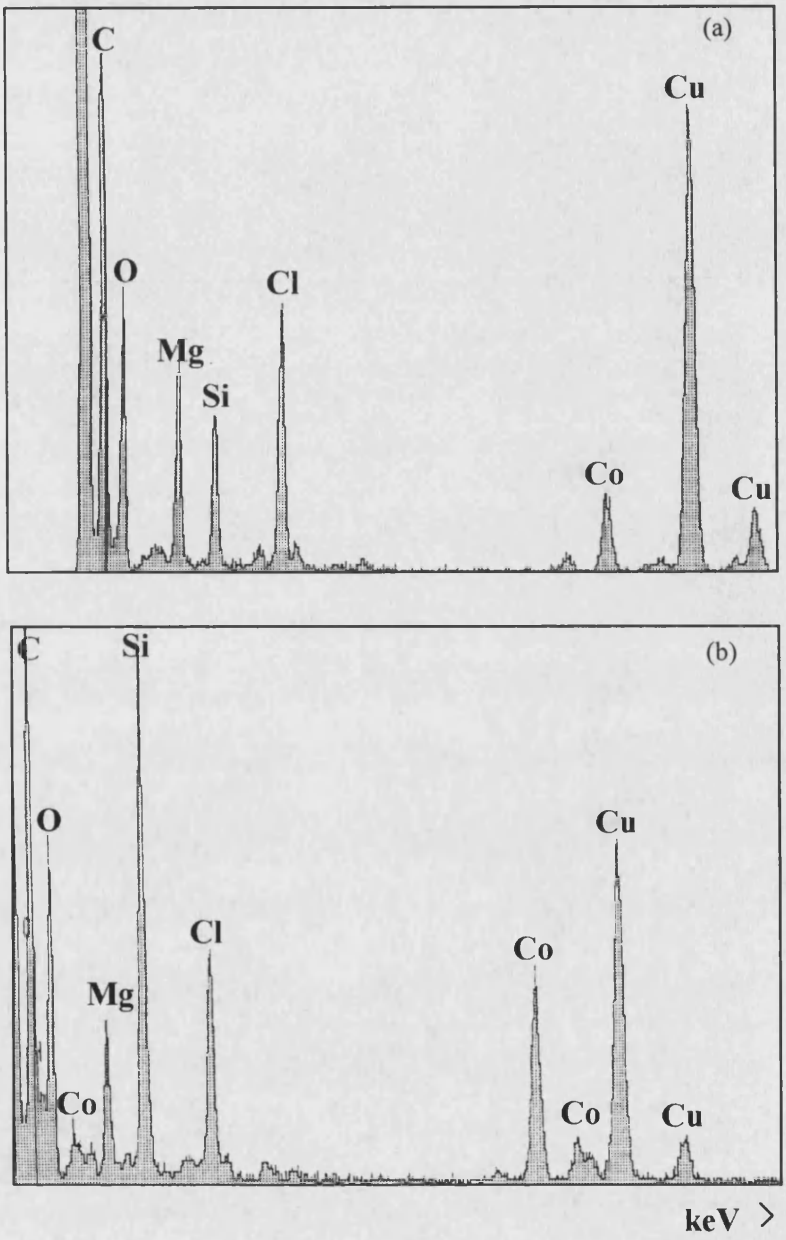

Figure 5.19 EDXA data for (a) Mg-EDTMS and (b) Mg-H^{+}EDTMS following incubation in Co(II)-containing solutions.

Paramagnetic cobalt(II) within Mg-H^+EDTMS had the effect of broadening the solid state ^{13}C CP MAS NMR linewidths, although signals arising from the organic moieties were still evident (Figure 5.20). Similar broadening was observed in the ^{29}Si MAS NMR spectra although the cobalt appeared to still provide a sufficient pathway for relaxation (Figure 5.21). Broadening of the NMR signals was similarly observed for the cobalt-exposed Mg-EDTMS.

Crude magnetic measurements obtained using a magnetic susceptibility balance demonstrated how the presence of cobalt(II) in the samples following reaction rendered the materials paramagnetic; before reaction the magnesium (organo)phyllosilicates were measured as diamagnetic. However, the copresence of diamagnetic low-spin Co(III) complexes could not be ruled out and no further quantitative use was made of the magnetic susceptibility data obtained.

Diffraction peaks from the 2:1 trioctahedral phyllosilicate framework were still present in the patterns of both samples following incubation (Figure 5.22). In addition, apart from a decrease in intensity of the d_{001} diffraction peak which indicated an increase in the turbostratic disorder of layers relative to each, the interlayer separation was apparently unchanged. The accommodation of cobalt (and chloride) involved a reorganization of the pendent organic groups in order to optimize the position of the ethylenediamine-derivatives for coordination, but this was achieved without significant alteration in the interlayer distance.

Little change was observed in the FTIR spectra of the (organo)phyllosilicates following incubation.

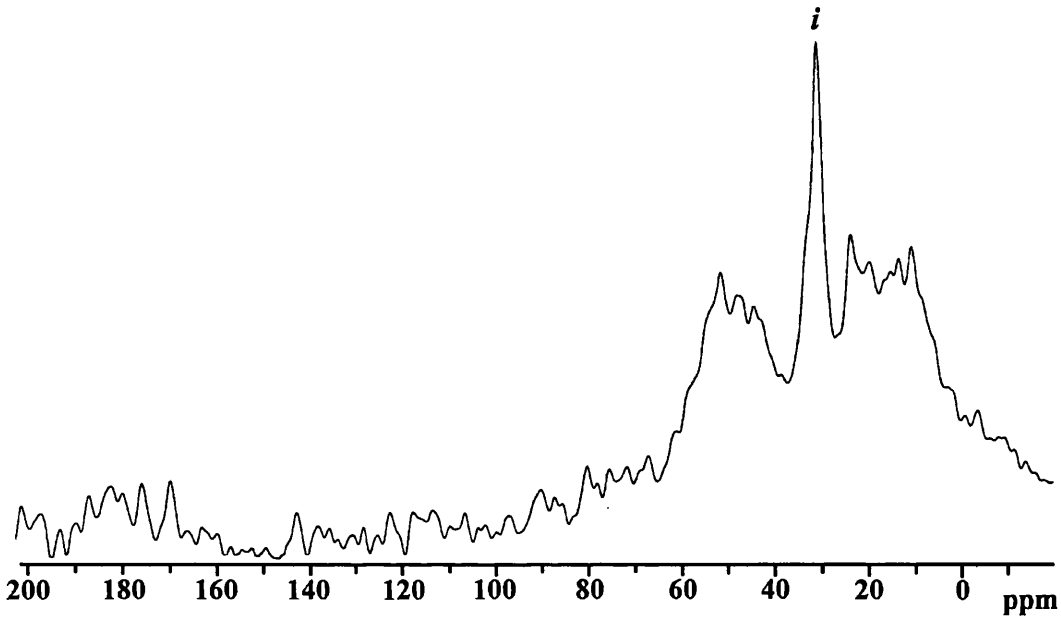

Figure 5.20 ^{13}C CP MAS NMR data for Mg-H^+EDTMS following incubation in Co(II)-containing solution. ***i*** = impurity.

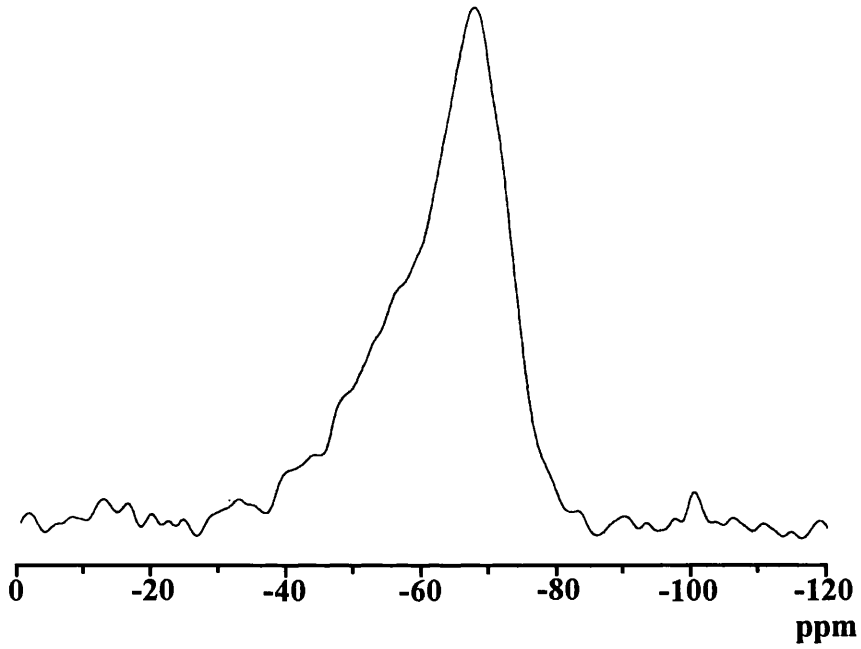

Figure 5.21 ^{29}Si DP MAS NMR spectrum for Mg-H^{+}EDTMS incubated in Co(II)-containing solution.

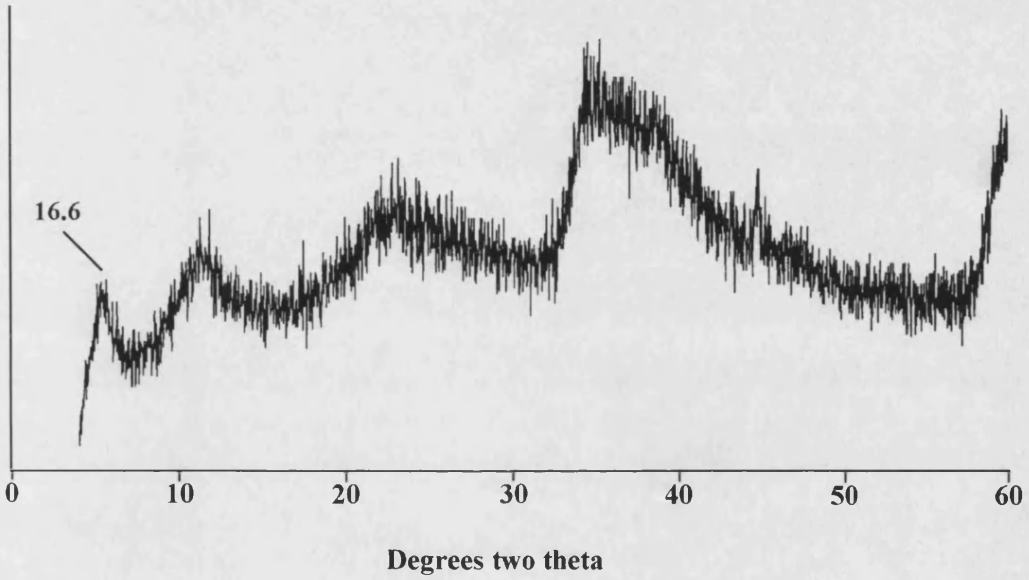

Figure 5.22 PXRD for Mg-EDTMS following incubation in Co(II)-containing solution. Interlayer spacing indicated in Å.

Formation of gold particles within magnesium (organo)phyllosilicates

The reduction of $HAuCl_4$ during the *in situ* formation of Mg-ATES under standard and methanolic, base-free synthesis conditions yielded red/purple and straw-coloured solid products respectively. The standard synthesis conditions utilized in this preparation used methanol in place of ethanol as co-solvent. Methanol will induce reduction of $HAuCl_4$ (Au(III)) to metallic gold, Au(0), and although having a lower affinity than thiol organic functionalities, amino groups also show a tendency to bind to gold surfaces (which may be in the form of gold nanoparticles). To this end, synthesis of the magnesium (organo)phyllosilicate was attempted in solutions suitable for reduction of $HAuCl_4$. Binding of gold particles in the interlayer regions of the layered material was envisaged.

The straw-colored product of the methanolic, base-free synthesis afforded a powder X-ray diffraction pattern containing 2:1 trioctahedral phyllosilicate reflections: 2θ= 20°-25°, 35°-40°, 59.6°. An unresolved and broad peak in the (001) region of the pattern encompassed *d*-spacings of 14 - 7.8 Å. The pattern was noisy and reflections from Au(0) could have been obscured in the background.

The synthesis of Mg-ATES under standard mixed methanol/water basic conditions in the presence of $HAuCl_4$ afforded a product exhibiting a d_{001}-spacing of 13.1 Å, in which the corresponding diffraction peak was well-defined (Figure 5.23). Despite the noisiness of the XRD pattern it was possible to discern clearly Au(0) reflections at *d*-values of 2.04 Å and 2.34 Å (Burkett *et al.*, 1997) which indicated that the reduction of Au(III) had been successful.

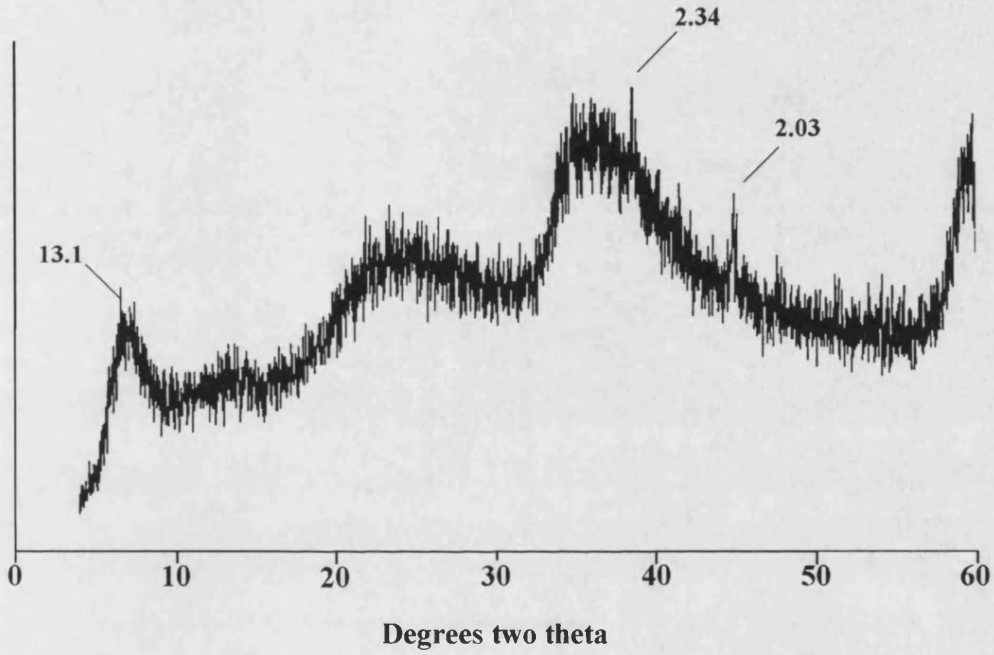

Figure 5.23 PXRD pattern for the product of reaction involving *in situ* formation of Mg-ATES under standard conditions in the presence of $HAuCl_4$. d_{001}-spacing indicated at 13.1 Å, Au(0) reflections indicated at 2.34 Å and 2.04 Å.

EDXA analysis on the product of the methanolic/ base free synthesis failed to detect an appreciable amount of gold in the organoclay particles. Similarly, transmission electron microscopy performed at the same time as EDXA did not image any electron dense particles typical of gold. In contrast, Mg-ATES prepared under standard synthesis conditions in the presence of $HAuCl_4$ showed electron dense regions of discreet nano-sized particles in association with the larger micron-sized organoclay particles when viewed under TEM (Figure 5.24a). Samples were prepared for observation under the microscope by dispersion under sonication in ethanol. The dimensions of the particles were of uniform size, approximately 5 nm in diameter.

Consideration of the XRD data for the latter sample threw question over the 5 nm gold particles being located in the interlayer region of the (organo)phyllosilicate. The d_{001} reflection in the pattern was broad but had a maximum at 13.1 Å, 1.2 Å less than that obtained for Mg-ATES prepared under standard conditions in the absence of $HAuCl_4$. Gold(0) reflections were easily discerned: 2.04 Å and 2.34 Å. This result suggested not only a more contracted, disordered arrangement of the pendent organic groups within the interlayer, but also discounted the possibility of 5 nm gold particles also being located in the interlayer. It is likely that the particles imaged by TEM were bound by exposed amine groups on the external surfaces of the clay particles.

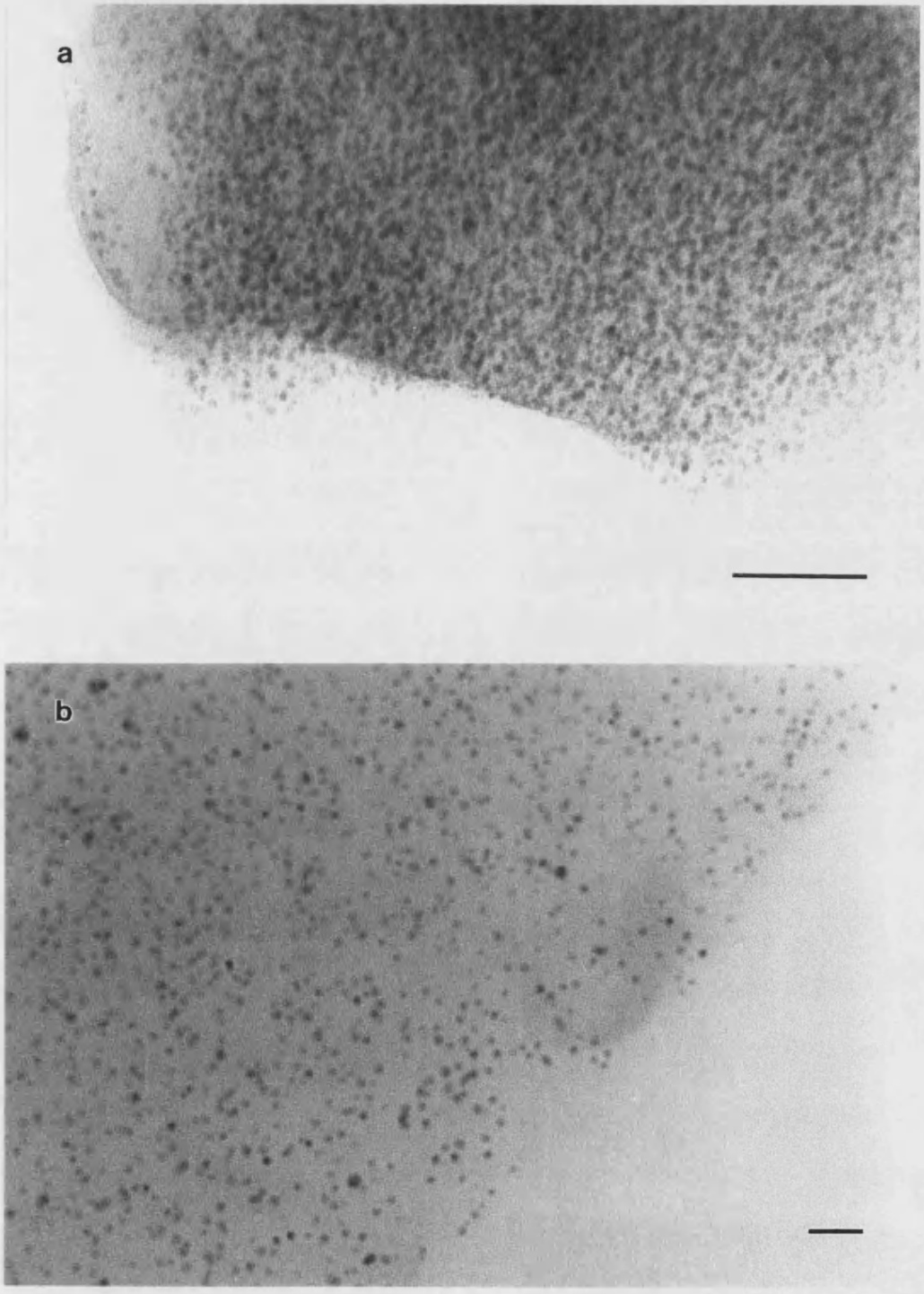

Figure 5.24 Transmission electron micrographs for Mg-ATES formed in the presence of $HAuCl_4$ under standard synthesis conditions. A micrograph of a thin section through an organoclay particle is shown in (b). Scale bars = (a) 50 nm, (b) 20 nm.

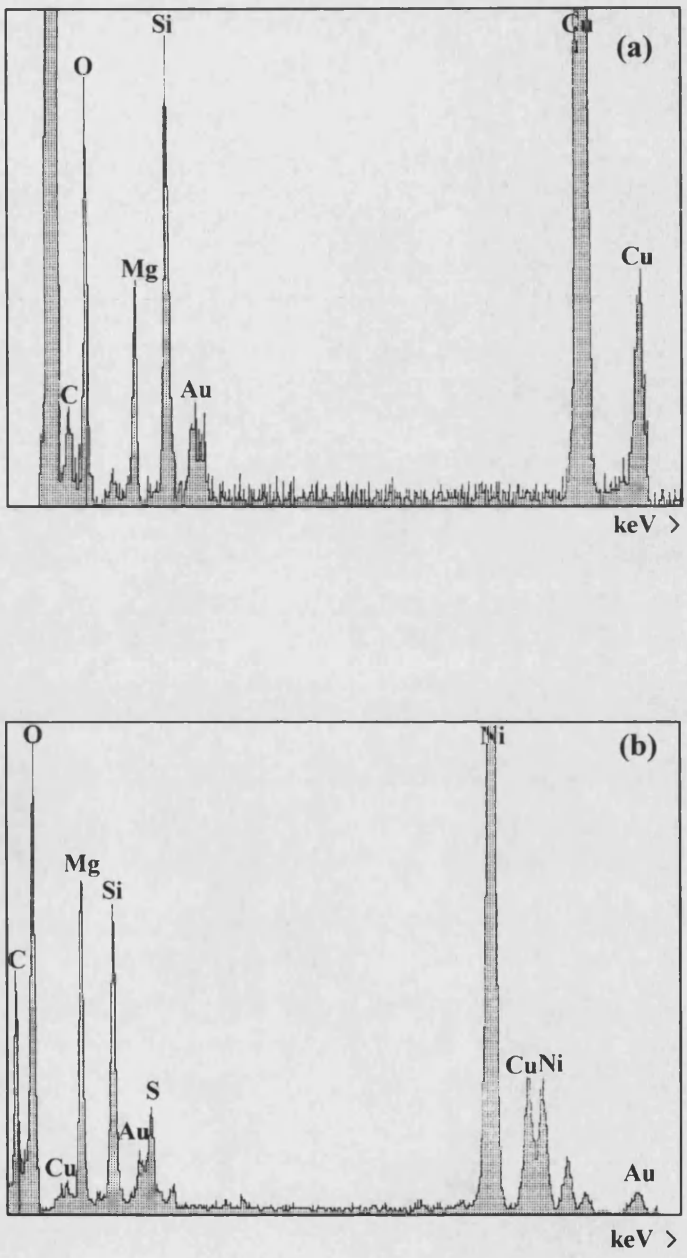

Figure 5.25 EDXA data for the products of (a) the standard synthesis involving *in situ* formation of Mg-EDTMS in the presence of HAuCl4 (thin section) and (b) the reduction of $AuCl_4$ in the presence of pre-formed Mg-EDTMS.

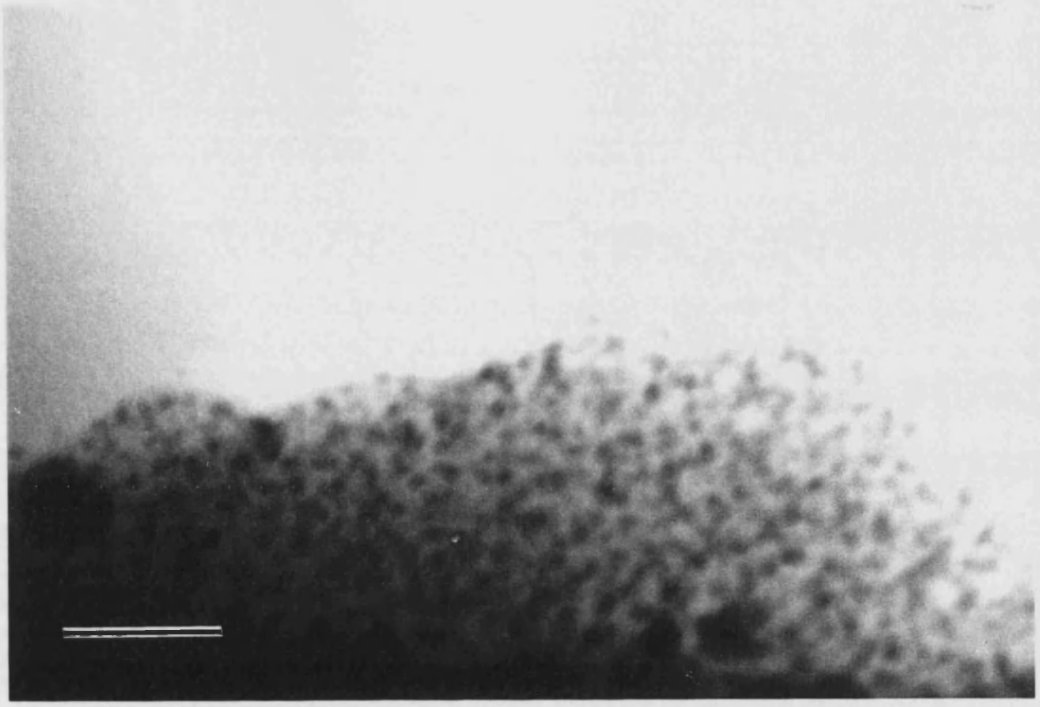

Figure 5.26 Transmission electron micrograph for the solid product of the reaction involving the reduction of HAuCl4 in the presence of preformed Mg-EDTMS (scale bar = 20 nm).

A more accurate picture of the situation within the micron-sized clay particles was provided by imaging thin sections of the sample. Discreet 2 nm gold particles dotted throughout the clay matter were evident (Figure 5.24b) and a gold signal was also detected by EDXA (Figure 5.25a). The uniformity of the gold particle size suggested that the particles were formed in association, at least, with the amine groups, although due to their dimensions were unlikely to be located in the interlayer spaces of the layered (organo)phyllosilicate phase.

It is possible that formation of the inorganic structure proceeded with buckling of the inorganic sheets around the gold particles, which prevented gold particle aggregation, but also hindered the formation of an ordered gold-intercalated (organo)phyllosilicate phase. An expanded d_{001} reflection may have been unobservable due it being outside the working range (d < 22 Å) of the diffractometer in use but this seemed unlikely. The 13.1 Å diffraction peak instead probably arose from an ordered (organo)phyllosilicate phase, formed in association with no gold.

Since the synthesis of an organoclay with concomitant binding of gold nanoparticles within the interlayer region appeared unsuccessful, preliminary experiments were carried out on the binding of gold nanoparticles within a preformed Mg-EDTMS. This experiment employed the synthetic approach of Burkett *et al.* (1997), who had observed the gold binding effect of a pre-synthesized thiol-derivatized magnesium (organo)phyllosilicate. $HAuCl_4$ was reduced in methanol in the presence of dispersed Mg-EDTMS particles. Preliminary TEM images (Figure 5.26) and EDXA (Figure 5.25b) analysis indicated the successful association of discreet 1 - 2 nm particles on the edges of the clay particles and no bulk aggregates of

gold were observed. Unfortunately time constraints prevented further analysis on this sample.

Synthesis of magnesium (organo)phyllosilicates containing layer-bridging organics

The polymerization of bis(trialkoxysilyl) monomers [$(R'O)_3Si\text{-}R\text{-}Si(OR')_3$] has been previously utilized in sol-gel chemistry to fabricate highly cross-linked polysilsesquioxane gels (Loy and Shea, 1995). These materials consist of a network of tetrahedral silicon atoms interconnected by three siloxane bonds. The fourth silicon linkage is joined to an aryl or alkyl spacer which is in turn connected to a second silicon tetrahedron. The nature of these "building blocks" allows for their systematic variation and the potential for controlled alteration of the overall microstructure and porosity of the material.

It was thus of interest to replace the organotrialkoxysilanes used in the synthesis of magnesium (organo)phyllosilicates with alkylene and arylene-bridged bis(trialkoxysilyl) species, which undergo similar hydrolysis and condensation reactions to form siloxane-type bonds. It was envisaged that layered (organo)phyllosilicates could be fabricated with adjacent inorganic layers covalently connected by bridging organic R groups; the organic spacers forming an integral part of the chemical connectivity of the material, rather than being pendent groups in the structure. The materials would be analogues of the α-zirconium organophosphonate-type, metal(IV) diphosphonates $M^{IV}(O_3P\text{-}R\text{-}PO_3)$ (Alberti *et al.*, 1993).

Syntheses were attempted utilizing 1,6-bis(trimethoxysilyl)hexane and 1,4-bis(trimethoxysilylethyl)benzene (Scheme 5.1), the organic spacer groups being

chosen for their flexibility and rigidity respectively. Typical precipitation in the reaction mixture occurred upon addition of the sodium hydroxide solution. In the case of the 1,4-bis(trimethoxysilylethyl)benzene-containing mixture the reaction mixture had a noticeable pink tint to it, which was due to light scattering from the aromatic ring (Loy *et al.*, 1996). There was no such tint to the precipitation during the hexylene-bridged (organo)phyllosilicate preparation. Under basic reaction conditions hydrolysis and condensation of the arylene-bridged monomers were likely to occur at a faster rate than for the alkylene-bridged (Loy *et al.*, 1996).

XRD data resulting from the preparation using the benzyldiethylene-bridged triethoxysilane indicated the successful formation of a 2:1 trioctahedral phyllosilicate structure, with an interlayer spacing of 11.5 Å (Figure 5.27). The reflections were, however, considerably broadened and, in particular, the intensity and broadness of the reflection between 17° and 30° 2θ implied a significant amount of a disordered (amorphous) phase also present in the sample. Furthermore, the position of the (001) reflection and dimension of the interlayer spacing was inconsistent with a perpendicular orientation for the diethylbenzene spacers relative to the inorganic sheets. If this were the case, an interlayer spacing closer to 20 Å would be expected. Instead, a severely tilted or disordered orientation could be implied and the low intensity of the d_{001} peak suggested a poor degree of short range ordering of the layers relative to each other.

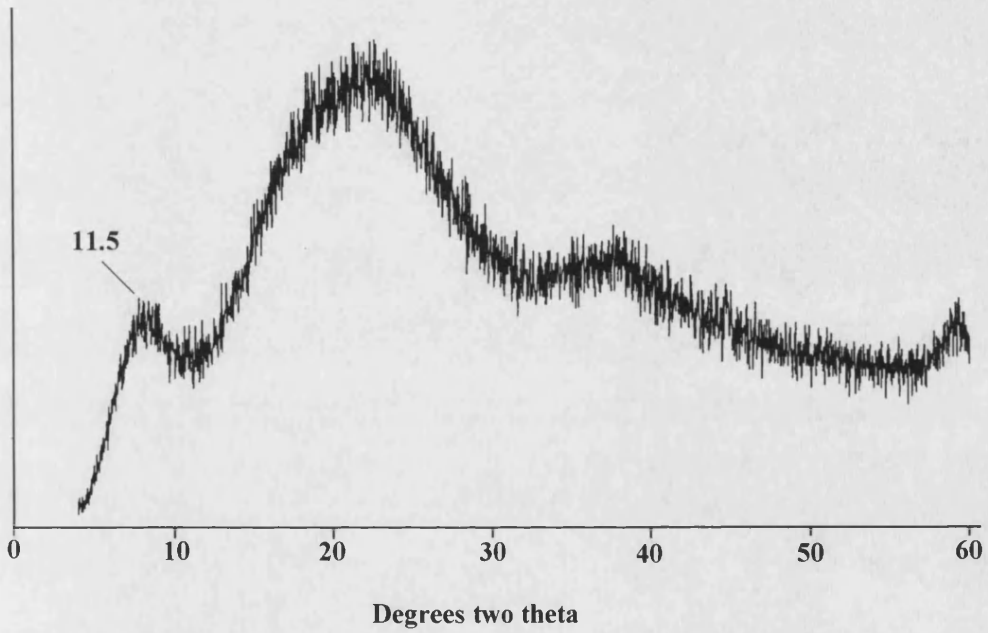

Figure 5.27 PXRD pattern for benzyldiethylene-bridged magnesium (organo)phyllosilicate. Interlayer spacing indicated in Å.

The generation of the (organo)phyllosilicate structure may have been favoured due to suitable condensation kinetics between the arylene-bridged bis(trimethoxysilyl) monomers and the aqua magnesium cations, and intermolecular interactions between the organic groups may also be a contributing factor to structure formation. However, a problem recognized early on in the preparation of metal(IV) diphosphonates was that crowding within the interlayer regions, owing to the small distance between adjacent attachments in the inorganic layer, resulted in poorly crystallized materials (Alberti *et al.*, 1993). Similar steric effects are likely to have imposed geometric constraints on the generation of the aryl-bridged magnesium (organo)phyllosilicate and may account for the high degree of packing defects and vacancies in the structure resulting in the poor crystallinity evidenced by XRD. Steric factors may also have led to microscopic phase domains affording amorphous material.

^{13}C CP MAS NMR data (Figure 5.28) could be assigned to intact diethylbenzene groups: (δ = 15.1, 29.2, 127.5, 143.1 and 167.1 ppm). Non-quaternary suppression indicated a single resonance arising from the carbons in the 1 and 4 positions of the benzene ring (143.1 ppm) and no highly mobile carbons were detected indicating a rigid environment for the organic spacers. This lent further support to the XRD data for a disordered arrangement of the organics.

A vibration at 1250 cm^{-1} in the FTIR spectrum further confirmed the integrity of the Si-C bond towards the reaction conditions employed and peaks at 500 cm^{-1} (Mg-O) and 1000-1150 cm^{-1} (Mg-O-Si, Si-O-Si) indicated the formation of the inorganic framework. Ethylene group vibrations were also evidenced at 2850-2950 cm^{-1}, and a broad unresolved vibration between 1400 cm^{-1} and 1650 cm^{-1} was attributed to various aromatic ring and alkyl absorptions.

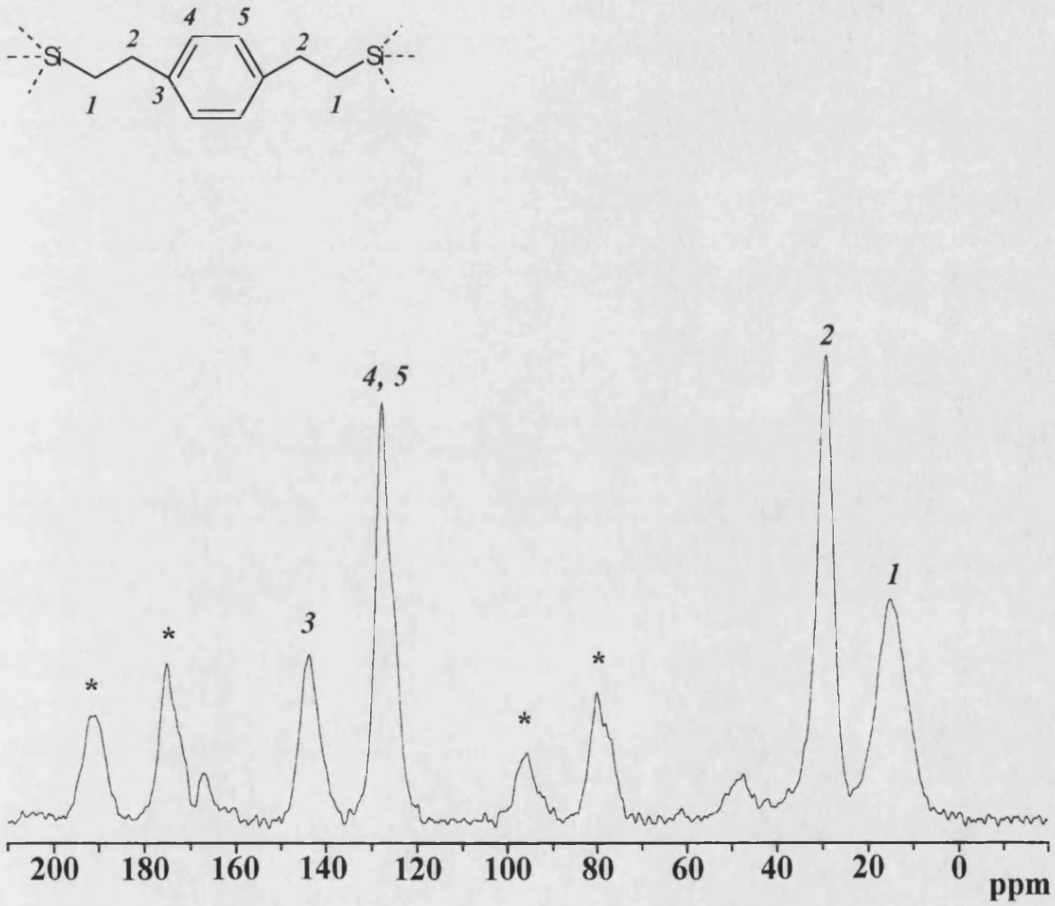

Figure 5.28 ^{13}C CP MAS NMR spectrum of benzyldiethylene-bridged magnesium (organo)phyllosilicate. * indicate spinning sidebands.

	Chemical Shift (ppm)	%
T^1	-49	12.3
T^2	-58	38.6
T^3	-67	49.1

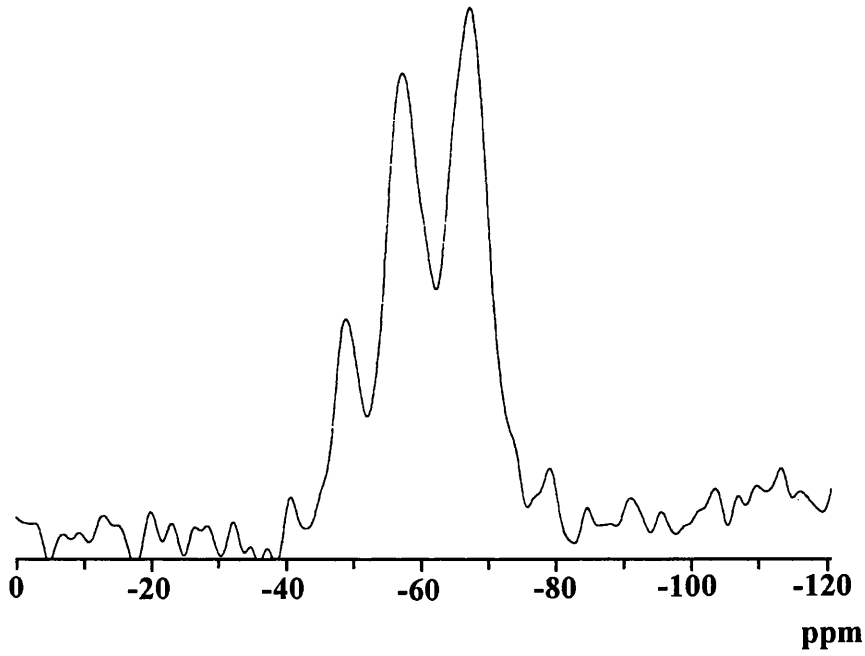

Figure 5.29 ^{29}Si DP MAS NMR of benzyldiethylene-bridged magnesium (organo)phyllosilicate.

Well-resolved ^{29}Si MAS NMR data indicated good condensation within the sample (Figure 5.29), with fully condensed T^3 silicon species (possessing three siloxane-type bonds), contributing almost 50 % of the overall condensation. The contribution from amorphous material could not, however, be determined.

Thermal analysis for this sample (Figure 5.30) showed a 5 % weight loss, below 150 °C attributed to water in the sample. Decomposition of the organic functionalities ensued around 350 °C and continued to 600 °C (28 %). Between 600 °C and 800 °C a further 5 % loss in weight was recorded most likely due to further organic decomposition.

XRD data (Figure 5.31) for the product of the synthesis involving 1,6-bis(trimethoxysilyl)hexane was inconsistent with formation of the 2:1 tri-octahedral phyllosilicate structure, and instead the location and relative intensities of most of the reflections indicated predominantly brucite formation (JCPDS card 7-239). An intense reflection around 10° 2θ (d = ~8 Å) was most probably attributable to a disordered silica-containing phase (Loy *et al.*, 1996) indicating phase separation of the silicon and magnesium components. Clearly, reaction conditions were not optimized for the generation of the layered 2:1 sheet structure, with the slower condensation kinetics of the hexylene-bridged bis(trimethoxysilyl) relative to the faster hydrolyzing magnesium metal cation leading to phase separation. The flexibility of the hexylene spacer may also have a propensity to form disordered material and not facilitate the formation of the layered magnesium (organo)phyllosilicate. Reports on organic-bridged poysilsesquioxane gels showed that those containing flexible aliphatic spacers to contain little porosity, with the organic being unsuitable as "molecular scaffold" to generate porosity in the structure (Shea *et al.*, 1992; Oviatt *et al.*, 1993).

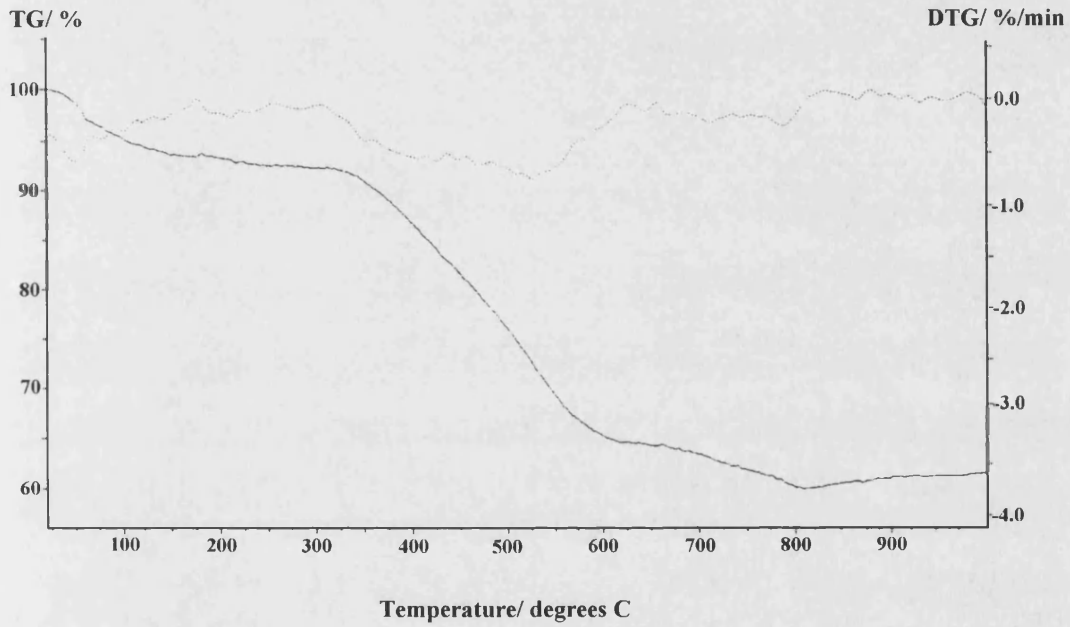

Figure 5.30 Thermogravimetric analysis data for benzyldiethylene-bridged magnesium (organo)phyllosilicate

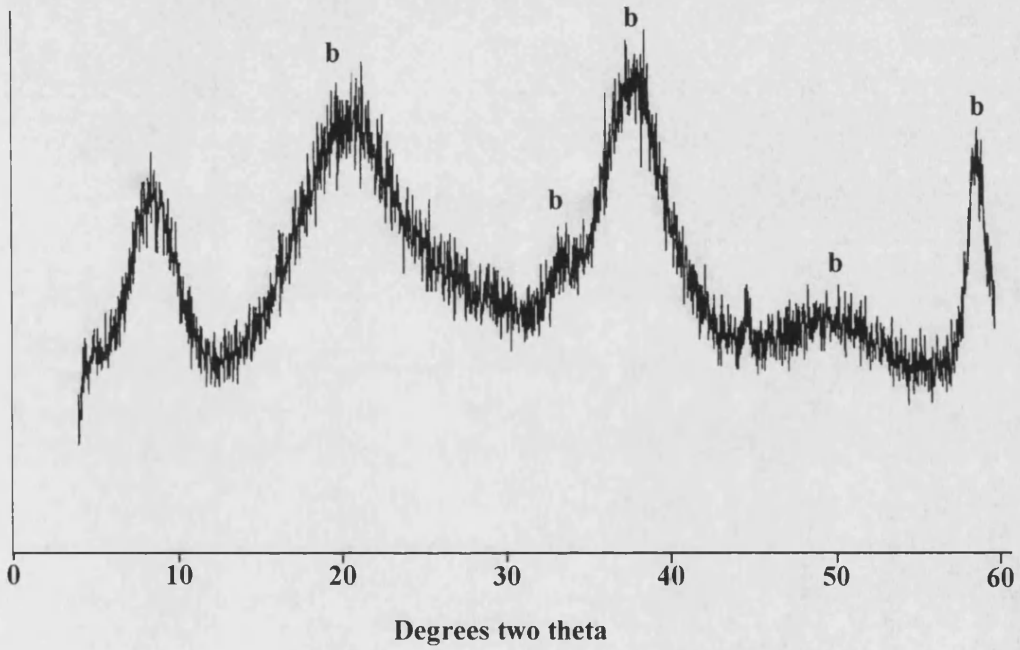

Figure 5.31 PXRD pattern for the hexylene-bridged magnesium (organo)phyllosilicate, **b** indicate reflections from a brucite phase.

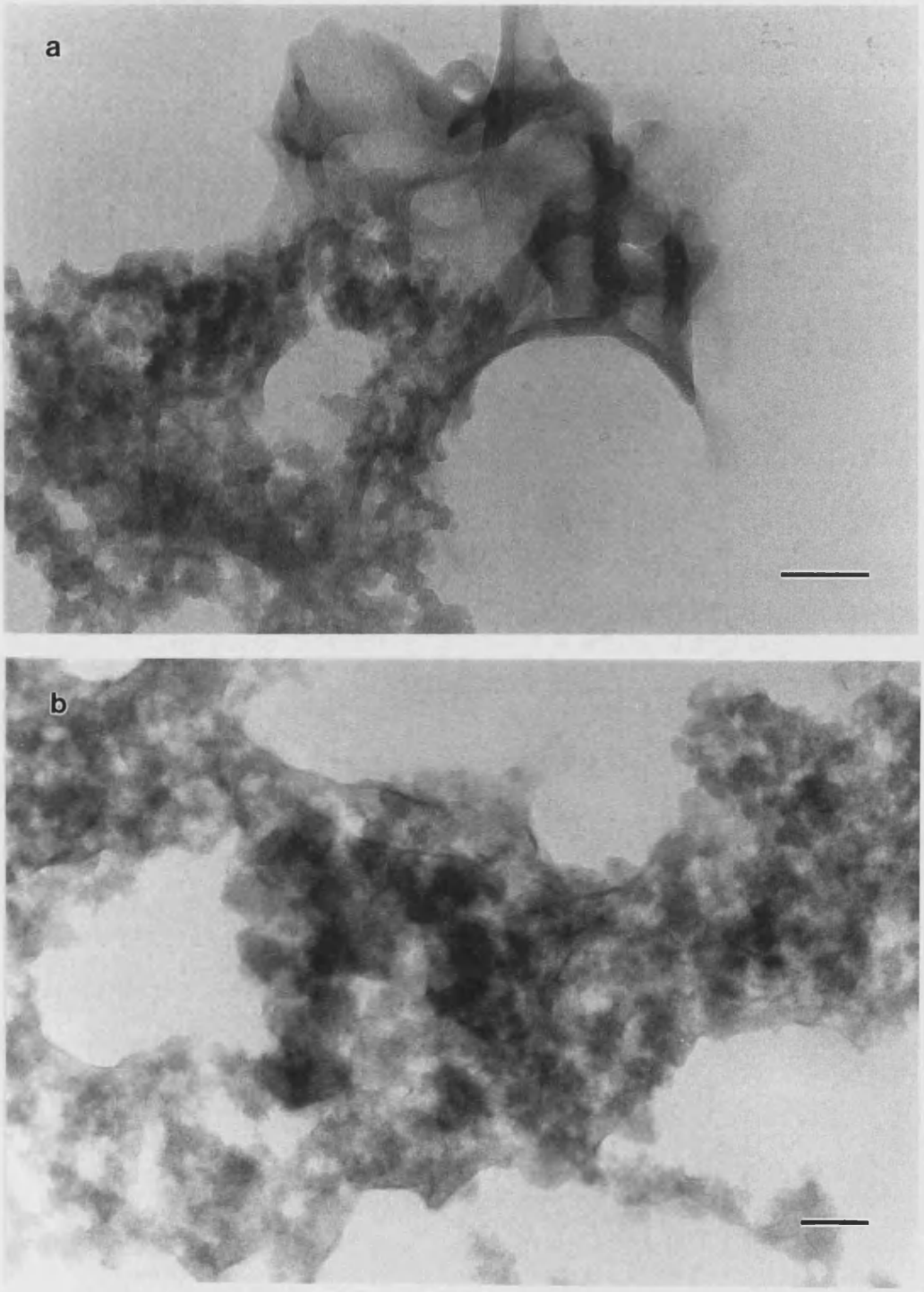

Figure 5.33 Transmission electron micrographs for the (a) benzyldiethylene-bridged and (b) hexylene-bridged magnesium (organo)phyllosilicates (scale bars = 100 nm).

Solid state ^{13}C and ^{29}Si NMR and FTIR data were also collected for this sample, but due to the indication from the XRD pattern of no (organo)phyllosilicate structure being formed in the reaction, the data are not presented here. However, what was apparent from these data were that the integrity of the Si-C bond and organic substituent was retained indicating that future work on this system may be successful.

Heterogeneity in the benzyldiethylene-bridged sample was revealed by transmission electron microscopy. Figure 5.32a shows different morphologies within the sample. Evidence for a layered clay-like phase is seen in the upper region of the micrograph, whilst in the lower region a disordered amorphous phase is indicated. TEM analysis on the product of the hexylene-bridged bis(triethoxysilyl) monomer preparation showed only the disordered phase morphology (Figure 5.32b).

The data presented for preliminary experiments involving these precursors are interesting and illustrate the potential for further investigation of this system as a way of preparing pillared (organo)phyllosilicates. The results indicated how the nature and structure of the bis(trimethoxysilyl) precursors and the optimization of experimental conditions are important parameters involved in the formation of the layered structure. Unfortunately, due to time constraints, further experiments were not possible although work will continue within the research group on the synthesis of these materials.

Solid state ^{13}C and ^{29}Si NMR and FTIR data were also collected for this sample, but due to the indication from the XRD pattern of no (organo)phyllosilicate structure being formed in the reaction, the data is not presented here. However, what was apparent from this data was that the integrity of the Si-C bond and organic substituent was retained indicating that future work on this system may be successful.

Heterogeneity in the benzyldiethylene-bridged sample was revealed by transmission electron microscopy. Figure 5.32a shows different morphologies within the sample. Evidence for a layered clay-like phase is seen in the upper region of the micrograph, whilst in the lower region a disordered amorphous phase is indicated. TEM analysis on the product of the hexylene-bridged bis(triethoxysilyl) monomer preparation showed only the disordered phase morphology (Figure 5.32b).

The data presented for preliminary experiments involving these precursors are interesting and illustrate the potential for further investigation of this system as a way of preparing pillared (organo)phyllosilicates. The results indicated how the nature and structure of the bis(trimethoxysilyl) precursors and the optimization of experimental conditions are important parameters involved in the formation of the layered structure. Unfortunately, due to time constraints, further experiments were not possible although work will continue within the research group on the synthesis of these materials.

5.4 *Conclusions*

A successful bimolecular intermolecular reaction between clay-bound epoxide functionalities and a guest thiol nucleophile led to intercalation of a new functional group (carboxylate or ester) in the gallery region by reaction. Bimolecular intramolecular reactions were achieved by polymerization of adjacent epoxide and methacrylate substituents of the magnesium (organo)phyllosilicates. New composite materials consisting of an organic polymeric/oligomeric component molecularly dispersed and covalently bound to the inorganic polymer sheets were synthesized. The structural integrity of the inorganic framework was retained during the inter- and intramolecular reactions.

Clay-bound cobalt-organocomplexes were formed in the interlayer region of a magnesium (organo)phyllosilicate through ligation of cobalt(II/III) ions by ethylenediamine functionalities. The exact nature of the complex is as yet undetermined although work is under way to elucidate the structure.

Attempts to incorporate 2-dimensional arrays of gold nanoparticles in the interlayer region of an amine-functionalized (organo)phyllosilicate proved unsuccessful although discreet uniformly-sized nanoparticles were obtained indicating some controlling influence of the organic amine groups on their formation.

A viable synthetic approach to the synthesis of pillared (organo)phyllosilicates using organic-bridged bis(triethoxysilyl) monomers seems promising, providing suitable reaction conditions and choice of precursor can be made. In particular the use of rigid organic spacer groups, such as diethylbenzene may aid formation of the layered structure.

In summary, various investigations aimed at exploiting the nature and properties of the organic functionalities have shown how a range of future applications are possible for these nanocomposite materials.

CHAPTER 6

RECOMMENDATIONS FOR FUTURE WORK

RECOMMENDATIONS FOR FUTURE WORK

The work on the intercalation of biologically-relevant negatively-charged organic species in layered double hydroxides (Chapter 3) illustrated the potential for preparing a range of bioinorganic nanocomposites. The immobilization of other biologically-relevant polyanionic macromolecules, such as DNA and negatively-charged proteins such as egg yolk phosvitin, should also be considered. Furthermore, the marrying of technologically-useful individual properties of the polymer and LDHs may impart novel and interesting properties on the polymer nanocomposite and the bioactivity, biocompatability and biodegradability of the polyaspartate-containing nanocomposite is worth further investigation.

Results from Chapter 4, which focused on the synthesis and characterization of a variety of organically-functionalized magnesium phyllosilicates showed how the formation of the layered structures appeared to require complementarity between the hydrolysis/condensation behaviours of the organofunctional trialkoxysilane and the magnesium metal cations which were both influenced by the reaction conditions. Changes in the mechanism of formation of the phyllosilicate framework with changes in reaction conditions were also indicated from the characterization data.

Future work on the synthesis of these materials may concentrate on controlling the reaction conditions to optimize the formation of the phyllosilicate, to improve the crystallinity of the product and limit the formation of amorphous materials which complicates interpretation of the characterisation data. The use of aluminium (Ukrainczyk *et al.*, 1997) or nickel (Fukushima and Tani, 1995) in place of magnesium to constitute the octahedral sheet and differences in their respective

hydrolysis behaviours, (pK_1* [Al] = ~ 4.5-5; pK_1* [Ni]= ~ 6.5-10.6) compared to magnesium may provide a further variable to the reaction mixture.

The tunability of the properties of the magnesium (organo)phyllosilicate through choice of organic functionality offers a wealth of applications. Due to time constraints only a few of the these were explored and futher work on some of the projects discussed in Chapter 5 is currently underway. In particular, further characterization of the cobalt(II/III)-ethylenediamine complexes and an investigation into possible dioxygen binding affinities will utilize diffuse-reflectance UV/VIS spectrophotometry, electron paramagnetic resonance and possibly cyclic voltammetry. Selective metal-sequestration may also be possible using suitably functionalized hybrids and controlled experiments should be carried out to test this.

Post-synthesis organic group conversions were shown to be possible though the ring-opening of clay-bound epoxide groups with guest thiol nucleophiles to incorporate hydroxysulphide functionalities. Numerous other conversions in the organic and organometallic chemist's handbook are available provided suitable reaction conditions are found. Bimolecular reactions may be possible which alter not only the functionality, but also the reactivity, charge, and hydrophobicity/hydrophilicity of the interlayer region.

The delamination of the individual sheets of magnesium (organo)phyllosilicates using suitable exfoliation techniques, such as sonication in a suitable choice of organic solvent or through the incorporation of larger guest species in the interlayers may allow for the construction of multilayer films, rather like those observed upon spreading of organoammonium clay complexes on aqueous solutions (Kotov, *et al.*, 1994). Bulk nanocomposites (Oriakhi *et al.*, 1995) generated *via*

flocculation from dispersions containing exfoliated organoclay sheets and hydrophobic/hydrophilic inorganic/organic species may also be accessible.

Chapter 5 showed how epoxide moieties within a magnesium (organo)phyllosilicate could be crosslinked. An extension of this approach would involve infiltration of an epoxy resin into the epoxide-rich hydrophobic interlayer region of the clay. Upon curing, intragallery crosslinking between clay-bound epoxides and resin epoxide groups as well as intrapolymer crosslinking may be possible, and afford exfoliated clay nanocomposites in which the mineral sheets are covalently-attached to the polymer matrix. Mechanical and thermal properties could be compared with those of typical exfoliated clay-polymer materials (Lan *et al.*, 1995).

Polymer intercalation using polymer melts or from solution exploiting favourable enthalpic interactions between the polymer and organic functionalities in the interlayer may also provide an accessible route to layered polymer nanocomposites.

Future work on the synthesis of pillared magnesium (organo)phyllosilicates through the use of organically-bridged bis(trialkoxysilyl) monomers should attempt to reduce the possible steric crowding in the interlayer region, which may be possible through replacement of a number of the layer-bridging pillars with small O_3Si-R groups (R = H, CH_3). Optimization of the reaction conditions when employing mixed organofunctional alkoxysilane systems is likely to be required.

CHAPTER 7

REFERENCES

REFERENCES

G. Alberti, "Syntheses, crystalline structure, and ion-exchange properties of insoluble acid salts of tetravalent metals and their salt forms", *Acc. Chem. Res.*, **11**, 163 - 170, (1978).

G. Alberti, U. Costantino, S. Allulli and N. Tomassini, "Crystalline $Zr(R\text{-}PO_3)_2$ and $Zr(ROPO_3)_2$ compounds (R = organic radical). A new class of materials having layered structure of the zirconium phosphate type", *J. Inorg. Nucl. Chem.*, **40**, 1113 - 1117, (1978).

G. Alberti, U. Costantino, F. Marmottini, R. Vivani and P. Zappelli, "Zirconium phosphite (3,3',5,5'-tetramethylbiphenyl)diphosphonate, a microporous, layered inorganic-organic polymer", *Angew. Chem. Int. Ed. Engl.*, **32**, 1357 - 1359, (1993).

L. Albiston, K. R. Franklin, E. Lee and J. B. A. F. Saunders, "Rheology and microstructure of aqueous layered double hydroxide dispersions", *J. Mater. Chem*, **6**, 871 - 877, (1996).

P. Aranda and E. Ruiz-Hitzky, "Poly(ethylene oxide)-silicate intercalation materials", *Chem. Mater.*, **4**, 1395 - 1403, (1992).

D. D. Archibald and S. Mann, "Template mineralization of self-assembled anisotropic lipid microstructures", *Nature*, **364**, 430 - 433, (1993).

G. S. Attard, J. C. Glyde and C. G. Göltner, "Liquid-crystalline phases as templates for the synthesis of mesoporous silica" *Nature*, **378**, 366 - 368, (1995).

G. S. Attard, P. N. Bartlett, N. R. B. Coleman, J. M. Elliot, J. R. Owen and J. H. Wang, "Mesoporous platinum films from lyotropic liquid crystalline phases", *Science*, **278**, 838 - 840, (1997).

S. A. Bagshaw, F. Di Renzo, F. Fajula, "Preparation of metal-incorporated MSU mesoporous molecular sieves. Ti incorporation *via* a totally nonionic route", *J. Chem. Soc., Chem. Commun.*, 2209 - 2210, (1996).

R. M. Barrer and L. W. R. Dicks, "Chemistry of soil minerals. IV. Synthetic alkylammonium montmorillonites and hectorites", *J. Chem. Soc. A*, 1523 - 1529, (1967).

J. S. Beck, J. C. Vartuli, W. J. Roth, M. E. Leonowicz, C. T. Kresge, K. D. Schmitt, C. T. -W. Chu, D. H. Olson, E. W. Sheppard, S. B. McCullen, J. B. Higgins and J. Schlenker, "A new family of mesoporous molecular sieves prepared with liquid crystal templates", *J. Amer. Chem. Soc.*, **114**, 10834, (1992).

P. Behrens, "Mesoporous solids", *Adv. Mater.*, **5**, 127 - 132, (1993).

C. M. Bell, M. F. Arenat, L. Gomez, R. H. Schmehl and T. E. Mallouk, "Growth of lamellar Hofmann clathrate films by sequential ligand exchange reactions: assembling a coordination solid one layer at a time", *J. Am. Chem. Soc.*, **116**, 8374 - 8375, (1994).

M. Bellotto, B. Rebours, O. Clause, J. Lynch, D. Bazin and E. Ekaïm, "A reexamination of hydrotalcite crystal chemistry", *J. Phys. Chem.*, **100**, 8527 - 8534, (1996).

P. A. Bianconi, J. Lin and A. R. Strzelecki, "Crystallization of an inorganic phase controlled by a polymer matrix", *Nature*, **349**, 315, (1991).

R. Bissessur, M. G. Kanatzidis, J. L. Schindler and C. R. Kannewurf, "Encapsulation of polymer into MoS_2 and metal to insulator transition in metastable MoS_2", *J. Chem. Soc., Chem. Commun.*, 1582 - 1585, (1993).

A. Blumstein, S. L. Malhotra and A. C. Watterson, *Polym. Prepr. Amer. Chem. Soc. Div. Polym. Chem.*, 9, 167-175, (1968).

S. Bonnet, C. Forano, D. de Roy, J. P. Besse, P. Maillard and M. Momenteau, "Synthesis of hybrid organo-mineral materials: anionic tetraphenylporphyrins in layered double hydroxides", *Chem. Mater.*, **8**, 1962 - 1968, (1996).

S. A. Boyd, J. F. Lee and M. M. Mortland, "Attenuating organic contaminant mobility by soil modification", *Nature*, **333**, 345 -347, (1988).

P. V. Braun, P. Osenar and S. I. Stupp, "Semiconducting superlattices templated by molecular assemblies", *Nature*, **380**, 325 - 328, (1996).

C. J. Brinker and G. W. Scherer (Eds.), in Sol-gel science-the physics and chemistry of sol-gel processing, Publ. Academic Press, (1990).

G. Brown and G. W. Brindley (Eds.), in Crystal structures of clay minerals and their X-ray identification, Publ. Mineralogical Society, London, (1980).

B. Bujoli, O. Pena, P. Pavadeau, J. L. Bideau, C. Payne and J. Rouxel, "Synthesis, structure and magnetic properties of a new lamellar iron phosphonate, $Fe^{II}(C_2H_5PO_3)$. H_2O, *Chem. Mater.*, **5**, 583 -587, (1993).

J.Burgress, in Metal ions in solution, Publ. Ellis Horwood Ltd., (1978).

S. L. Burkett, S. D. Sims and S. Mann, "Synthesis of hybrid inorganic-organic mesoporous silica by cocondensation of siloxane and organosiloxane precursors", *J. Chem. Soc., Chem. Commun.*, 1367 - 1368, (1996).

S. L. Burkett, A. Press and S. Mann, "Synthesis, characterization, and reactivity of layered inorganic:organic nanocomposites based on 2:1 trioctahedral phyllosilicates", *Chem. Mater.*, **9**, 1071, (1997).

K. O. Burkey and E. L. Gross, "Effect of carboxyl group modification on redox properties and electron donation capability of spinach plastocyanin", *Biochem.*, **20**, 5495-5499, (1981).

G. Cao and T. E. Mallouk, "Topochemical diacetylene polymerization in layered metal phosphate salts", *J. Solid. State. Chem.*, **94**, 59, (1991).

G. Cao, H. -G. Hong and T. E. Mallouk, "Layered metal phosphates and phosphonates: from crystals to monolayers", *Acc. Chem. Res.*, **25**, 420 - 427, (1992).

S. Carlino and M. J. Hudson, "Reaction of molten sebacic acid with a layered (Mg/Al) double hydroxide", *J. Mater. Chem.*, **4**, 99 - 104, (1994).

S. Carlino and M. J. Hudson, "Thermal intercalation of layered double hydroxides: capric acid into an Mg-Al LDH", *J. Mater. Chem.*, **5**, 1433 - 1442, (1995).

K.A. Carrado, P. Thiyagarajan, R. E. Winans and R. E. Botto, "Hydrothermal crystallization of porphyrin-containing layer silicates", *Inorg. Chem.*, **30**, 794 - 799, (1991).

K. A. Carrado, "Preparation of hectorite clays utilizing organic and organometallic complexes during hydrothermal crystallization", *Ind. Eng. Chem. Res.*, **31**, 1654 - 1659, (1992).

K. A. Carrado, J. E. Forman, R. E. Botto and R. E. Winans, "Incorporation of phthalocyanines by cationic and anionic clays via ion exchange and direct synthesis", *Chem. Mater.*, **5**, 472 - 478, (1993).

F. Cavani, F. Trifiro and A. Vaccari, "Hydrotalcite-type anionic clays: preparation, properties and applications", *Catal. Today*, **11**, 173, (1991).

T. Challier and R. C. T. Slade, "Nanocomposite materials: polyaniline-intercalated layered double hydroxides", *J. Mater. Chem.*, **4**, 367 - 371, (1994).

J. H. Cheung, A. F. Rou and M. F. Rubner, "Fabrication of electrically conductive Langmuir-Blodgett multilayer films of polyaniline", *Thin Solid Films*, **244**, 990 - 994, (1994).

K. Chibwe and W. Jones, "Intercalation of organic and inorganic anions into layered double hydroxides", *J. Chem. Soc., Chem. Commun.*, 926 - 927, (1989).

A. Clearfield, M. Kieke, J. Kwan, J. L. Colon and R. -C. Wang, "Intercalation of dodecyl sulfate into layered double hydroxides", *J. Inclus. Phenom. Molec. Recognition. Chem.*, **11**, 361-378, (1991).

K. C. Cole, "A new approach to modeling the cure kinetics of epoxy amine thermosetting resins. 1. Mathematical development", *Macromolecules*, **24**, 3093 - 3097, (1991).

N. B. Colthup, L. H. Daly and S. E. Wilberley, in Introduction to infrared and Raman spectroscopy, Publ. Academic Press,(1964).

V. R. L. Constantino and T. J. Pinnavaia, "Basic properties of Mg^{2+}_{1-x} Al^{3+}_{x} layered double hydroxides intercalated by carbonate, hydroxide, chloride and sulfate anions", *Inorg. Chem.*, **34**, 883 - 892, (1995).

A. D. Cross and R. A. Jones (Eds.), in An introduction to practical infra-red spectroscopy., Publ. Butterworths, London, (1969).

S. M. Davis, R. F. Howe and J. H. Lunsford, "Formation of dioxygen adducts of cobalt(II) amine complexes in a cation exchange resin", *J. Inorg. Nucl. Chem.*, **39**, 1069 - 1072, (1977).

J. F. Díaz, K. J. Balkus Jr., F. Bedioui, V. Kurshev and L. Kevan, "Synthesis and characterization of cobalt-complex functionalized MCM-41", *Chem. Mater.*, **9**, 61 - 67, (1997).

Y. Ding, D. J. Jones, P. Maireles-Torres and J. Rozière, "Two-dimensional nanocomposites: alternating inorganic-organic polymer layers in zirconium phosphate", *Chem. Mater.*, **7**, 562 - 571, (1995).

J. E. Donachy and C. S. Sikes, "Thermal polycondensation synthesis of biomimetic serine-containing derivatives of polyaspartate - potent inhibitors of calcium carbonate and phosphate crystallization", *J. Polym. Sci., Part A: Polym. Chem.*, **32**, 789 - 795, (1994).

M. A. Drezdon, "Synthesis of isopolymetalate-pillared hydrotalcite *via* organic-anion-pillared precursors", *Inorg. Chem.*, **27**, 4628 - 4632, (1988).

P. K. Dutta and Zaykoski, "Dioxygen complexes of cobalt (II) ethylenediamine in zeolite Y cages: a resonance Raman spectroscopic study", *J. Phys. Chem.*, **93**, 2603 - 2607, (1989).

S. D. Evans, A. Ulman, K. E. Goppert-Berarducci and J. Gerenser, "Self-assembled multilayers of ω-mercaptoalkanoic acids - selective ionic interactions", *J. Am. Chem. Soc.*, **113**, 5866 - 5868, (1991).

X. Feng, G. E. Fryxell, L. -Q. Wang, A. Y. Kim, J. Liu and K. M. Kemner, "Functionalized monolayers on ordered mesoporous supports", *Science*, **276**, 923 - 926, (1997).

G. S. Ferguson and E. R. Kleinfeld, "Mosaic tiling in molecular dimensions", *Adv. Mater.*, **7**, 414 - 416, (1995).

C. E. Fowler, S. L. Burkett and S. Mann, "Synthesis and characterization of ordered organo-silica-surfactant mesophases with functionalized MCM-41-type architecture", *J. Chem. Soc., Chem. Commun.*, **18**, 1769 - 1770, (1997).

Y. Fukushima and S. Inagaki, "Synthesis of an intercalated compound of montmorillonite and 6-polyamide", *J. Inclusion. Phenom.*, **5**, 473 - 482, (1987).

Y. Fukushima and M. Tani, "An organic/inorganic hybrid layered polymer: methacrylate-magnesium (nickel) phyllosilicate", *J. Chem. Soc., Chem. Commun.*, 241 - 242, (1995).

C. A. Fyfe (Ed.), in Solid state NMR for chemists, Publ. CFC Press, (1983).

G. L. Gaines Jr., "Deposition of colloidal particles in monolayers and multilayers", *Thin Solid Films*, **99**, 243 - 248, (1983).

A. Galarneau, A. Barodawalla and T. J. Pinnavaia, "Porous clay heterostructures formed by gallery-templated synthesis", *Nature*, **374**, 529 - 531, (1995).

R. H. Glaser, G. Wilkes and C. E. Bronnimann, "Solid-state silicon-29 NMR of TEOS-based multifunctional sol-gel materials", *J. Non-Cryst. Solids*, **113**, 73 - 87, (1989).

C. G. Göltner and M. Antonietti, "Mesoporous materials by templating of liquid-crystalline phases", *Adv. Mater.*, **9**, 431 - 440, (1997).

H. Harder, "Clay mineral formation under lateritic weathering conditions", *Clay Minerals*, **12**, 281, (1977).

B. R. Heywood and S. Mann, "Template-directed nucleation and growth of inorganic materials", *Adv. Mater.*, **6**, 9 - 20, (1994).

R. F. Howe and J. H. Lunsford, "Oxygen adducts of cobalt(II)-ethylenediamine complexes in X- and Y-type zeolites", *J. Phys. Chem.*, **79**, 1836 - 1842, (1975).

Q. Huo, D. I. Margolese, U. Ciesla, P. Feng, T. E. Gier, P. Sieger, R. Leon, P. M. Petroff, F. Schüth and G. D. Stucky, "Generalized synthesis of periodic surfactant/inorganic composite materials", *Nature*, **368**, 317 - 321, (1994).

Q. Huo, R. Leon, P. M. Petroff, G. D. Stucky, "Mesostructure design with gemini surfactants: supercage formation in a three-dimensional hexagonal array", *Science*, **268**, 1324 - 1327, (1995).

R. K. Iler, "Multilayers of colloidal particles", *J. Colloid. Interf. Sci.*, **21**, 569 - 594, (1966).

D. Ingersoll, P. J. Kulesza and L. R. Faulkner, "Polyoxometalate-based layered composite films on electrodes - preparation through alternate immersions in modification solutions", *J. Eectrochem. Soc.*, **141**, 140 - 147, (1994).

H. Ishida, C. H. Chang, J. L. Koenig, "The structure of aminofunctional silane coupling agents: 1. γ-Aminopropyltriethoxtsilane and its analogues", *Polymer*, **23**, 251 - 257, (1982).

M. G. Kanatzidis, C. -G. Wu, H. O. Marcy, D. C. DeGroot and C. R. Kannewurf, "Conductive polymer/oxide bronze nanocomposites. Intercalated polythiophene in V_2O_5 xerogels", *Chem. Mater.*, **2**, 222 - 224, (1990).

M. G. Kanatzidis, R. Bissessur, D. C. DeGroot, J. L. Schindler and C. R. Kannewurf, "New intercalation compounds of conjugated polymers. Encapsulation of polyaniline in MoS_2", *Chem. Mater.*, **5**, 595 - 596, (1993).

C. Kato, K. Kurado and M. Misawa, "Preparation of montmorillonite-nylon complexes and their thermal properties", *Clays Clay Miner.*, **27**, 129 - 136, (1979).

C. Kato, K. Kurado and H. Takahara, "Preparation and electrical properties of quaternary ammonium montmorillonite-polystyrene complexes", *Clays Clay Miner.*, **29**, 294, (1981).

H. E. Katz, G. Scheller, T. M. Putvinski, M. L. Schilling, W. L. Wilson and C. E. D. Chidsey, "Polar orientation of dyes in robust multilayers by zirconium phosphate-phosphonate interlayers", *Science*, **254**, 1485 - 1487, (1991).

S. W. Keller, H. -N. Kim and T. E. Mallouk, "Layer-by-layer assembly of intercalation compounds and heterostructures on surfaces: Toward molecular "beaker" epitaxy", *J. Amer. Chem. Soc.*, **116**, 8817-8818, (1994).

M. Kermarec, J. Y. Carriat, P. Burattin, M. Che and A. Decarreau, " FTIR identification of the supported phases produced in the preparation of silica-supported nickel catalysts", *J. Phys. Chem*, **98**, 12008 - 12017, (1994).

H. -N. Kim, S. W. Keller, T. Mallouk, J. Schmidt and G. Decher, "Characterization of zirconium phosphate/polycation thin films grown by sequential adsorption reactions", *Chem. Mater.*, **9**, 1414 - 1421, (1997).

T. Kijima, S. Ueno and M, Goto, "Uptake of amino-acids by zirconium phosphates. Part 2. Intercalation of L-histidine, L-lysine, and L-arginine by α-zirconium phosphate", *J. Chem. Soc., Dalton Trans.*, 2499 - 2503, (1982).

T. Kijima and S. Ueno, "Uptake of amino-acids by zirconium phosphate. Part 3. intercalation of L-histidine, L-lysine, and L-arginine by γ-zirconium phosphate", *J. Chem. Soc., Dalton Trans.*, 61 - 65, (1986).

E. R. Kleinfeld and G. S. Ferguson, "Stepwise formation of multilayered nanostructural films from macromolecular precursors", *Science*, **265**, 370 - 373, (1994).

R. A. Komoroski (Ed.), in High resolution NMR spectroscopy of synthetic polymers in bulk, Publ. VCH Publishers, Inc. (1986).

F. Kooli, I. C. Chisem, M. Vucelic and W. Jones, "Synthesis and properties of terephthalate and benzoate intercalates of Mg-Al layered double hydroxides possessing varying layer charge", *Chem. Mater.*, **8**, 1969 - 1977, (1996).

N. A. Kotov, F. C. Meldrum, J. H. Fendler, E. Tombácz and I. Dékány, "Spreading of clay organocomplexes on aqueous solutions: construction of Langmuir-Blodgett clay organocomplex multilayer films", *Langmuir*, **10**, 3797-3804, (1994).

C. T. Kresge, M. E. Leonowicz, W. J. Roth, J. C. Vartuli and J. S. Beck, "Ordered mesoporous molecular sieves synthesized in a liquid-crystal template mechanism", *Nature*, **359**, 710 - 712, (1992).

R. Krishnamoorti, R. A. Vaia and E. P. Giannelis, Structure and dynamics of polymer-layered silicate nanocomposites", *Chem. Mater.*, **8**, 1728 - 1734, (1996).

A. Krysztafkiewicz and L. Domka, "Surface-modified microporous talc as fillers of polymers and pigments", *J. Mater. Chem.*, **7**, 1655 - 1659, (1997).

T. Lan, P. D. Kaviratna and T. J. Pinnavaia, "Mechanism of clay tactoid exfoliation in epoxy-clay nanocomposites", *Chem. Mater.*, **7**, 2144 - 2150, (1995).

M. E Landis, B. A. Aufdembrink, P. Chu, I. D. Johnson, G. W. Kirker and M. K. Rubin, "Preparation of molecular sieves from dense, layered metal oxides", *J. Amer. Chem. Soc.*, **11**, 3189 -3190, (1991).

P. Laszlo, "Chemical reactions on clays", *Science*, **235**, 1473 - 1477, (1987).

H. Lee, L. J. Kepley, H. -G. Hong and T. E. Mallouk, "Inorganic analogues of Langmuir-Blodgett films: adsorption of ordered zirconium 1,10-decanebisphosphonate multilayers on silicon surfaces", *J. Am. Chem. Soc.*, **110**, 618 - 620, (1988).

H. Lee, L. J. Kepley, H. -G. Hong, S. Achter and T. E. Mallouk,"Adsorption of ordered zirconium phosphonate multilayer films on silicon and gold surfaces", *J. Phys. Chem.*, **92**, 2597 - 2601, (1988).

J. F. Lee, M. M. Mortland, S. A. Boyd and C. T. Chiou, "Shape selective adsorption of aromatic molecules from water by tetramethylammonium smectite", *J. Chem. Soc., Faraday. Trans. I*, **85**, 2953 - 2954, (1989).

J. P. Lemmon and M. M. Lerner, "Preparation and characterization of nanocomposites of polyethers and molybdenum disulfide", *Chem. Mater.*, **6**, 207-210, (1994).

Y. -J. Liu, D. C. DeGroot, J. L. Schindler, C. R. Kannewurk and M. G. Kanatzidis, "Intercalation of poly(ethylene oxide) in V_2O_5 xerogel", *Chem. Mater.*, **3**, 992 - 994, (1991).

D. A. Loy and K. J. Shea, "Bridged polysilsesquioxanes: highly porous hybrid organic-inorganic materials", *Chem. Rev.*, **95**, 1431 - 1442, (1995).

D. A. Loy, G. M. Jamison, B. M. Baugher, S. A. Myers, R. A. Assink and K. J. Shea, "Sol-gel synthesis of hybrid organic-inorganic materials. Hexylene- and phenylene-bridged polysiloxanes", *Chem. Mater.*, **8**, 656 - 663, (1996)

Y. Lvov, H. Haas, G. Decher, H. Möhwald and A. Kakachev, "Assembly of polyelectrolyte molecular films onto plasma-treated glass", *J. Phys. Chem.*, **97**, 12835 - 12841, (1993).

D. M. C. MacEwan in The X-ray identification of crystal structures of clay minerals, Ed. G. Brown, Publ. Mineralogical Society London, Chp. 4, (1961).

S. Mann. J. P. Hannington and R. J. P. Williams, "Phospholipid vesicles as a model for biomineralization", *Nature*, **324**, 565 - 567, (1986).

S. Mann, D. D. Archibald, J. M. Didymus, B. R. Heywood, F. C. Meldrum and V. J. Wade, "Biomineralization - biomimetic potential at the inorganic-organic interface", *Mater. Res. Bull.*, **17**, 32 - 36, (1992).

S. Mann, "Molecular tectonics in biomineralization and biomimetic materials chemistry", *Nature*, **365**, 499 - 505, (1993).

S. Mann and G. A. Ozin, "Synthesis of inorganic materials with complex form", *Nature*, **382**, 313 - 318, (1996).

S. Mann, S. L. Burkett, S. A. Davis, C. E. Fowler, N. H. Mendelson, S. D. Sims, D. Walsh and N. T. Whilton, "Sol-gel synthesis of organized matter", unpublished, (1997).

K. M. McGrath, D. M. Dabbs, N. Yao, I. A. Aksay and S. M. Grüner, "Formation of a silicate L_3 phase with continuously adjustable pore sizes", *Science*, **277**, 552 - 556, (1997).

F. C. Meldrum, V. J. Wade, D. L. Nimmo, B. R. Heywood and S. Mann, "Synthesis of inorganic nanophase materials in supramolecular protein cages", *Nature*, **349**, 684 - 687, (1991).

F. C. Meldrum, B. R. Heywood and S. Mann, "Magnetoferritin - *in vitro* synthesis of a novel magnetic protein", *Science*, **257**, 522 - 523, (1992).

R. B. Merrifield, "Solid phase peptide synthesis I. The synthesis of a tetrapeptide", *J. Amer. Chem. Soc.*, **85**, 2149 - 2150, (1963).

P. B. Messersmith and E. P. Giannelis, "Polymer-layered silicate nanocomposites: *in situ* intercalative polymerization of ε-caprolactone in layered silicates", *Chem. Mater.*, **5**, 1064 - 1066, (1993).

P. B. Messersmith and S. I. Stupp, "Synthesis of nanocomposites: organoceramics", *J. Mater. Res.*, **7**, 2599 - 2611, (1992).

P. B. Messersmith and S. I. Stupp, "High-temperature chemical and microstructural trnasformations of a nanocomposite organoceramic", *Chem. Mater.*, **7**, 454 - 460, (1995).

M. Meyer, C. Wallberg, K. Kurihara and J. H. Fendler, "Photosensitized charge separation and hydrogen production in reversed micelle entrapped platinized colloidal cadmium sulphide", *J. Chem. Soc., Chem. Commun.*, 90 - 91, (1984).

M. Meyn, K. Beneke and G. Lagaly, "Anion-exchange reactions of layered double hydroxides", *Inorg. Chem.*, **29**, 5201 - 5207, (1990).

S. Miyata, "Anion-exchange properties of hydrotalcite-like compounds", *Clays Clay Miner.*, **31**, 305 - 311, (1983).

T. Mizutani, Y. Fukushima and O. Kamigaito, "Mechanism of the copolymerization of silicic acid and metal ions in aqueous media", *Bull. Chem. Soc. Jpn.*, **63**, 618 - 619, (1990).

T. Mitzutani, Y. Fukushima, A. Okada and O. Kamigaito, "Synthesis of nickel and magnesium phyllosilicates with 1:1 and 2:1 layer structures", *Bull. Chem. Soc. Jpn.*, **63**. 2094 - 2098, (1990)

A. Monnier, F. Schüth, Q. Huo, D. Kumar, D. Margolese, R. S. Maxwell, G. D. Stucky, M. Krishnamurty, P. Petroff, A. Firouzi, M. Janicke and B. Chmelka, "Cooperative formation of inorganic-organic interfaces in the synthesis of silicate mesostructures", *Science*, **261**, 1299 - 1303, (1993).

H. Muraishi, "The reaction of magnesium hydroxide with soluble silica under hydrothermal conditions below the critical temperature", *Bull. Chem. Soc. Jpn.*, **54**, 878 - 883, (1981).

A. Naito, S. Ganapathy and C. A. McDowell, "High resolution solid state ^{13}C NMR spectra of carbons bonded to nitrogen in a sample spinning at the magic angle", *J. Chem. Phys.*, **74**, 5393, (1981).

L. Netzer and J. Sagiv, "A new approach to construction of artificial monolayer assemblies", *J. Am. Chem. Soc.*, **105**, 674 - 676, (1983).

M. Ogawa, "Formation of novel oriented transparent films of layered silica-surfactant composites", *J. Am. Chem. Soc.*, **116**, 7941 - 7942, (1994).

C. Oriakhi and M. M. Lerner, "Poly(pyrrole) and poly(thiophene)/clay nanocomposites *via* latex-colloid interaction", *Mater. Res. Bull.*, **30**, 723-729, (1995).

C. O. Oriakhi, I. V. Farr and M. M. Lerner, "Incorporation of poly(acrylic acid), poly(vinylsulfonate) and poy(styrenesulfonate) within layered double hydroxides", *J. Mater. Chem.*, **6**, 103 - 107, (1996).

H. W. Oviatt Jr., K. J. Shea and J. H. Small, "Alkylene-bridged silsesquioxane sol-gel synthesis and xerogel characterization. Molecular requirements for porosity", *Chem. Mater.* **5**, 943 - 950, (1993).

G. A. Ozin, "Nanochemistry: synthesis in diminishing dimensions", *Adv. Mater.*, **4**, 612 - 649, (1992).

I. Y. Park, K. Kurado and C. Kato, "Direct synthesis of intercalation compounds between a layered double hydroxide and an anionic dye", *J. Chem. Soc., Dalton Trans.*, 3071 - 3074, (1990).

L. M. Parker, N. B. Milestone and R. H. Newman, "The use of hydrotalcite as an anion absorbant", *Ind. Eng. Chem. Res.*, **34**, 1196 - 1202, (1995).

E. Paus, "Reaction of α-mannosidase from *phaseolus vulgaris* with group-specific reagents. Essential carboxyl groups", *Biochim. Biophys. Acta.*, **526**, 507 - 518, (1978).

C. Petit, P. Lixon and M. P. Pileni, "*In situ* synthesis of silver nanocluster in AOT reverse micelles", *J. Phys. Chem.*, **97**, 12974 - 12983, (1993).

G. Phillip and H. Schmidt, "New materials for contact lenses prepared from Si- and Ti- alkoxides by the sol-gel process", *J. Non-Crystalline Solids*, **63**, 283, (1984).

T. J. Pinnavaia, "Intercalated clay catalysts", *Science*, **220**, 365 - 371, (1983).

T. J. Pinnavaia, T. Lan, P. D. Kaviratna and M. S. Wang, "Clay-polymer nanocomposites: polyether and polyimide systems", *Mater. Res. Soc. Symp. Proc.*, **346**, 81 - 88, (1994).

W. H. Pirkle and P. L. Rinaldi, "General method for the synthesis of high enantiomeric purity chiral epoxides", *J. Org. Chem.*, **43**, 3803 - 3807, (1978).

E. R. Pohl and F. D. Osterholtz, in Molecular characterization of composite interfaces, Eds. H. Ishida and G. Kumar, Publ. Plenum, p157, (1985).

L. Raki, D. G. Rancourt and C. Detellier, "Preparation, characterization and Mössbauer spectroscopy of organic anion intercalated pyroaurite-like layered double hydroxides", *Chem. Mater.*, **7**, 221 - 224, (1995)

K. M. Reddy, I. Moudrakovski, A. Sayari, "Synthesis of mesoporous vanadium silicate molecular sieves", *J. Chem. Soc., Chem. Commun.*, 1059 - 1060, (1994).

W. T. Reichle, "Catalytic reactions by thermally activated, synthetic anionic clay minerals", *J. Catal.*, **94**, 547 - 557, (1985).

W. T. Reichle, "Anionic clay minerals", *CHEMTECH*, **16**, 58 - 63, (1986).

E. Ruiz-Hitzky and J. M. Rojo, "Intracrystalline grafting on layer silicic acids", *Nature*, **287**, 28, (1980).

E. Ruiz-Hitzky, P. Aranda and B. Casal, "New polyethylene intercalation materials in vanadium oxide xerogel", *J. Mater. Chem.*, **2**, 581 - 582, (1992).

E. Ruiz-Hitzky, "Conducting polymers intercalated in layered solids", *Adv. Mater.*, **5**, 334, (1993).

E. Ruiz-Hitzky and P. Aranda, "Polymer-salt intercalation complexes in layer silicates", *Adv. Mater.*, **2**, 545 - 547, (1993).

K. Sakata and T. Kunitake, "A mulitlayered film of an ultrathin siloxane network", *J. Chem. Soc., Chem. Commun.*, 504 - 505, (1990).

D. W. Schaefer and K. D.Keefer, "Fractal aspects of ceramic synthesis", *Mater. Res. Soc. Symp. Proc.*, **73**, 277 -288, (1986).

R. A. Schoonheydt and J. Pelgrims, "Preparation, spectroscopy and reaction with oxygen of $[Co(en)_2]^{2+}$ on the surface of hectorite", *J. Chem. Soc., Faraday Trans. 2*, **79**, 1169 - 1180, (1983).

K. J. Shea, D. A. Loy and O. Webster, "Arylsilsesquioxane gels and related materials. New hybrids of organic and inorganic networks, *J. Am Chem. Soc.*, **114**, 6700 - 6710, (1992).

J. C. Sheehan and G. P. Hess, "A new method of forming peptide bonds", *J. Am. Chem. Soc.*, **77**, 1067 - 1069, (1955).

M. Soma and Y. Soma, "Intercalation of tetrathiafulvene (TTF) into montmorillonite by reaction with the interlayer cations", *Chem. Lett.*, 405 - 408, (1988).

M. S. Stul, A. Maes and J. D. Bock, "The adsorption of n-aliphatic alcohols from dilute aqueous solutions on alkylammonium-montmorillonites", *Clays Clay Miner.*, **26**, 309 - 317, (1978).

Y. Sugahara, N. Yokoyama, K. Kurado and C. Kato, "AIN formation from a hydrotalcite polyacrylonitrile intercalation compound by carbothermal reduction", *Ceram. Int.*, **14**, 163 - 167, (1988).

H. Tagaya, S. Sato, H. Morioka, J. Kadokawa, M. Karasu and K. Chiba, "Preferential intercalation of isomers of naphthalenecarboxylate ions into the interlayer of layered double hydroxides", *Chem. Mater.*, **5**, 1431 - 1433, (1993).

P. T. Tanev and T. J. Pinnavaia, "A neutral templating route to mesoporous molecular sieves", *Science*, **267**, 865 - 867, (1995).

P. T. Tanev and T. J. Pinnavaia, "Biomimetic templating of porous lamellar silicas by vesicular surfactant assemblies", *Science*, **271**, 1267 - 1269, (1996).

N. Tillman, A. Ulman and T. L. Penner, "Formation of multilayers by self assembly", *Langmuir*, **5**, 101 - 111, (1989).

L. Ukrainczyk, R. A. Bellman and A. B. Anderson, "Template synthesis and characterization of layered Al- and Mg-silisesquioxanes", *J. Phys. Chem. B*,**101**, 531 - 539, (1997).

R. A. Vaia, H. Ishii and E. P. Giannelis, "Synthesis and properties of two-dimensional nanostructures by direct intercalation of polymer melts in layered silicates", *Chem. Mater.*, **5**, 1694 - 1696, (1993).

M. H. P. Van Genderen, M. Pfaadt, C. Möller, S. Valiyaveettil and H. W. Speiss, "Dynamics of high temperature membrane models composed of 5-alkoxyisophthalic

acids as investigated by ^{2}H-NMR spectroscopy", *J. Amer. Chem. Soc.*, **118**, 3661 - 3665, (1996).

H. Van Olphen, in An introduction to clay colloid chemistry, Publ. Wiley-Interscience: New York, (1977).

J. C. Vartuli, C. T. Kresge, W. J. Roth, S. B. McCullen, J. S. Beck, K. D. Schmitt, M. E. Leonowicz, J. D. Lutner and E. W. Sheppard, "Designed synthesis of mesopore molecular sieve systems using surfactant directing agents", *Prepr. Amer. Chem. Soc. Div. Pet. Chem.*, **40**, 269 - 271,(1995).

D. Walsh, J. D. Hopwood and S. Mann, "Crystal tectonics - construction of reticulated calcium phosphate frameworks in bicontinuous reverse microemulsions", *Science*, **264**, 1576 - 1578, (1994).

M. S. Wang and T. J. Pinnavaia, "Clay-polymer nanocomposite formed from acidic derivatives of montmorillonite and an epoxy resin", *Chem. Mater.*, **6**, 468 - 474, (1994).

Z. Wang, T. Lan and T. J. Pinnavaia, "Hybrid organic-inorganic nanocomposites formed from an epoxy polymer and a layered silicic acid (magadiite)", *Chem. Mater.*, **8**, 2200 - 2204, (1996).

H. J. Watzke and C. Dieschbourg, "Novel silica biopolymer nanocomposites - the silica sol-gel process in biopolymer organogels", *Adv. Colloid. Interf. Sci.*, **50**, 1 - 14, (1994).

M. S. Whittingham and A. J. Jacobson (Eds.), in Intercalation chemistry, Publ. Academic Press, (1982).

S. K .Wolk, G. Swift, Y. H. Paik, K. M. Yocom, R. L. Smith and E. S. Simon, "One- and two-dimensional nuclear magnetic resonance characterization of poly(aspartic acid) prepared by thermal polymerization of L-aspartic acid", *Macromolecules*, **27**, 7613 - 7620, (1994).

K. K. W. Wong, N. T. Whilton, H. Colfen, T. Douglas and S. Mann, manuscript in preparation, (1997).

J. L. Woodhead and A. D. B. Malcolm, "The essential carboxyl group in restriction endonuclease *Eco*RI", *Eur. J. Biochem.*, **120**, 125-128, (1981).

J. Wu and M. M. Lerner, "Structural, thermal, and electrical characterization of layered nanocomposites derived from Na-montmorillonite and polyethers", *Chem. Mater.*, **5**, 835 - 838, (1993).

S. Yamanaka, "Synthesis and characterization of organic derivatives of zirconium phosphate", *Inorg. Chem.*, **15**, 2811 - 2817, (1976).

T. Yanagisawa, C. Yokoyama, K. Kurado and C. Kato, "Synthesis of layered polysilicic acid-acrylamide intercalation compounds and polymerization in the interlayer spaces", *Bull. Chem. Soc. Jpn.*, **63**, 47 - 50, (1990).

W. Zhang, M. Fröba, J. Wang, P. T. Tanev, J. Wong and T. J. Pinnavaia, "Mesoporous titanosilicate molecular sieves prepared at ambient temperature by electrostatic (S^+I^-, $S^+X^-I^+$) and neutral S°I°) assembly pathways - a comparison of physical properties and catalytic activity for peroxide oxidations", *J. Am. Chem. Soc.*, **118**, 9164 - 9171, (1996).

APPENDIX

A BRIEF INTRODUCTION TO THE CROSS-POLARIZATION (CP) MAGIC ANGLE SPINNING (MAS) NMR EXPERIMENT

A BRIEF INTRODUCTION TO THE CROSS-POLARIZATION (CP) MAGIC ANGLE SPINNING (MAS) NMR EXPERIMENT

A.1 *The CP MAS experiment*

Much chemical and structural information has been gained from isotropic shift measurements by high resolution NMR in solution. The random tumbling of molecules in solution allows for complete averaging of anisotropic spin interactions (proton dipolar broadening, carbon chemical shift anisotropy) with the result that the spectra contain signals with very narrow line widths (<1 Hz). In solids, where such motion is rare, anisotropic interactions are at most incompletely averaged, and the width of the lines in a solid-state spectrum is much greater (several kilohertz). The CP MAS experiment (Lowe, 1959; Andrew, 1971), however, has extended high-resolution NMR studies to the solid state. The crux of this experiment involves alteration of the polarizations of low-γ nuclei by exploiting the dipolar coupling to high-γ nuclei, to afford well-resolved NMR spectra of organic solids.

The CP MAS experiment involves the use of:

1) CP (Pines *et al.*, 1973) techniques to increase the signal/noise and bypass the T_1 relaxation processes of the dilute nuclei being observed.

2) High-power proton decoupling (spin locking) during acquisition to remove the dipolar interactions.

3) Continuous magic angle sample spinning [MAS (Lowe, 1959; Andrew, 1971)] to remove the chemical shift anisotropy.

The experiment will be discussed with a view to obtaining well-resolved ^{13}C NMR spectra, although it applies to other spin-$^1/_2$ nuclei which can have weak mutual coupling either by virtue of low natural abundance or a small magnetic moment (e.g., ^{31}P, ^{29}Si, ^{15}N)

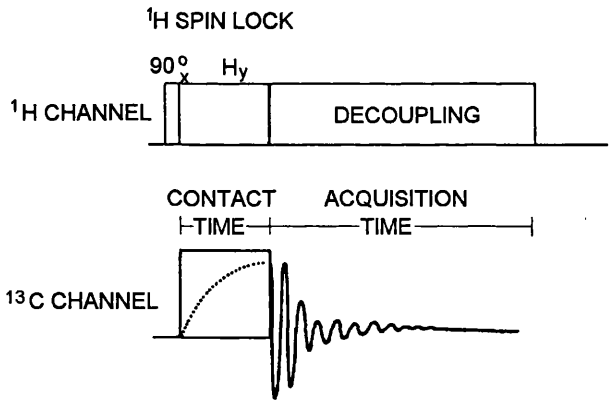

Figure A.1 A typical ^{13}C-^1H cross-polarization sequence. Redrawn from Komoroski, 1986.

Cross polarization involves the generation of the ^{13}C NMR signal by using the energy and relaxation properties of the protons. The first step of the ^{13}C-^1H cross polarization sequence involves rotation of the proton magnetization 90° to the y'-axis in the rotating frame by a strong on-resonance $\pi/2$ pulse applied along the x'-axis and

then "spin locked" along y' by an on-resonance "spin locking" pulse applied along y'. In the rotating frame the protons are now characterized by a very low spin temperature, given by:

$$T_R = (H_{1H}/H_0)T1$$

where T_R = spin temperature of the proton reservoir in the rotating frame

H_{1H} = applied rf

H_0 = static magnetic field

T_1 = lattice temperature

achieved by lowering of the effective field seen by the protons (H_{1H}).

In the second step the ^1H spins are kept locked along y' for a time period t. During this time period a strong on-resonance pulse is applied to the ^{13}C spins which also orient in the y' direction in the ^{13}C rotating plane. Both sets of spins become 'locked', and by correct choice of magnitudes of the spin-locking fields H_{1H} and H_{1C}, the net carbon magnetization may be enhanced by proton-carbon cross-polarization. The magnitudes of the two fields are chosen so that the equality, called the Hartmann-Hahn condition is established (Hartmann and Hahn, 1962; McArthur *et al.*, 1969)

$$\gamma_{1H}.H_{1H} = \gamma_{13C}.\ H_{1C}$$

where γ = gyromagnetic ratio of ^1H or ^{13}C nuclei,

H = rf pulse applied to ^{1}H or ^{13}C nuclei.

Since the separation of the ^{13}C upper and lower spin levels is only $^{1}/_{4}$ of the separation of the corresponding proton levels at the same temperature (since $\gamma_{1_H} \cong 4\gamma_{13_C}$), the ^{13}C locking field, H_{1C} must be four times H_{1H} to satisfy the equality. Carbon and proton spins, with identical oscillatory components in their respective rotating frames, can thus cross relax efficiently by the energy-conserving spin flips normally reserved for identical nuclei. Since the ^{13}C spins are very dilute in the system, they will adopt the more favourable spin distribution of the proton system, while the total proton magnetization will be little affected.

After carbon magnetization has built up during the matching or 'contact' period (t), the carbon field, H_{1C}, is switched off and the carbon free-induction delay (FID) is recorded. The proton field is kept on (and spin-locked) during this period to provide heteronuclear decoupling of the proton-carbon dipolar interactions.

A recycle time is inserted between pulse sequences during which there are no carbon or proton pulses and both carbon and proton spin systems relax towards their equilibrium values in H_0.

Because the chemical shift anisotropy is described by a second rank tensor, high-speed magic angle sample spinning (Andrew, 1971) is often used in conjunction with the cross-polarization experiment to improve the resolution. By fashioning the solid into a rotor (or placing inside a hollow rotor) and aligning the axis of rotation of

the rotor at 54.7° relative to H_0, chemical shift anisotropic dispersions are averaged to their isotropic average chemical shift value.

A.2 *Selection of Nonprotonated Carbons*

A modification of the CP MAS experiment allows for differentiation of carbons with directly-bonded protons from those carbons without protons (Opella and Frey, 1979). Figure A.2 illustrates the pulse sequence used to suppress signals from protonated carbons in solid samples.

The experiment consists of a normal CP period followed by the insertion of a short delay (25-100 μs) in which both the ^{13}C and ^{1}H rf fields are turned off. The ^{1}H field is reapplied (to decouple the dipolar interactions) and data acquisition begun. In the 'dephasing' delay any carbon which is strongly interacting with protons loses magnetization quickly through rapid 'dephasing' of the ^{13}C spins, such that during the acquisition of the carbon free-induction decay, only non-protonated carbons which were not dephased during the delay contribute to the spectrum. In a rigid solid any CH or CH_2 signal is thus removed. A drawback to the approach is that molecular motion can reduce the strength of dipolar coupling (and dephasing); thus a rapidly rotating group could appear as if protons were farther away. Hence methyl carbons often appear, but at reduced intensity because of their fast "internal" rotation.

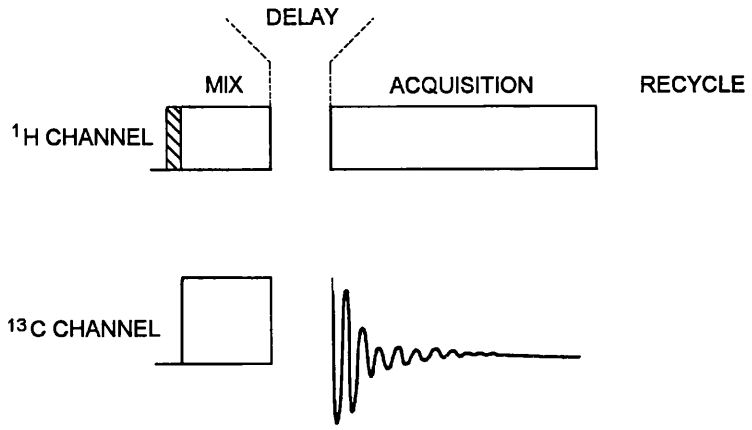

Figure A.2 Schematic of the pulse sequence applied in non-quaternary suppression (NQS) experiments. Redrawn from Opella and Frey, 1979.

A.3 *Quantitative ^{29}Si MAS NMR*

The problem of CP MAS experiments is their being quantitatively unreliable due to differential cross-polarization rates and possibly differential decays of the magnetization of individual dilute nuclei, and an alternative approach using MAS alone can be used to obtain ^{29}Si MAS NMR at high magnetic field strengths (Fyfe, 1983). Direct polarization is achieved via a simple 90° pulse technique resulting in direct polarization and a loss in the signal/noise ratio. The high magnetic field gives sufficient sensitivity to obtain ^{29}Si spectra and the resolution is good allowing for efficient deconvolution of the peaks.

A.4 *References*

E. R. Andrew, *Prog. Nucl. Magn. Reson.*, **8**, 1, (1971).

C. A. Fyfe (Ed.), in Solid state NMR for chemists, Publ. CFC Press, (1983).

S. R. Hartmann and E. L. Hahn, *Phys. Rev.*, **128**, 2042, (1962).

R. A. Komoroski (Ed.), in High resolution NMR spectroscopy of synthetic polymers in bulk, Publ. VCH, (1986).

I. J. Lowe, *Phys. Rev. Lett.*, **2**, 285, (1959).

D. A. McArthur, E. L. Hahn and R. E. Walstedt, *Phys. Rev.*, **188**, 609, (1969)

S. J. Opella and M. H. Frey, *J. Am. Chem. Soc.*, **101**, 5854, (1979).

A. Pines, M. G. Gibby and J. S. Waugh, *J. Chem. Phys.*, **59**, 569, (1973).